FINAL REPORT
FOR THE
BACKSCATTER ULTRAVIOLET (BUV) INSTRUMENT

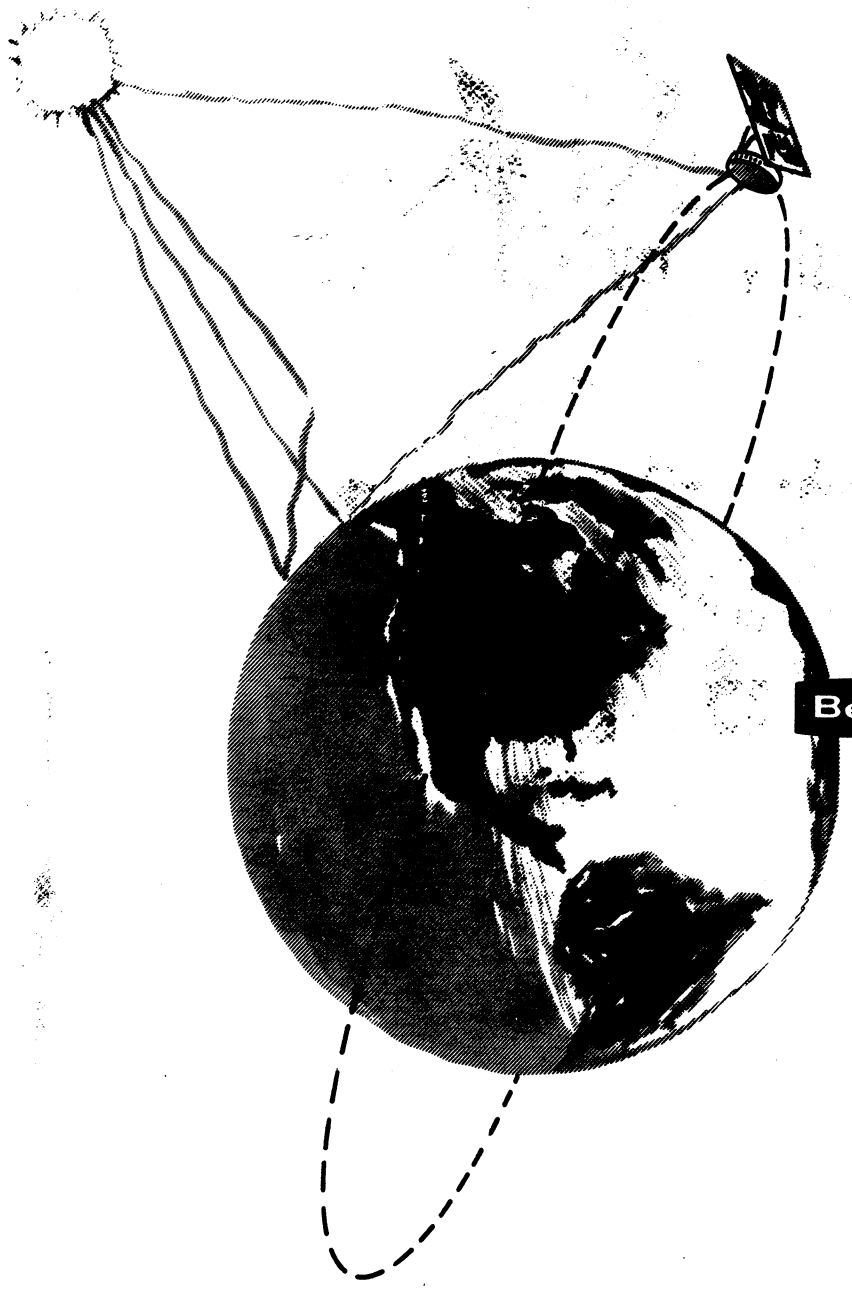

VOLUME 2

Prepared by

Beckman INSTRUMENTS, INC.

ADVANCED TECHNOLOGY OPERATIONS
FULLERTON, CALIFORNIA • 92634

for

Goddard Space Flight Center
Greenbelt, Maryland

FR-2475-101

Volume II

Final Report

for the

BACKSCATTER ULTRAVIOLET (BUV) INSTRUMENT

Contract No. NAS5-10381

Covering the Period:

(April 1967 to June 1970)

Goddard Space Flight Center

Contracting Officer: Henry Arista
Technical Monitor: Arlin J. Krueger

Prepared By:

Beckman® INSTRUMENTS, INC.
ADVANCED TECHNOLOGY OPERATIONS
FULLERTON, CALIFORNIA • 92634

Project Manager: Merton A. Robinson

Prepared For

GODDARD SPACE FLIGHT CENTER
Greenbelt, Maryland

for Balloon
13W

8/14/74

Bert

Your coffee isn't hot enough for me.

The solar irradiance at 2700 Å

is $\frac{25\,\mu W}{m^2\,Å} = \frac{.025\,\mu W}{cm^2\,nm}$

The lamp irradiance at 2700 Å at 50 cm. distance is $\frac{.0549\,\mu W}{cm^2\,nm}$

$\frac{.0549}{.025} = 2.196$ — at 50 cm distance the lamp is 2.196 times as bright as the sun

Therefore, to simulate the sun, I must back off by a factor of $\sqrt{2.196} = 1.4819$

Therefore new distance is 74.1 cm or 29.17 inches

Check?

HReid

DOCUMENTS REQUIREMENTS LIST

ITEM NO.	REFERENCE PARAGRAPH: WORK STATEMENT	REFERENCE PARAGRAPH: OTHER	DOCUMENT	SUBMIT TO NASA	UPDATING BY CONTRACTOR	DISTRIBUTION CODE (SEE NOTE 1)	NASA/LRC ACTION REQUIRED SEE NOTE 2
1	Ex 1, P-5.1 Ex 3, P-1.6		Configuration Control Plan	30 Days after Contract Award	As Required	B-4, C-1, G-3	Approval
2	Ex 1, P-4.4		Subcontractor Quality Program Plans	45 Days After Subcontract Award	As Required	B-4, C-1, G-3	Approval
3	Ex 1, P-3.9.3.10		Subcontractor Parts Program	As Required Prior to Subcontracting	As Required	B-4, C-1, G-3	Review
4	Ex 1, P-4.6	NHB 5300.4(1A) p-1A308 NHB 5300.4(1B) p-1B603	Materials, Parts, Components, and Process Specifications	As Required	As Required	B-4, C-1, G-3	Approval
5	Ex 1,P-5.3.2		Engineering Design Changes	As Generated	As Required	B-6, C-1, G-6	Approval
6	Ex 1, 3.9.2	NHB 5300.4(1A) p-1A308	Materials & Process Lists	30 Days Prior to PDR	As Required	B-4, C-1, G-3	Approval
7	Ex 1, 3.9.3		Sensor Authorized Parts List	a. 45 Days After Award b. 90 Days After Award	a. No. b. Monthly	B-4, C-1, G-10	a. Review b. Approval
8	Ex 1, p-3.9.3.4		Parts Identification List	8 Months After Award	Monthly as Required	B-4, C-1, G-3	Review
9	Ex 1, p-3.8 p-3.9.3.14 Ex 3,p-1.9	NHB5300A (1A),p-1A 306 S-312-p-1	Malfunction Reports/ a. Preliminary (copies 1 & 2 b. Final (copies 4 & 5)	Within 2 Days After Malfunction Within 14 Days After Malfunction	No No	B-4, C-1, G-5 copies 1 & 2 B-4, C-1 G-5 copies 4 & 5	 Approval

FINISH 541

LINEARITY TEST - Q.L. LAMP

INITIAL LAMP TO DIFFUSER DIST. 50 FT.

DIST (in cm)	KEITHLEY w/o DIF	KEITHLEY WITH DIF
0	.31 x10⁻⁹	.29 x10⁻¹⁰
50	.32	.315
100	.34	.325
110	.365	.34
200	.38	.36
250	.41	.38
300	.44	.395
350	.48	.41
400	.52	.44
450	.57	.465
500	.62	.51
550	.68	.55
600	.76	.62
650	.85	.67
700	.95	.76
750	.125x10⁻⁸	.84
800	.137	.93
850	.155	.107x10⁻⁹
900	.178	.120
950	.210	.138
1000	.255	.162
1050	.312	.195
1100	.375	.235
1150	.465	.290
1200	.615	.380
1250	.835	.51
1300	.122x10⁻⁷	.092x10⁻⁸
1350	.208	.145
1400	.41	.275
1450	.125x10⁻⁶	.75
1500	.288 x10⁻⁶	.162x10⁻⁷

INVERSION

SET UP:

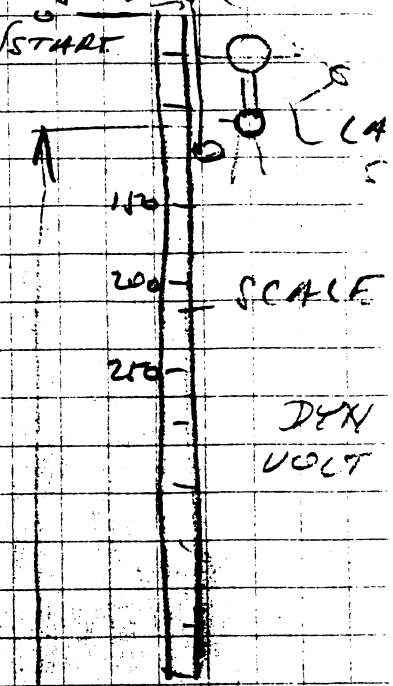

Q.L. LAMP WAS INSTALLED 50' FROM ZUV. THE LAMP WAS THEN MOVED TOWARD THE ZUV IN 50cm STEPS AND READINGS TAKEN WITH AND W/O THE DIFFUSER

Volume II

TABLE OF CONTENTS

LIST OF ILLUSTRATIONS

LIST OF ILLUSTRATIONS (continued)

LIST OF ILLUSTRATIONS (continued)

LIST OF ILLUSTRATIONS (continued)

LIST OF TABLES

SECTION IV

MECHANICS

4.1 MECHANICAL REQUIREMENTS

The technical challenges in designing the mechanical portion of the BUV instrument can be grouped into the following categories:

1. Combine two separate units with their optical and electronic systems, monochromators, and photometer into one extremely compact assembly fitting into bay No. 9 of the NIMBUS satellite.
2. Provide high-accuracy repeatability and reliability in areas where optical components had to be located, held, and moved.
3. Provide an essentially monometallic design to eliminate changes in the system due to thermal gradients.
4. All moving components have to move with a minimum of applied force and at the same time stay in place after motion is performed.
5. Thermally isolate the BUV Instrument from the NIMBUS ring.
6. Interface with the NIMBUS satellite as shown in Figure 4-1.

4.2 THERMAL ANALYSIS

Beckman has reviewed all thermal analyses conducted during this program. Tests were performed to verify the thermal design integrity. The results of these studies and tests indicate that the thermal design philosophy as defined by Beckman has produced an acceptable environment for the BUV optics.

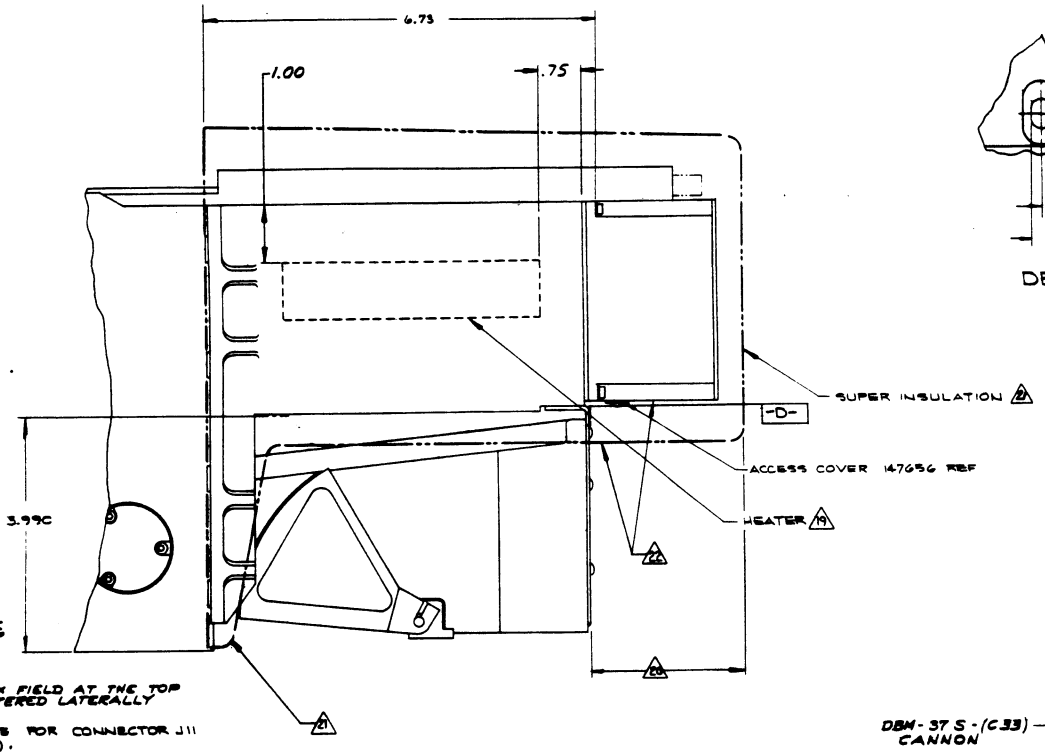

DBM-37S-(C33)
CANNON

(28) INSTALL INSULATING STRIP PER G.E. INSTALLING PROCEDURE AND DRAWING NO. ER49J213116.

(26) APPLY NAMEPLATE WITH HYSOL ADHESIVE 9309 AFTER CLEANING SURFACES WITH ACETONE.

(25) THIS DIMENSION DEFINES THE MAX FIELD AT THE TOP OF THE DIFFUSER, TO BE CENTERED LATERALLY ABOUT OPTICAL ℄.

23. THERMAL PROTECTION OF CABLE FOR CONNECTOR J11 TO BE SUPPLIED BY NASA (G.S.).

(24) WHEN INSTALLING SUPERINSULATION ASSURE ELECTRICAL GROUND SEPARATION BETWEEN ELECTROMETER HOUSING AND SENSOR HOUSING.

(21) SUPERINSULATION SHELL CONFIGURATION SEE G.E. DRAWING 47 E 213222.

(22) SIDE PORTION OF THE SUPERINSULATION FACING THE FIELD-DEFINING-HORNS TO BE PAINTED BLACK WITH NEXTEL, OR EQUIV, OVER AREA SHOWN.

(19) COMPENSATION HEATER TO BE INSTALLED ON BUV HOUSING BY NASA (GE) IN AREA SHOWN.

(18) TO BE MARKED BY GENERAL ELECTRIC CO. PER GE SPEC 118A1526, CLASS 21.

(17) SUPPLIED BY BECKMAN PART NO. 147171 & 147688. FOR ASSY SEE DETAIL C.

(16) RADIATION PORTS WITHIN SUPER INSULATION TO BE FINISHED WITH PV 100. SEE PAINTING PROCEDURE DWG 149199

(15) WIRE MESH REPLACEMENT PARTS TO BE SUPPLIED BY BECKMAN (PART NO. 146881). ALL CUT EDGES OF WIRE MESH TO BE SEALED.

(14) MODIFIED DIMENSION FOR EXTENSION AS REQUESTED IN LETTER TO NASA BUV TECHNICAL OFFICER DATED DEC. 1, 1967.

(13) THE SPACECRAFT INBOARD WALL SHALL CONTAIN NO LIGHTNING HOLES AND SHALL BE FINISHED WITH GLYCEROL PHTHLATE.

(12) BUTTON HEIGHT TO BE DETERMINED AT ASSEMBLY FOR MINIMUM CLEARANCE.

(11) NO. 8-32 x 3/4" LONG CRES SOCKET HEAD CAP SCREW TO BE TORQUED TO 18-20 INCH LBS (AFTER MODULE CLAMPS ARE SET).

10. THE BUV SENSOR MODULE WILL BE MOUNTED IN BAY 9 OF THE NIMBUS D SPACECRAFT.

9. THE INSIDE OF THE NIMBUS BAY IN WHICH THE SENSOR MODULE IS MOUNTED SHALL BE COATED WITH ALODINE 600 WITH EXCEPTION OF THE INBOARD SIDE WHICH SHALL BE COATED WITH GLYCEROL PHTHLATE.

8. THE BUV INSTRUMENT IS NOT TO BE EXPOSED TO HUMIDITY TESTING AS REQUIRED IN SECTION 3.1 OF GSFC ENVIRONMENTAL SPECIFICATION S-633-P-14. HIGH HUMIDITY AND/OR MOISTURE CONDENSATION WILL CAUSE SERIOUS DAMAGE TO THE COATED OPTICAL SURFACES.

(7) THE TEMPERATURE CONTROL SHUTTERS ON THE SPACECRAFT ARE TO BE FIXED IN A CLOSED POSITION AND A LAYER OF SUPER INSULATION IS TO BE INSTALLED BY G.E. BETWEEN THE TEMPERATURE CONTROL SURFACE AND THE SHUTTERS.

(6) COAT WITH CAT-A-LAC BLACK.

(5) REPLACE WIRE MESH FOR EACH NEW INSTALLATION. (SEE NOTE (15)).

(4) MIRROR COVER NOT TO BE REMOVED BY G.E. PERSONNEL.

(3) FORCE APPLIED PER CLAMP TO BE 144 ± 72 LBS.

(2) BECKMAN WILL APPLY REFLECTIVE TAPE BII NO. 148216 (3M NO. Y-9360) TO AREA INDICATED.

1. FINISH ALL EXPOSED MAGNESIUM SURFACES WITH DOW #9 PER MIL-M-3171, TYPE 4.

NOTES: UNLESS OTHERWISE SPECIFIED

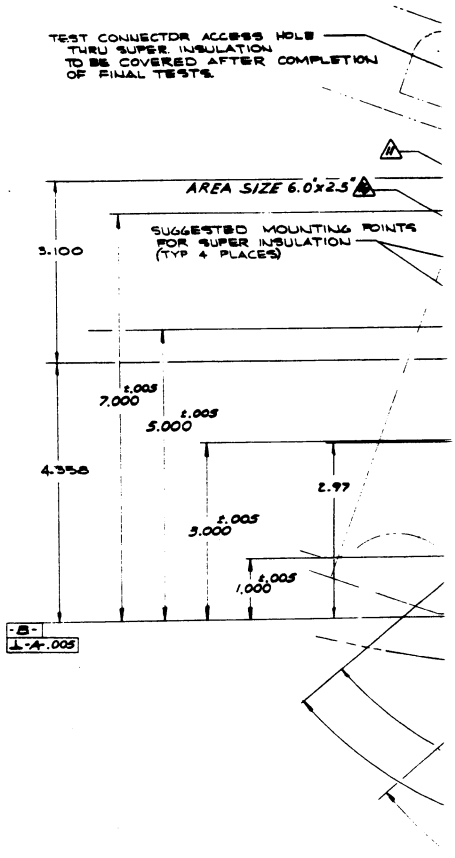

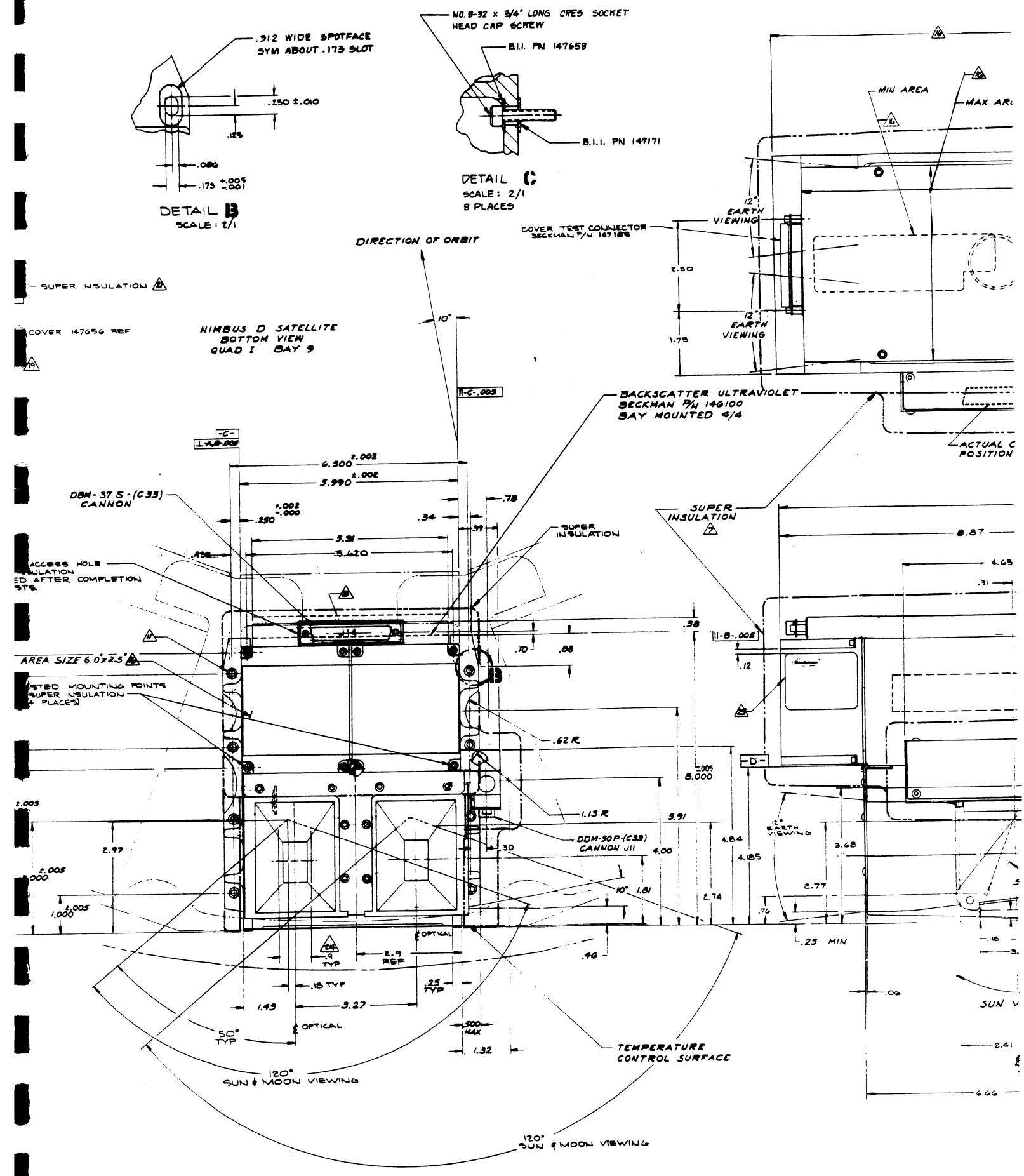
.312 WIDE SPOTFACE SYM ABOUT .173 SLOT
.250 ±.010
.125
.086
.173 +.005 -.001
DETAIL B
SCALE: 2/1
NO. 8-32 x 3/4" LONG CRES SOCKET HEAD CAP SCREW
B.I.I. PN 147658
B.I.I. PN 147171
DETAIL C
SCALE: 2/1
8 PLACES
MIN AREA
MAX AR
12° EARTH VIEWING
COVER TEST CONNECTOR BECKMAN P/N 147188
2.80
1.75
12° EARTH VIEWING
DIRECTION OF ORBIT
SUPER INSULATION
COVER 147656 REF
NIMBUS D SATELLITE
BOTTOM VIEW
QUAD I BAY 9
10°
11-C-.005
BACKSCATTER ULTRAVIOLET
BECKMAN P/N 146100
BAY MOUNTED 4/4
ACTUAL C
POSITION
-C-
6.500 ±.002
5.990 ±.002
DBM-37 S-(C33)
CANNON
.250 +.002 -.000
.78
.34
.99
SUPER INSULATION
5.31
5.620
.438
ACCESS HOLE
INSULATION
ED AFTER COMPLETION
STS.
SUPER INSULATION
8.87
4.63
.31
.38
11-B-.005
.10
.88
.12
AREA SIZE 6.0"x2.5"
STBD MOUNTING POINTS
SUPER INSULATION
4 PLACES)
.62 R
-D-
±.005
8.000
1.13 R
5.91
DDM-50P-(C33)
CANNON J11
4.00
.30
4.84
4.185
12° EARTH VIEWING
3.68
2.77
10°
1.81
2.74
.76
.25 MIN
.005
2.97
.005
.000
.005
1.000
℄ OPTICAL
.9 TYP
2.9 REF
.46
.18 TYP
.25 TYP
1.43
3.27
50° TYP
℄ OPTICAL
.500 MAX
1.32
.06
SUN V
2.41
6.66
TEMPERATURE CONTROL SURFACE
120° SUN & MOON VIEWING
120° SUN & MOON VIEWING

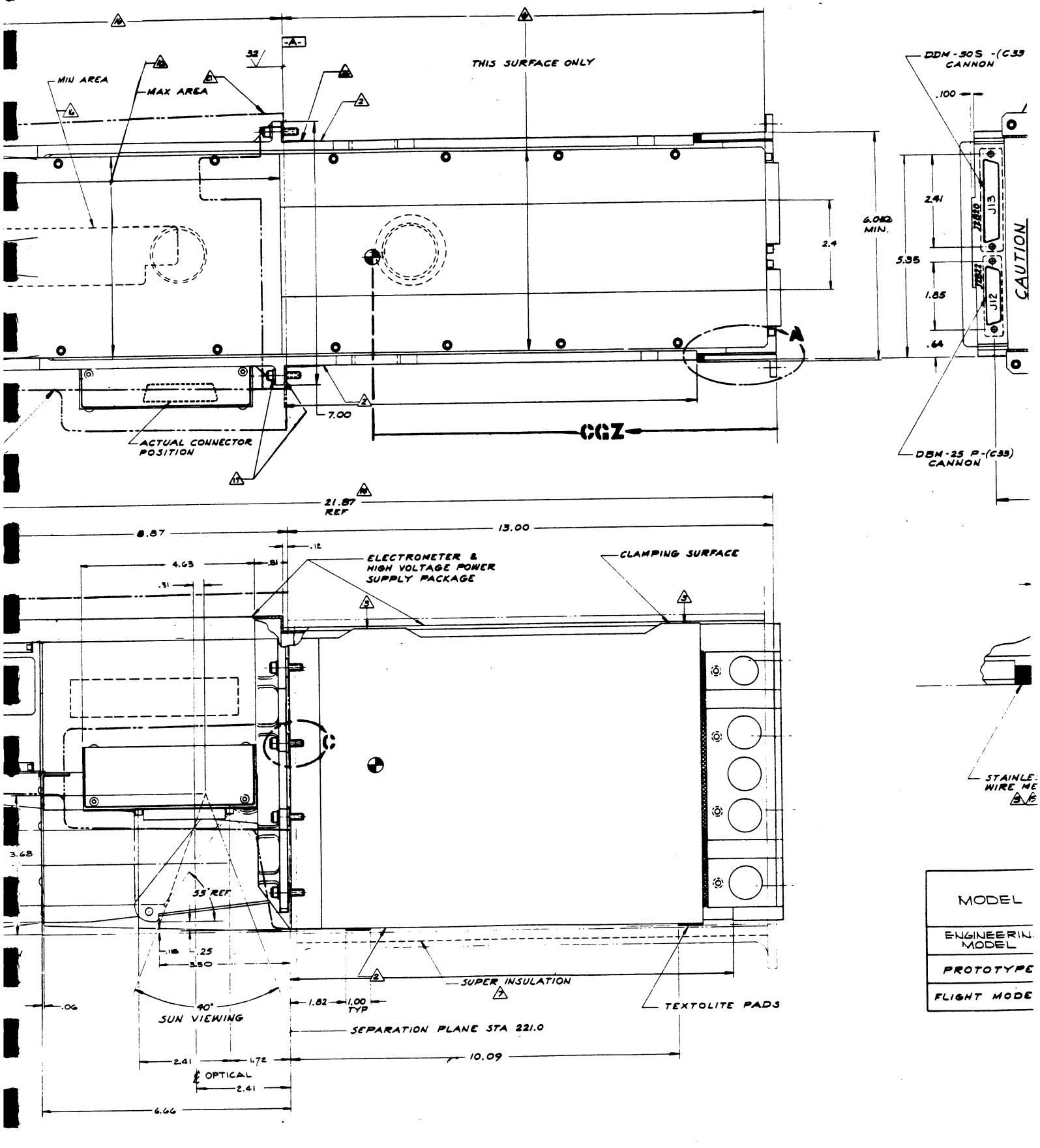
MIN AREA
MAX AREA
32
-A-
THIS SURFACE ONLY
DDM-50S -(C33 CANNON
.100
2.41
5.35
1.85
.64
J13
J12
CAUTION
6.082 MIN.
2.4
7.00
CGZ
ACTUAL CONNECTOR POSITION
DBM-25 P-(C33) CANNON
21.87 REF
8.87
13.00
.12
4.63
.81
.31
ELECTROMETER & HIGH VOLTAGE POWER SUPPLY PACKAGE
CLAMPING SURFACE
3.68
55° REF
.18
.25
3.50
SUPER INSULATION
.06
40°
SUN VIEWING
1.82
1.00 TYP
TEXTOLITE PADS
SEPARATION PLANE STA 221.0
2.41
1.72
10.09
OPTICAL
2.41
6.66
STAINLE
WIRE ME
MODEL
ENGINEERIN
MODEL
PROTOTYPE
FLIGHT MODE

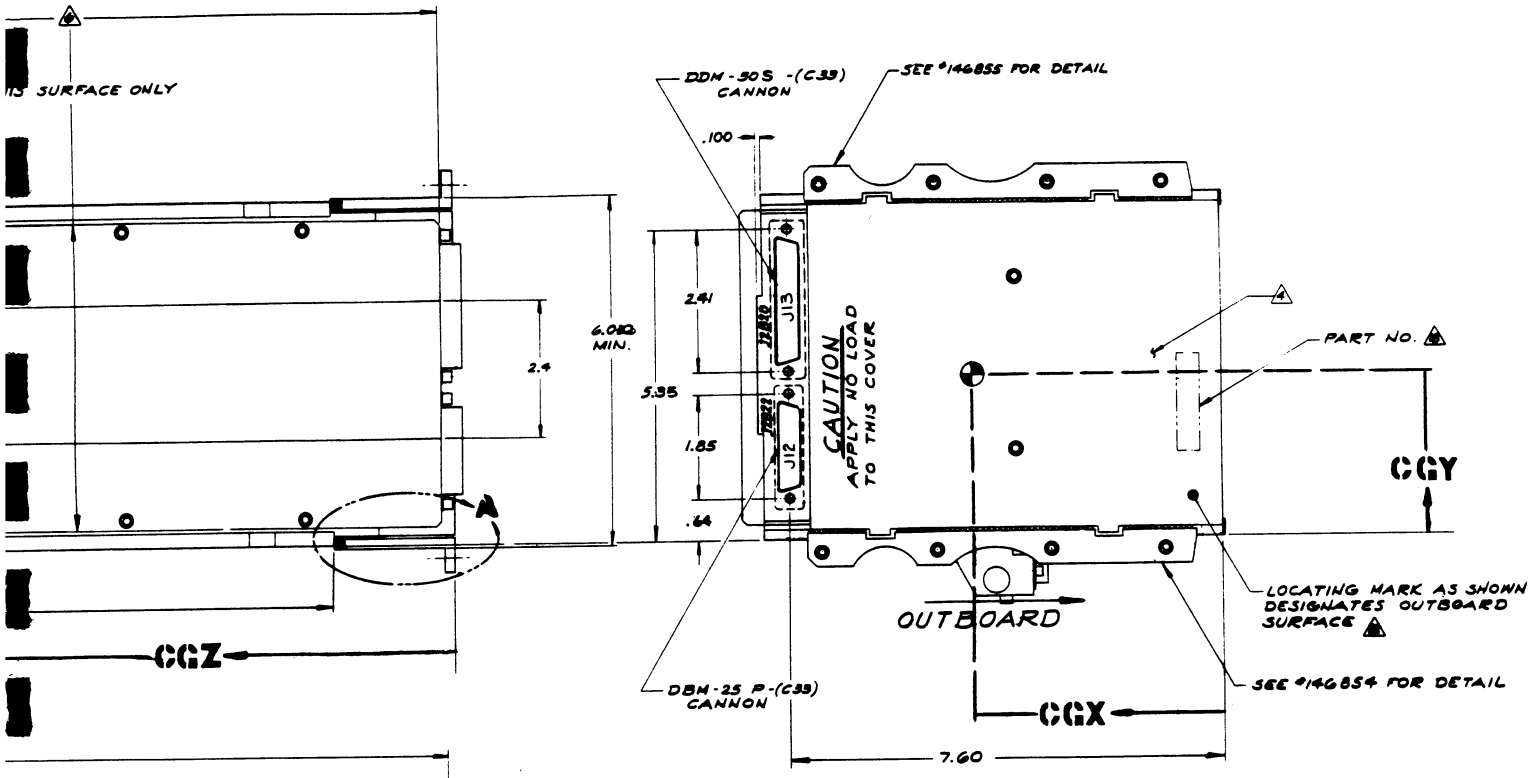

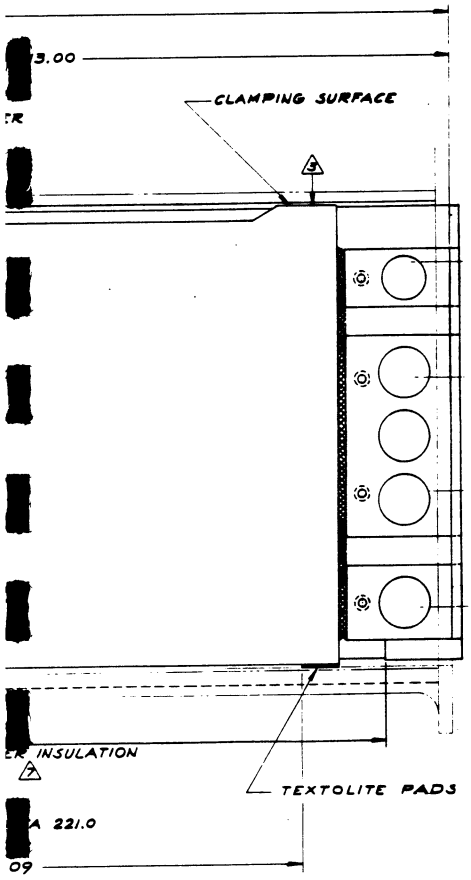

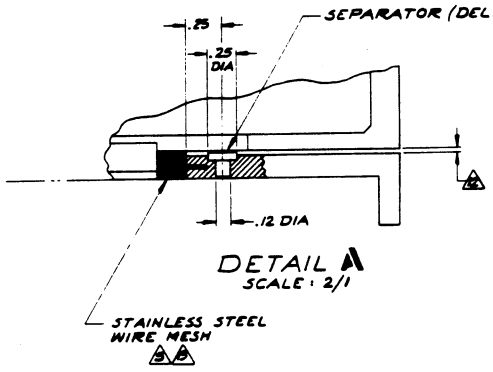

MODEL	LOCATION OF CENTER OF GRAVITY		
	X-AXIS	Y-AXIS	Z-AXIS
ENGINEERING MODEL	4.4	2.9	10.9
PROTOTYPE	4.55	2.81	11.05
FLIGHT MODEL	4.68	2.62	11.03

Figure 4-1. BUV-NIMBUS Interface Control Drawing

4.2.1 Thermal Environment

The BUV must operate within the tolerance of the optical specification, while it is exposed to two thermal environments: the "Nimbus environment" as established by the sensory ring thermal control system and the "Test Environment". These environments can be briefly stated as the following:

Nimbus thermal environment

Structure temperature	25 ±10°C
Experiment to structure temperature differential	5°C maximum
Instantaneous structural temperature differential	10°C maximum
Day-Night structural temperature differential	10°C maximum

Test thermal environment (Thermal-Vacuum test)

Isothermal temperature changes from -5°C to +45°C while in an evacuated chamber at 10^{-5} mm Hg.

4.2.2 Thermal Effects on the Optics

The optical system of the BUV must measure backscattered radiation from the earth at various wavelengths within an allowable tolerance of ±.2Å. To maintain the optical alignment within the ±.2Å tolerance, thermal expansions and gradients which could alter and shift optical surfaces had to be minimized and considered within the thermal design.

4.2.2.1 Thermal Expansions

The "Test Environment" subjected the BUV to isothermal temperature changes of 50°C. Under that condition, all components of the BUV expanded and contracted

causing changes in the optical parameters. Expansion of the housing side walls increased the focal length of the monochromator; the radius of curvature of the spherical mirror increased as the mirrors expanded, etc. Within the temperature ranges of the "test environment", however, the only changes in physical dimensions caused by thermal expansions which affected performance were changes in the grating and the wavelength cam.

The grating is attached to a cast magnesium mount and is tilted as the arm of the mount follows the contour of the wavelength cam. Increases in the radius of the cam increase the tilt of the grating and shift the wavelength. The grating itself is effected by temperature since its groove spacing changes and produces wavelength error as the grating expands. Originally, the grating was made from BSC-2 glass and the cam was 7075 aluminum.

The thermal expansion of the cam and the grating were considered individually. The following is a derivation of wavelength error at the exit slit of the monochromator due to changes in the temperature of the grating.

$$d\lambda = \alpha \lambda \Delta T$$

where: $d\lambda$ = change in wavelength (angstrom)

α = coefficient of thermal expansion (1/°C)

λ = wavelength (angstrom)

ΔT = change in temperature (°C)

For the maximum wavelength of 3400Å and with the coefficient of expansion for BSC-2 glass which is 83×10^{-7} per degree centigrade, a temperature change of 7°C will shift the wavelength the full 0.2Å tolerance. Considering quartz,

which has a lower coefficient of expansion (α = 5.5 x 10^{-7}/°C), a temperature change of 107°C was required to shift the wavelength 0.2Å for the same wavelength. Obviously, changing the grating material to quartz was required to maintain calibration tolerance for the "Test Environment".

The geometrical relationship of the grating mount, the wavelength cam and the housing had to be maintained during temperature changes. If the components were monometallic, their omni-directional expansion would always maintain the same geometrical relation. However, the original cam was aluminum while the housing and mount were magnesium. The lower coefficient of expansion of aluminum caused a change in the geometry which was proportional to the difference between the coefficient of expansions of aluminum and magnesium.

On an average, an increase of 0.0002 inches on the radius of the cam shifts the wavelength 0.2Å. Therefore, the maximum permissible temperature change was determined by considering a radius increase of 0.0002 inches. The following equation was used:

$$\Delta T = \frac{(\Delta R)}{\left(\alpha_{mag} - \alpha_{alum}\right) R_{max}}$$

where: ΔT = temperature change (°C)

ΔR = change in radius = 0.0002 inches (maximum)

α_{mag} = magnesium coefficient of thermal expansion = 25.2 x 10^{-6}/°C

α_{alum} = aluminum coefficient of thermal expansion = 22 x 10^{-6}/°C

R_{max} = maximum cam radius = 2.0685 inches

Substituting the numbers in the equation, a temperature change of 24°C produced the total 0.2Å tolerance shift. Since the requirement was for a 50°C

temperature change, a closer match of expansion coefficients between the cam and its related components was required. A magnesium cam which was flame sprayed to provide a satisfactory wear surface was the final design solution. With the magnesium cam, the assembly was monometallic and temperature independent. Therefore, since the magnesium cam was temperature independent, the quartz grating produced the total wavelength shift from temperature changes. Since it was demonstrated above that those shifts were acceptable, the BUV will function within tolerance during the "Test Environment".

4.2.2.2 Thermal Gradients

The "Nimbus Environment" subjects the BUV to various thermal gradients. The instantaneous structural temperature differential as well as the day-night temperature fluctuations produce temperature gradients within the BUV which could result in the tilting of the collimating mirrors. The allowable temperature gradient across the collimating mirrors was determined as follows:

The exit slit of the BUV is 1.2 mm wide and provides for a 10Å bandwidth. Therefore, the spectral dispersion at the exit slit is 10Å/1.2 mm = 8.33Å/mm. The tolerance on the wavelength at the exit slit is ±0.2Å. The corresponding displacement for the tolerance is 0.2Å/8.33Å/mm = 0.024 mm. In other words, the wavelength can be shifted ±0.024 mm for the monochromator to remain within tolerance.

In a computerized ray trace analysis, with all other optical surfaces fixed, the collimating mirrors were tilted at various angles and the displacement of the wavelength at the exit plane was computed. The results of this study are presented in Figure 4-2. For the 0.024 mm permissible shift, an angle of 0.0031° resulted. This angle is equivalent to 54.1×10^{-6} radians.

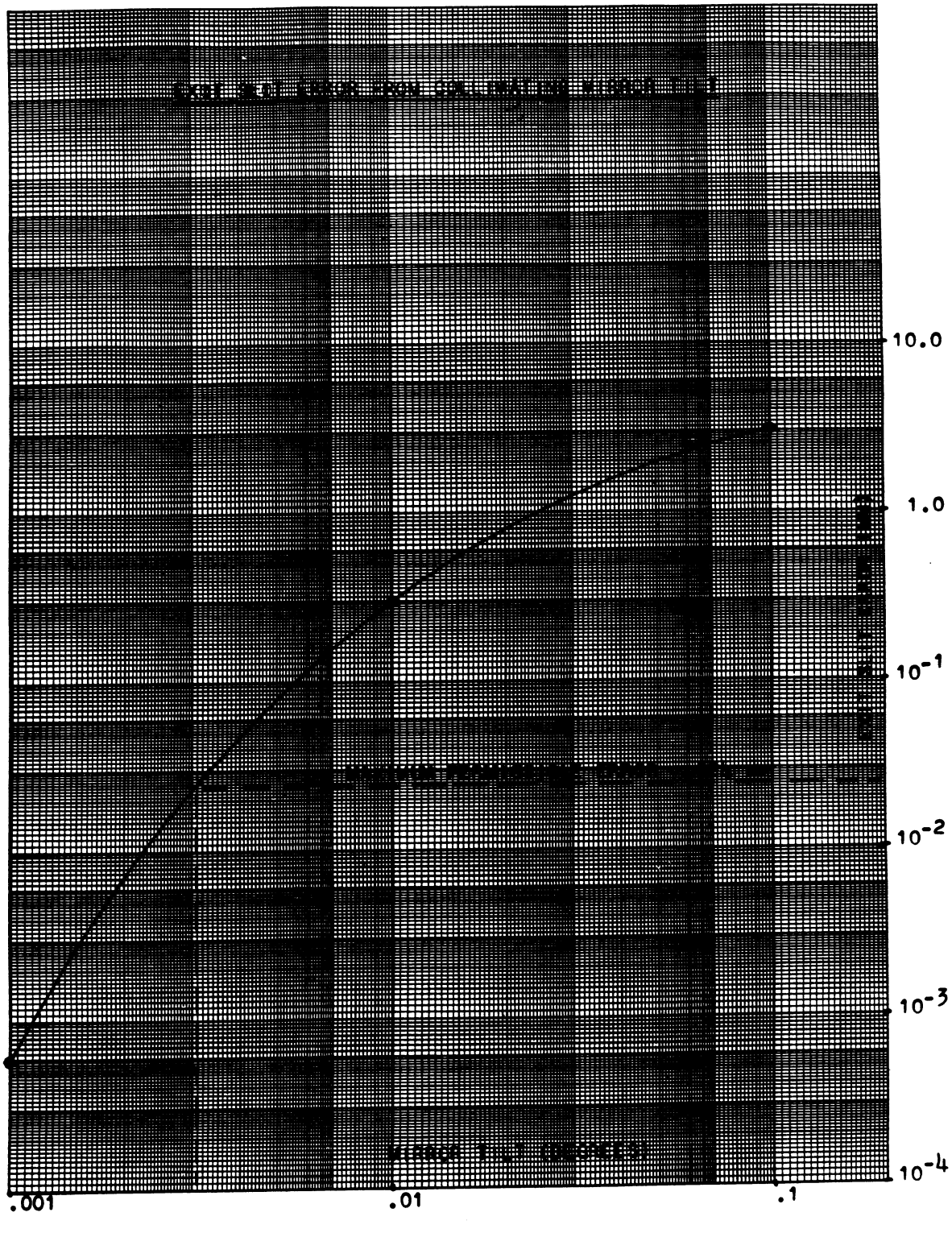

Figure 4-2. Exit Slit Error From Collimating Mirror Tilt

The geometry of the monochromator is shown in Figure 4-3.

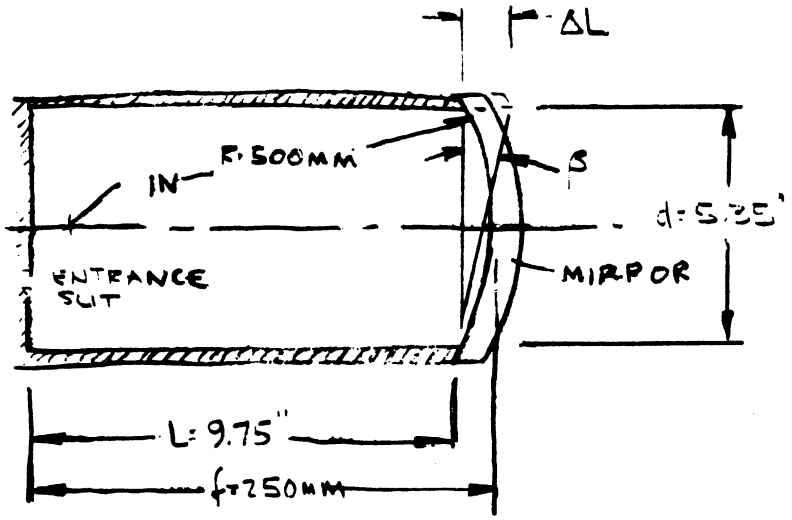

Figure 4-3. Monochromator

A temperature gradient (ΔT) from one mirror supporting wall to the other would tilt the mirrors due to thermal expansions. The increase in wall length is

$$\Delta L = \alpha L \Delta T$$

where α is the coefficient of expansion. For magnesium, $\alpha = 25.2 \times 10^{-6}$ per degree centigrade. The angular tilt of the mirror resulting from the increase in wall length is

$$\tan \beta = \frac{\Delta L}{d} ,$$

But for small angles, $\tan \beta \approx \beta$, so

$$\beta = \frac{\Delta L}{d}$$

With the permissible mirror tilt of 54.1×10^{-6} radians, the permissible length is:

$$\Delta L = \beta d = 5.35'' \ (54.1 \times 10^{-6}) = .00029''$$

Finally, the permissible temperature gradient is

$$\Delta T = \frac{\Delta L}{\alpha L} = \frac{.00029}{25.2(10^{-6})(9.75)}$$

$$= 1.18°C$$

Since this gradient was far less than the possible 10°C spacecraft gradient, a thermal design was established to limit the BUV internal gradient to a value less than 1°C.

4.2.3 Power Dissipation

In addition to the thermal environment, internal heat dissipation of the electronics was also considered in the BUV thermal design. Table 4-1 indicates the total power dissipated in the BUV and the heat transferred to the spacecraft. Figure 4-4 indicates the actual distribution of the heat within the instrument.

4.2.4 Thermal Design

To make the BUV optical requirements compatible with its thermal environment, the following method of passive thermal control was incorporated:

- Super-insulate the BUV's exposed bottom and top surfaces.
- Isolate the field defining cone and diffuser plate assembly from the BUV.

LOCATION	COMPONENT	DISSIPATION (MW)	TRANSFERRED TO S/C (MW)	NOTES
Bay #9 Internal to BUV Sensor	Motor, Cam Drive	306	306	Conducted & Radiated to Bay #9 (1074 mw)
	Motor, Diffuser	1	1	
	Motor, Monochromator	48	48	
	Motor, Photometer	49	49	
	Photomultipliers	512	512	
	Encoder	155	155	
	Lamp	3	3	
Bay #9 Electronics Attached to BUV Sensor	Lower Sensor Electronics	564	0	Radiated to Space
	Upper Sensor Electronics	694	694	Radiated to Inner Ring
	Electrometers	1501	0	Radiated to Space
	TOTALS - SENSOR BAY (#9)	≈3900	1768	
Bay #8 3/0 Module	3/0 Electronics Module	≈8100		
	TOTAL - BUV	12 watts ±.5 watts		

Table 4-1. Power Dissipation Average

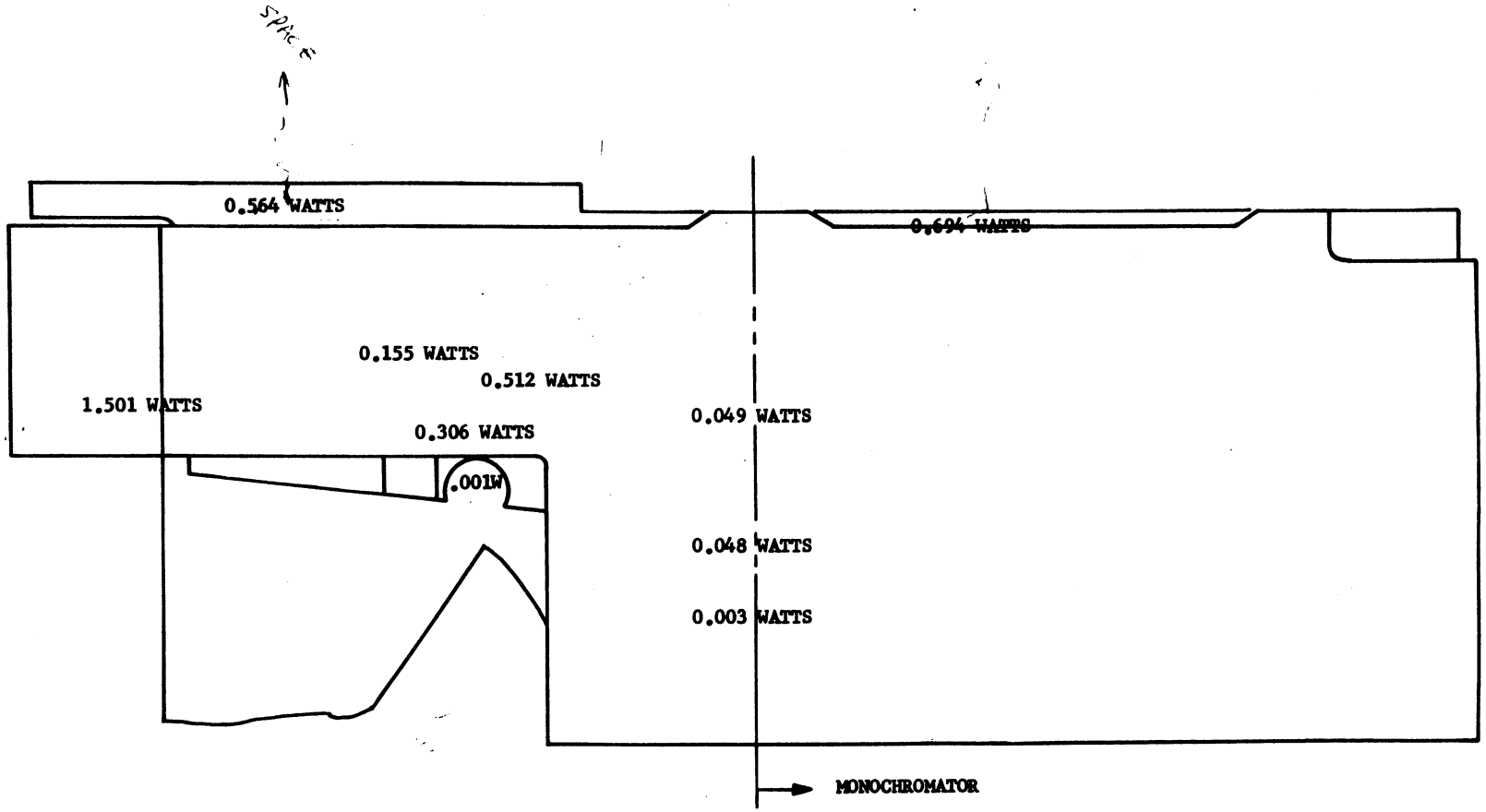

NOTE:
ELECTRONIC MODULE (3/0 MODULE)
DISSIPATION 7.8 WATTS

Figure 4-4. BUV Sensor Module Power Dissipation Distribution Diagram

- Isolate the electronics from the BUV, and radiate their power to space or to the spacecraft.
- Provide a high thermal resistance between the BUV and spacecraft.

This thermal design is represented in Figure 4-5 and indicated on the Beckman BUV/Interface drawing (Figure 4-1).

4.2.4.1 Super-Insulation

The need for super-insulation (SI) was substantiated early in the program by performing an energy balance on the BUV for two cases: one with SI and one without. When SI was not used, a painted surface with an emissivity of 0.85 and an absorbtivity of 0.3 was used. Both cases incorporated the other items mentioned above and also considered the internal heat dissipation. The peaks of the absorbed energy flux were truncated for both the day and night values to approximately account for the thermal capacitance of the BUV. Also, two conditions were considered for each case; the spacecraft at an isothermal temperature of 25°C and the spacecraft with a standing thermal gradient across the BUV of 10°C (35°C - 25°C = 10°C gradient). The results of this study were as follows:

Case	Spacecraft Condition	BUV Mean Temperature Day	Night
Super-Insulation (SI)	Isothermal	25.5°C	25.5°C
	10°C Gradient	30.5°C	30.5°C
No Insulation	Isothermal	20°C	17.8°C
	10°C Gradient	24°C	22°C

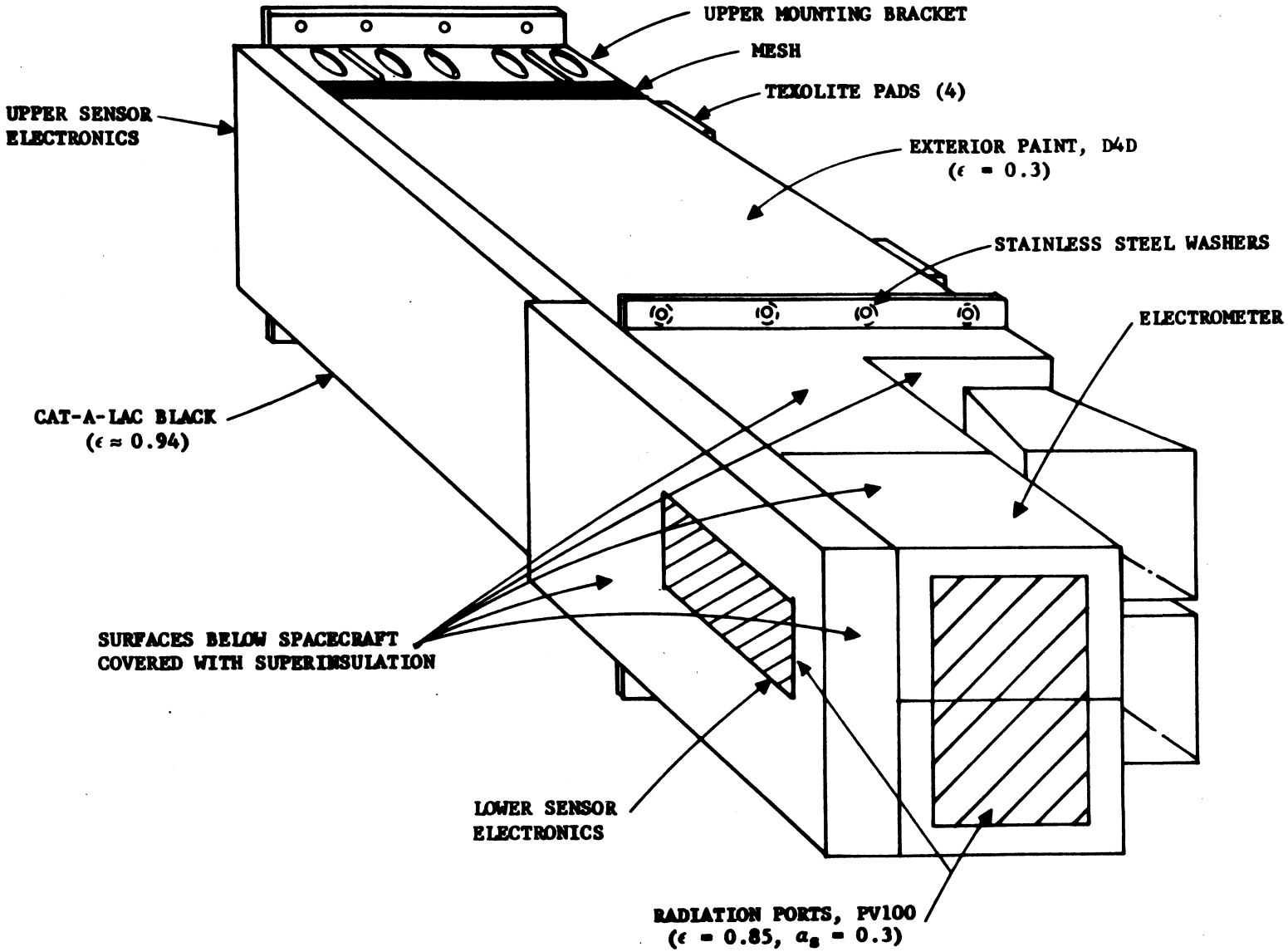

Figure 4-5. BUV Sensor Module Passive Thermal Control System

The results can be briefly summarized by stating that the BUV did not vary in temperature from day to night with SI as it did without the insulation. Since thermal gradients within the BUV had to be minimized, SI provided the best design.

Perhaps of more importance than the temperature variations was the heat transfer required for equilibrium in each case. By investigating more fully the energy equation for the SI case, it was realized that the only energy flowing through the BUV is the internal dissipation and the radiation absorbed through the entrance slit. To achieve equilibrium without the SI, however, energy had to flow from the spacecraft through the BUV. About 9 and 14 watts were required during the day and the night, respectively, with an isothermal spacecraft. The transfer of heat of this magnitude through the BUV would have created excessive internal temperature gradients.

4.2.4.2 Component Isolation

Isolation of the electronics and the field defining cone diffuser plate assembly reduced the thermal input to the BUV and eliminated sources of thermal gradients. The electronics, if not isolated, would have transferred energy into the BUV housing and produced thermal gradients. The upper sensor electronics would have produced a gradient from one side relative to the other. This gradient would have tilted the collimating mirrors as described in Paragraph 4.2.2.2, so isolation was absolutely necessary. The field defining cones contain multi-reflecting grooves to restrict stray light. Because of the multi-reflections, the cones approach black-body cavities. To eliminate temperature and thermal energy fluctuations which would have been induced into the BUV by the black-body cavities, thermal isolation of the cones was desirable.

With the electronics thermally isolated from the BUV, it was necessary to radiate the power dissipation. The electronics below the spacecraft radiated to space and earth, while the electronics within the spacecraft radiated directly to the spacecraft. This placed the following requirements upon the BUV:

- Provide a high emissivity surface on the upper sensor electronics to optimize radiation with the spacecraft (Cat-A-Lac Black, $\epsilon \approx 0.94$).
- Provide high emissivity-low solar absorptivity surfaces on the lower sensor electronics and electrometer (PV100, $\epsilon = 0.85$ $\alpha_s = 0.3$).

The spacecraft also provided the following:

- A high emissivity surface on the inner bay wall (Glyceryl Phthalate, $\epsilon = 0.83$).
- Radiation viewing ports for the electronics in the super-insulation.
- Elimination of the inner-bay-wall lightening holes to prohibit radiation with the SIRS and IDCS.

4.2.4.3 BUV/Spacecraft Thermal Interface

The susceptibility of BUV to thermal gradients required that the BUV Instrument mounting and thermal control deviate from the standard Nimbus methods. The standard Nimbus thermal control system could have imposed a 10° Centigrade (C) gradient across the instrument. Less than a 1°C gradient was acceptable across the BUV to maintain wavelength calibration as shown in Paragraph 4.2.2.2. To limit the BUV gradient, a scheme of partial thermal isolation was required.

The scheme used is graphically shown in Figure 4-6. The thermal isolation was defined by solving for the magnitude of the interface resistances required to limit the temperature drop across BUV to 1°C.

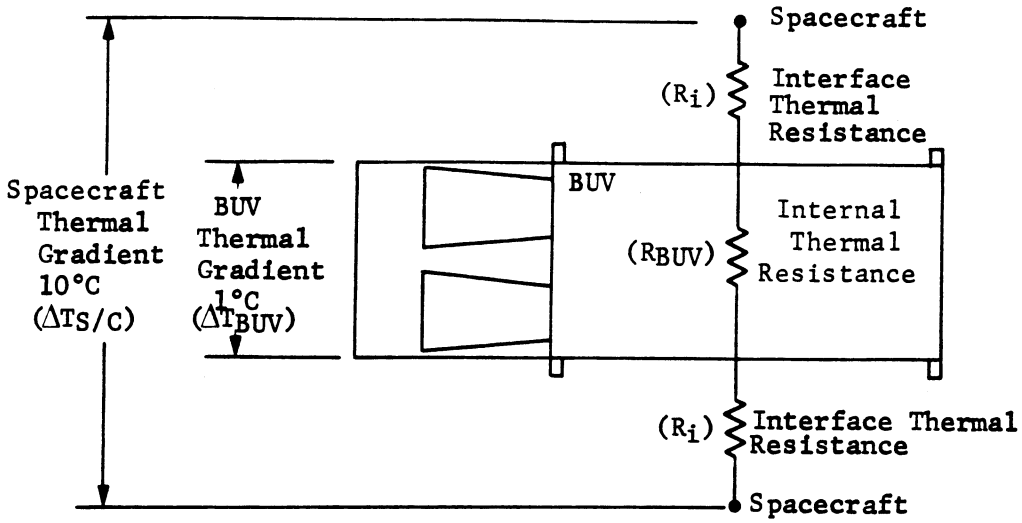

Figure 4-6. BUV Instrument Thermal Isolation Diagram

For steady-state equilibrium, the heat transferred (q) through the BUV must be equal to the heat transferred (q) through the total network as written in the following two equations:

$$q = \frac{\Delta T_{BUV}}{R_{BUV}} ; \qquad q = \frac{\Delta T_{Total}}{R_{Total}} = \frac{10°C}{2\ R_i + R_{BUV}}$$

Equating the two equations and solving for R yields:

$$R_i = 1/2 \left[10°C \frac{R_{BUV}}{\Delta T_{BUV}} - R_{BUV} \right]$$

This equation was solved to define the magnitude of interface resistance required to limit the temperature drop across the BUV. The internal resistance

of the BUV was determined to be 0.13°F HR/BTU. To restrict the gradient across BUV to the 1.18°C required for limitation of mirror tilt, an interface resistance of 0.475°F HR/BTU was found to be required by solving the above equation. This interface resistance consists of parallel radiation and conduction resistances and represents a minimum value required. Higher resistances, of course, would further limit the heat transferred through the network and further reduce the gradient across the BUV.

The physical accomplishment of the needed thermal interface resistance imposed requirements on both the BUV and the spacecraft. The BUV requirements were the following:

- Reduce conduction contact area between the lower mounting flange and the spacecraft by using stainless steel washers.
- Reduce conduction contact with the spacecraft thermal control surface by using four small Textolite pads.
- Increase conduction resistance of the upper mounting bracket with the use of monel mesh and lightening holes in the magnesium brackets.
- Minimize radiation to the spacecraft by painting the BUV exterior walls with a low emissivity paint (D4D).

The spacecraft requirements were the following:

- Minimize radiation with the optical portion of the sensor by finishing the bay walls, except the inner wall, with Alodine 600 ($\epsilon \approx .15$).
- Locally modify the spacecraft to accept the point loads produced by the Textolite pads.

- Remove the holes in the thermal control surface and cover it with super-insulation to eliminate solar flux and space viewing.

4.2.4 Thermal Analysis

In addition to the first order analysis performed during the establishment of the thermal design, Beckman performed a multi-nodal computer thermal analysis on the BUV. This analysis considered the BUV as 276 discrete isothermal nodes which were inter-connected by 332 conduction, 73 joint, and 61 radiation resistances.

Figures 4-7, 4-8, 4-9, and 4-10 show the mean temperature distribution (in degrees Rankine, R) in the housing, diffuser plates, field defining horn, and electronics. This temperature distribution was based upon the following assumptions:

- Steady state solution
- 10°C spacecraft gradient (546°R to 528°R)
- Average electronic power dissipation per Paragraph 4.2.3
- Averaged solar and albedo flux
- Thermal design as defined in Paragraph 4.2.4

This temperature distribution was evaluated to determine the angular shift of the collimating mirrors and the resultant wavelength shift (Paragraph 4.2.2.2). The results indicate that a shift of 0.1Å will occur. Since this was only one-half the allowable wavelength shift, the adequacy of the thermal design was verified.

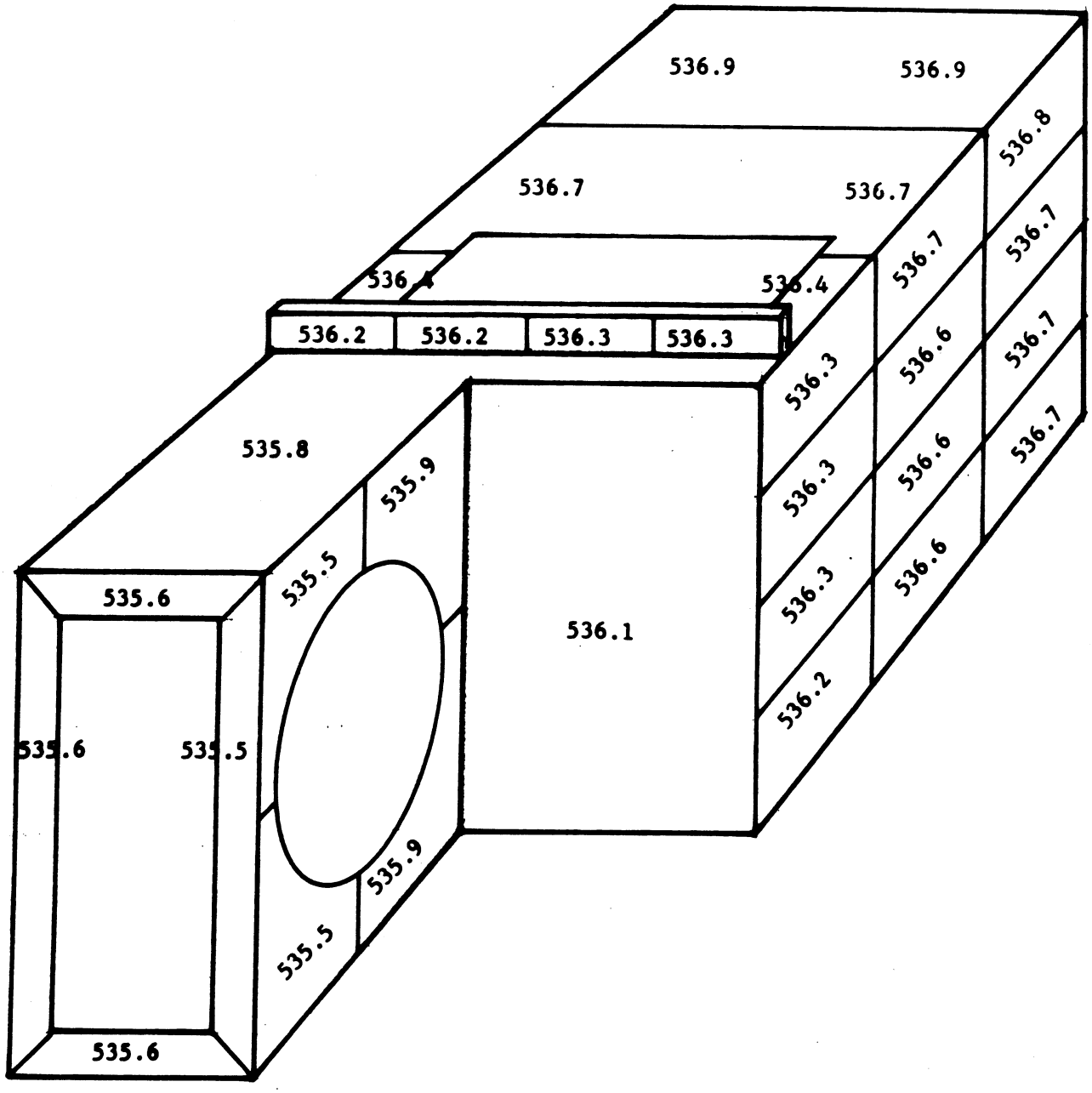

Figure 4-7. Temperature Distribution (°R) BUV Housing (1 of 2)

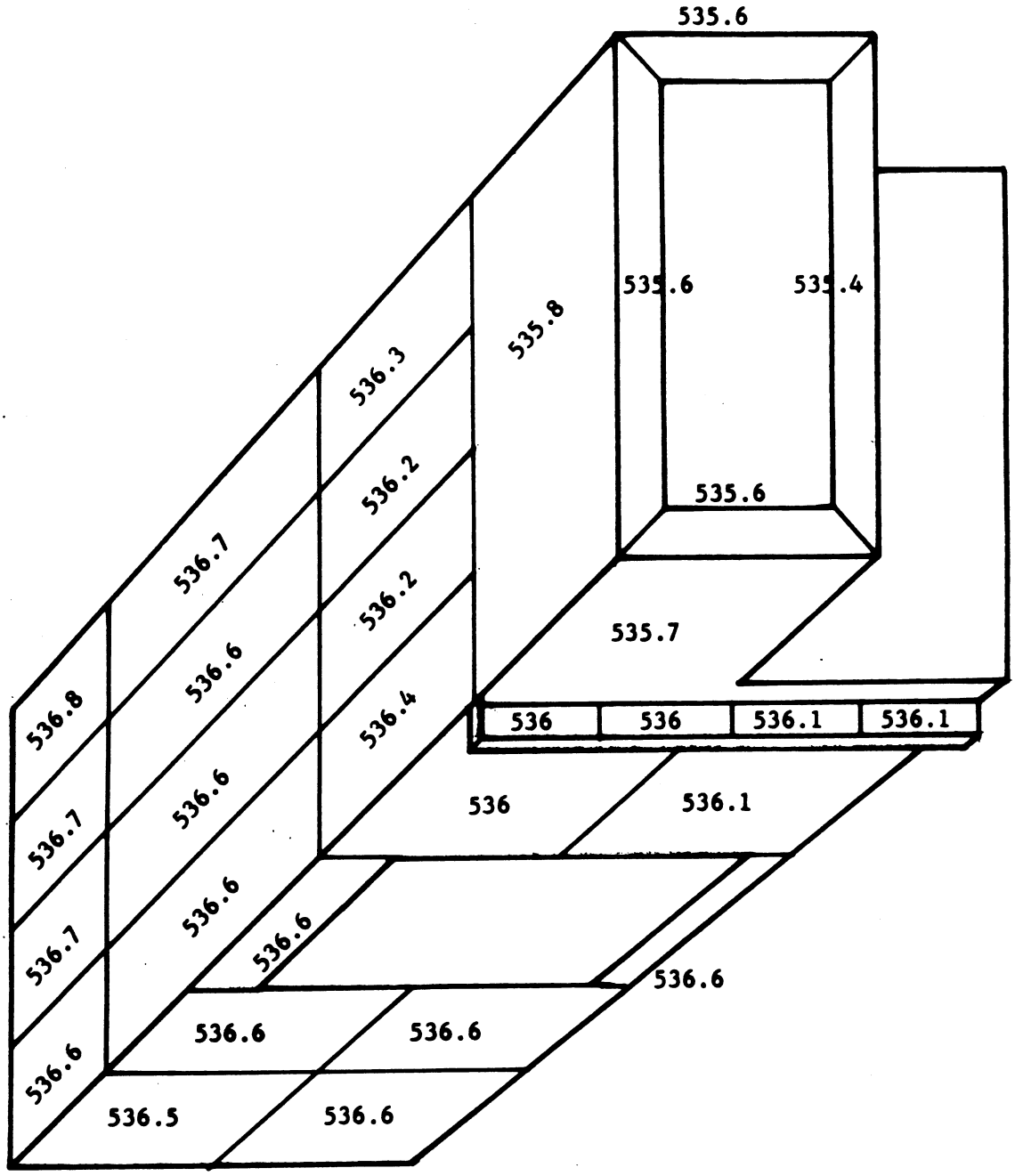

Figure 4-8. Temperature Distribution (°R) BUV Housing (2 of 2)

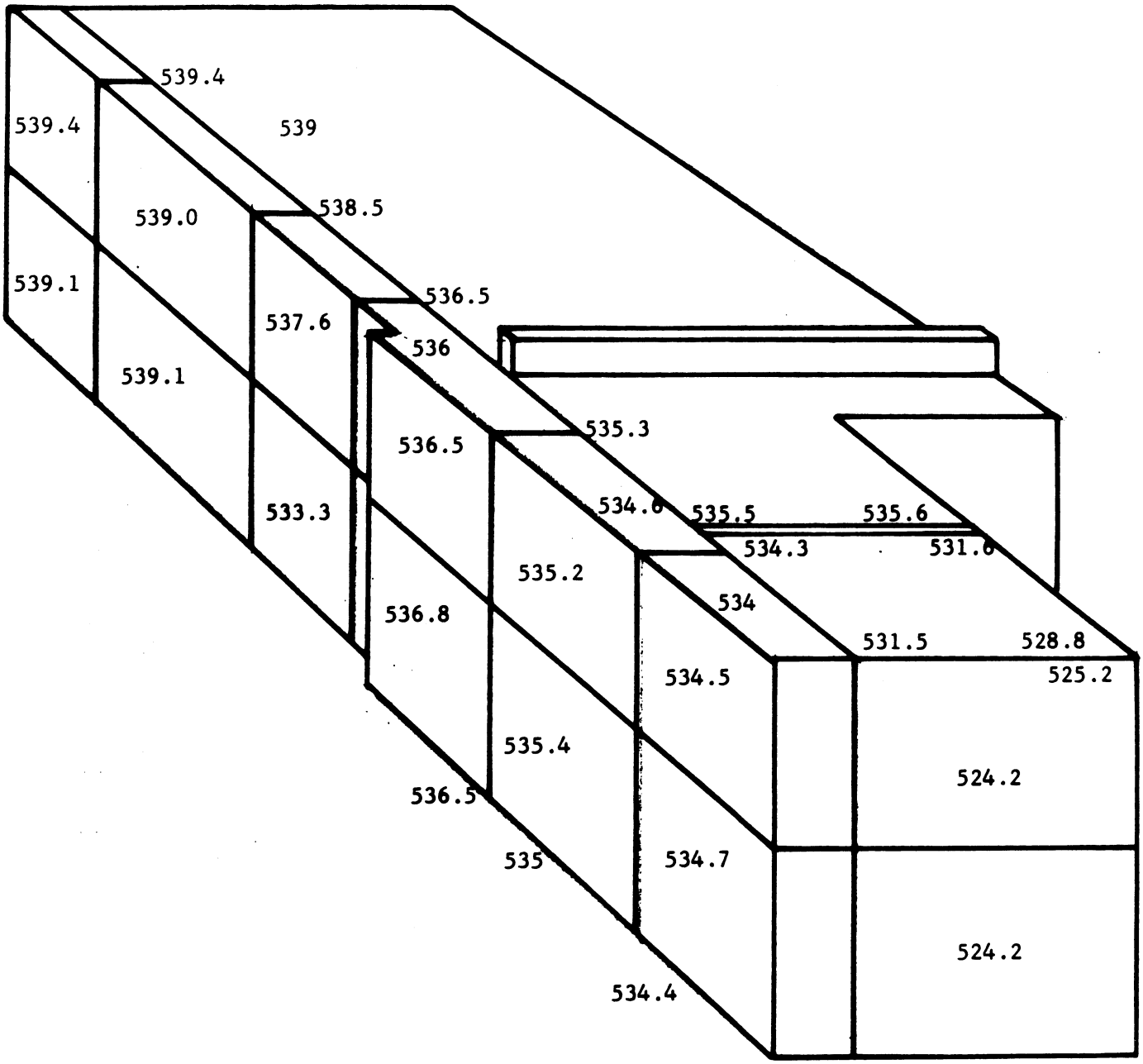

Figure 4-9. Temperature Distribution (°F) Electronics

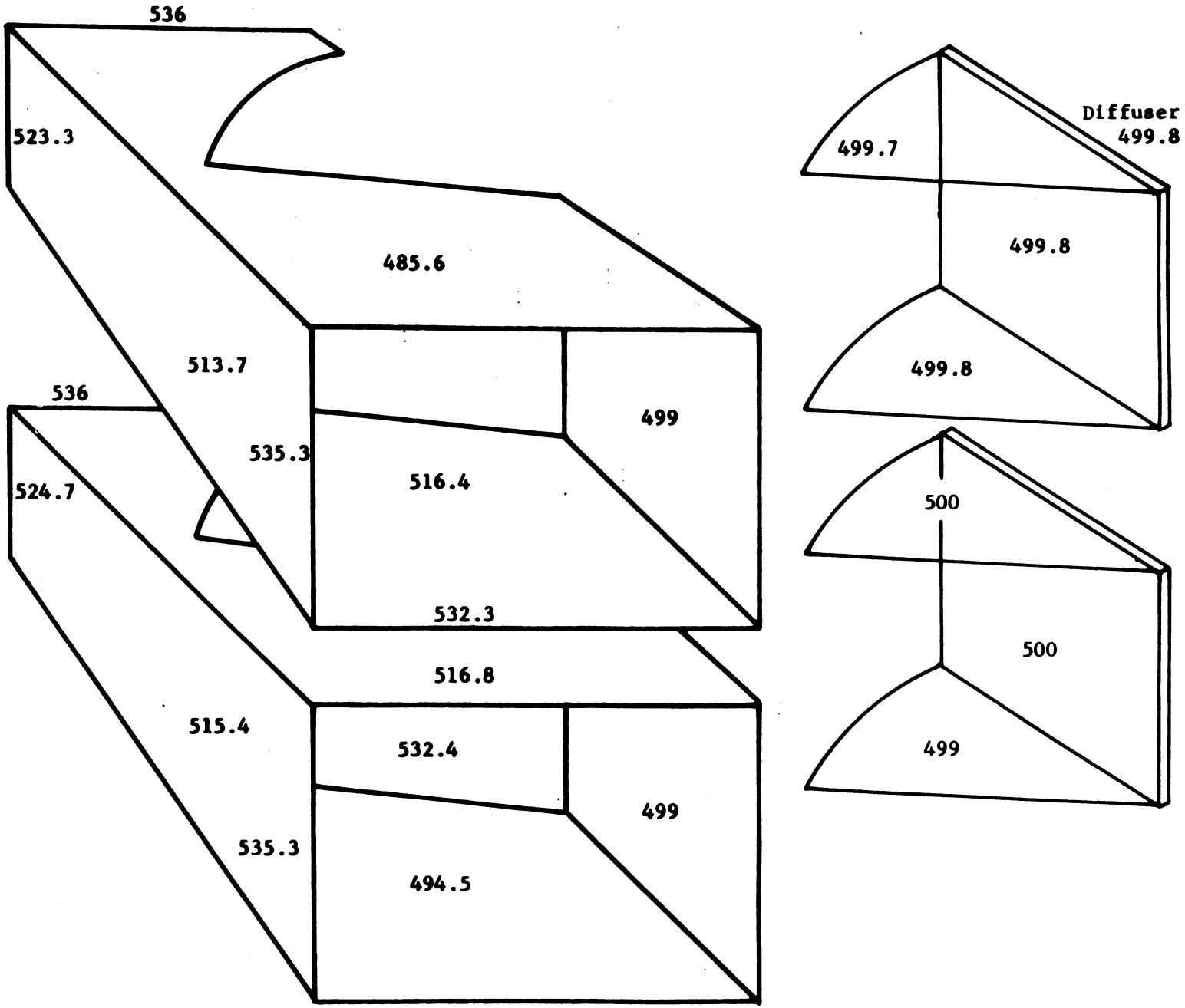

Figure 4-10. Temperature Distribution (°R) Field Defining Horns and Diffusers

4.2.5 Testing

During design verification testing of the BUV, the instrument was subjected to laboratory and thermal vacuum testing to verify the thermal design. During these conditions, the instrument maintained an acceptable temperature distribution, and under no condition was a significant wavelength shift experienced due to thermal gradients.

4.3 MATERIAL SELECTION

Much attention was given to the selection of materials to conform to a proven and approved selection; the only serious problem encountered was with the choice of Bearing Lubricant (Paragraph 4.4.10). Solutions to material problems such as the hard facing of the wavelength cam are described in the individual paragraphs.

4.4 MECHANISM DESCRIPTION AND ANALYSIS

4.4.1 Housing

The main Sensor Housing for the P103 and F104 instruments is cast out of E233 Magnesium. Precise machining was required to accommodate the numerous intricate mechanisms and subassemblies.

The choice of magnesium was made after extensive evaluation and comparison with aluminum. The weight saving, together with the damping quality of magnesium, prevented major problems with the mechanisms during vibration testing. An added advantage was the ability to apply a dark, almost black, finish to all magnesium components without the need for paint. The coating used is a Dow No. 9 anodize finish and has the advantage of not producing a significant buildup which could affect dimensional precision.

4.4.2 Stress Analysis

A complete analysis of the most highly stressed areas in the BUV casting was performed. Conditions considered included static loads due to mounting clamps and dynamic loads due to g-levels reached during sinusoidal and random vibration.

Beckman's design goal was to design the casting such that stresses would be below 10 percent of the actual yield strength of the casting material. This assured long-term stability of optical alignment by reducing the possibility of creepage. The analysis which follows shows that the most highly stressed areas are below 10 percent of the yield strength.

4.4.2.1 Static Loading Analysis of Mounting Clamps

The BUV Instrument is retained in the bay by eight No. 8 screws preloaded to 20 in.-lbs. A clamping force of 144 ±72 lbs is applied on each of four pads to hold the Instrument against the thermal control surface. This mounting arrangement is shown in Figure 4-11.

F_p = Preload of Mounting Screws

F_c = Clamping Force

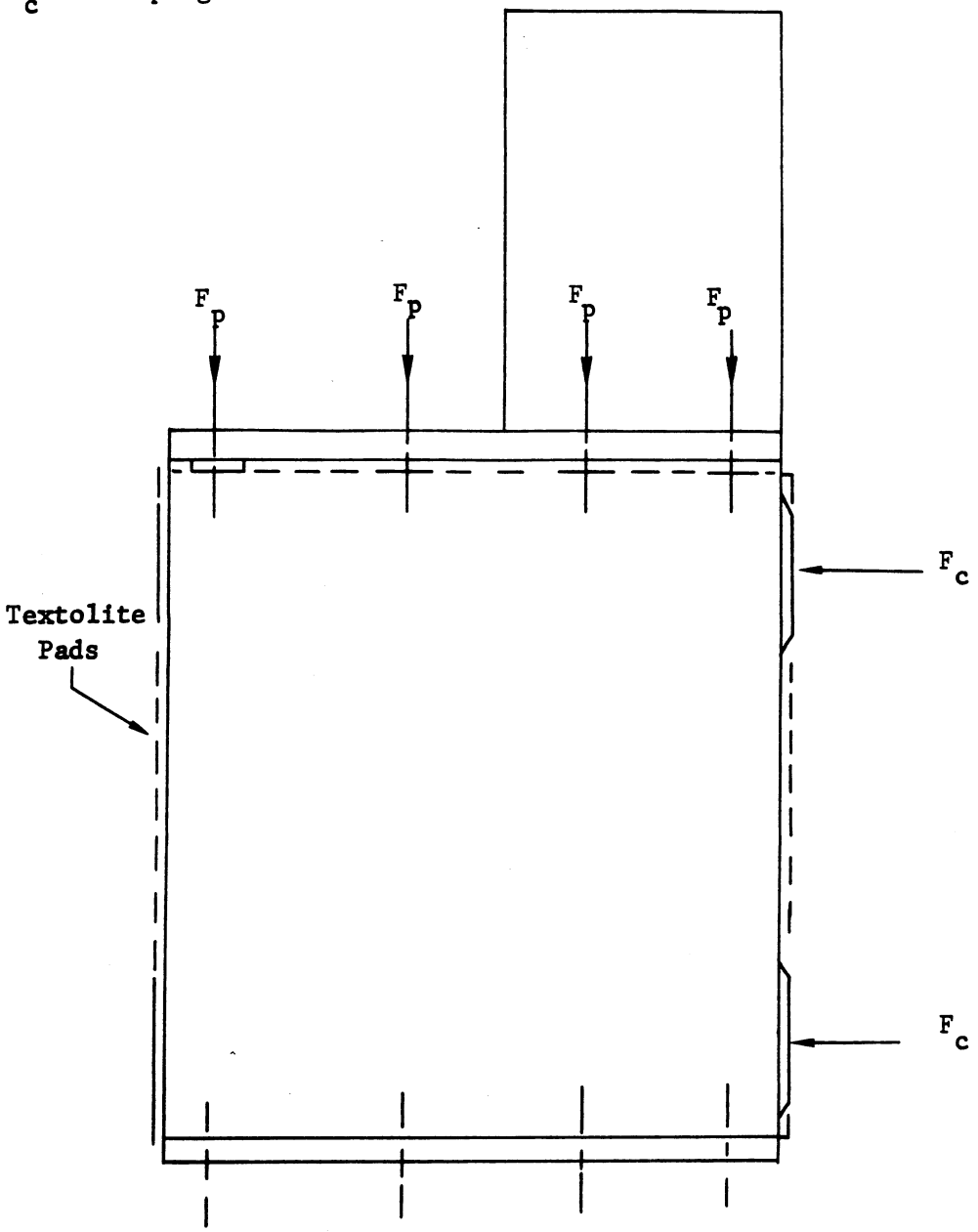

Figure 4-11. Mounting Arrangement Diagram

A. Bearing Load (Figure 4-12)

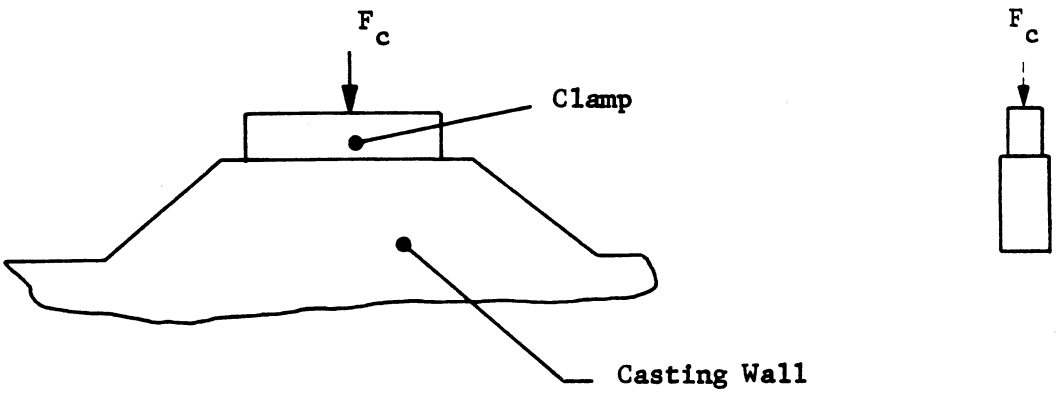

Figure 4-12. Bearing Load Diagram

A bearing load exists at the clamping pad due to the concentrated area of the clamp. The bearing stress due to this load is, therefore:

$$\sigma_B = F_c/A$$

$$\sigma_B = \frac{216 \text{ lbs.}}{0.1115 \text{in.}^2}$$

$$\sigma_B = 1936 \text{ psi}$$

$F_c = 144 \pm 72$ lbs.

A = Clamping Area

= 0.18in. x 0.62in.

The bearing strength of EZ33A is:

$$\sigma_{By}(\text{yield}) = 40{,}000 \text{ psi}^{(1)}$$

$$\sigma_{Bu}(\text{ultimate}) = 57{,}000 \text{ psi}$$

It was previously decided by Beckman to maintain the BUV Instrument's stress level below one-tenth the materials yield strength. To maintain the stress below $0.1\sigma_{By}$ requires that the stress level be below 4,000 psi. The factor of safety for this loading case is then:

$$F.S. = \frac{0.1\sigma_{By}}{\sigma_B} = \frac{4000}{1936} = 2.1$$

B. Housing Stresses

The clamping force is distributed through the full length of the casting wall directly under the clamping area. The configuration for the casting wall directly under the clamps is not the same for the upper and lower mounting clamps. The cross-sectional loading area for each case is shown in Figure 4-13. and 4-14. The loading case for the lower clamps is a column consisting of the

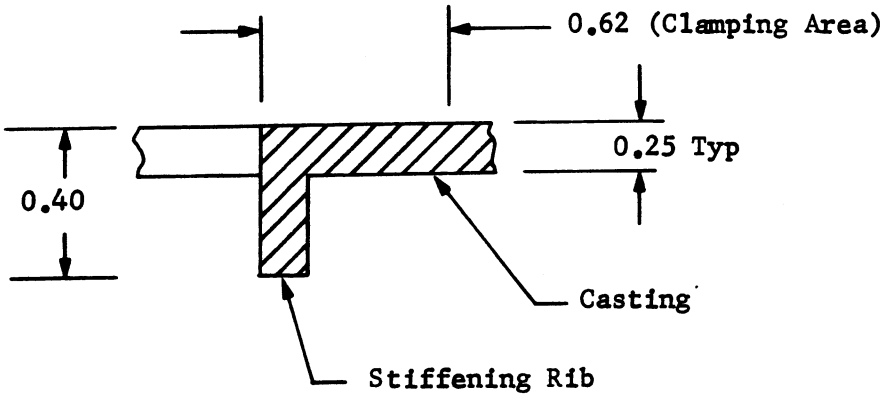

Figure 4-13. Column Area For Lower Clamps

(1) Dow Chemical Corporation, Physical Properties of Magnesium Casting Alloys, Table II.

casting wall and a stiffening rib. Interference with the optical path prevented the use of a stiffening rib at the upper clamps so the loading case is a column consisting of the casting wall which is built up in the area of the clamps.

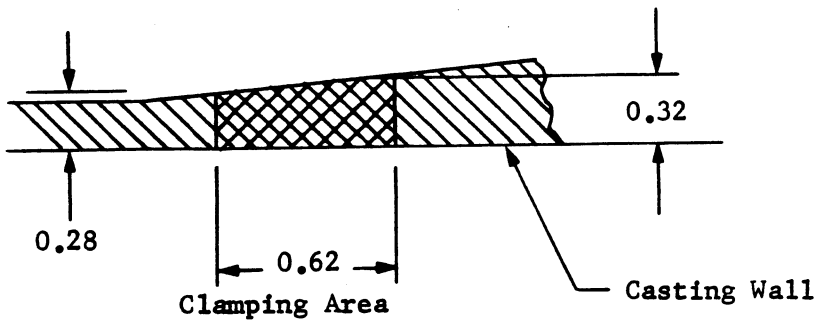

Figure 4-14. Column Area For Upper Clamps

The compressive stress in the casting due to the lower clamps (Figure 4-13) is then:

$$\sigma_c = \frac{F_c}{A} = \frac{216 \text{ in.}}{(177\text{in.})(0.25\text{in.})} = 1{,}123 \text{ psi}$$

The compressive stress in the casting due to the upper clamps (Figure 4-14) is:

$$A = (0.28)(0.62) + 1/2(0.04)(0.62)$$
$$A = 0.1858 \text{ in.}^2$$

$$\sigma_c = \frac{216 \text{ lbs.}}{0.1858\text{in.}^2}$$

$$\sigma_c = 1163 \text{ psi}$$

The compressive stress of EZ33A is:

$$\sigma_{cy} = 14{,}000 \text{ psi}^{(2)}$$

(2) MIL Handbook - 5A Metallic Materials & Elements for Aerospace Vehicle Structures

The minimum factor of safety for this criteria is then:

$$F.S. = \frac{0.1\sigma_{cy}}{\sigma_c} = \frac{1400 \text{ psi}}{1163 \text{ psi}} = 1.2$$

4.4.2.2 Dynamic Load Analysis of Mounting Clamps

The Instrument will be subjected to vibration under the following conditions:

Sinusoidal	Thrust Axis (g)	Transverse Axis (g)
5 - 200cps	15	10
100 - 2000cps	10	10

Random	Frequency (cps)	Spectral Density g^2/cps	g - rms
Thrust Axis	20 - 2000	0.2	20
Transverse Axis	20 - 2000	0.2	20

These acceleration levels will impose an additional load on the casting wall in the vicinity of the clamps. Neglecting the affect of the 8 mounting screws on the lower flange and assuming the loads are equally distributed among the clamps, the column force previously considered becomes:

$$F_c' = F_c + \frac{mgQ}{N}$$

where F_c = clamping force = 216 lbs. (max)

m = mass of the casting

g = acceleration level

Q = transmissibility factor

N = number of clamps = 4

The transmissibility factor for random vibration is assumed to be 3, since for a Gaussian distribution the probability that the instantaneous acceleration

will exceed three times the rms acceleration is only about 0.003[3]. A transmissibility factor of 6 is assumed for sinusoidal vibration, since this was the maximum Q-factor obtained from the breadboard vibration test.

$$F_c' = 216 \text{ lbs} + \frac{(31.41\text{lbs})(20g)(3)}{4}$$

$$F_c' = 216 \text{ lbs} + 472 \text{ lbs} = 688 \text{ lbs.}$$

From this it would appear that the g-force acting on the housing exceeds the preload force thereby increasing the compressive stress to:

$$\sigma_c' = \frac{688 \text{ lbs.}}{(0.77\text{in.})(0.25\text{in.})} = 3{,}580 \text{ psi}$$

$$\sigma_c' = 3{,}580$$

Although this loading case yields an acceptable level of stress from the standpoint of material strength it is overly conservative since no consideration was given to the frictional resistance of the bolts on the lower mounting flange which retain the BUV Instrument in the bay. Referring back to Figure 4-11, a preload force F_p is shown on each of eight bolts. A more detailed illustration of the mounting configuration is shown in Figure 4-15.

$$F_p = \frac{T}{Kd} \quad (4)$$

where: T = tightening Torque, in.-lb.

K = torque coefficient

= 0.22 for No. 8

D = major dia. of screw

(3) Wirsching, P.H., Random Vibrations, Product Engineering, Vol.22, p.108,1964.

(4) Shigley, J. E., Mechanical Engineering Design, p. 246

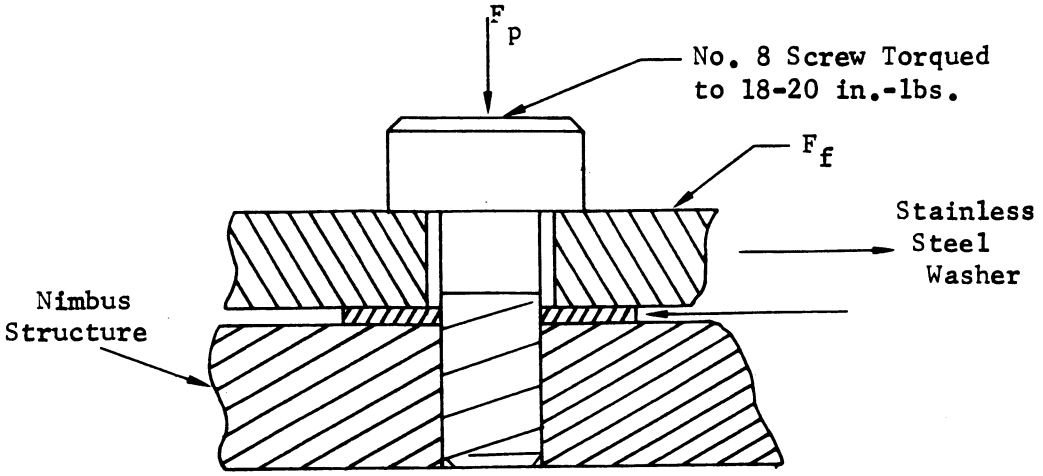

Figure 4-15. Mounting Configuration Diagram

Including the frictional resistance of the mounting bolts, the force against the clamping area becomes:

$$F_c' = F_c + \frac{mgQ}{N} - 8F_f$$

$$F_f = \mu F_p \qquad \text{assume } \mu = 0.1$$

$$F_c' = 216 \text{ lbs.} + 472 \text{ lbs.} - 8(0.1)(544 \text{ lbs.})$$

$$F_c' = 252 \text{ lbs.}$$

The increase in clamping force due to the g-force acting on the housing is only 36 lbs and increases the stress level to:

$$c = \frac{252 \text{ lbs.}}{0.308 \text{in}^2} = 818 \text{ psi}$$

For this criteria the factor of safety becomes:

$$F.S. = \frac{0.1 \text{ cy}}{0.308 \text{in.}^2} = \frac{1400}{818} = 1.7$$

4.4.2.3 Stress in Mounting Flange (Figure 4-16)

A. Bending Stress

The maximum clearance between the casting wall and the Nimbus bay mounting surface is:[5]

$$S_{max} = \frac{6.042 - 5.992}{2} = \frac{0.050}{2}$$

If the dimensions of the upper mounting bracket and the insulation separator are controlled, the maximum possible deflection will be 0.005 inch.

If the upper end of the casting is permitted to deflect to S_{max}, the maximum possible bending moment would be exerted on the lower mounting flange (Figure 4-17).

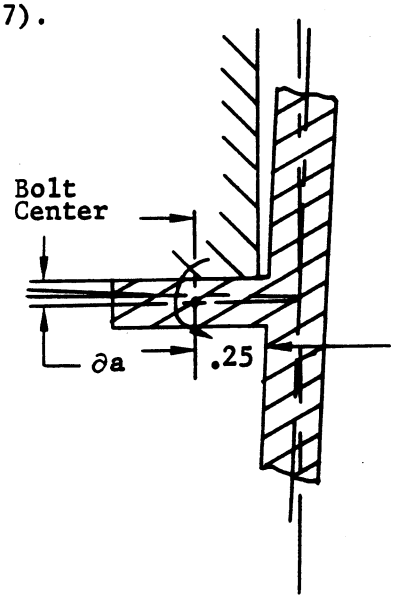

Figure 4-17. Lower Mounting

$$\partial_a = \frac{.25(0.005)}{11} = 11.4 \times 10^{-5} \text{ in.}$$

Bending Stress:

$$\sigma_B = \frac{MC}{I}$$

M = Bending moment, in-lb

C = Distance to extreme

I = Moment of inertia of cross section

$$\sigma_B = \frac{M\ell^2}{2EI}$$ (6)

(5) Nimbus Handbook for Experimenters, Figure 13,

(6) Timoshenko, Elements of Strength of Materials, P. 212.

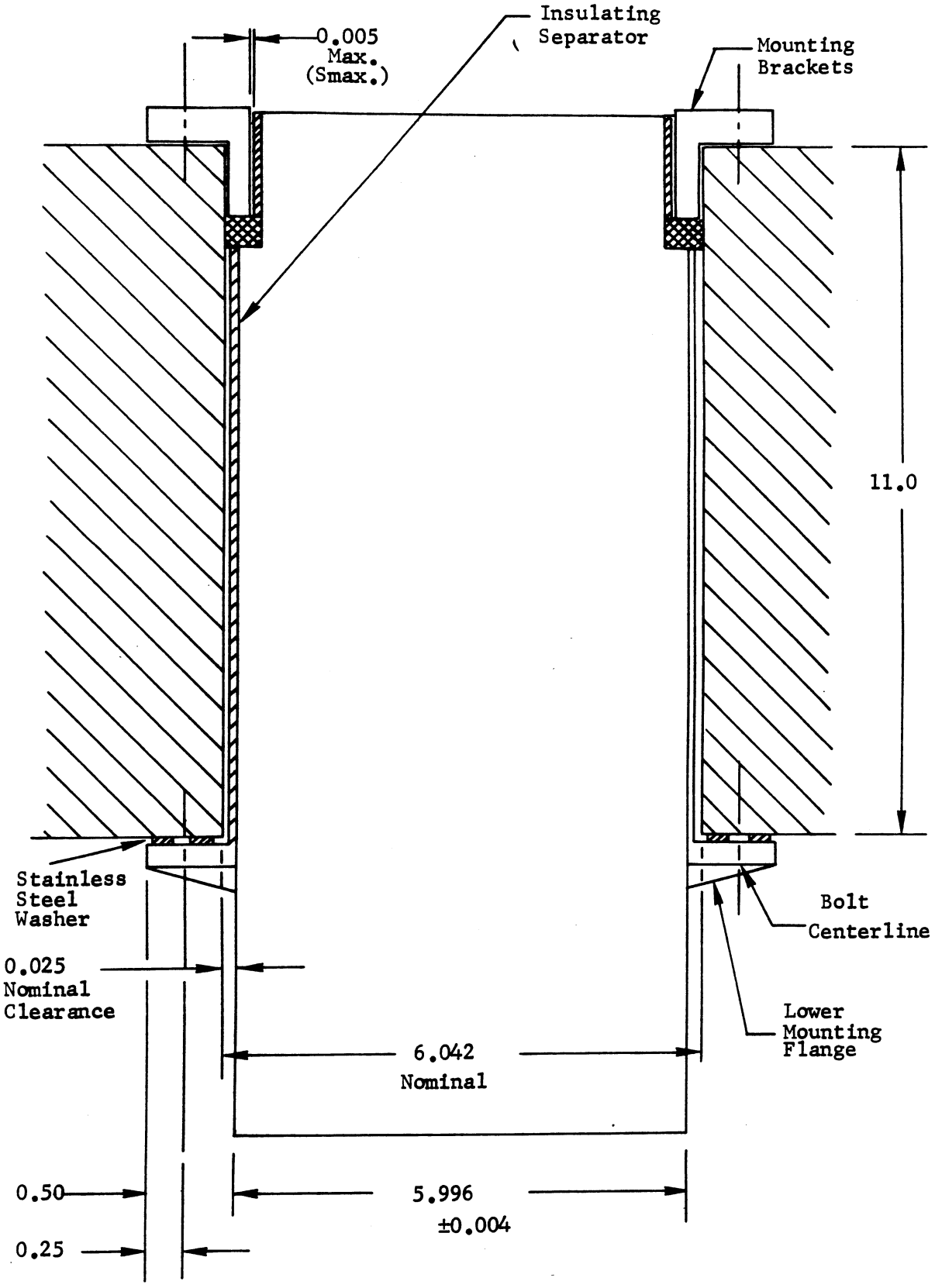

Figure 4-16. Configuration Mounting Diagram

$$M = \frac{2EI\ \partial a}{\ell^2}$$

$$\sigma_B = \frac{MC}{I} = \left(\frac{2EI\ \partial a}{\ell^2}\right)\ \frac{C}{I}$$

$$\sigma_B = \frac{2E\ \partial aC}{\ell^2}$$

$$\sigma_B = \frac{2(6.5 \times 10^6\ \text{psi})(0.00008\ \text{in.})(0.125\ \text{in.})}{(0.25\ \text{in.})}$$

$$\sigma_B = 229\ \text{lb/in2}$$

The factor of safety for this criteria [7] is:

$$\text{F.S.} = \frac{0.1\ \text{By}}{\sigma_B} = \frac{0.1(40{,}000\ \text{psi})}{229} = 17.5$$

B. Shear Stress in Lower Mounting Flange

$$\sigma\text{shear} = \frac{F}{2A}$$

$$F = 31.4\ \text{lbm}\ (60g) = 1883\ \text{lbs.}$$

$$A = 0.25\ \text{in}\ (8\text{in.}) = 2\ \text{in}^2$$

$$\sigma\text{shear} = \frac{1883\ \text{lb}_f}{2(2\text{in}^2)} = 472\ \text{lb/in}^2$$

$$\sigma\text{shear} = 472\ \text{psi}$$

where: F = External force from g-loading

A = Area of one flange

---

(7) Dow Chemical Corp., Properties of Magnesium Alloy Castings.

4.4.2.4 Stress in Bolts which Hold the Instrument in the Bay

A. Loading Case 1.

Bolts are preloaded and acted upon by external force due to g-load.

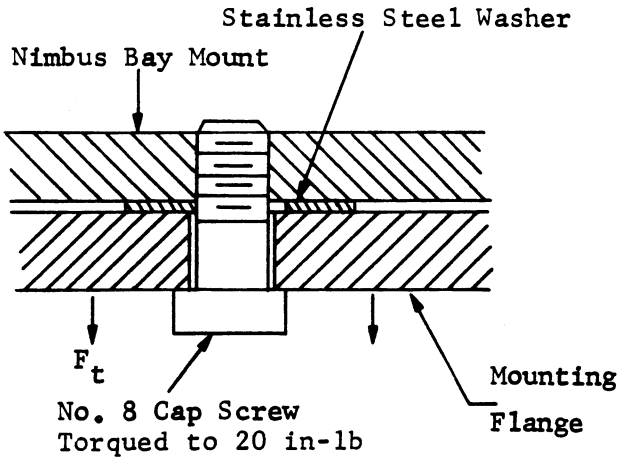

Figure 4-18. Stress on Attaching bolt

1. Determine Resultant Load on Cap Screw

Definition of terms:

F = Resultant tensile load on cap screw

Ft = Total external load on bolted assembly

Fi = Initial preload on bolt due only to tightening

Fb = Portion of Ft taken by bolt

Fm = Portion of Ft taken by connected members

k = Stiffness constant of each member

$$k = F/\partial = \frac{AE}{\ell} \text{ (Hookes Law)}$$

2. Total External Load

M = Mass of instrument

g = Design acceleration under random vibration

$$g = 3(20\ g\ R.M.S.) = 60\ g$$

$$Ft = \frac{(31.4\ lb\ m.)\ (60\ g)}{8\ (screws)}$$

$$Ft = 235\ lb_f$$

3. Initial Preload

$$T = K\ Fi\ d^{(8)}$$

$$Fi = \frac{T}{Kd} = \frac{20\ in.\ lbs.}{(0.22)(0.164\ in.)}$$

$$Fi = 544\ lb_f$$

where:

K = Torque Coef. = 0.22 (No. 8 screw)

d = Major Diameter of screw

T = Tightening torque

As external load is applied, deformation of bolt increases while the deformation of members decreases.

$\Delta\partial b = \Delta\partial m$

$\Delta\partial b = Fb/kb$

$\Delta\partial m = Fm/km$

∂b = Deformation of bolt

∂m = Deformation of members

---

(8) Shigley, Mech. Engr. Design, p. 246.

$$km = kw + kf$$

where: kw = Stiffness constant of bolt

kf = Stiffness constant of washer

$$\frac{Fm}{km} = \frac{Fb}{kb}$$

(or)

$$\frac{Fm}{kw + Kf} = \frac{Fb}{kb}; \qquad Fb = \frac{kb\ Fm}{Kw + kF}$$

Since $Ft = Fb + Fm$

$$Fb = \frac{kb\ (Ft - Fb)}{kw + kf} = \frac{Ft\ kb}{kw + kf + kb}$$

4. Resultant Load on Bolt

$$F = Fb + Fi$$

$$F = \frac{Ft\ Kb}{kn + kf + kb} + Fi$$

(Screw)

$$kb = \frac{AbEb}{\ell b}$$

$$kb = \frac{(0.0104\ in^2)(30 \times 10^6\ psi)}{(0.29\ in.)}$$

$$kb = 1.077 \times 10^6\ \frac{lb}{in}$$

A = Area of member in compression or tension

E = Modulus of elasticity of screw

ℓ = Height of member in compression or tension

(Washer)

$$kw = \frac{Aw\ Ew}{n}$$

$$Aw = 0.1727\ in^2$$

$$w = 0.030$$

$$kw = \frac{0.173\ in^2\ (30 \times 10^6\ psi)}{(0.030\ in.)}$$

$$kw = 173 \times 10^6\ lb/in$$

(Flange) $kf = \frac{AfEf}{f}$

Af = Same area as washer

$Ef = 6.5 \times 10^6$ psi

$f = 0.25$ in

$$kf = \frac{(0.1727 \text{ in}^2)\ (6.5 \times 10^6 \text{ psi})}{(0.25 \text{ in})}$$

$kf = 4.48 \times 10^6$ psi

(Screw) $$Fb = \frac{Ftkw}{kw + kf + kb} = \frac{(195.2 \text{ lbs})\ (1.077)}{(173 + 4.48 + 1.077)}$$

$Fb = 1.177$ lbs

$F = Fb + Fi$ (Resultant tensile load on screw)

$F = 1.18\ lb_f + 544\ lb_f$

$F = 545\ lb_f$

5. Conclusion

The preload is the only significant tensile force acting on the screws for this loading case and is well below the allowable tensile strength for a No. 8 cap screw (1120 lbs min.)[9]. Safety factor = 1.97.

B. Loading Case 2

Bolts put in tension due to deflection of upper end of housing

1. During vibration it is possible for the upper end of the housing to deflect 0.005 maximum (Figure 4-19). This will cause a tensile force to act on the bolts in one of the flanges.

---

[9] Military Standard MS 16995

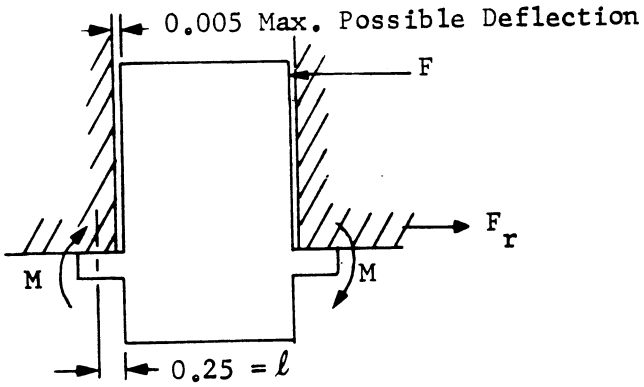

Figure 4-19. Possible Deflection Due to Vibration

The stress in the mounting flange was examined and the bending moment at the screw location was:

$$M = \frac{2EI\,\partial a}{\ell^2} \quad (10)$$

If F = Tensile load on screw:

$$M = 4p\ell \text{ (4 screws)}$$

$$P = \frac{M}{4\ell} = \frac{2EI\,\partial a}{4\ell^3}$$

$$I = \frac{bh^3}{12} = \frac{8(0.25)^3}{12}$$

$$I = 0.01041 \text{ in}^3$$

$$P = \frac{2(6.5 \times 10^6 \text{ psi})(0.01041 \text{ in}^3)(0.00014 \text{ in})}{4(0.25 \text{ in})^3}$$

$$P = 303 \text{ lb}_f$$

(10) Timoshenko, Elements of Strength of Materials, p. 212

2. Conclusion

The tensile load due to deflection of the upper end of the housing does not exceed the preload on the screws (544) so no additional load has been added to the screws.

4.4.2.5 Vibration Analysis of Lower End of Casting

The lower end of the casting contains the photomultiplier tubes, cam, and the cam bearing insert. The electrometers are attached to the end of the extension. Because the extension is essentially represented by a cantilevered beam loaded by these components, it is important that the approximate resonant frequency, deflection, and stress level induced in the casting be determined.

Figure 4-20 illustrates the condition being considered, and Table 4-2 lists the major components loading the extension and their location from the mounting flange.

Deflection	Component	Weight (lbs.)	Distance, Z (inches)
y_1	Cam & Motor	0.55	2.74
y_2	Photomultiplier, Tubes, Mnts, & Shields (2)	2.75	3.25
y_3	Electrometer Extension	1.50	7.62
y_4	Cam Bearing Insert	0.42	2.74
y_5	Weight of Lower End of Casting	1.60	Distributed

Table 4-2. Major Components Loading the Lower End Casting Extension

The natural frequency[11] is found by:

(11) Freberg and Kemler, Elements of Mechanical Vibrations, p. 28.

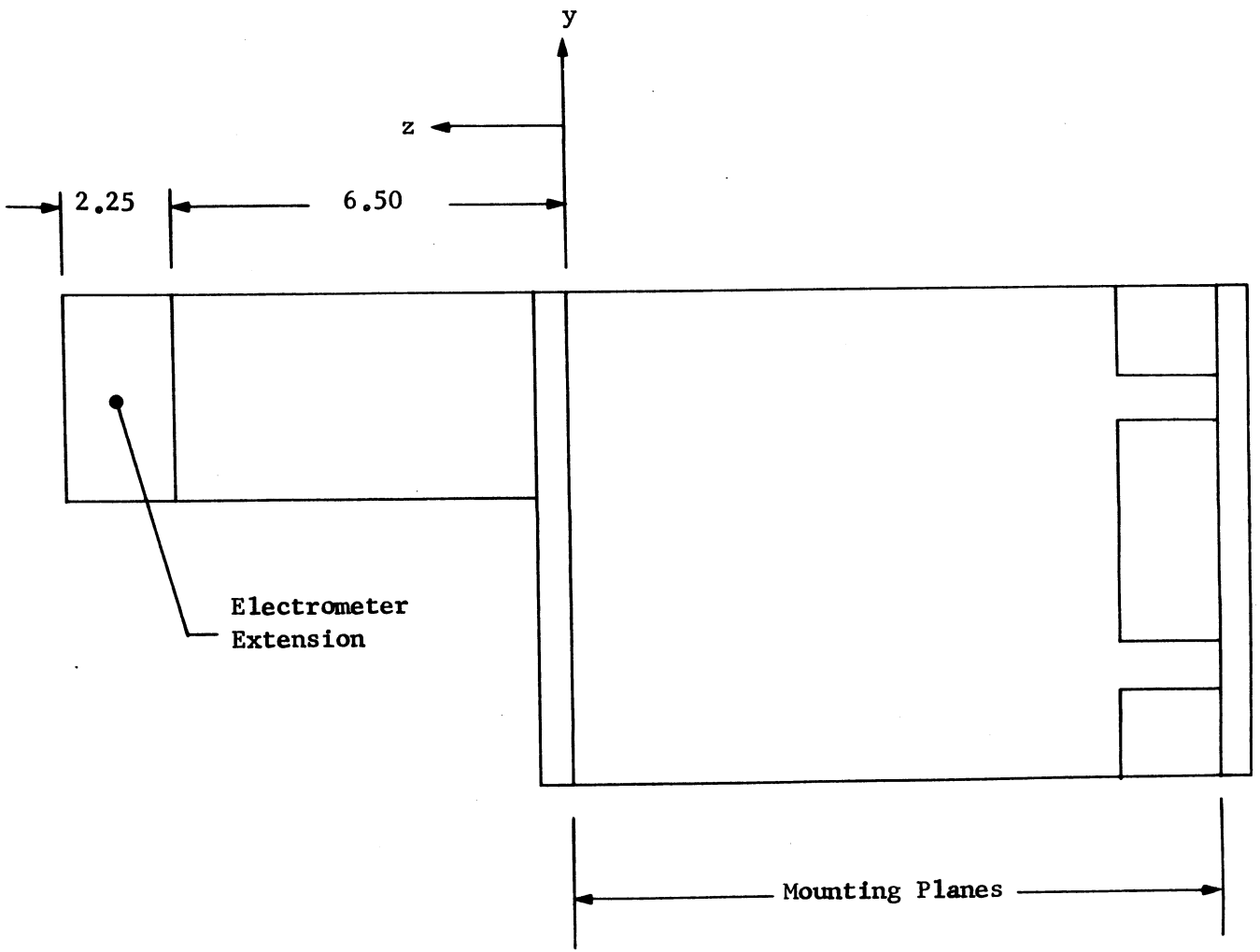

Figure 4-20. Lower End Casting Extension Diagram

$$f_n = \frac{1}{2\pi}\sqrt{\frac{g}{\delta_{st}}} \quad \text{cycles per second}$$

where g = Acceleration of gravity = $\frac{386 \text{ in.}}{\text{sec.}^2}$

δ_{st} = Static deflection

The lower end of the casting is basically a box configuration (Figure 4-21). Because of the large opening for the cam bearing insert, most of one wall of the box is removed.

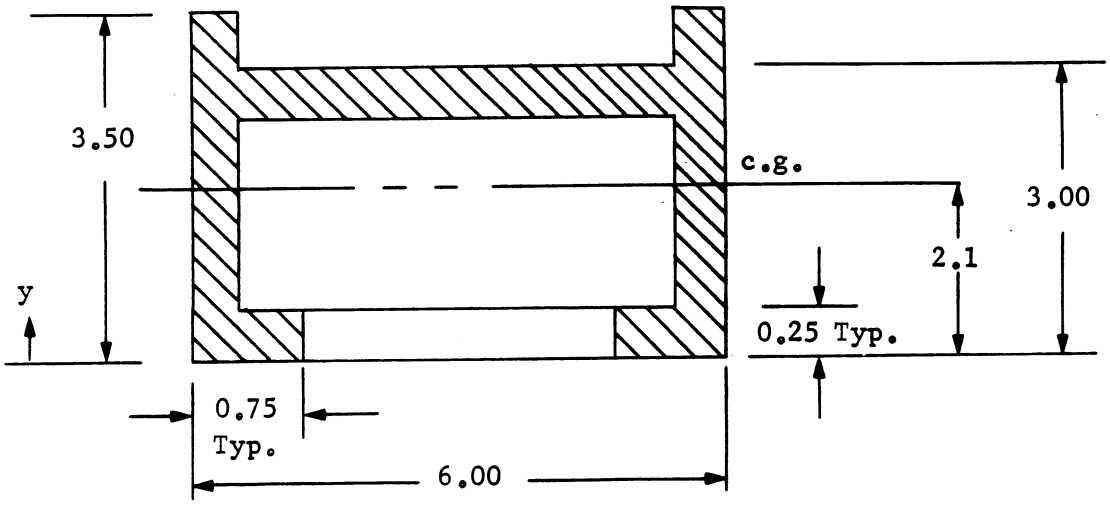

Figure 4-21. Lower End Casting Cross-Sectional View

The static deflection of the casting is determined by superimposing the solution for each loading condition.

$$y = y_1 + y_2 + y_3 + y_4 + y_5$$

In general, $\bar{I} = \frac{bh^3}{12}$, $I = \bar{I} + Ad^2$

where, I is about the bending neutral axis of casting crossection;

$\bar{I}$ is about centroid of element;

b and h are the dimensions of a rectangular area;

A is the area; and

d is the distance between the centroidal axis of the area and the centroidal axis of the casting.

The centroidal axis of the casting for the minimum moment of inertia is:

$$y = \frac{\Sigma \bar{y}A}{\Sigma A} = \frac{7.05}{3.38} = 2.1 \text{ (centroid of casting section)}$$

The minimum moment of inertia is:

$$I = 2\left[\frac{.25\ (3.5)^3}{12} + .25\ (3.5)\ (.35)^2\right] + \left[\frac{5.5\ (.25)^3}{12} + 5.5\ (.25)\ (.77)^2\right]$$

$$+ \left[\frac{1.0\ (.25)^3}{12} + 1.0\ (.25)\ (1.98)^2\right]$$

$$I = 3.80 \text{ in.}^4$$

The loading case for y_1, y_2, y_3, y_4 is shown in Figures 4-22 and 4-23.

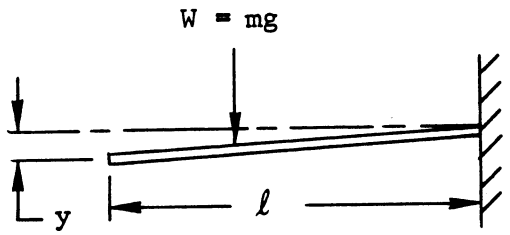

$$y_{max} = \frac{1}{6}\ \frac{W}{EI}\ (3z^2\ell - z^3)$$

Figure 4-22. Loading Condition For y_1, y_2, y_3, y_4

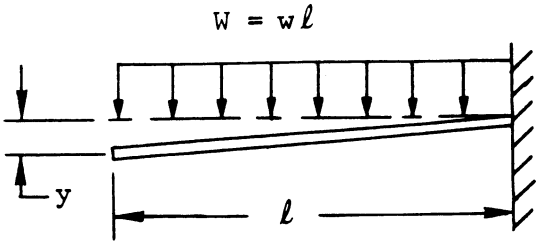

$$y_{max} = \frac{1}{8}\frac{W\ell^3}{EI}$$

Figure 4-23. Loading Condition for y_5

$$y_1 = \frac{1}{6}\frac{(.5516)}{(6.5 \times 10^6 \text{ psi})(3.80 \text{ in.}^4)} 3\left[(2.74 \text{ in.})^2 (6.50 \text{ in.}) - (2.74 \text{ in.})^3\right]$$

$$= 0.467 \times 10^{-6} \text{ inches}$$

$$y_2 = \frac{1}{6}\frac{(2.75 \text{ lbs})}{(6.5 \times 10^6 \text{ psi})(3.80 \text{ in.}^4)} 3\left[(3.25 \text{ in.})^2 (6.50 \text{ in.}) - (3.25 \text{ in.})^3\right]$$

$$= 3.185 \times 10^{-6} \text{ inches}$$

$$y_3 = \frac{1}{3}\frac{(1.50 \text{ lbs})(6.5 \text{ in.})^3}{(6.5 \times 10^6 \text{ psi})(3.80 \text{ in.}^4)} = 5.559 \times 10^{-6} \text{ inches}$$

$$y_4 = \frac{1}{6}\frac{(.42 \text{ lbs})}{(6.5 \times 10^6 \text{ psi})(3.80 \text{ in.}^4)} 3\left[(2.74 \text{ in.})^2 (6.5 \text{ in.}) - (2.74 \text{ in.})^3\right]$$

$$= 0.357 \times 10^{-6} \text{ inches}$$

$$y_5 = \frac{1}{8}\frac{(1.60 \text{ lbs})(6.50 \text{ in.})^3}{6.5 \times 10^6 \text{ psi } (3.80 \text{ in.}^4)} = 2.224 \times 10^{-6} \text{ inches}$$

$$y = \Sigma y_n = 11.792 \times 10^{-6} \text{ inches}$$

$$f_n = \frac{1}{2\pi} \sqrt{\frac{386 \text{ in./sec}^2}{11.792 \times 10^{-6} \text{ in.}}}$$

$$f_n = 910 \text{ cps}$$

The bending stress in the casting is determined by:

$$\sigma_B = \frac{Mc}{I}$$

where: M = bending moment, in.-lb.

C = distance to extreme fiber, in.

I = moment of inertia, $in.^4$

σ_B = bending stress, psi

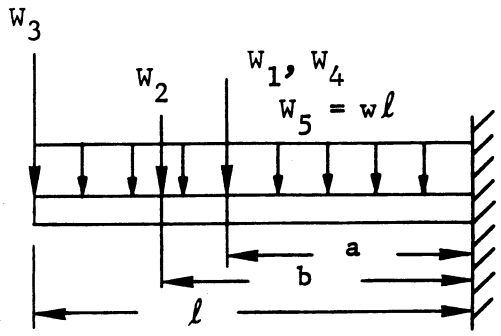

Figure 4-24. Bending Stress Diagram

$$M = (W_1 + W_4)\ (a) + W_2\ (b) + W_3\ (\ell) + 1/2\ W_5\ell$$

$$M = (.55 \text{ lbs.} + .42 \text{ lbs.})\ (2.74 \text{ in.}) + 2.75 \text{ lbs.}\ (3.25 \text{ in.})$$
$$+ (1.50 \text{ lbs})\ (6.50 \text{ in.}) + 1/2\ (1.6 \text{ lbs.})\ (3.25 \text{ in.})$$

$$M = 23.9 \text{ in.-lbs.}$$

Assuming g = 20g for random vibration and a transmissibility of Q = 3, the bending stress becomes:

$$\sigma = \frac{Mg\ Qc}{I} = \frac{(23.9\ \text{in.-lb.})\ (20g)\ (3)\ (2.1\ \text{in.})}{3.80\ \text{in.}^4}$$

$$\sigma = 792\ \text{psi}$$

This case is overly pessimistic since the cam bearing insert is a structural member to some degree and would therefore increase the moment of inertia. This would cause the resonant frequency of the casting to increase. The bending stress for the "worse case" considered is 792 psi which is a low stress since the bending strength of EZ33A is 40,000 psi (yield), 57,000 psi (ultimate)[1]. The factor of safety for this criteria is:

$$\text{F.S.} = \frac{0.1\ \sigma_{By}}{\sigma_B} = \frac{4{,}000\ \text{psi}}{792\ \text{psi}} = 5.1$$

The casting deflection under this g loading becomes

$$y = gy = 11.79 \times 10^{-6}\ \text{in.}\ (60g) = .00071\ \text{in.}$$

A deflection of this magnitude and location will not effect optical alignment and will occur only during launch.

---

1 Dow Chemical Company, Properties of Magnesium Alloy Castings. Table II, Bulletin 141-176.

4.4.3 Shutters

The shutters consist of a fixed outer sleeve and a rotating inner sleeve with openings of slightly larger dimension than the theoretical light beam size and shape. The radial clearance between sleeves is 0.0015 in. The material used is Magnesium with a Dow No. 9 anodic anodize coating. The outer sleeve is fitted precisely (0.0005 diametrical clearance) into bored cavities within the cast instrument housing. Closely identical shutters have been manufactured, installed, and tested for the P103 and F104 Instruments. A photo of the shutter is shown in Figure 4-25. The entrance shutter has four operating positions as shown in Figure 4-26. The exit shutter has two operating positions. The relationship between shutters is also shown.

The operation of the unit by functional sequence is as follows:

1. Monitor

   Entrance shutter open

   Exit shutter open

2. Dark current

   Entrance shutter closed

   Exit shutter closed

3. Photometric calibration

   Entrance shutter closed

   Exit shutter rotated to intermediate position permitting its built-in mirror to pick up energy from a Tritium UV emitting source and directing it into the Monochromator. The configuration of the rotating part of the shutter is such as to simultaneously block light from entering

Figure 4-25. Entrance Shutter Assembly

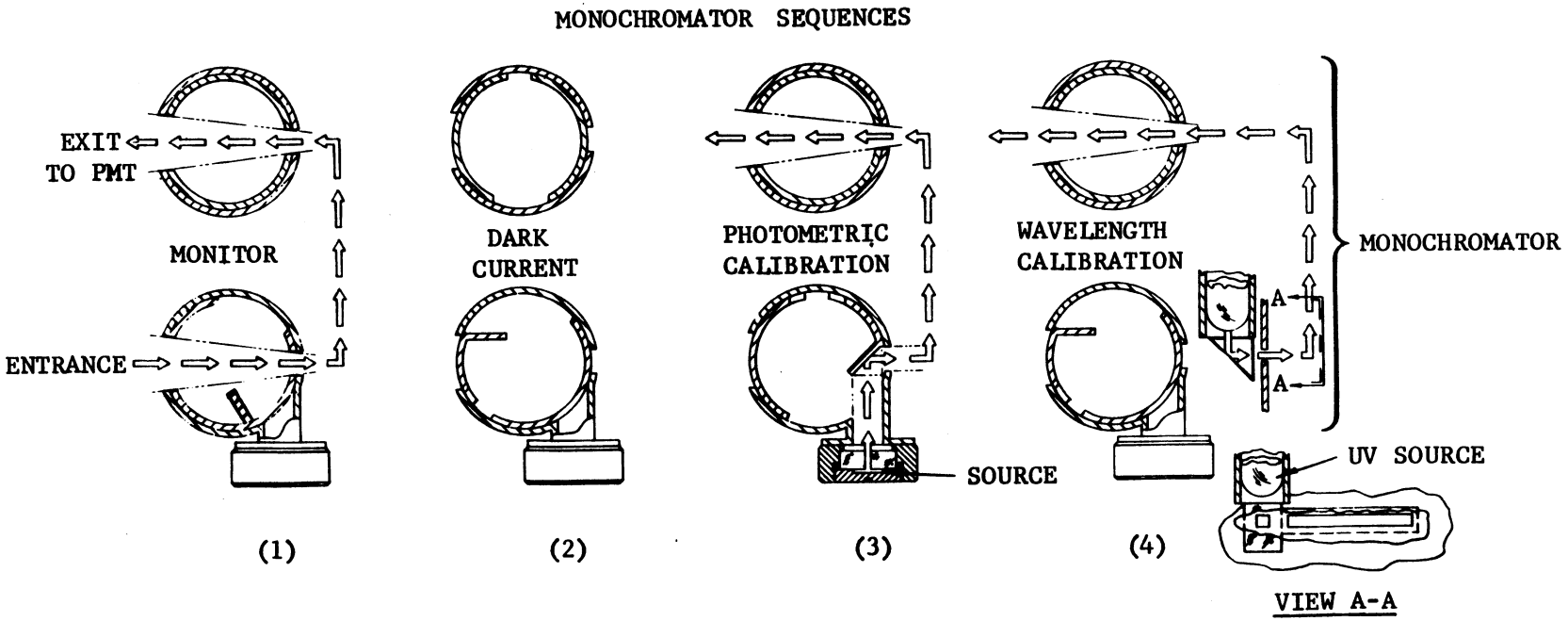

Figure 4-26. Shutter Sequence Chart

the entrance port and permit light to enter from the photometric calibration source.

4. Wavelength calibration

   Entrance shutter closed

   Exit shutter open

In this position, energy from the wavelength calibration lamp is introduced into the Monochromator.

Both shutters are driven by the same motor (stepper motor) coupled to a Geneva Mechanism. The Geneva Mechanism consists of a common driver and two individual driven stars (Figures 4-27 and 4-28).

One of the significant advantages of the rotary shutter is the ease with which extremely close matching diametrical tolerances can be maintained. This, in conjunction with a curved leak path and the black surface finish, cuts light leakage to a minimum.

Housekeeping information concerning the shutter position is obtained by an encoder assembly consisting of reed switches actuated by a small magnet as part of a disk which is coupled to the driver of the Geneva Mechanism. Instrument logic dictates rotational direction of the stepper motor and stop positions of the driver.

4.4.4 Geneva Mechanism

The Geneva Mechanism (Figures 4-27 and 4-28) positions the entrance and exit shutters for the monochromator. A general discussion of the mechanism is followed by a detailed analysis of the forces and torques caused by the combined effect of both dynamic and static loadings.

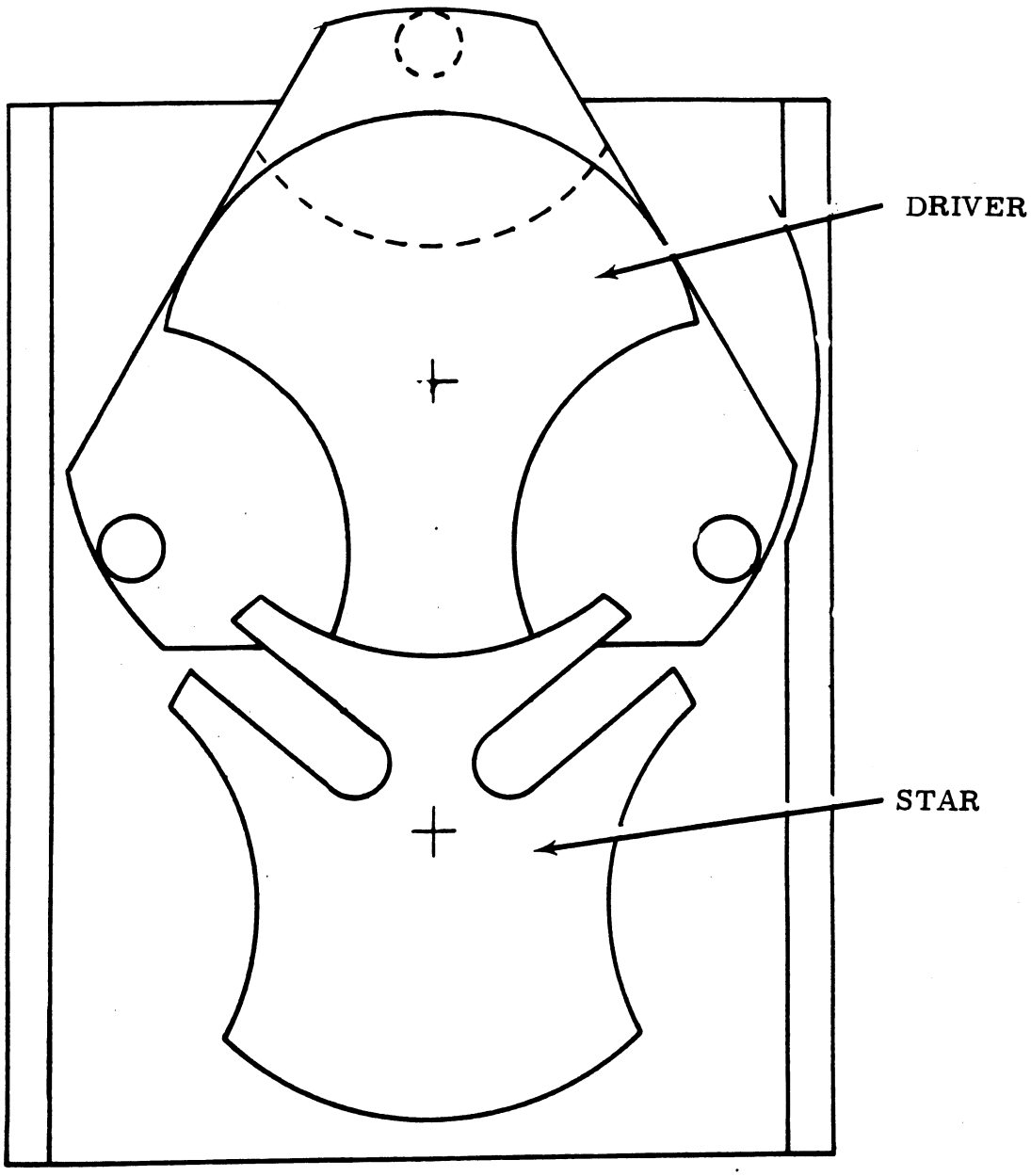

Figure 4-27. Geneva Mechanism (rear)

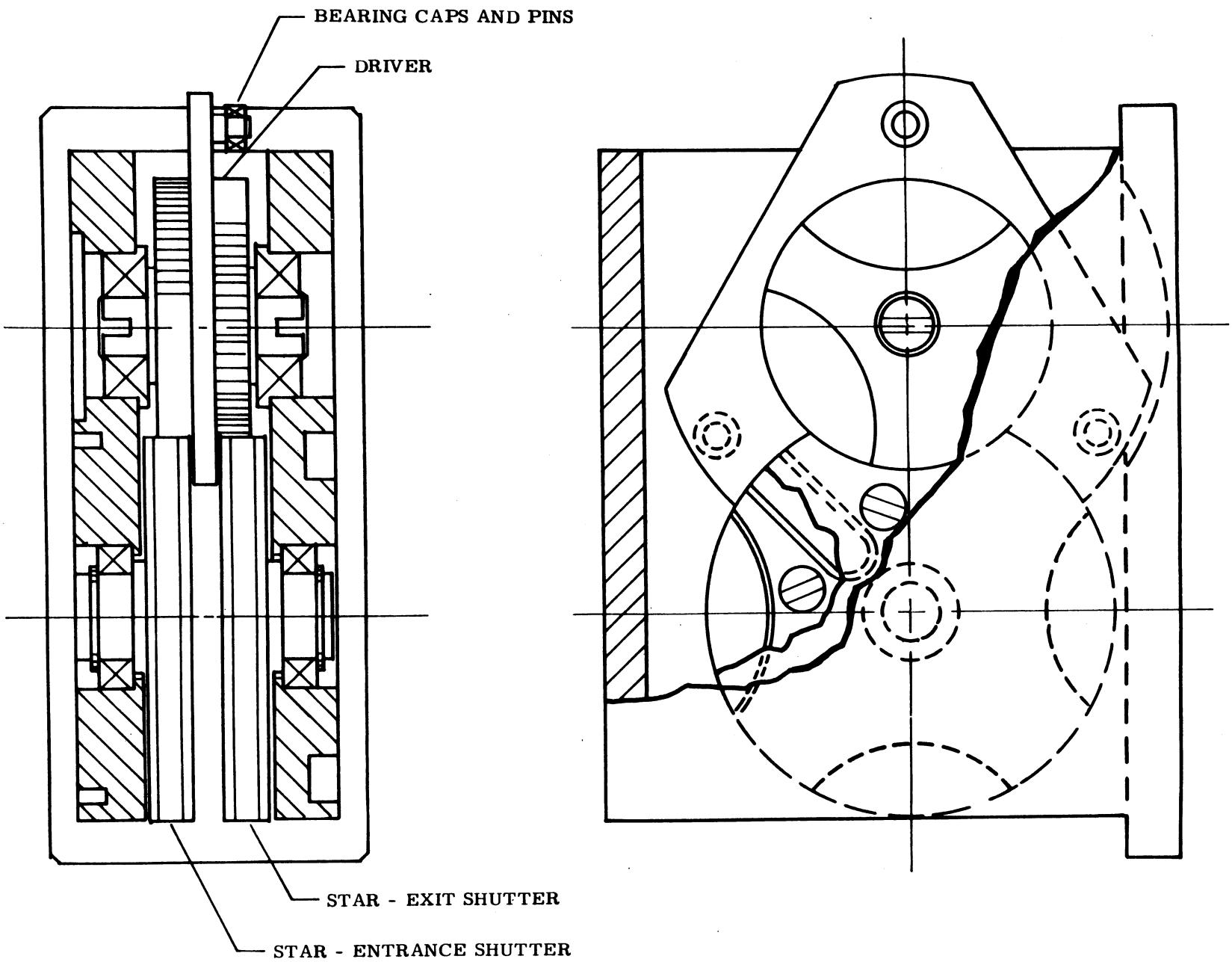

Figure 4-28. Geneva Mechanism (front)

4.4.4.1 Mechanism Functional Description

The basic advantage of the Geneva mechanism as a positioning device is that it permits a phasable method for independent positioning of the entrance and exit shutters. The inherent positioning and locking characteristics, smoothness of operation at slow speeds, and simplicity in design made this mechanism particularly adaptable to the BUV Instrument.

Special considerations were necessary to allow use of this mechanism in a space environment. Primary areas of concern were lubrication of bearings and elimination of metallic contact between all moving surfaces. The mechanism has only three moving parts: the drive wheel and two Geneva wheels (one for each shutter). A ball bearing was incorporated on the drive wheel to establish rolling rather than sliding contact between the drive pin and Geneva wheel indexing slot. The Geneva wheel itself consists of a sandwich construction of aluminum and duroid. Duroid is Teflon with a glass fiber and MoS_2 filler. This material provides a non-metallic surface having a low coefficient of friction and good wear characteristics for the motion of the drive pin when engaged in the Geneva wheel slot and on the detent surfaces. All ball bearings in the mechanism are lubricated with "Krytox" 240 AC (a fluorinated grease). All critical machining of the Geneva wheel and of the Geneva housing is performed on a J16 bore mill.

These special considerations along with very close control over manufacturing of the mechanism have resulted in successful operation in both P103 and F104 Instruments.

4.4.4.2 Geometry

The basic geometry of the Geneva mechanism is shown in Figure 4-29. The drive wheel pin rolls in the slot to drive the wheel. At the instant contact is being made or broken the roller axis is perpendicular to the slot. For any position of the drive pin:

$$\beta = \text{Sin}^{-1}\left[\frac{r_1}{\rho}\ \text{Sin}\ \alpha\right]$$

A diagram of the motion is shown in Figure 4-30.

Nomenclature

a = Center distance, in.

r = Crank radius, center drive wheel to roller, in.

ρ = Effective wheel radius, wheel axis to roller axis, in.

α = Crank position, deg.

α_o = Half indexing drive wheel angle, deg.

β = Wheel position, deg.

β_o = Half angle between two adjacent wheel slots, deg.

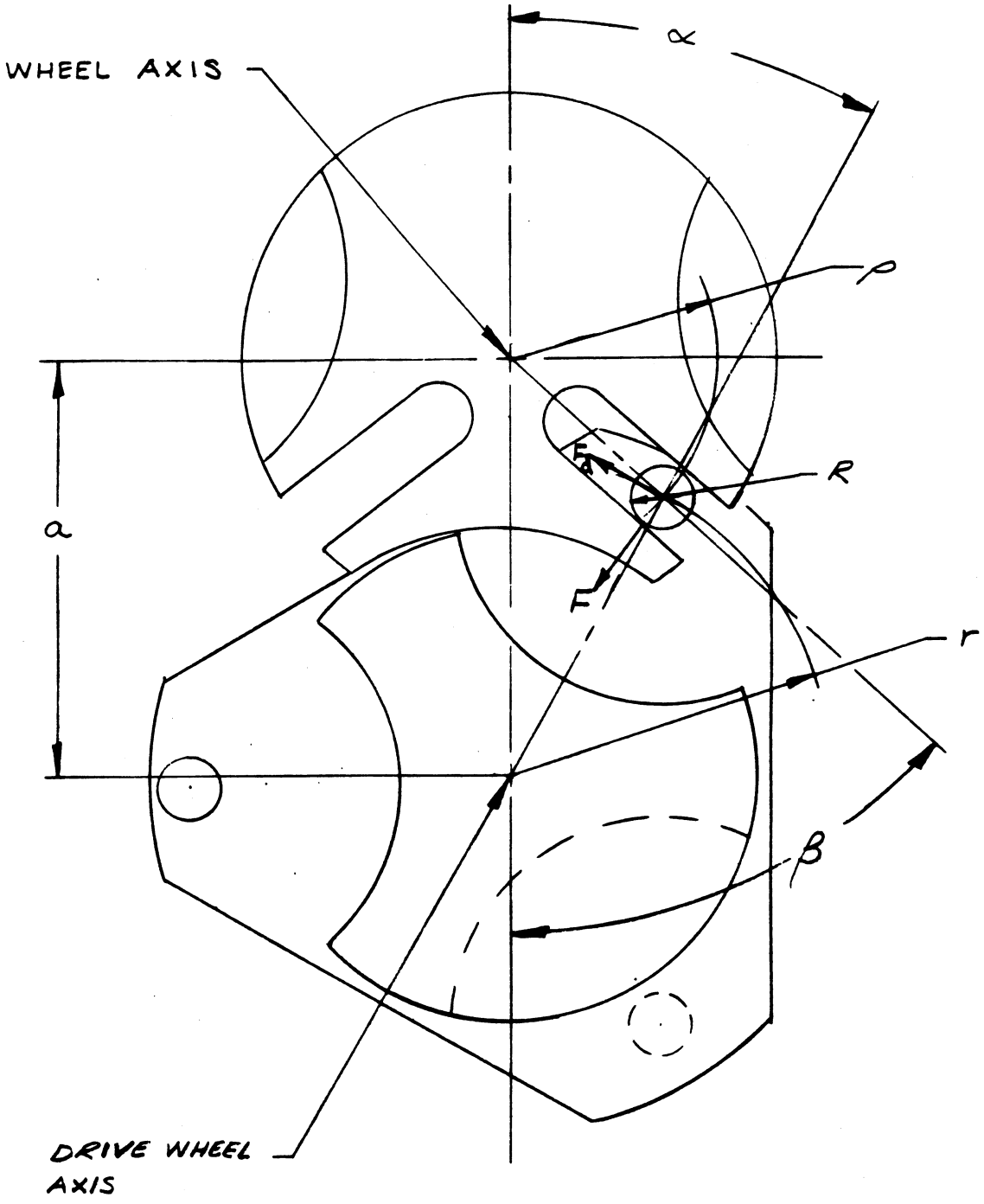

Figure 4-29. Basic Geometry

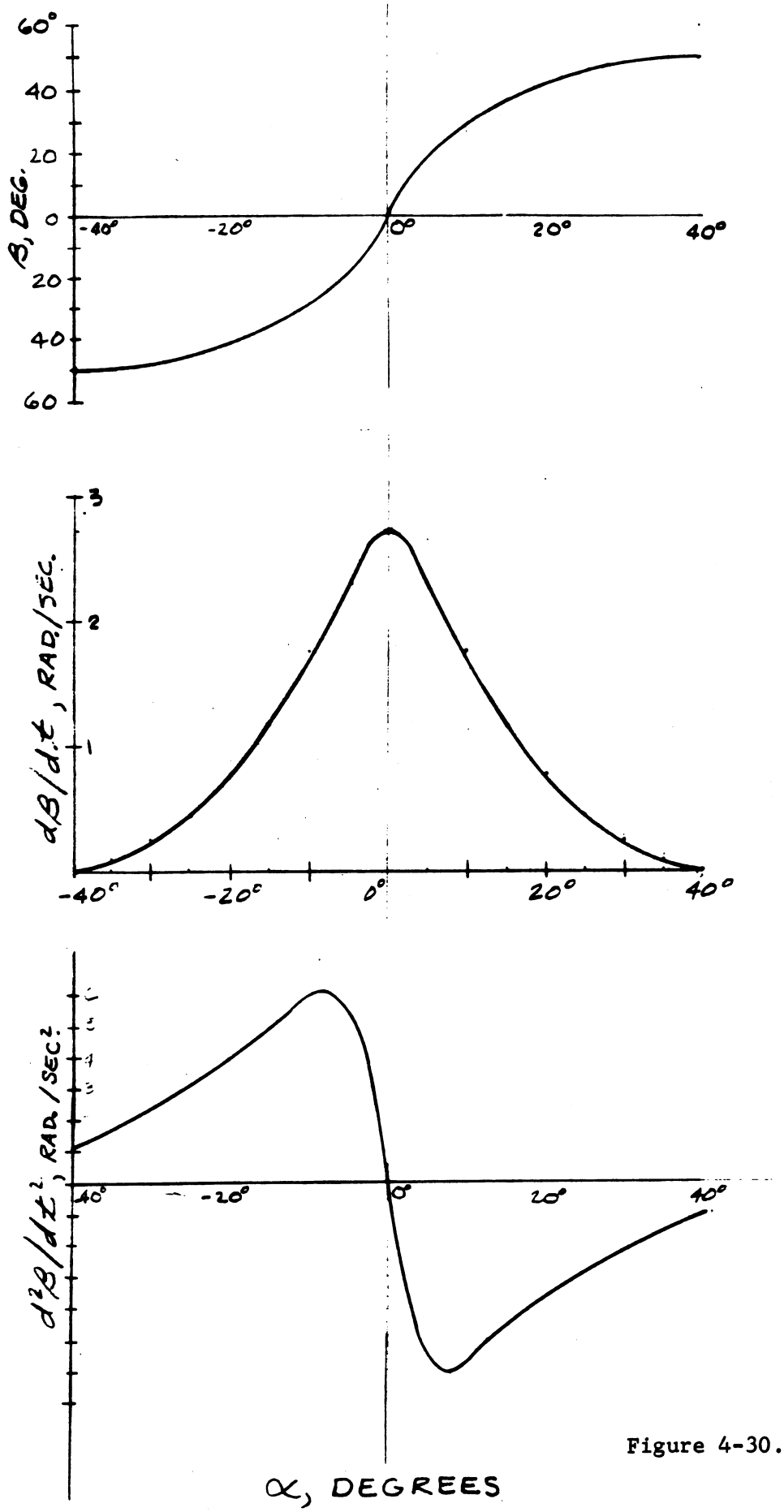

Figure 4-30. Diagram of Motion

ω_d = Drive wheel angular velocity, rad/sec

ω_w = Wheel angular velocity, rad/sec

ω_R = Roller angular velocity, rad/sec

ϵ_w = Wheel angular acceleration, rad/sec^2

V_s = Relative velocity of roller along wheel slot, fps

R = Roller radius, in.

I = Total equivalent rotational inertia of mechanism being driven by the Geneva wheel, lb m - in^2

I_w = Moment of inertia of wheel, lb m - in^2

F = Roller contact force, lb

M_d = Driving torque, lb - in

T_B = Rolling torque of ball bearings used in the mechanism

4.4.4.3 Kinematics

A. Angular Velocity of ω_w of the Wheel

Angular velocity ω_w of the wheel is a function of angular position α of the roller drive pin, Figure 4-29.

$$(1)\quad \omega_w = \frac{d\beta}{dt}\ ; \qquad \beta = \mathrm{Sin}^{-1}\left(\frac{r\ \mathrm{Sin}\ \alpha}{\rho}\right)$$

$$\rho = \sqrt{r^2 + a^2 - 2ra\ \mathrm{Cos}\ \alpha} = a\sqrt{1 + \mathrm{Sin}^2\ \beta_o - 2\ \mathrm{Sin}\ \beta_o\ \mathrm{Cos}\ \alpha}$$

Then,

$$(2)\quad \beta = \mathrm{Sin}^{-1}\ \frac{\mathrm{Sin}\ \beta_o\ \mathrm{Sin}\ \alpha}{\sqrt{1 + \mathrm{Sin}^2\ \beta_o - 2\ \mathrm{Sin}\ \beta_o\ \mathrm{Cos}\ \alpha}}$$

Assuming drive wheel rotates with unit angular velocity $\frac{d\beta}{dt}$ may be replaced by $\frac{d\beta}{d\alpha}$.

$$(3)\quad \frac{d\beta}{d\alpha} = \frac{\text{Sin } \beta_o \text{ (Cos } \alpha - \text{Sin } \beta_o)}{1 + \text{Sin}^2 \beta_o - 2 \text{ Sin } \beta_o \text{ Cos } \alpha}$$

It is apparent that maximum angular velocity occurs at $\alpha = 0$:

$$(4)\quad \left(\frac{d\beta}{d\alpha}\right)_o = \frac{\text{Sin } \beta_o}{1 - \text{Sin } \beta_o}$$

B. Angular Acceleration of Wheel, ϵ_w

Differentiating expression (3) leads to the angular acceleration of the Geneva wheel:

$$(5)\quad \frac{d^2\beta}{d^2} = \frac{\text{Sin } \beta_o \text{ Cos}^2 \beta_o \text{ Sin } \alpha}{\left(1 + \text{Sin}^2 \beta_o - 2 \text{ Sin } \beta_o \text{ Cos } \alpha\right)^2}$$

The third differential of expression (3) is

$$(6)\quad \frac{d^3\beta}{d\alpha^3} = -\text{Sin } \beta_o \text{ Cos}^2 \beta_o \left[\frac{2 \text{ Sin } \beta_o \text{ Cos } \alpha + (1+\text{Sin } \beta_o) \text{ Cos } \alpha - 4 \text{ Sin } \beta_o}{\left(1 + \text{Sin}^2 \beta_o - 2 \text{ Sin } \beta_o \text{ Cos } \alpha\right)^3}\right]$$

Setting this expression equal to zero yield the wheel position at which maximum acceleration occurs, $\frac{d^3\beta}{d\alpha^3} = 0$ or,

$$(7)\quad 25 \text{ in } \beta_o \text{ Cos}^2 \alpha + (1 + \text{Sin}^2 \beta_o) \text{ Cos } \alpha - 4 \text{ Sin } \beta_o = 0$$

Solving for α:

$$(8)\quad \text{Cos } \alpha = \frac{1 + \text{Sin}^2 \beta_o}{4 \text{ Sin } \beta_o} \pm \sqrt{\left(\frac{1 + \text{Sin}^2 \beta_o}{4 \text{ Sin } \beta_o}\right)^2 + 2}$$

Therefore:

$$(9)\quad \alpha_{max} = \text{Cos}^{-1} \left[-\frac{1 + \text{Sin}^2 \beta_o}{4 \text{ Sin } \beta_o} + \sqrt{\left(\frac{1 + \text{Sin } \beta_o}{4 \text{ Sin } \beta_o}\right)^2 + 2}\right]$$

$$\frac{d^2\beta}{d\alpha^2}_{max} = -\frac{\text{Sin } \beta_o \text{ Cos}^2 \beta_o \text{ Sin } \alpha_{max}}{\left(1 + \text{Sin}^2 \beta_o - 2 \text{ Sin } \beta_o \text{ Cos } \alpha_{max}\right)^2}$$

(10) $\omega_d = \frac{\pi}{180} \frac{p \times n}{R}$

where: p = Pulse rate of motor, pulse/sec

n = Step angle, deg/pulse

R = Gear ratio

$$\omega_d = \frac{\pi}{180} \frac{(50 \text{ pulses/sec}) (90 \text{ deg/pulse})}{(93:1)}$$

$$\omega_d = .844 \text{ rad/sec}$$

Therefore, maximum velocity is:

$$\left(\frac{d\beta}{dt}\right)_{max} = \left(\frac{d\beta}{d\alpha}\right)_o \frac{d\alpha}{dt} = \frac{\omega_d \text{ Sin } \beta_o}{1 - \text{Sin } \beta_o}$$

$$\left(\frac{d\beta}{dt}\right)_{max} = \frac{(.844 \text{ rad/sec}) \quad (\text{Sin } 50°)}{1 - \text{Sin } 50°} = 2.76 \text{ rad/sec}$$

$$\omega_{w \text{ max}} = \left(\frac{d\beta}{dt}\right)_{max} = 2.76 \text{ rad/sec (26.4 rpm)}$$

Maximum acceleration is:

Ref. (9) $$\alpha_{max} = \text{Cos}^{-1} \left[- \frac{1 + (.587)}{4(.766)} + \sqrt{\left(\frac{1 + .582}{4(.766)}\right)^2 + 2} \right]$$

$$\alpha_{max} = \text{Cos}^{-1} .989 = .148 \text{ rad } (8°30')$$

$$\frac{d^2\beta}{dt^2} = \left(\frac{d^2\beta}{d\alpha^2}\right)_{max} \left(\frac{d\alpha^2}{dt^2}\right) = - \frac{.766 \ (.413) \ (.1478) \ (.844)^2}{\left[1 + .587 - 2(.766) \ (.989)\right]^2}$$

$$\epsilon_{w \text{ max}} = \left(\frac{d^2\beta}{dt^2}\right)_{max} = 6.13 \text{ rad/sec}^2$$

C. Roller Velocity

The roller moves radially inward in the wheel slot during the first half of each cycle, and outward during the second half. For any position of the drive wheel,

$$V_s = \omega_w \rho \quad \text{and} \quad \omega_R = \frac{\omega_w \rho}{R}$$

Maximum roller velocity occurs at:

$$\left(\frac{d\beta}{d\alpha}\right)_{max} = \frac{\text{Sin } \beta_o}{1 - \text{Sin } \beta_o} \quad \text{and} \quad \rho = a - r_1$$

$$\left(\omega_R\right)_{max} = \left(\frac{d\beta}{d\alpha}\right)_{max} \left(\frac{d\alpha}{dt}\right) \frac{a - r_1}{R} = (2.76 \text{ rad/sec}) \left(\frac{.293 \text{ in.}}{.094 \text{ in.}}\right)$$

$$\left(\omega_R\right)_{max} = 8.62 \text{ rad/sec}$$

4.4.4.4 Kinetics

A. Driving Torque

The driving torque or total drive wheel shaft torque required to drive the mechanism is a function of the drive roller position.

$$T = (I_w + I) \epsilon_{w_{max}} + \Sigma T_B$$

$$\Sigma T_B = T_{(\text{drive wheel})} + T_{(\text{Geneva wheel})} + T_{(\text{shutter})}$$

$$\Sigma T_B = .20 \text{ in.-ounces (measured)}$$

$$T = \frac{(9.45 \times 10^{-3} \text{ lb-in}^2 + 30.5 \times 10^{-3} \text{ lb-in}^2)\ (6.13 \text{ rad/sec}^2)}{16\ (32.2 \text{ lb/slug})} + (.20 \text{ ounce-inches})$$

$$T = .68 \text{ ounce-inches}$$

The output torque of the stepper motor is .09 in.-ounces when operating at 50 pulses/sec. Available torque at the gearhead output shaft is:

$$T_G = (.09 \text{ in.-ounces}) (93:1) = 8.37 \text{ ounce-in.}$$

The resulting safety factor is

$$S.F. = \frac{8.37}{.68} = 12.3$$

The inertial capacity of the motor is .05 gm-cm^2 when operating with the above torque load. Total inertial load consists of the shutter, Geneva wheel, and drive wheel.

$$I_T = I_w + I + I_D = 1.68 \times 10^{-3} \text{ slug-in.}^2$$

The inertial capacity of the motor is increased by the square of the gear ratio:

$$.05 \text{ gm-cm}^2 = 1.707 \times 10^{-5} \text{ slug-in.}^2$$

It is evident that the inertial capacity of the motor exceeds the inertial load by nearly a factor of 90.

$$S.F. = \frac{(1.707 \times 10^{-5}) (93:)^2}{1.68 \times 10^{-3}} = 87.8$$

B. Roller Force

The magnitude of the contact force between the roller and the Geneva slot is a function of wheel position and is maximum when T is maximum. This force is always perpendicular to the slot surface.

$$F = \frac{T}{\rho} \qquad a = 1.25 \text{ in.}$$

$$\rho = \left[r^2 + a^2 - 2\,ra\,\text{Cos}\,\alpha\right]^{1/2} \qquad r = .957 \text{ in.}$$

$$\alpha = 8°30'$$

$$\rho = \left[(.957 \text{ in.})^2 + (1.25 \text{ in.})^2 - 2(.957 \text{ in.})\,(1.25 \text{ in.})\,(.989)\right]^{1/2}$$

$$\rho = .335 \text{ in.}$$

$$F_{max} = \frac{T_{max}}{\rho_{max}} = \frac{.68 \text{ in.-ounces}}{.335 \text{ in.}}$$

$$F_{max} = 2.03 \text{ ounces}$$

4.4.4.5 Tabulation of Results

Angular Velocity of Drive Wheel	=	.84 rad/sec
Angular Velocity of Geneva Wheel	=	2.76 rad/sec (max)
Angular Velocity of Drive Roller Pin	=	8.62 rad/sec (max)
Angular Acceleration of Geneva Wheel	=	6.13 rad/sec^2 (max)
Driving Torque	=	.68 ounce-in.
Roller Force	=	2.03 ounces

4.4.4.6 Conclusions

This analysis has shown that the operating loads, velocities and accelerations are very low and that the stepper motor has adequate power to drive the

mechanism, with reserve power capabilities of approximately a factor of 10. No mechanical problems inherent to the design have been observed on either the P103 or F104 Instrument Geneva mechanisms.

4.4.4.7 References

1. Greenwood, Douglas C., Geneva Wheel Design, Product Engineering, May 26, 1958.
2. Jensen, Preven, W., Geneva Mechanisms, Design Data; Design News, September 29, 1965.
3. Fenton, R. G., Geneva Mechanisms, Machine Design, January 21, 1965.
4. Lichtwitz, Otto, Mechanisms for Intermittent Motion, Machine Design, December 1951.
5. Johnson, Ray C., Geneva Mechanisms, Machine Design, March 22, 1956.

4.4.5 Wavelength Cam and Cam Drive

To maintain the monometallic concept of the instrument, the cam was fabricated of magnesium metal. A hard surface was needed on the surface of the cam which contacts the cam follower. This task was achieved by application of a tungsten-carbide plasma spray of approximately 0.008" thickness which was then precision ground and lapped. During removal of about half of the hard coating, the radius of the cam with its twelve monitor and seven primary wavelength calibration steps was worked to within ±0.0001" of theoretical dimension. An auxiliary extension made out of Duroid was installed close to the high radius of the cam. This extension covered about 7° of the cam circumference,

and protruded 0.004" above the high step (3398Å). During the launch mode, the extension is brought into position and lifts the wavelength arm just adjacent to the cam follower bearings. On the opposite end, the arm rests against a nylatron stop. This "caging" feature (Figure 4-31) effectively prevents contact between cam-follower bearings and cam periphery, preventing possible damage during launch.

The cam is driven by a No. 10 tandem gearhead stepper-motor assembly. Coupling is achieved through an interfacing part made of Duroid. Because Duroid is an insulating material, heat flow from the driver to the cam is prevented. Also, possible mating surface cold welding in the hard vacuum of space is prevented.

The cam shaft extending on both sides of the cam rests in matched pairs of dual bearings. The dual bearings were chosen to equalize small bearing errors and thus increase the accuracy of the cam-wavelength arm-grating combination.

Balancing of the cam, including auxiliary cam and encoder disk, was done statically to within better than 1/4 gram. Balancing was achieved to computed figures permitting maximum permissible removal of material on the cam disk. Residual unbalance was corrected by adding coin shaped disks of Kenametal on the "light" side.

4.4.6 Wavelength Arm and Grating Mount Assembly

One of the most critical subassemblies is the combined wavelength arm and grating support. The assembly was cast from magnesium and designed for minimum weight and maximum stability. To maintain the integrity of support and alignment, and because of critical space limitations, both gratings were

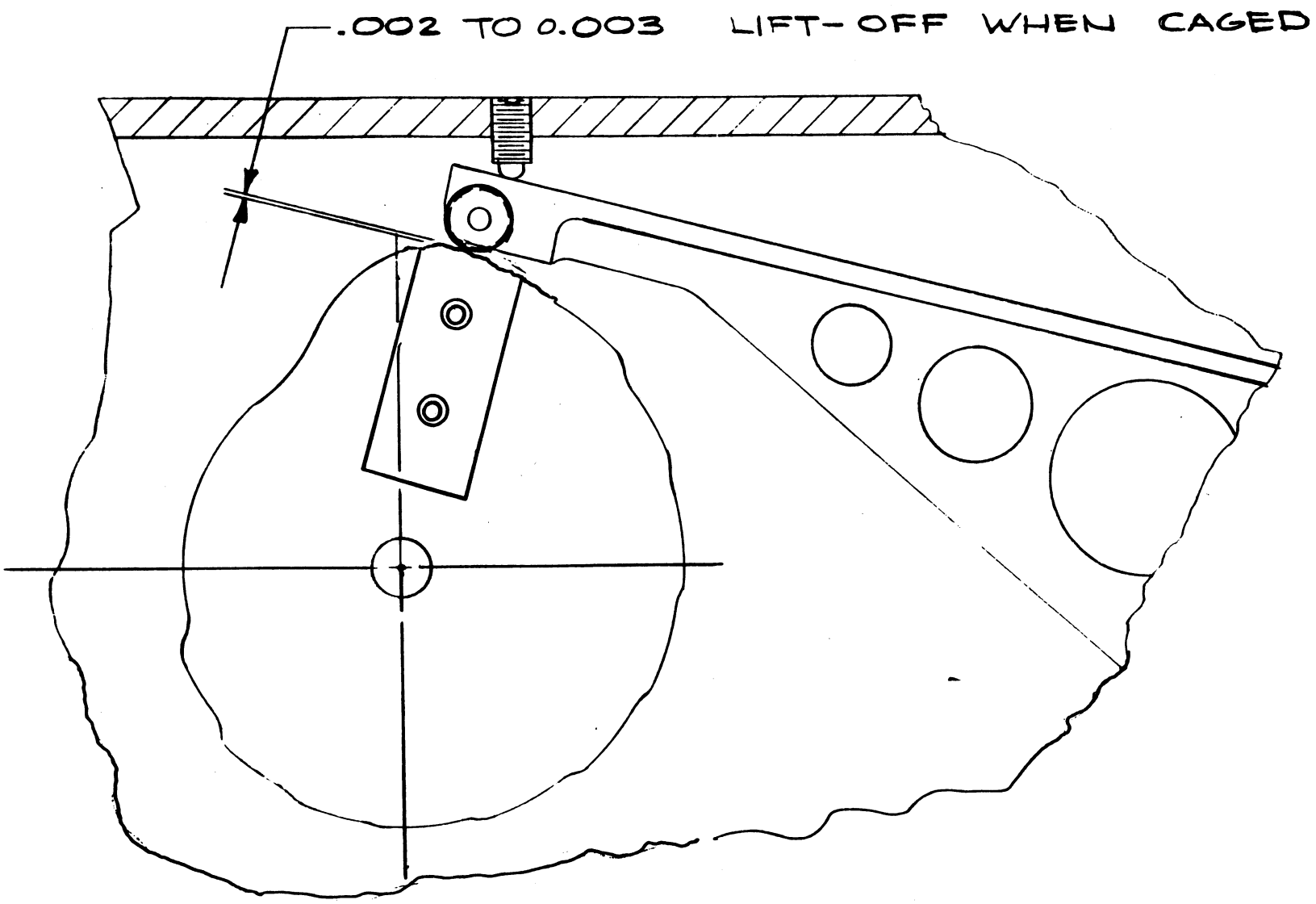

Figure 4-31. Caging Mechanism

supported from the back and loaded from the front surface. To obtain accuracy in alignment of the gratings within the optical monochromator system, a fixture with the geometrical distribution representing the cam and wavelength arm bearing support was built. Grating alignment then was accomplished to within ±2° sec of arc with an autocollimator. The gratings are mounted on precision lapped fixed pads as an integral part of the grating mounts.

The arm rests in class 7 ball bearings mounted directly into the supporting ends of the wavelength arm. The end of the arm contains the cam follower bearings consisting of a matched set of 3/8" diameter class 7 bearings. The dual bearing set provided the following major features:

- Equalization of small inaccuracies inherent in the bearings and on the cam surface.
- Distribution of bearing load onto the cam.

As further explained in Paragraph 4.4.5, the bearings are <u>not</u> resting on the cam during vibration testing or at launch. This important feature prevents any damage that could affect the accuracy or performance of the grating-wavelength arm and cam.

To prevent damaging oscillation of the grating support with its extending arm during environmental testing and at launch, the subassembly was statically balanced to within better than 1 gram. Balancing was achieved by the addition of small c' weights made out of Kennertium(1).

---

(1) Trademark of Kennametal, Inc.

4.4.7 Cam Encoder, Encoder Source, and Sensor Mount

The cam encoder (Figures 4-32 and 4-33) provides positional information to the electronic subsystem to allow proper cam sequencing. Attached to a shoulder on the cam is a disk perforated by a series of holes which generate the code shown in Table 4-3. The hole pattern is monitored by five miniature sensors and sources recessed in small printed circuit boards. Initial adjustment (phasing) between cam and encoder is achieved by rotating the disk vs. cam within the allowance of the slotted disk mounting holes. After the final adjustment, the disk is permanently pinned in place.

4.4.8 Mounting of Optical Components

4.4.8.1 Collimating Mirrors

The most critical optical component mounting task was accurately placing the two collimating mirrors at the upper end of the housing. Consistent with BUV design philosophy, optical system components are directly mounted to the supports. These supports or mounting surfaces, in turn, are machined to extremely close tolerance based on results of the computerized ray trace.

In this particular case, the mounting surfaces had to match the concave spherical surface of the mirrors. Pre-machining was done on a jig-borer. Final touch-up was done with a lapping plate having a surface equivalent to the radius of the mirror.

Clamping to the surface and securing of the mirrors was accomplished within extremely tight space limitations by the use of wave spring-straps to load the mirrors individually against the casting. A small tensile load was first applied to the straps as they were placed around the mirror back. The mirror cover was then placed over both mirrors and loaded and bolted in position.

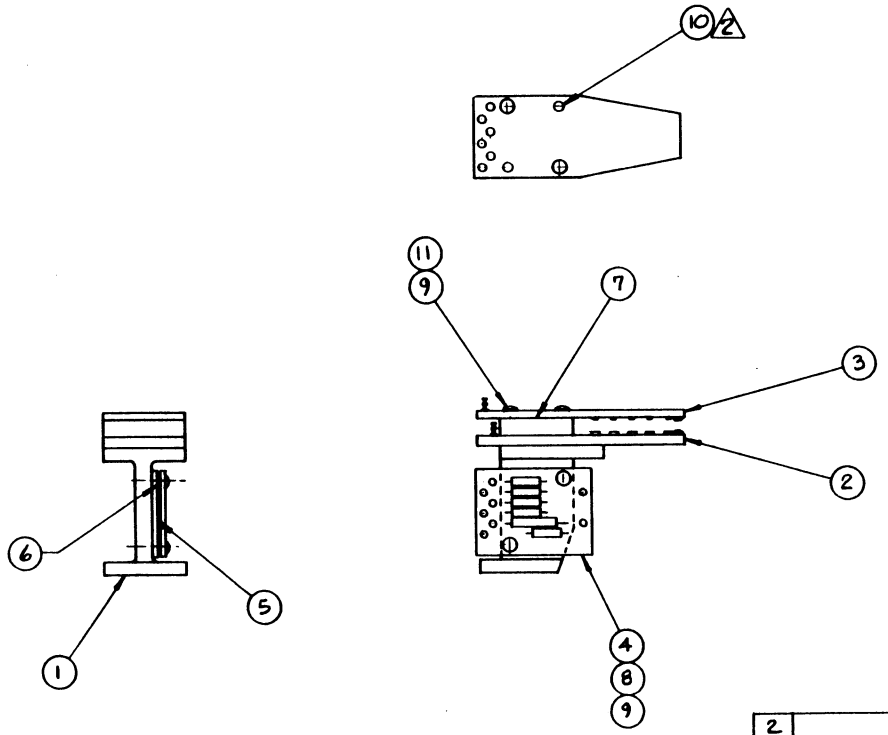

QTY REQD	BECKMAN NO.	ITEM NO.	NOMENCLATURE OR DESCRIPTION	PART OR IDENTIFYING NO.	CODE IDENT	MATERIAL	SPEC, NOTES, SIZES, VENDORS
2		11	SCREW, BUTTON HD CAP			ALLOY STL BLACK	2-56 x 5/8 LG
2		10	DOWEL PIN 3/32 DIA	D4-625			
4		9	WASHER, FLAT #2	NAS620-C3L			
2		8	SCREW, BUTTON HD CAP			ALLOY STL BLACK	2-56 x 1/4 LG
1	147618	7	SPACER				
2	147644	6	SPACER				
1	147621	5	INSULATOR				
1	147615	4	RESISTOR & CAPACITOR ASSY				
1	147616	3	SENSOR ASSY				
1	147617	2	SOURCE ASSY				
1	147037	1	SUPPORT				

LIST OF MATERIALS OR PARTS LIST

2 PRESS FIT IN ITEM 1 & SLIP FIT IN ITEMS 2, 3, & 7.

1. REF: SCHEMATIC DIAGRAM 147634

NOTES:

Figure 4-32. Cam Encoder Assembly

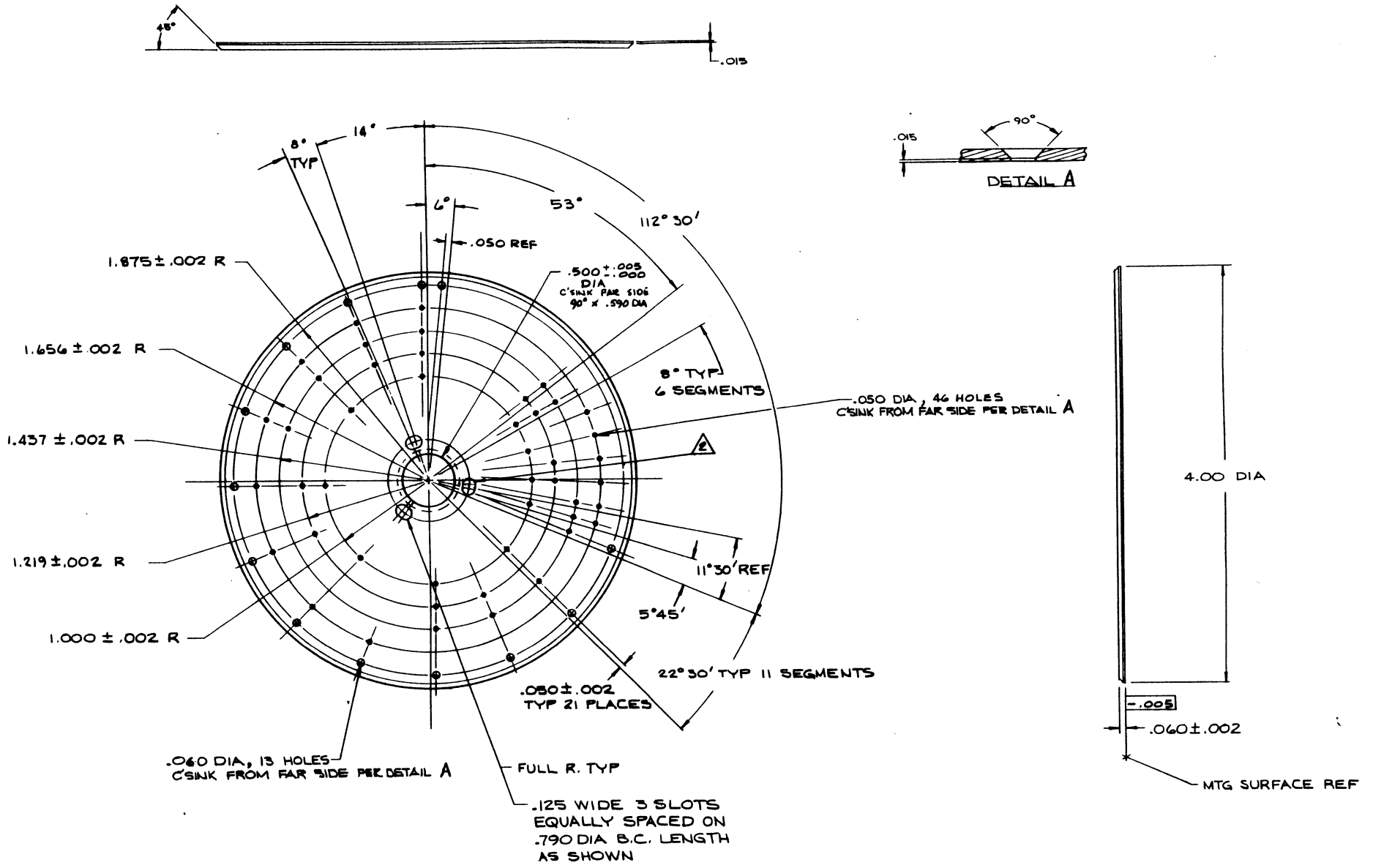

Figure 4-33. Encoder Disc

2 ON ASSY LOCATE THIS SLOT INLINE WITH TOOLING HOLE ON CAM.

1 ANGULAR TOLERANCES ± 0°15' NON-CUMULATIVE

NOTES:

	Wavelength (Angstroms)	Cam Code λ 1	λ 2	λ 4	λ 8	λ 16
1	3398	H	H	H	H	H
2	3312	X	H	H	H	H
3	3175	H	X	H	H	H
4	3125	X	X	H	H	H
5	3058	H	H	X	H	H
6	3019	X	H	X	H	H
7	2975	H	X	X	H	H
8	2922	X	X	X	H	H
9	2876	H	H	H	X	H
10	2830	X	H	H	X	H
11	2735	H	X	H	X	H
12	2555	X	X	H	X	H
13	2522	X	X	H	H	X
14	2527	H	H	X	H	X
15	2532	X	H	X	H	X
16	2537	H	X	X	H	X
17	2542	X	X	X	H	X
18	2547	H	H	H	X	X
19	2552	X	H	H	X	X
20	Caged			X	X	H

H = Hole, 0 V to Logic

X = No Hole, +4 V to Logic

Table 4-3. Cam Disc Coding

4.4.8.2 Mirror Mount Stress Analysis

The instrument is subjected to random and sinusoidal vibration during launch. The design acceleration is:

$$g_D = 3 \text{ (20 g - rms) Random} = 60 \text{ g} \quad (1)$$

The chances that the instantaneous acceleration will exceed three times the rms acceleration is only about 0.003.(2)

A. Spring Design

Consider the spring configuration shown in Figure 4-34 for loading the mirrors.

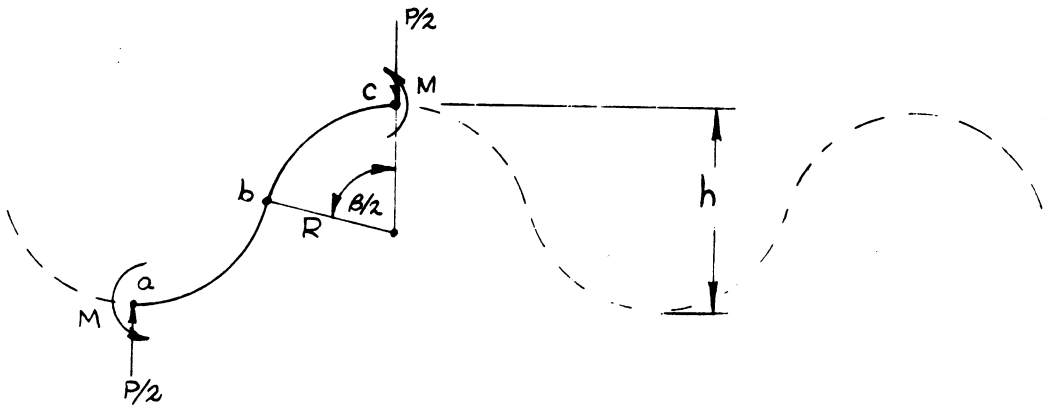

Figure 4-34. Spring Configuration

1. GSFC Specification, An Environmental Spec. for Nimbus B Subsystems, p. 5.
2. Product Engineering, June 22, 1964, p. 108.

Since the members under consideration may be treated as being very slender, it is only necessary to take into account the elastic strain energy caused by bending. The statement of Castigliano's principle in polar coordinates applicable to this case is:

$$Y = \frac{1}{EI}\int M \frac{\delta M}{\delta P} R\, d\theta \quad [1] \qquad (1)$$

The bending moment in section ab and section bc is:

$$M_{ab} = M_{bc} = M - \frac{PR}{2} \sin\theta \qquad (2)$$

The total deflection is therefor:

$$Y = \frac{1}{EI}\int M_{ab} \frac{\delta M_{ab}}{\delta P} R\, d\theta + \frac{1}{EI}\int M_{bc} \frac{\delta M_{bc}}{\delta P} R\, d\theta \qquad (3)$$

$$M = \frac{PR}{2} \sin \beta/2 \qquad (4)$$

$$M_{ab} = M_{bc} = M - \frac{P}{2} R \sin\theta = \frac{PR}{2} (\sin \beta/2 - \sin\theta) \qquad (5)$$

$$Y = \frac{2}{EI}\int_0^{\beta/2} \frac{PR}{2} (\sin \beta/2 - \sin\theta) \frac{\delta}{\delta P} \left[\frac{PR}{2} (\sin\beta/2 - \sin\theta)\right] R d\theta$$

$$Y = \frac{PR^3}{2EI}\int_0^{\beta/2} (\sin\beta/2 - \sin\theta)^2\, d\theta$$

$$Y = \frac{P(R\sin \beta/2)^3}{6\,EI} \quad \text{(Maximum Deflection)} \qquad (6)$$

The purpose of the wave springs is to provide sufficient preload such that during vibration the mirrors will remain seated against the casting.

---

1. Timoshenko, Elements of Strength of Materials, 4th edition, p. 247.

$F = mg$

$F = (1.3 \text{ lbm})\ (60 \text{ g}) = 78 \text{ lbf}$

$F = 78 \text{ lbf}$

where: F = Max. weight of mirror during vibration.

M = Mass of mirror (1.3 lbm)

g = Design acceleration (60 g)

The design preload must exceed 78 lbf

$F = 78 \text{ lbf}\ (1.5 \text{ S.F.}) = 117 \text{ lbf.}$

The spring configuration shown in Figure 4-34 will yield five points of contact on the back of the mirror.

$$P = \frac{117 \text{ lbf}}{2 \text{ (springs)} 5} = 11.7 \text{ lbf}$$

$P = 11.7 \text{ lbf.}$

For the configuration shown in Figure 4-34.

R = .156 in. (Radius of curvature)

h = .187 in. (height)

$E = 17 \times 10^6$ psi (Beryllium Copper)

t = .010 in. (thickness)

W = .375 in. (width of spring)

$$I = \frac{Wt^3}{12} = \frac{.375 \text{ in.} (.010 \text{ in})^3}{12}$$

$$I = 31.3 \times 10^{-9} \text{ in.}^4$$

$$\beta/2 = 90° - \text{in}^{-1} \frac{(R - h/2)}{R} = 90° - \sin^{-1} \frac{.062}{.156}$$

$$\beta/2 = 90^\circ - 23.5^\circ = 66.5^\circ$$

$$\beta/2 = 66.5^\circ$$

Deflection from equation (6)

$$Y = \frac{11.7 \text{ lbf } (.156 \text{ in. } \sin 66.5^\circ)^3}{2\ (17 \times 10^6 \text{ psi})\ (3.13 \times 10^{-8} \text{ in}^4}$$

$$Y = .011 \text{ in (Preload defection of wave spring)}$$

B. Stress Level in Wave Spring

The maximum bending moment is:

$$M_{max} = \frac{PR}{2} \sin \beta/2$$

$$\sigma = \frac{MC}{I} = \frac{M}{Z} \qquad Z = \frac{wt^2}{6}$$

$$\sigma = \frac{3\ PR \sin\beta/2}{wt^2}$$

$$= \frac{3(11.7 \text{ lbf})(.156 \text{ in})(.917)}{(.375 \text{in.})(.010 \text{ in})^2}$$

$$= 93{,}400 \text{ psi}$$

Yield strength of beryllium-copper (HT) is 150,000 psi.[1] This yields a safety factor of 1.6.

C. Compressive Stress on Back Side of Mirror Due to Wave Spring

Each convolution of the wave spring causes a line contact force to be exerted on the mirror. Although this force is directly over the mirror contact surface the stress level in the mirror should be examined.

---

1. Metals Handbook, p. 1038.

This loading case is analogous to the case of a flat plate in line contact with a cylinder as presented by Roark.[1]

$$\text{Max } S_c = \sqrt{\frac{p}{D\left[\frac{1-\nu_1^2}{E_1} + \frac{1-\nu_2^2}{E_2}\right]}}$$

$$S_c = \sqrt{\frac{31.2 \text{ lb/in}}{.312 \text{ in}\left[\frac{.974}{10.4 \times 10^6 \text{ psi}} + \frac{.910}{17 \times 10^6 \text{ psi}}\right]}}$$

$$S_c = 26{,}100 \text{ psi}$$

$$p = \frac{P}{w} = \frac{11.7 \text{ lb}}{.375 \text{ in}} = 31.2 \frac{\text{lb}}{\text{in}}$$

ν = Poisson's ratio

ν_1 = .16 Fused quartz)

ν_2 = .30 (Berylium-copper)

E_1 = 10.4×10^6 psi

E_2 = 17×10^6 psi

D = 2 R = .312 in

S_c = Compressive stress

D. Conclusion

The compressive strength of fuxed quartz is greater than 160,000 psi.[2] This yields a minimum factor of safety of 6.

---

1. Roark, Formulas for Stress and Strain, p. 320.

2. General Electric Fused Quartz Catalog, p. 5.

E. Contact Stress (Compressive) of Mirror Surface in Contact with Housing

The mirror is seated on two sides of the housing. These surfaces are lapped to the spherical radius of the mirrors to provide a maximum area of uniform seating surface.

$$A = 2\ (.20\ \text{in})\ (3.25\ \text{in}) = 1.30\ \text{in}^2$$

$$F = 117\ \text{lbf.}$$

$$\sigma_c = \frac{117\ \text{lbf}}{1.30\ \text{in}^2} = 90\ \text{psi}$$

4.4.8.3 Grating Mount

Installation of the gratings is similar to the collimating mirrors. The cover on the mirrors was changed to an open frame that permits access to the surface of the gratings. The opening of the frame was designed to provide proper masking of the optical image. Possible side motion or tilting of the grating is prevented by lateral stops as an integral part of the grating mount-wavelength arm assembly. These stops are precision machined and lapped to align the ruling pattern of each grating in line with the rotating axis of the grating mount.

4.4.8.4 Prisms

The peculiar shapes of the prism and especially of the roof prism presented some mounting problems. No mounting surface contact with any of the internally reflecting surfaces could be tolerated. Permanent alignment had to be maintained under the rather severe requirements of environmental testing. Mounting was against solid precision machined surfaces with loading across supporting areas.

4.4.8.5 Lenses

Only two lenses were part of the total optical system. The lens adjacent to the exit slit had a flat section on the periphery which excluded the use of a loading ring. Instead, a semicircular spring made out of Beryllium copper with individual fingers provided the necessary loading force.

The lens in the photometer section is mounted in a conventional way with a threaded ring in its tubular mount. The same mount contains the 3800Å interference filter.

4.4.9 Diffuser Field-Defining Horn

4.4.9.1 Assembly and Mechanism

This assembly permits introduction of a diffuser plate in front of the entrance of the monochromator, and in front of the entrance to the photometer. In this position, diffused sunlight is reflected from the surface of the diffuser plates into both the monochromator and photometer, providing primary photometric calibration; normal viewing to the earth is blocked at this time.

During the monitor cycle for both the monochromator and photometer, the diffuser plates are stored out of the normal viewing path, and openings in the field-defining horns for the plates are closed.

To reduce the size and weight of the plates and the related mechanism, it was necessary to move the components as close as possible to the entrance to take advantage of the converging beam. The shutter and diffuser plates were combined into one relatively small assembly and attached directly onto the field-defining horns.

The shutters are coupled to the drive motor by a gear segment cut on the periphery of the shutter side (Figure 4-1). This segment engages a gear mounted on the exit shaft of a No. 8 motor-gearhead assembly attached to the main housing.

The gear drive is completely exposed to space environments, i.e., vacuum, UV radiation, etc. To avoid lubrication problems, the gear is fabricated from Nylatron GS, a molybdenum disulphide-filled nylon. The shutter is cut from magnesium plate and coated with a Dow No. 9 finish. This combination performed well under all environmental testing.

The shutters with mounted diffuser plates are part of the light-baffling system at the entrance to both the monochromator and photometer (Figure 4-1), obviating further baffling inside the optical systems. The field-defining horns were cast out of a glass-filled epoxy formulation which permitted casting of extremely fine detail with the baffle edges maintained to a 0.002-inch radius. The high strength of the cast epoxy part also permitted it to be used as a structural part for the bearing support. This arrangement provided a compact design to fit into the extremely small space available.

During vibration testing, the assembly reached primary and secondary resonant peaks due to the generally thin wall construction of the total assembly. Measured g-levels of up to 60 g's (10X input) did not result in damage or affect subsequent performance.

4.4.9.2 Diffuser Drive

A. Angular Velocity

$$W = \frac{(90 \text{ DEG/PULSE})(50 \text{ PULSE/sec})\ 2\pi}{(24:1)(7.72:1)(360 \text{ DEG})}$$

First stage gearing, 24:1

Second stage gearing, 7.72:1

W = .424 radians/sec

B. Rotational Inertia

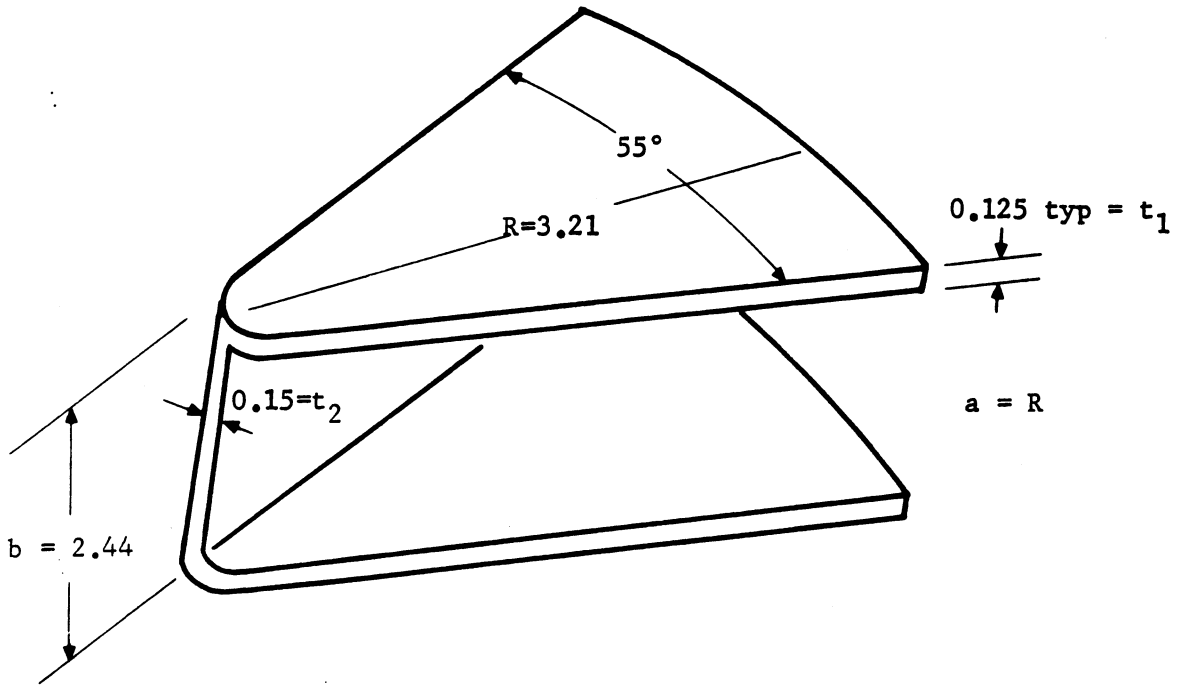

$$I = \frac{\pi \rho\ {}^{4}t_1\ \theta^2}{360^2} + \frac{3\ \rho\ a^3\ bt_2}{4}$$

$$I = \frac{(.067\ \text{lbm/in}^3)(3.21\ \text{in})^4(.125\ \text{in})(55)^2}{(360)^2} + \frac{3\ (.067\ \frac{\text{lbm}}{\text{in}^3})\ (3.21\ \text{in})^3(2.31\ \text{in})(.15\ \text{in})}{4}$$

$$I = .642\ \text{lbm - in}^2$$

C. Angular Momentum

$$H = IW = (.642\ \text{lbm - in}^2)(.424\ \text{radian/sec}$$

$$H = .272\ \frac{\text{lbm - in}^2}{\text{sec}} = 5.87 \times 10^{-5}\ \text{ft - lb}_f\text{ - sec}$$

$$H_t = H\ (\text{Photometer}) + H\ (\text{Monochromator}) = 2H$$

$$H_t = 2\ (5.87 \times 10^{-5}\ \text{ft - lb}_f\text{ - sec})$$

$$H_t = 11.7 \times 10^{-5}\ \text{ft - lb}_f\text{ - sec}$$

4.4.10 Bearings and Bearing Lubrication

A significant problem arose during preliminary thermal vacuum testing. The 30 percent Krytox filled ball bearings of the motor gearhead assemblies failed at low temperatures due to thickening of the Krytox grease. At the same time, tests performed at NASA indicated that at vacuum levels encountered in space, enough volatile material from the bearing grease would be deposited on the optics to significantly deteriorate the optical system performance.

The problems were solved by reworking or replacing all bearings so that they contained only a grease-plated lubricant coating. The formulation for the grease plating solution consisted of 1 part of Krytox dissolved in 10 parts of Freon 11. After this treatment, no failures in low temperature vacuum were observed and no damage from outgassing was observed.

SECTION V

ELECTRONICS

5.1 GENERAL

To accommodate the wide intensity variation in ultraviolet energy between night time and day time conditions, the BUV instrument provides a usable intensity ratio range of approximately 10^9. To accomplish this, the signal processing electronics in the BUV uses a dc electrometer and pulse counting techniques for measurement of extreme by low-level signals.

The wide dynamic range is accommodated by a 2 level high voltage power supply, a 5-1/2 decade dc electrometer, and a pulse counting system.

The power supply adjusts the PMT (photomultiplier tube) gain to a value chosen to ensure that the electrometer output remains on-scale for all values of expected optical inputs.

The dc electrometer provides 3 automatically switched gain ranges, and incorporates an automatic reference adjust circuit for balancing out electrometer offset voltages. The electrometer output after further processing is sent to the logarithmic analog-to-digital converter.

Since the spacecraft will periodically encounter high radiation levels, a pulse counting system has been incorporated. The photocathode signals produced by the desired input light incident on the photomultiplier are primarily single photoelectrons. Radiation induced signals are often characterized by multiple photoelectron emissions, which may mask low-level light

measurements if only average current measurements are made. The BUV counts single photoelectron pulses at low light levels in the radiation environment by discriminating against multiple photoelectron pulses. Thus, spurious emissions such as those produced by charged particles incident on the photomultiplier tubes are identified. At higher light levels where pulse counting becomes inaccurate, current measurements are substituted for pulse rate measurements.

The signal processing channel for the pulse counting mode consists of a wide band electrometer (common to both dc and pulse counting system), a pulse amplifier and shaper, two discriminators (upper level and lower level) and an anti-coincidence circuit. All of these circuits form a one channel pulse height selector of single photoelectron pulses. This is followed by a digital accumulator.

The PMT is operated at two different sensitivities by adjusting the high voltage power supply to one of two discrete levels, either 2×10^6 (nominal) or 4×10^3 (M) and 50 (P). The high gain mode, during which pulse counting occurs, is the normal condition for night time operation; automatic reduction of the PMT gain occurs for high light levels. The low gain mode, during which automatic electrometer ranging occurs, is used for normal day time operation; an automatic increase in sensitivity to a higher PMT gain level will occur for low light levels.

When operating in the low voltage mode, the electrometer is allowed to automatically range switch to gains of 3×10^{10}, 2×10^9, or 10^7. The maximum PMT current is limited to 10^{-6} amperes, above which the high voltage is either

automatically commanded off or reduced. The high voltage supply is also internally current limited as a secondary protection against fast transient overloads on the PMT. Operating in conjunction with the signal processing chain are the four motor drive circuits, which position the monochromator and photometer shutters, the monochromator wavelength cam, and the diffuser plate mount during the data taking cycle.

The various data taking and calibration operations are controlled by the BUV word generator and by the calibration sequencer. Operation of the calibration sequencer may be modified by ground command, when required.

In addition to the 2-level high voltage supply, a separate supply periodically drives the wavelength calibration lamp, and two low voltage supplies (main instrument supply and housekeeping supply) interface directly with the spacecraft input power to operate the instrument.

5.2 NIMBUS ELECTRICAL INTERFACE

5.2.1 Inputs

- Major Frame Pulse (MFP), used to synchronize the BUV sequencer to the VIP sampling sequence
- VIP A_{16}, which drives the BUV word generator and controls the individual sample times
- VIP B, used in conjunction with VIP A for sample time control and also counted down to generate the 50 Hz motor drive frequency
- VIP C, which controls the serial shifting of the digital A output data
- 10 KHz, used in the motor drive and switching circuits, and to synchronize the two static inverters for avoiding beat frequency generation.

The BUV accepts the following eight commands:

- Power On - Execution of this command applies power to the instrument experiment subsystem and initializes the BUV sequencer. The first major frame pulse received upon completion of this sequence initiates the normal experiment cycle.

- Power Off - Execution of this command removes all power from the experiment proper. Telemetry is still available following execution of this command, as the housekeeping voltage is not switched.

- Deploy Diffuser - Execution of this command causes the diffuser plate to be deployed. The BUV logic stores the command and, upon receipt of the next BUV sub frame pulse (these pulses occur every 32 seconds coincident with every other VIP major frame pulse), the programmer initiates a deploy diffuser operation, followed 64 seconds later with an automatic store diffuser operation.

- Store Diffuser - Execution of this command causes the diffuser to be placed in the stored position. This command is a back-up for the automatic store diffuser command and is normally not required.

- Inhibit Calibration - Execution of this command prevents any calibration sequences from occurring until receipt of the enable calibration command. While the instrument is operating in the inhibit calibration mode, normal experiment data replaces the calibration data.

- Enable Calibrate - Execution of this command removes the calibration inhibit and returns control of the calibration sequences to the internal programmer. Calibrations which would have occurred had the calibrate not been inhibited are lost and the next calibration to be performed is that which normally occurs in that time slot.

- Launch Mode - Execution of this command causes the wavelength cam to be placed in the caged position and causes the shutters to be placed in the dark current position after receipt of the next BUV major frame pulse. In addition, the high voltage is removed from both photomultiplier tubes. The instrument remains in this configuration until receipt of a normal mode command.

- Normal Mode - Execution of this command enables the automatic cam drive and reapplies high voltage to the photomultiplier tubes. The shutters remain in the dark current position until the end of the first electronics calibrate (MCSA) cycle which follows receipt of the normal mode command. Since restoration of normal cam drive signals may not occur at an MFP time, the cam may require two or three BUV frame times to re-synchronize with the internal programmer.

5.2.2 Outputs

The BUV has a total of 32 outputs:

- Digital A channel, sampled at a rate of 5 per second, which supplies the main experiment data output.

- 19 digital B lines, each sampled 3 times every 16 seconds, made up of various status indicating signals.

- 12 analog outputs, sampled once every 16 seconds.

The 19 digital B signals are as follows:

1. Photometer shutter in the data (monitor) position.
2. Photometer shutter in the photometric calibrate position.
3. Photometer shutter in the dark current position.
4. Monochromator shutter in the data (monitor) position.
5. Monochromator shutter in the photometric calibrate position.
6. Monochromator shutter in the dark current position.
7. Deploy diffuser command received.
8. Store diffuser command received.
9. Diffuser in the deployed position.
10. Diffuser in the stored position.
11. Calibration enabled/disabled.
12. BUV mode launch/normal.
13. BUV power on/off.
14. Electronic calibrate (MCSA).
15. Photometric Calibrate (MCSB,C).
16. Wavelength calibrate lamp on/off.
17. Pre-wavelength calibrate yes/no.
18. MFP received (data cycle one or two).
19. 10 kiloHertz received yes/no.

The 12 analog signals are as follows:

1. Housing absolute temperature

2. Housing temperature gradient
3. Arm temperature gradient
4. PMT absolute temperature
5. Sensor electronics temperature
6. Motor current limiter temperature
7. Inverter No. 1 temperature
8. Inverter No. 2 temperature
9. Monochromator high voltage monitor
10. Photometer high voltage monitor
11. Housekeeping reference voltage
12. Plus 4 volts monitor.

5.3 ELECTRONICS DESIGN DESCRIPTION

The following discussions refer to major functional blocks, with individual schematics included for the important signal processing elements. For a detailed electronics analysis refer to Beckman document FM-2475-301, Instruction Manual for the BUV instrument, Vol. 1, previously submitted. The Manual contains the submodule schematics, the detailed theory of operation, and signal levels and waveforms of key signals within the instrument electronics.

5.3.1 Electrometer

The electrometer input stage is an insulated gate field effect transistor (IGFET) of the MOS type. Electrometer operation satisfies the two basic requirements:

1. In the hybrid mode, single photoelectron charge pulses are amplified such that the pulses may be discriminated from amplifier noise.

2. In the range switched analog mode, the input stage leakage and equivalent offset drift are significantly below the desired current threshold for each particular range.

During operations the electrometer is zero-corrected once each minor data frame (32 seconds) by a signal automatic reference adjust correction (ARAC). During this correction, the electrometer feedback is shorted out by a 1K ohm resistor, and the automatic reference adjustment corrects for errors at the electrometer summing point due to input stage offset and offset drifts. A block diagram of the electrometer is shown in Figure 5-1. Also shown are the individual submodule schematics of the electrometer (Figure 5-2), the automatic reference adjust (Figure 5-3) and the ARS relays (Figure 5-4).

5.3.2 Logarithmic Analog-to-Digital Converter

The logarithmic height-to-time conversion operation (a linear input signal is compared with a precision exponential time base) produces a clock gate signal. The duration of the clock gate signal is proportional to the logarithm of the input signal. An 8 bit quantization of this gate results in a quantizing uncertainty of ±1.2 percent, with dynamic range of 316 to 1 (2.5 decades) and a maximum gate length of 1.02 milliseconds.

5.3.2.1 Buffer Filter Amplifier (Figure 5-5)

The gain of these two inverting amplifiers provides an impedance match between the output of the electrometer and the input of the signal comparator. The Buffer Filter Amplifier response is limited (approximately 10 Hz) to average the pulse component of the waveform presented at the electrometer output. The output signal ranges from zero to 31.6 volts depending upon the anode current of the photomultiplier tube.

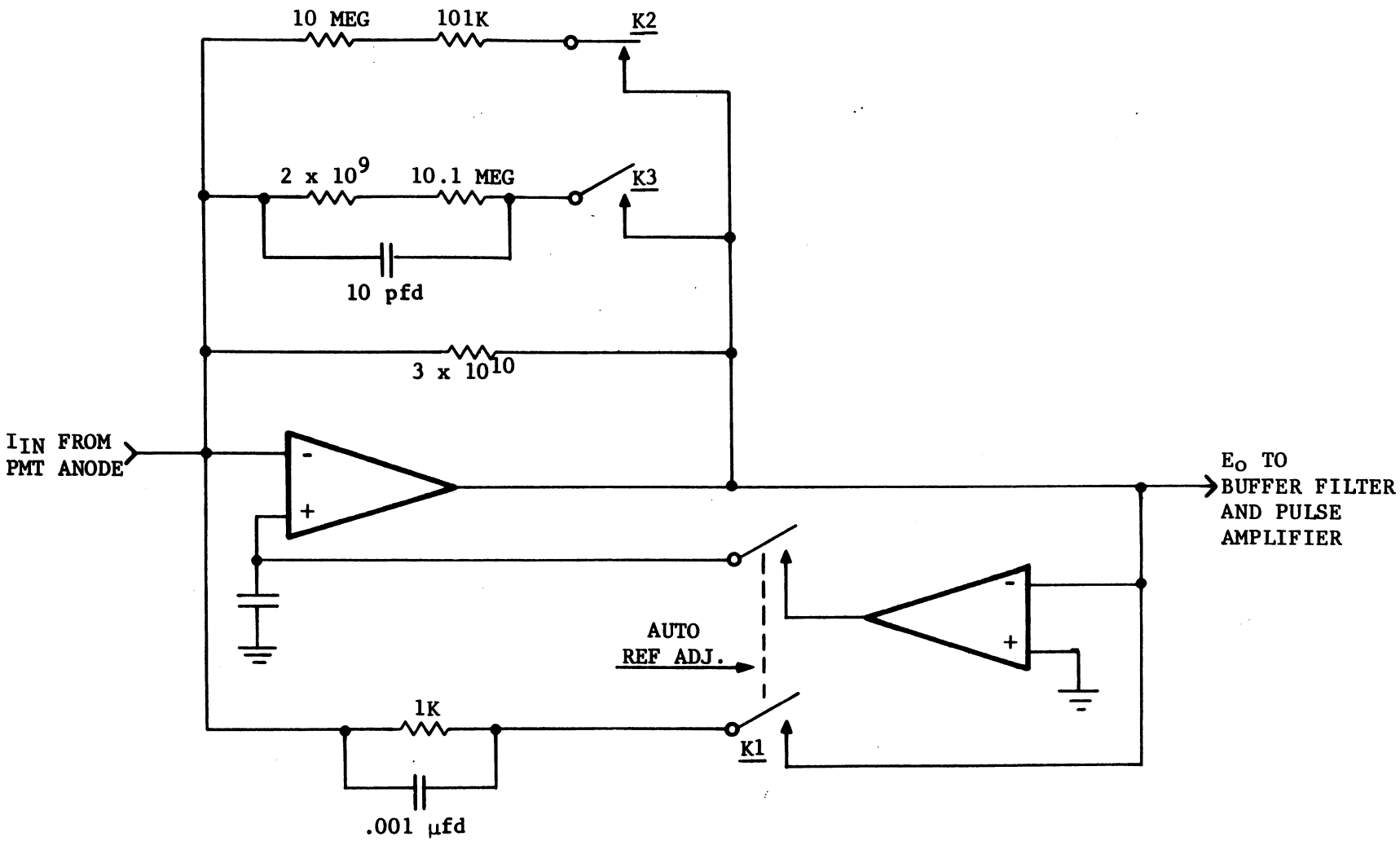

Figure 5-1. Electrometer Block Diagram

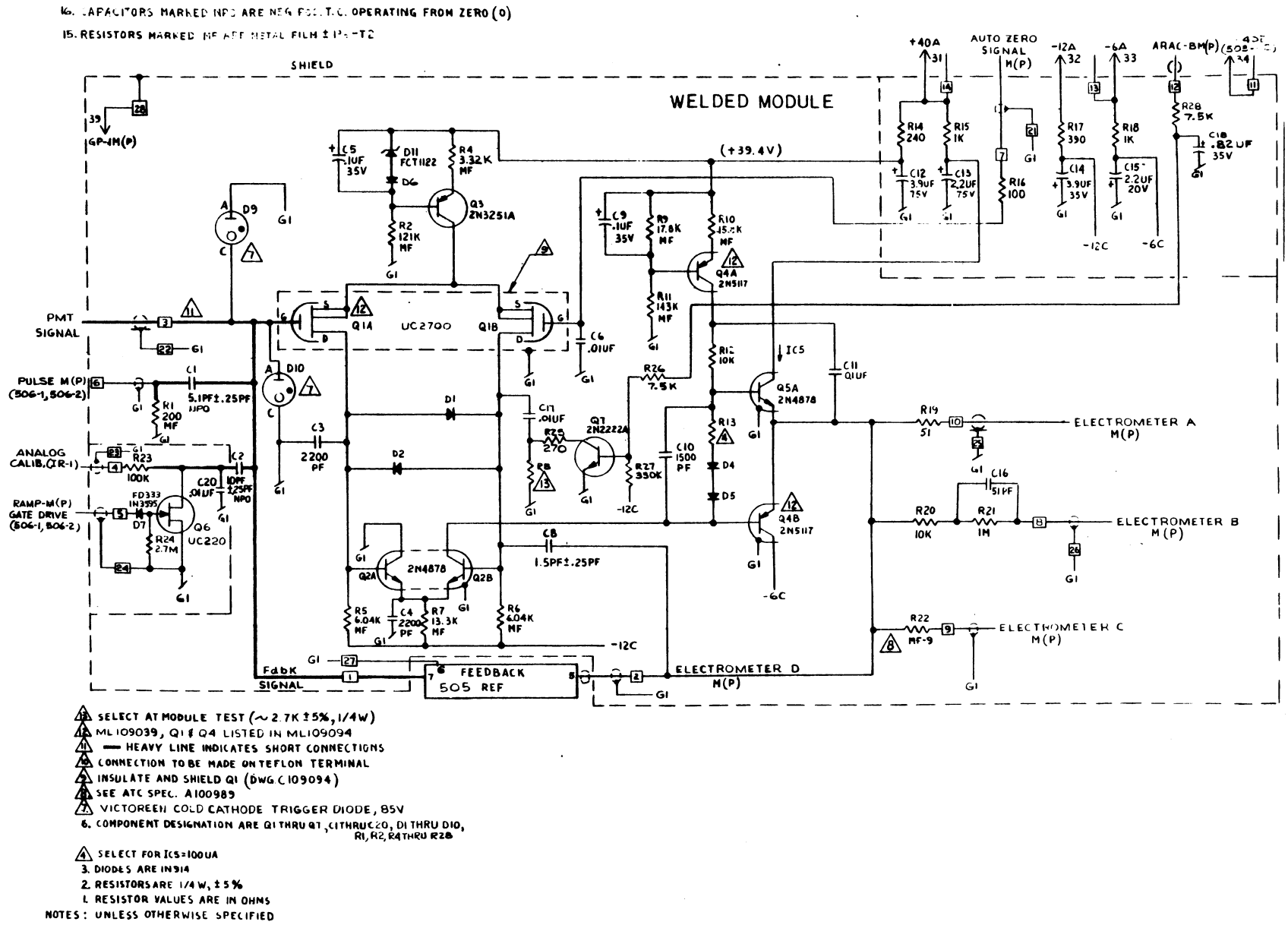

6. CAPACITORS MARKED NPO ARE NEG. P.P.M. T.C. OPERATING FROM ZERO (0)
15. RESISTORS MARKED MF ARE METAL FILM ± 1% -T2

△16 SELECT AT MODULE TEST (~2.7K ±5%, 1/4W)
△15 ML109039, Q1 & Q4 LISTED IN ML109094
△14 — HEAVY LINE INDICATES SHORT CONNECTIONS
△13 CONNECTION TO BE MADE ON TEFLON TERMINAL
△12 INSULATE AND SHIELD Q1 (DWG C109094)
△11 SEE ATC SPEC. A100989
△7 VICTOREEN COLD CATHODE TRIGGER DIODE, 85V
6. COMPONENT DESIGNATION ARE Q1 THRU Q7, C1 THRU C20, D1 THRU D10, R1, R2, R4 THRU R28

△4 SELECT FOR ICS=100UA
3. DIODES ARE IN914
2. RESISTORS ARE 1/4W, ±5%
1. RESISTOR VALUES ARE IN OHMS
NOTES: UNLESS OTHERWISE SPECIFIED

Figure 5-2. Electrometer 501, 502, Schematic Diagram

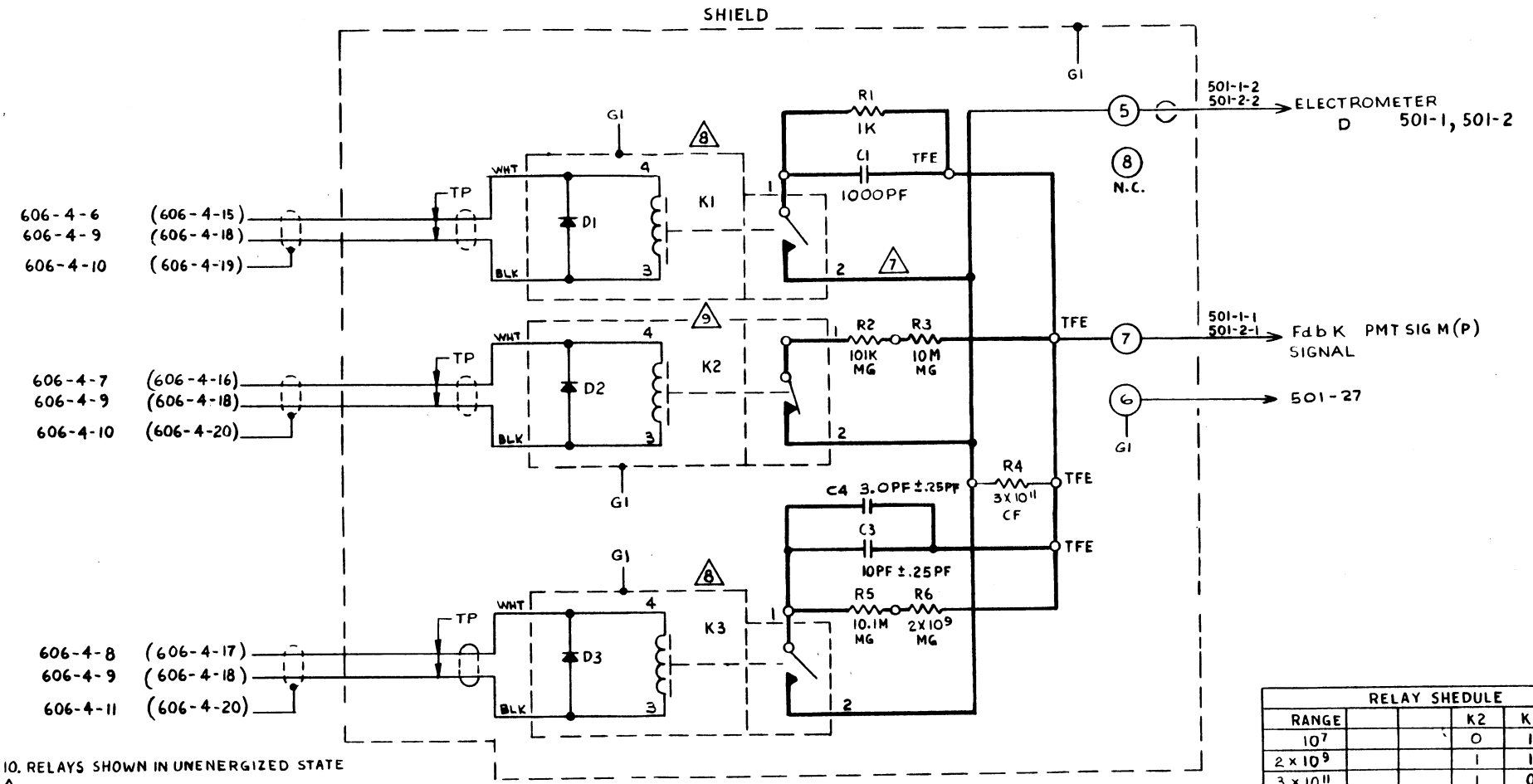

RELAY SHEDULE				
RANGE			K2	K3
10^7			0	1
2×10^9			1	1
3×10^{11}			1	0
10^7 + C			0	1
ARS RESET			0	1

"1" = ENERGIZED
"0" = UNENERGIZED

10. RELAYS SHOWN IN UNENERGIZED STATE
9. ELEC-TROL NO. 2106-2 SCREENED VERSION NO. R2108-2
8. ELEC-TROL NO. 2105-2 SCREENED VERSION NO. R2107-2
7. — HEAVY LINES INDICATES SHORT CONNECTIONS
6. MATERIAL LIST ML 109074
5. COMPONENT DESIGATIONS USED RITHRUR6, D1, D2, D3, K1, K2, K3, C1, C2, C3, C4
4. HEAVY LINES INDICATE SHORT CONNECTIONS
3. DIODES ARE IN3722 INCLUDED IN ELECTROL PART
2. RESISTORS ARE 1/8 W, ± 5%
1. RESISTOR VALUES ARE IN OHMS

NOTES: UNLESS OTHERWISE SPECIFIED

Figure 5-4. ARS Relays and Electrometer Feedback (505-1, 505-2) Schematic Diagram

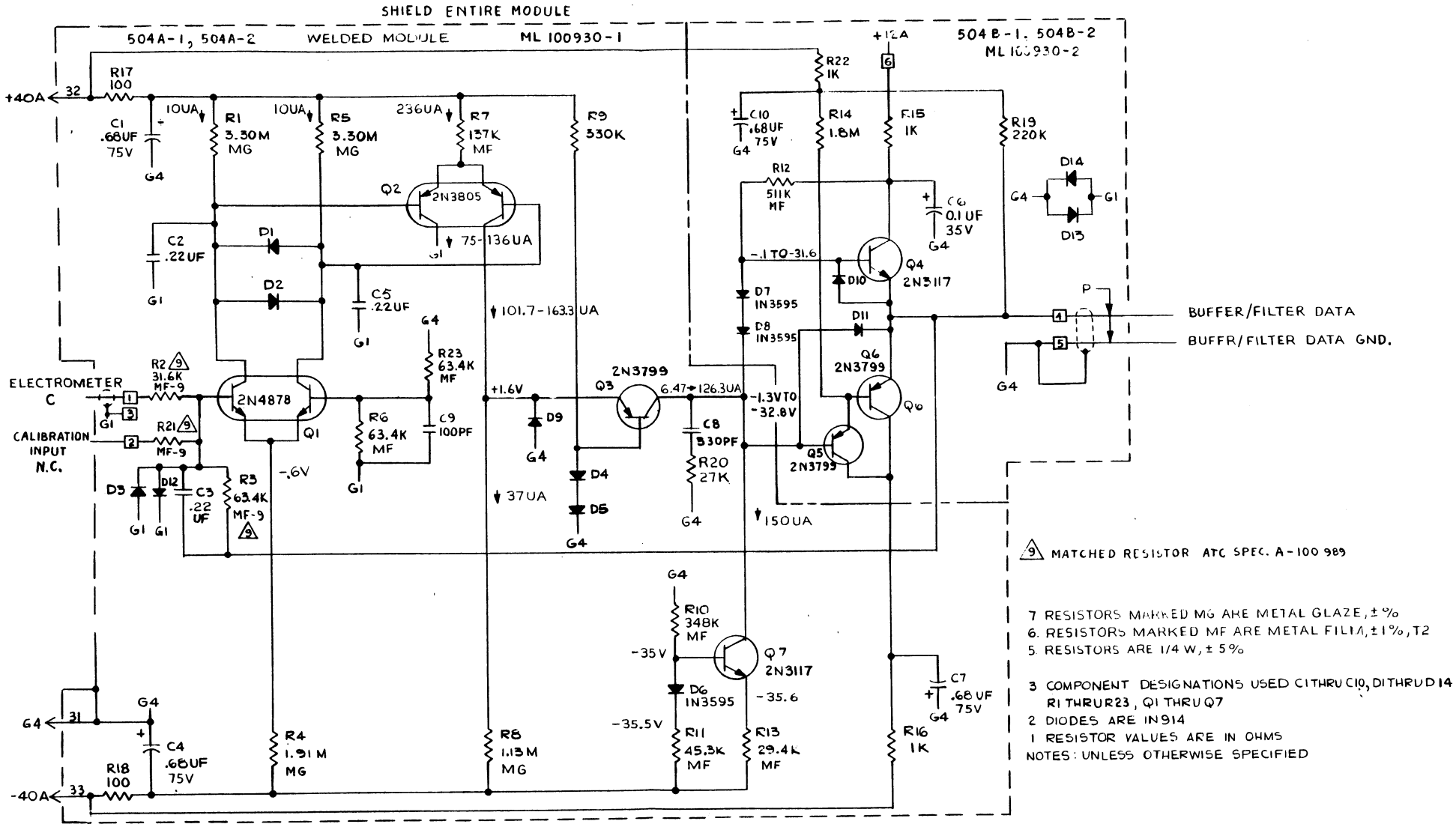

Figure 5-5. Log ADC Buffer and Filter (504-1, 504-2) Schematic Diagram

5.3.2.2 Exponential Time Base Generator (Figure 5-6)

This circuit provides the rising or positive exponential waveform used as the basis for comparing reference and signal voltages. During the conversion period, a 36 volt exponential waveform is generated with the actual conversion beginning when this waveform crosses the 100 millivolt level as detected by the 100 millivolt comparator.

5.3.2.3 Precision Millivolt Source (Figure 5-7)

The precision millivolt source provides a 93.5 millivolt output as the level at which the exponential waveform starts. The precision millivolt source also provides a 100 millivolt output to the 100 millivolt comparator, which is the point at which the conversion period begins.

5.3.2.4 100 Millivolt Comparator and Signal Comparator (Figures 5-8 and 5-9)

The 100 millivolt comparator senses the point in time at which the exponential waveform reaches 100 millivolts. At this time the comparator provides a positive-going signal to the pulse shaping logic.

The signal comparator senses the point in time at which the exponential waveform equals the buffer output voltage, and provides a negative-going level to the pulse shaping logic.

5.3.2.5 Pulse Shaping Logic

The pulse shaping logic receives the signals from the 100 millivolt comparator and the signal comparator in addition to the 1.05 millisecond conversion gate. The output of the pulse shaping logic is a square pulse, the width of which is directly proportional to the natural logarithm of the electrometer output voltage. Figure 5-10 shows a typical waveform timing relationship.

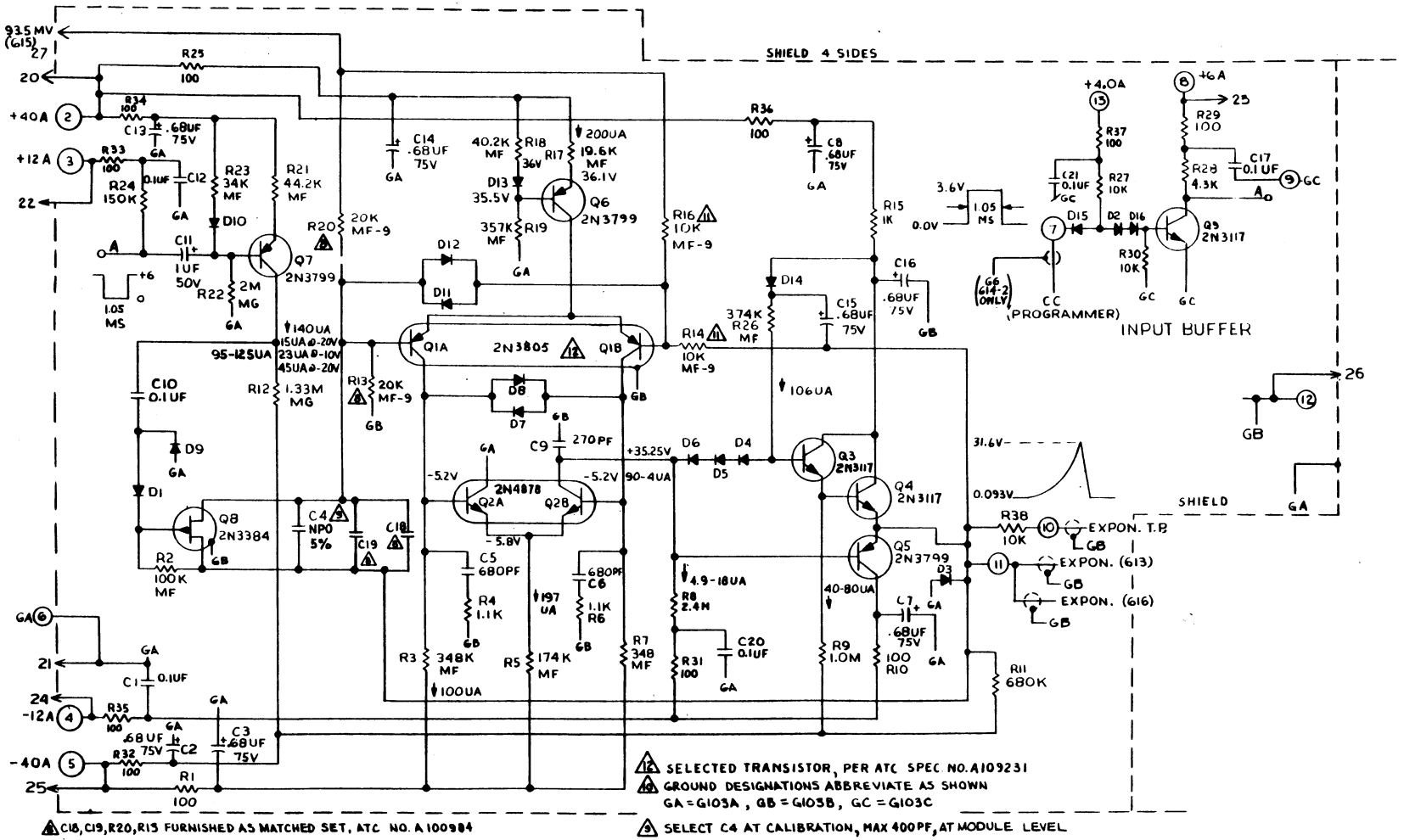

Figure 5-6. Exponential Time Base Generator, Schematic Diagram

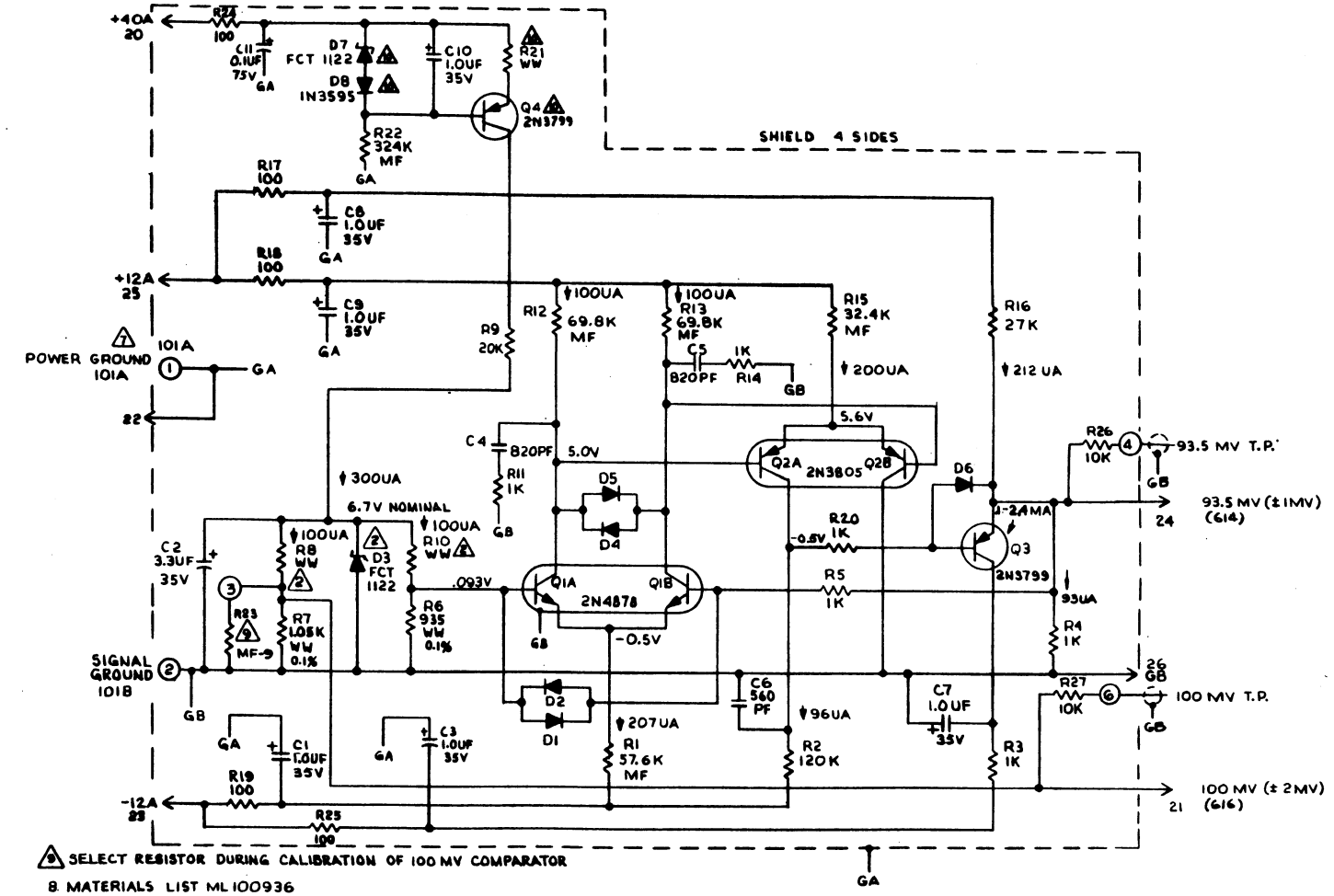

9 SELECT RESISTOR DURING CALIBRATION OF 100 MV COMPARATOR

8 MATERIALS LIST ML 100936

7 COMPONENT DESIGNATIONS USED C1 THRU C11, D1 THRU D8, R1 THRU R27, Q1 THRU Q4

6 RESISTOR MARKED MF ARE METAL FILM, ±1% T2.

5 RESISTORS ARE 1/4 W, ± 5%

4 RESISTORS ARE IN OHMS

3 GROUND DESIGNATIONS ABBREVIATE AS SHOWN
GA=G101A, GB=G101B

2 DIODE -RESISTOR NETWORK A109003

1. DIODES ARE IN914

NOTES: UNLESS OTHERWISE SPECIFIED

10 DIODE-TRANSISTOR-RESISTOR NETWORK A109006

11. RESISTORS MARKED MG ARE METAL GLAZE ±1%

Figure 5-7. Precision Millivolt Source, Schematic Diagram

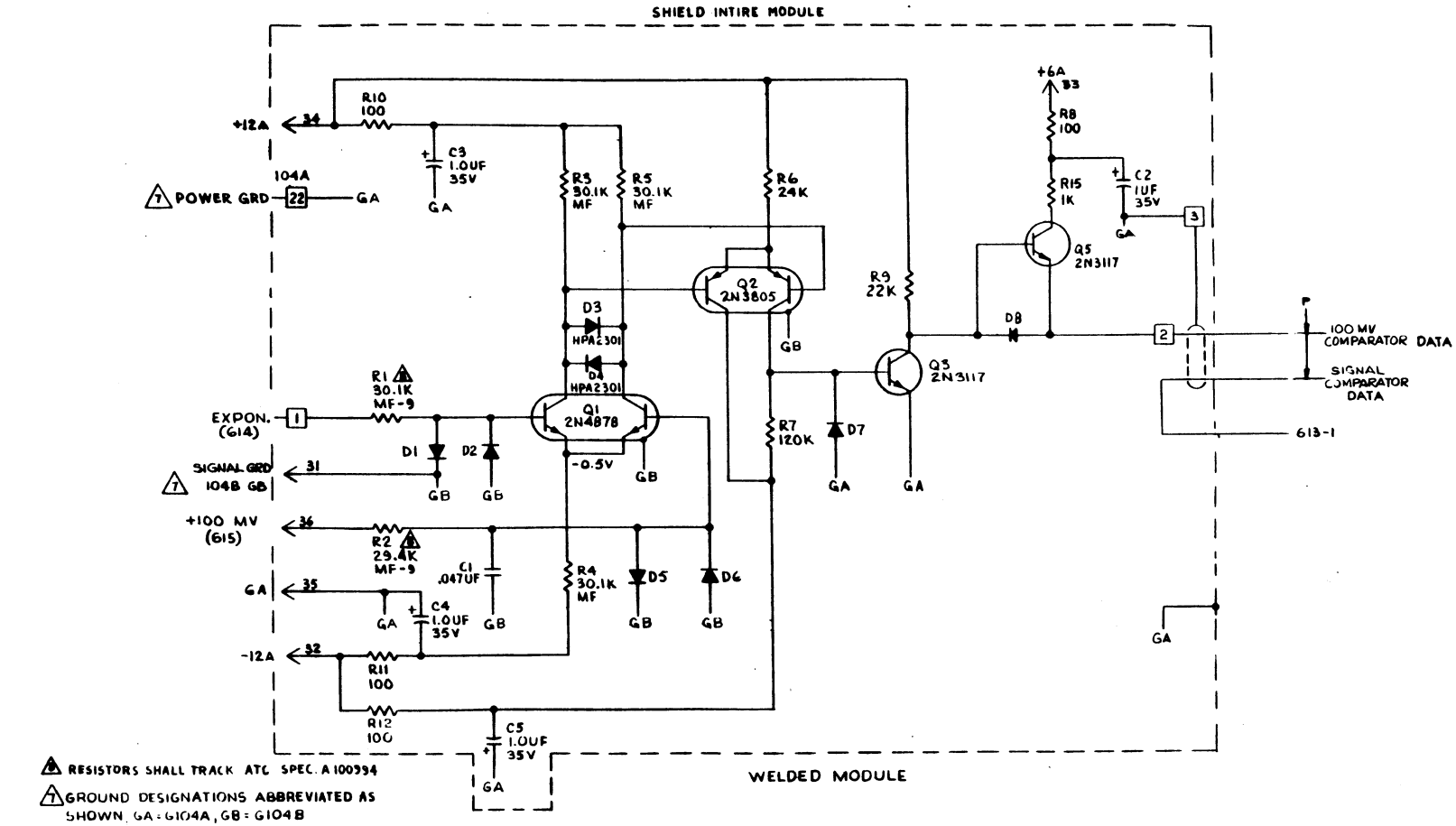

⚠ RESISTORS SHALL TRACK ATC SPEC. A100994

⚠ GROUND DESIGNATIONS ABBREVIATED AS SHOWN. GA = G104A, GB = G104B

6. RESISTORS MARKED MF ARE METAL FILM ±1%
5. MATERIALS LIST ML100938
4. COMPONENT DESIGNATION USED: Q1, Q2, Q3, Q5 D1 THRU D8, C1 THRU C5, R1 THRU R12, R15
3. DIODES ARE IN914
2. RESISTORS ARE 1/4W, ±5%
1. RESISTOR VALUES ARE IN OHMS

NOTES: UNLESS OTHERWISE SPECIFIED

Figure 5-8. 100-Millivolt Comparator, Schematic Diagram

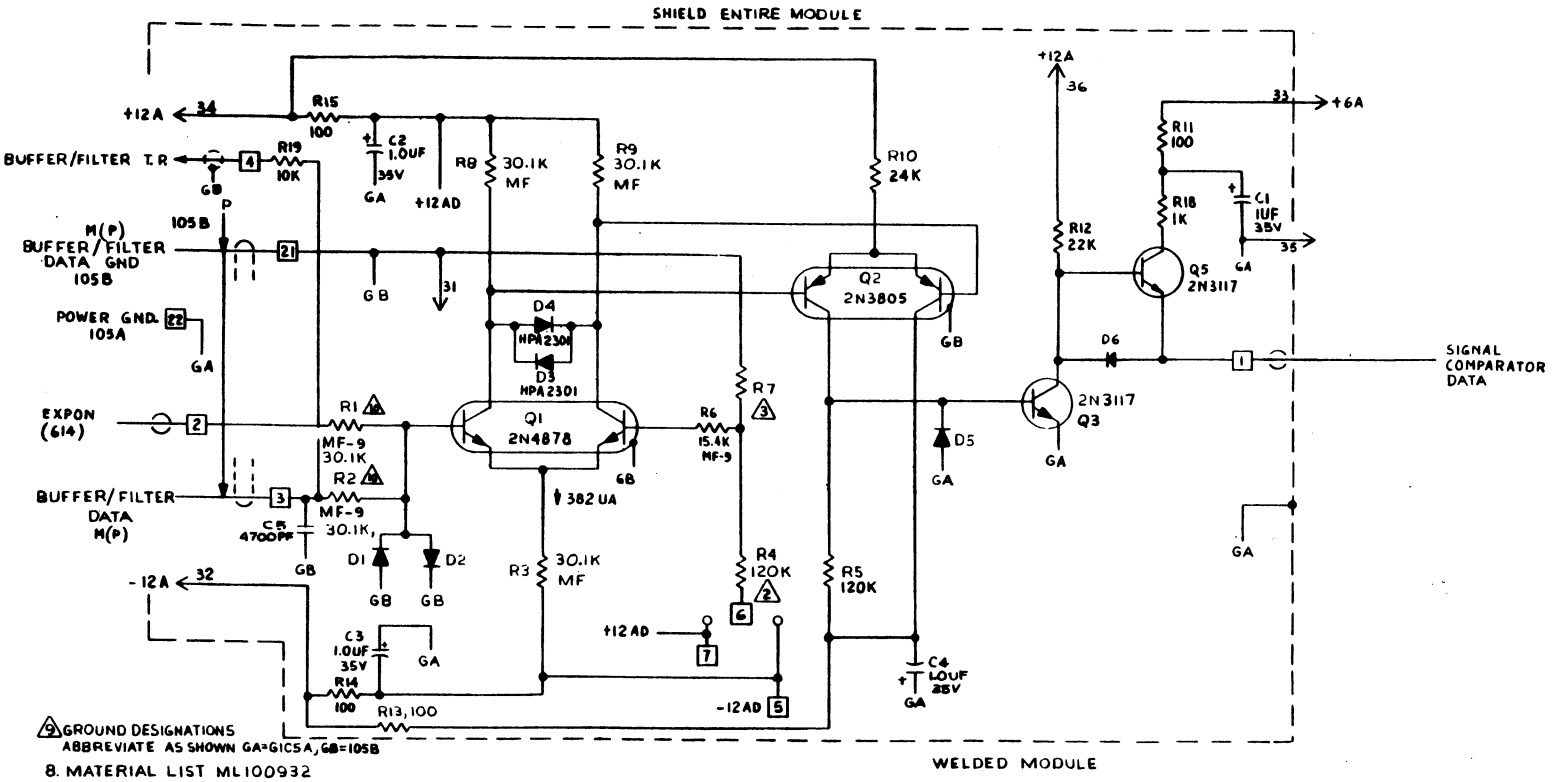

8. MATERIAL LIST ML100932

7 COMPONENT DESIGNATIONS USED D1 THRU D6, R1 THRU R15, R18, R19, C1 THRU C5, Q1, Q2, Q3, Q5

6. RESISTORS MARKED MF ARE METAL FILM ± 1%, T2

5. RESISTORS ARE 1/4 W, ± 5%

4. RESISTORS ARE IN OHMS

3 SELECT R7 AT CALIBRATION $0 \leq R7 \leq 33\Omega$

2 SELECT +12V OR -12V AT CALIBRATION

1. DIODES ARE IN914

NOTES: UNLESS OTHERWISE SPECIFIED

10 MATCHED RESISTORS ATC SPEC. A100999

11 JUMPER PINS 34 & 36 DURING TEST

Figure 5-9. Signal Comparator, Schematic Diagram

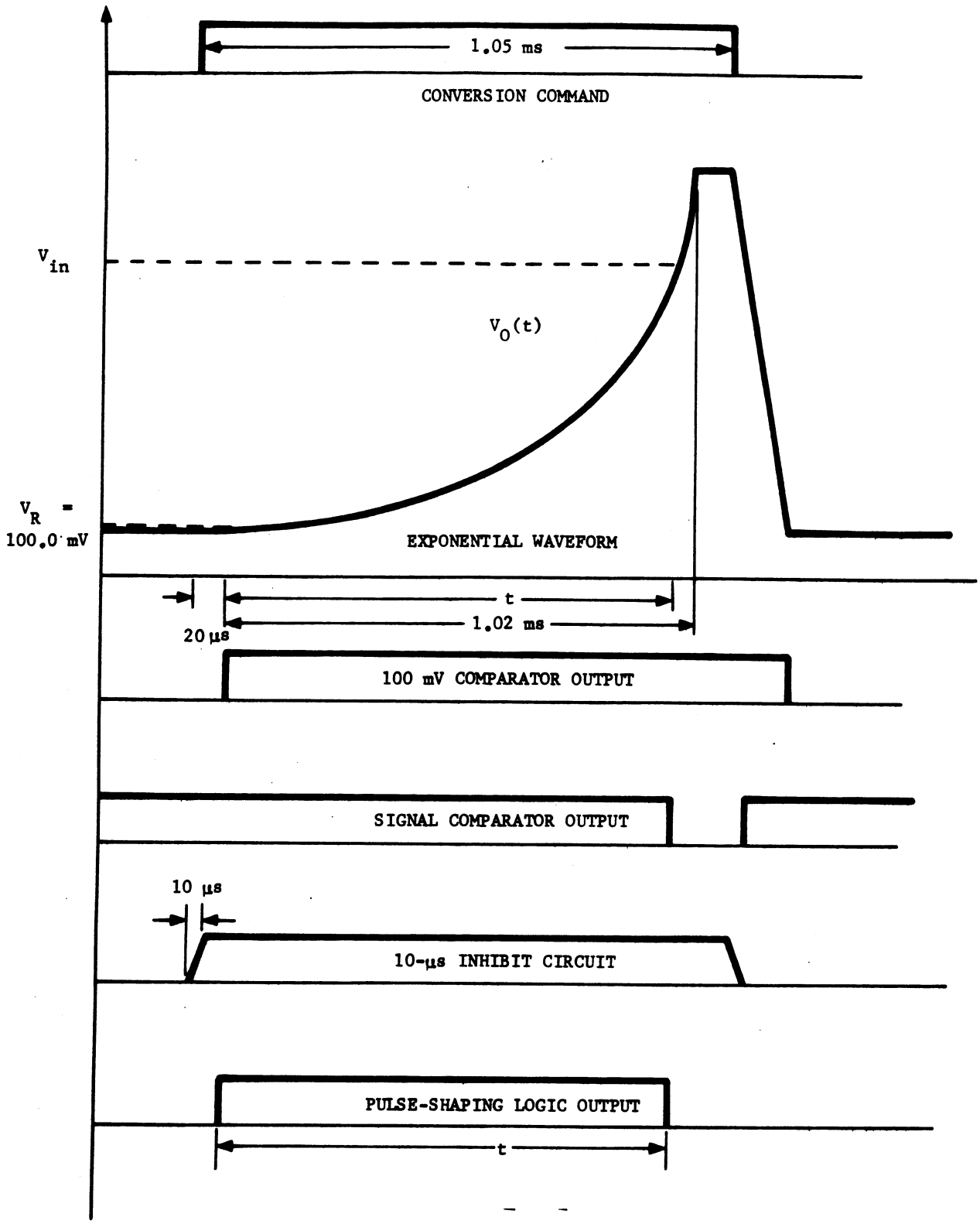

Figure 5-10. Timing Sequence

5.3.2.6 Logarithmic ADC Output Logic (Figure 5-11)

The logarithmic analog-to-digital data output accumulator consists of an 8 bit binary counter and a scaler to divide the four megahertz clock frequency by 16. Two additional bits of electrometer range information are inserted at the output of the accumulator. After the conversion is completed, the accumulator counting gates are inhibited and the accumulated count transferred to an output shift register. The VIP C pulses can then cause the transfer of data into the VIP through the data output buffer at the appropriate time. The divide by 16 scaler contributes a quantization uncertainty of 1/16 of a bit at the beginning of the conversion and a full bit uncertainty at the end of the conversion. Thus, the converted number could be 1-1/16 larger, or 17/32 bits on the average. A block diagram of the log ADC and the associated circuits is shown in Figure 5-12.

5.3.3 Pulse Counting

Pulse counting operation occurs during the PMT high gain mode only and provides accurate performance for anode pulse count rate up to 1 megahertz per second.

There are two identical pulse counting chains in the BUV, one for each channel. A block diagram is given in Figure 5-13. The amplification and shaping circuits (Figure 5-14) between the electrometer and the discriminators amplify the photoelectron pulses, preserving the shape and amplitude information to permit accurate discrimination against electrometer noise at the lower level and spurious pulses at the higher level. Discriminator levels are set at 150 millivolts for the low level and 4.0 volts for the high level. The lower level, while sufficiently high to produce negligible noise counting rates, is also low

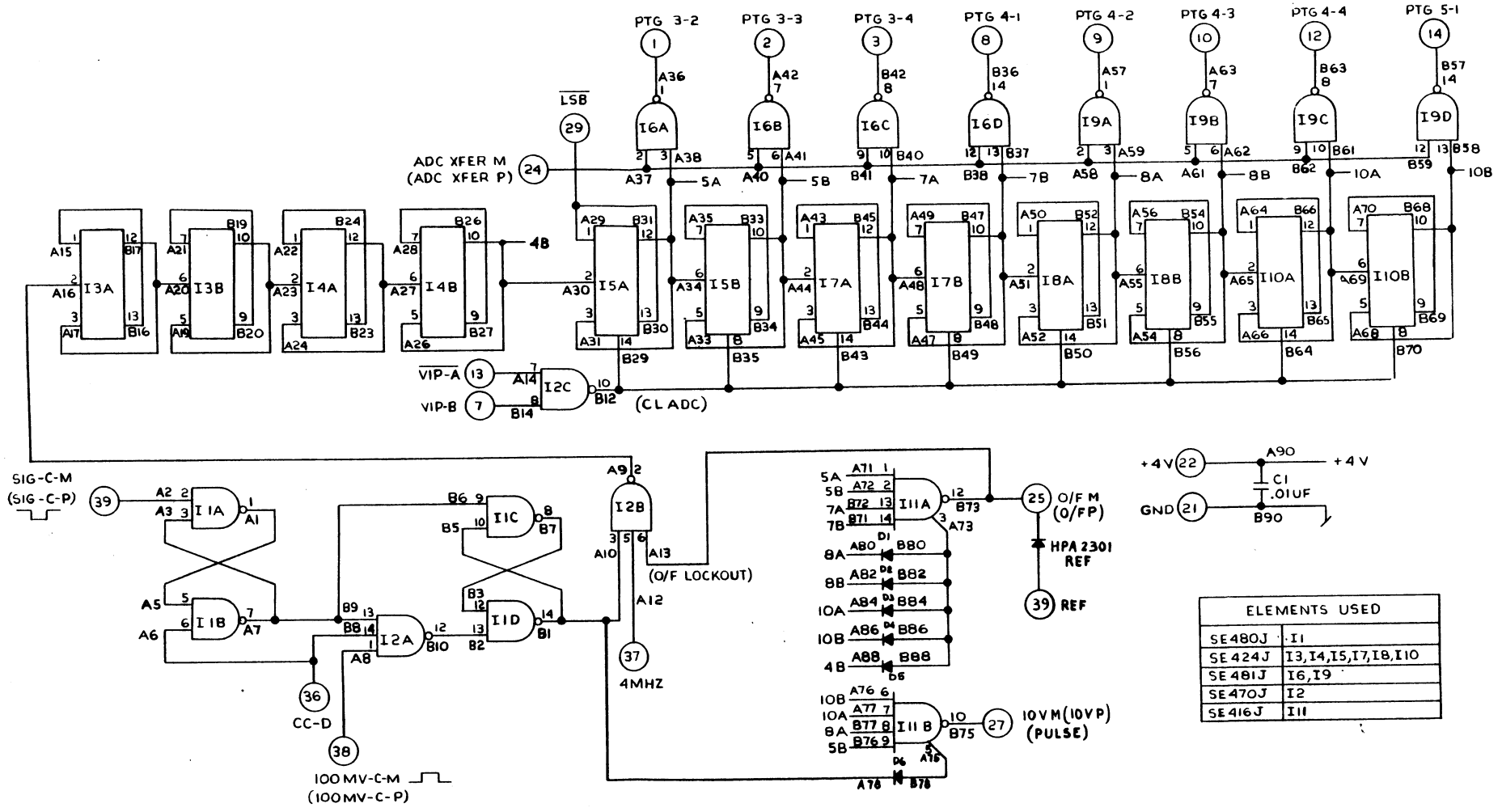

Figure 5-11. ADC Counter 110 (M) and 109 (P), Logic Diagram

3. PINS USED 20
2. MATERIAL LIST ML 109017
1. LOGIC SYMBOLS PER ATC D10000

NOTES: UNLESS OTHERWISE SPECIFIED

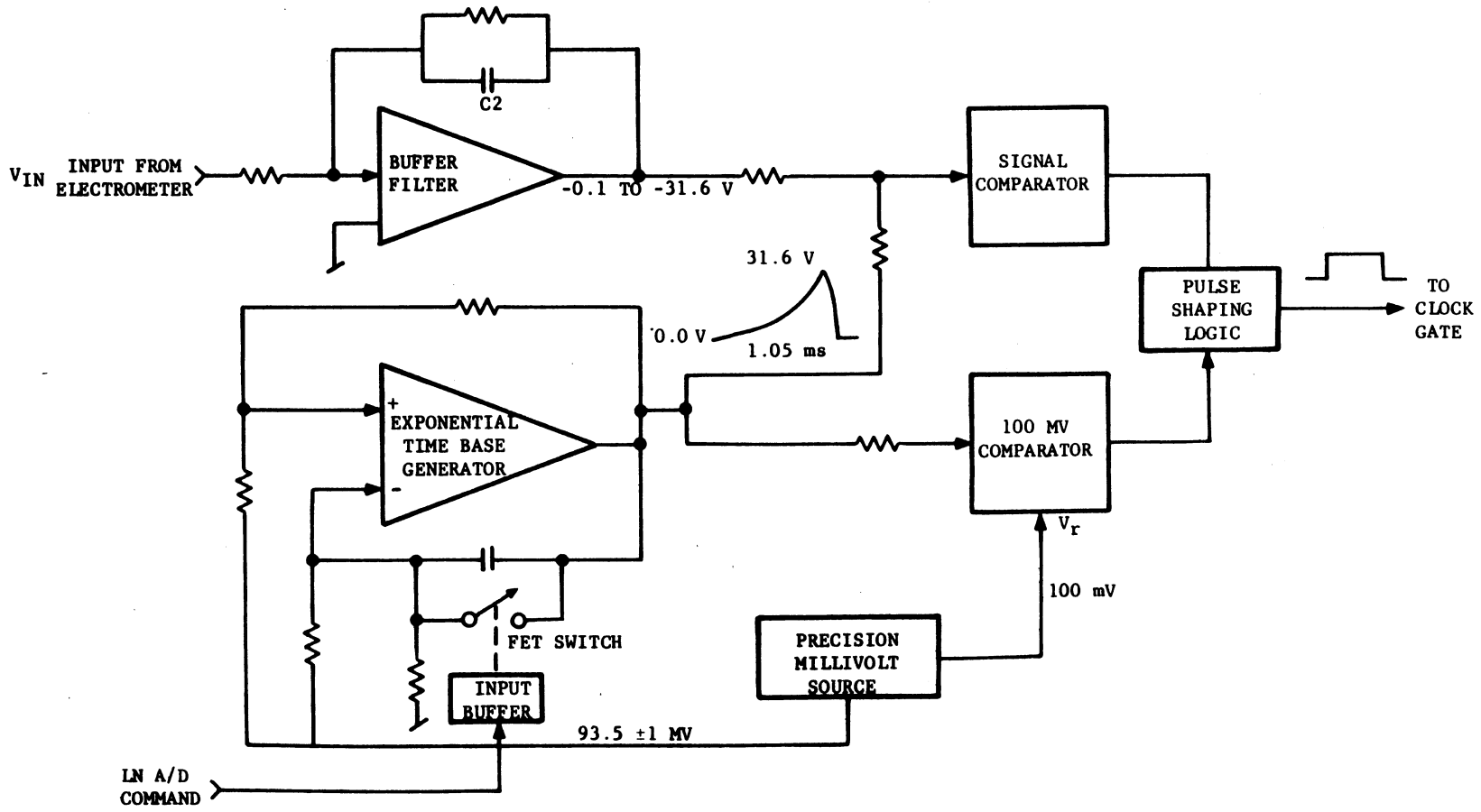

Figure 5-12. Logarithmic Analog-to-Digital Converter

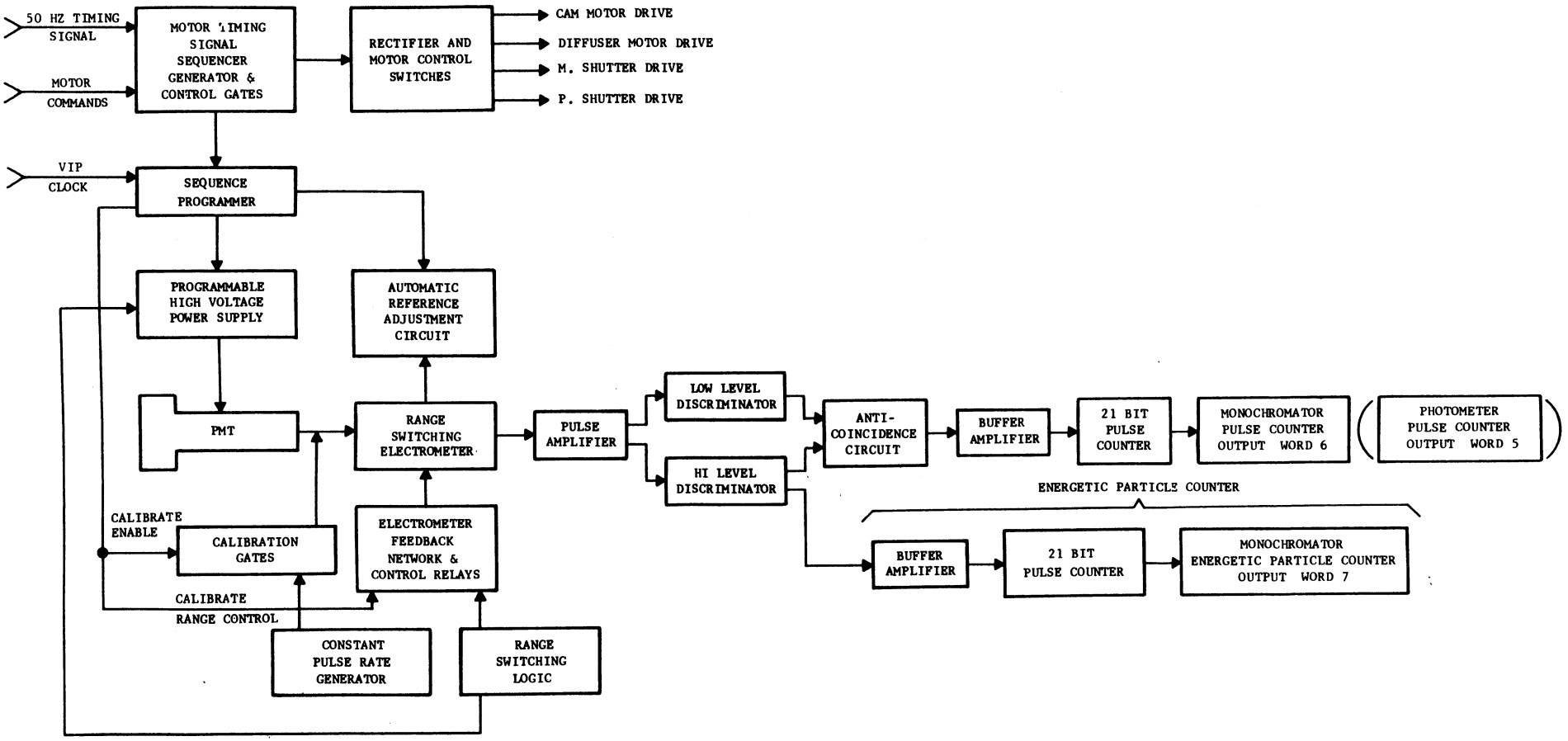

Figure 5-13. BUV Pulse Counting System

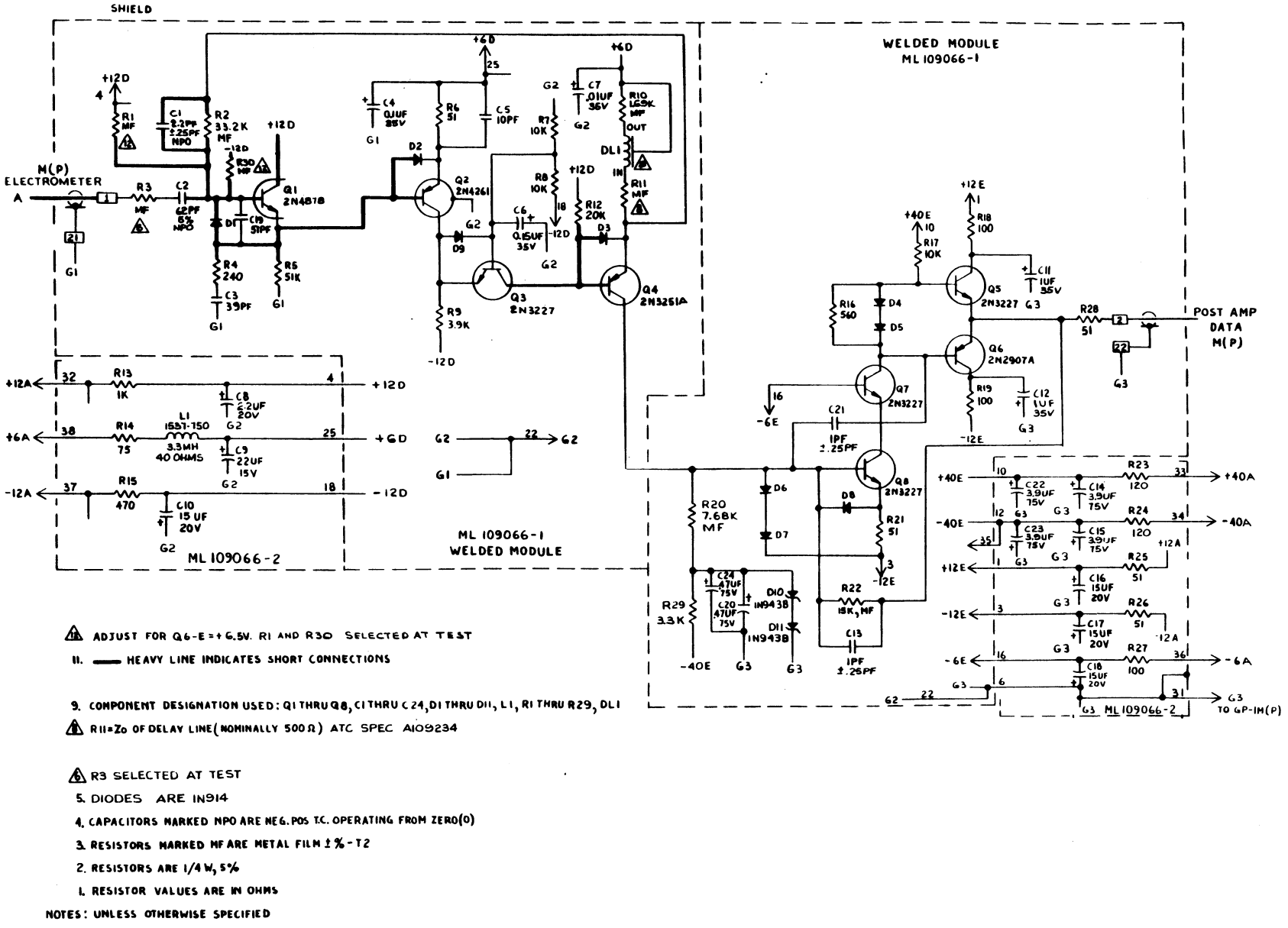

Figure 5-14. Pulse Amplifier 503-1, 503-2, Schematic Diagram

enough to pass a major portion of photoelectron pulses. The upper level similarly passes most single photoelectrons while excluding multiple photoelectrons on the order of 10 or more.

To make accurate counting rate measurements in systems with a dead time comparable to the average count rate period, the dead time must be accurately known and not vary as the function of pulse rate. The measured and true rates are related as follows:

$$R_T = \frac{R_M}{1 - R_M T_D}$$

where R_T = true rate,

R_M = measured rate,

T_D = dead time.

The discriminator circuits are shown in Figure 5-15. They are designed to accurately fix the dead time at approximately 1 microsecond independent of counting rates. (Refer to detailed specification, Section II, Paragraph 2.3, for the actual measured T_D of each channel.)

High energy particle pulses are rejected by examining the output of the low level discriminator (Figure 5-16) within the period of the high level discriminator (Figure 5-17). With an output from the low-level discriminator and none from the high-level discriminator, the input is assumed to be from a single photoelectron, and is sent on to the data accumulator register. If outputs exist simultaneously from both discriminators, it is assumed that a high energy particle generated this pulse and the results are not passed to the data register, but instead accumulated in a separate high energy particle counting register. Figure 5-18 is a schematic of the anti-coincidence circuit.

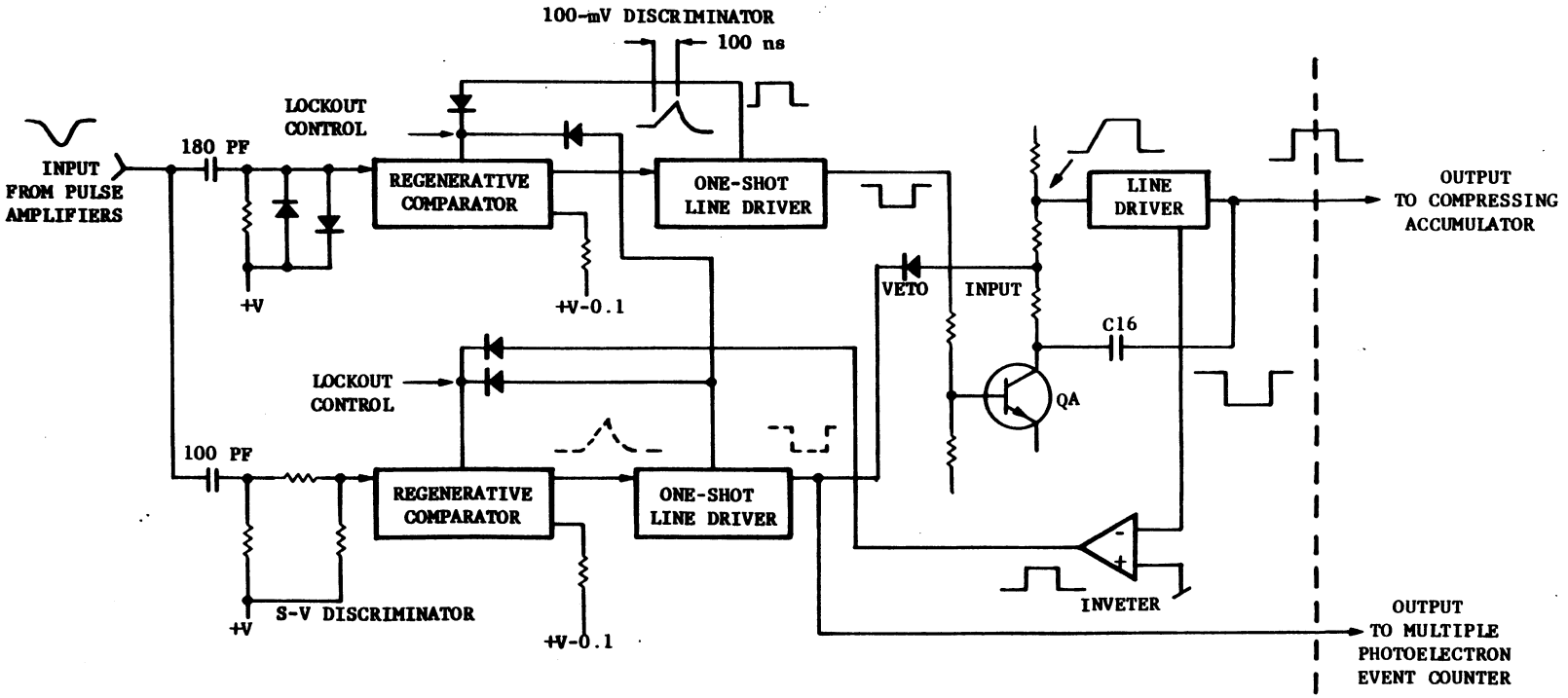

Figure 5-15. Discriminator-Anticoincidence Circuits

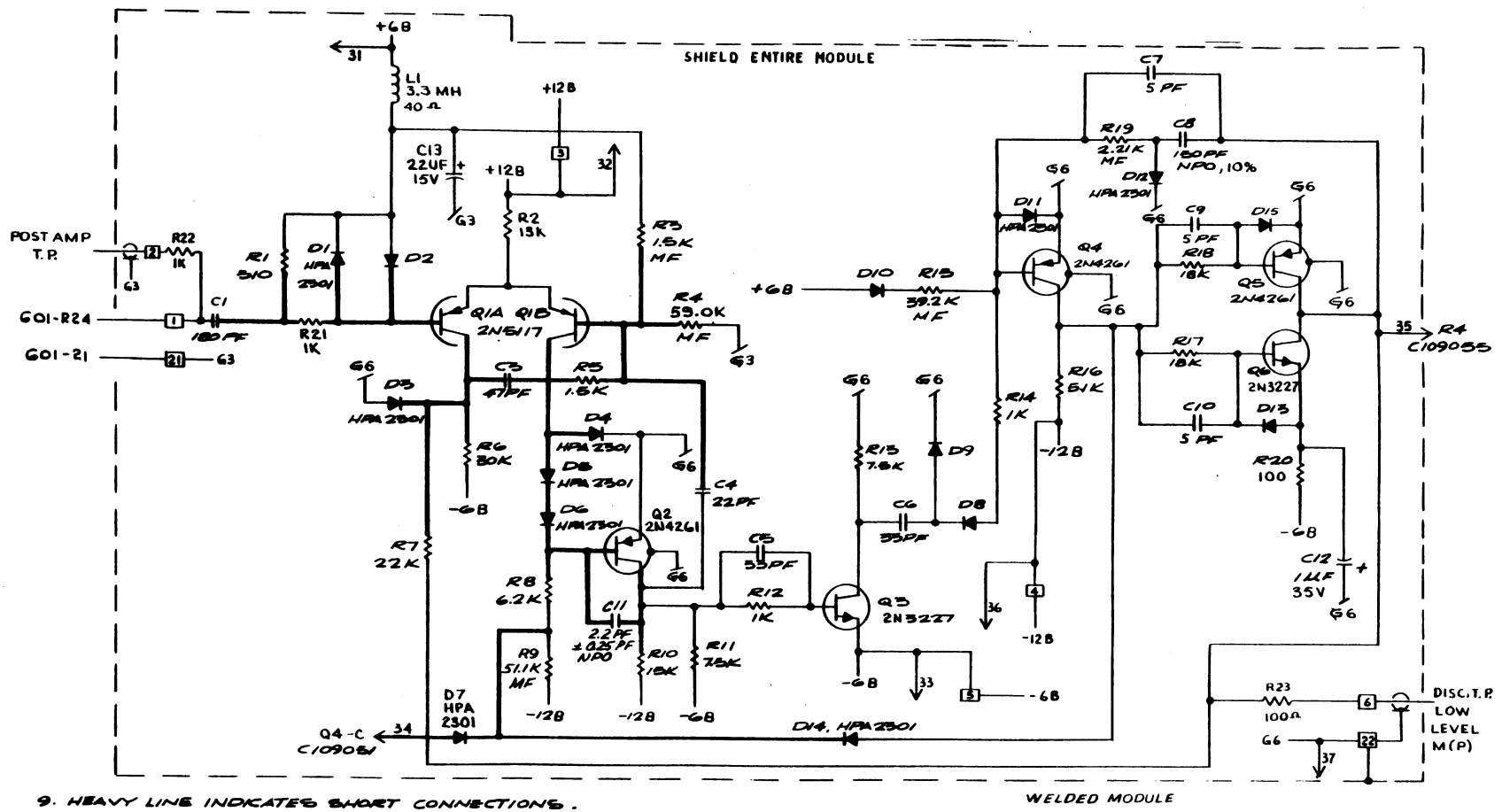

9. HEAVY LINE INDICATES SHORT CONNECTIONS.
8. CAPACITORS MARKED NPO ARE NEG POS T.C. OPERATING FROM ZERO (0).
7. RESISTORS MARKED MF ARE METAL FILM ±1%-T2.
6. COMPONENT DESIGNATIONS USED: R1 THRU R23 C1, C3 THRU C13, D1 THRU D15, Q1 THRU Q6, L1
5. ML 109052
3. DIODES ARE IN914.
2. RESISTORS ARE 1/4 W, ±5%
1. RESISTOR VALUES ARE OHMS.

NOTES: UNLESS OTHERWISE SPECIFIED

Figure 5-16. Low-Level Discriminator, Schematic Diagram

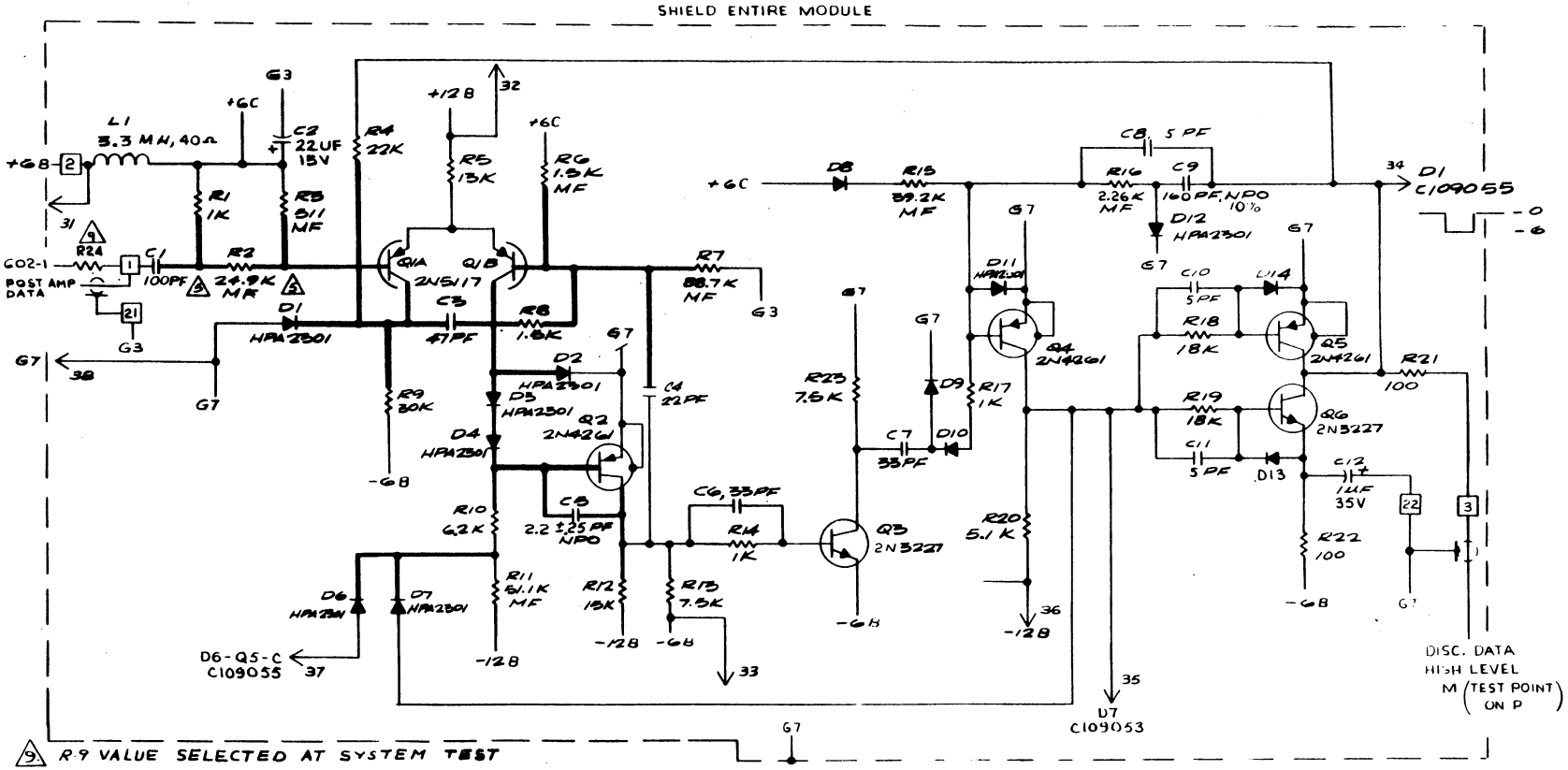

⚠9 R9 VALUE SELECTED AT SYSTEM TEST

8. REGISTORS MARKED MF ARE METAL FILM ± 1% -T2.
7. HEAVY LINES INDICATE SHORT CONNECTIONS.
6. CAPACITORS MARKED NPO ARE NEG POS T.C OPERATING FROM ZERO (0).

⚠5 THESE POINTS TO BE ISOLATED (NON-ADJACENT).

4. COMPONENT DESIGNATIONS USED: R1 THRU R24 C1 THRU C12, D1 THRU D14, Q1 THRU Q6, L1 NOT USED D5
3. DIODES ARE IN914.
2. RESISTOR ARE 1/4 W, 5%
1. RESISTOR VALUES ARE IN OHMS.

NOTES: UNLESS OTHERWISE SPECIFIED.

Figure 5-17. High-Level Discriminator, Schematic Diagram

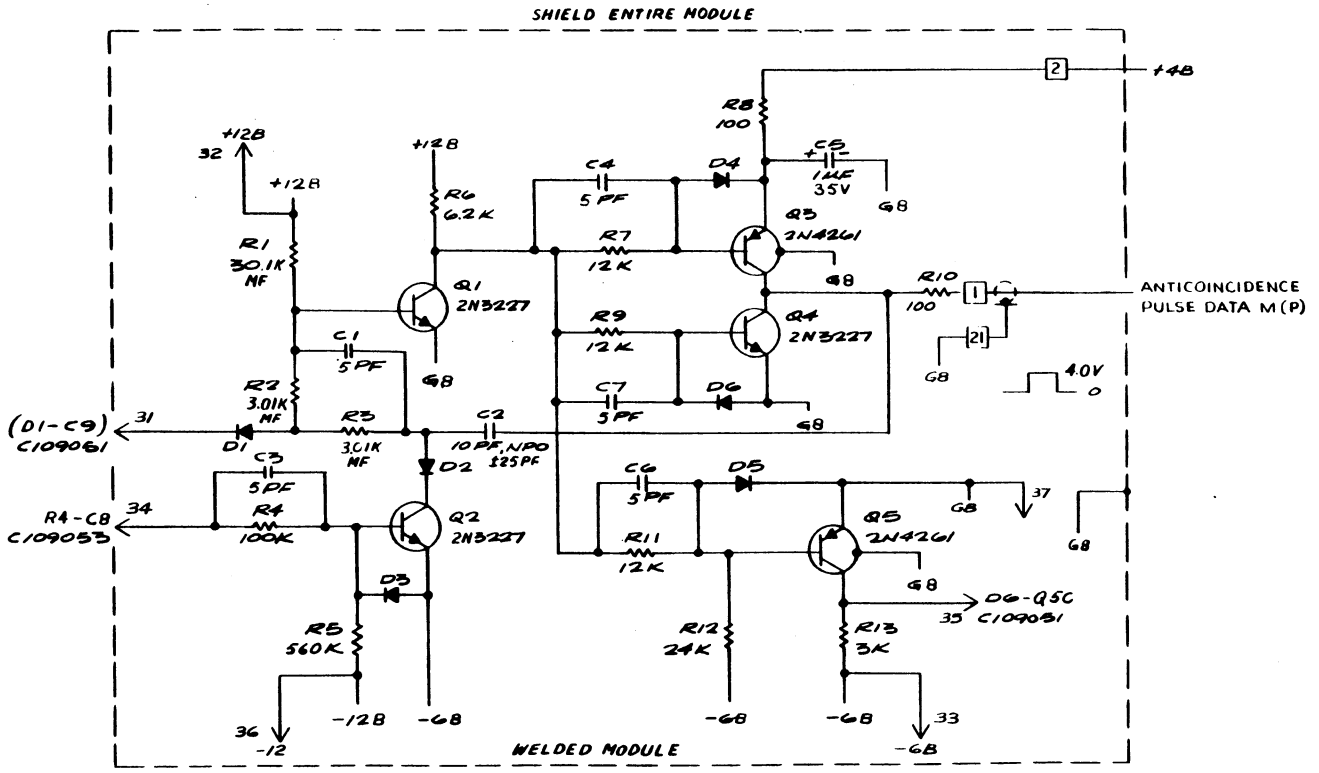

6. CAPACITORS MARKED NPO ARE NEG POS T.C. OPERATING FROM ZERO (0).
5. COMPONENT DESIGNATIONS USED: R1 THRU R13, C1 THRU C7 D1 THRU D6, Q1 THRU Q5.
4. MLC109054
3. DIODES ARE IN914.
2. RESISTORS ARE 1/4W, 5%.
1. RESISTOR VALUES ARE IN OHMS.

NOTES: UNLESS OTHERWISE SPECIFIED.

Figure 5-18. Anticoincidence Circuit, Schematic Diagram

5.3.4 Automatic Ranging

The automatic range sequencer (ARS) uses relays to change the electrometer feedback network, preventing over-scale or under-scale operations. This circuit also provides status information to the sequencer and controls the photomultiplier tube gain by changing high voltage level.

The ARS interfaces with the following circuits:

- o Electrometer
- o High voltage power supply
- o Sequencer.

The functional relationship of these circuits to the ARS is shown in Figure 5-19.

The ARS consists of control logic, relay driver programming logic, and two identical logic modules for individual control of the photometer and monochromator channels. These modules, with inputs from the programmer and the logarithmic analog-to-digital converter provide complete control of photomultiplier and electrometer gain plus protection for the photomultiplier tubes in the event of an overload condition (an anode current exceeding 1 microampere).

The signal level from the electrometer falls within a range of zero to 31.6 volts. Table 5-1 indicates the operating limits and constraints of the output voltage.

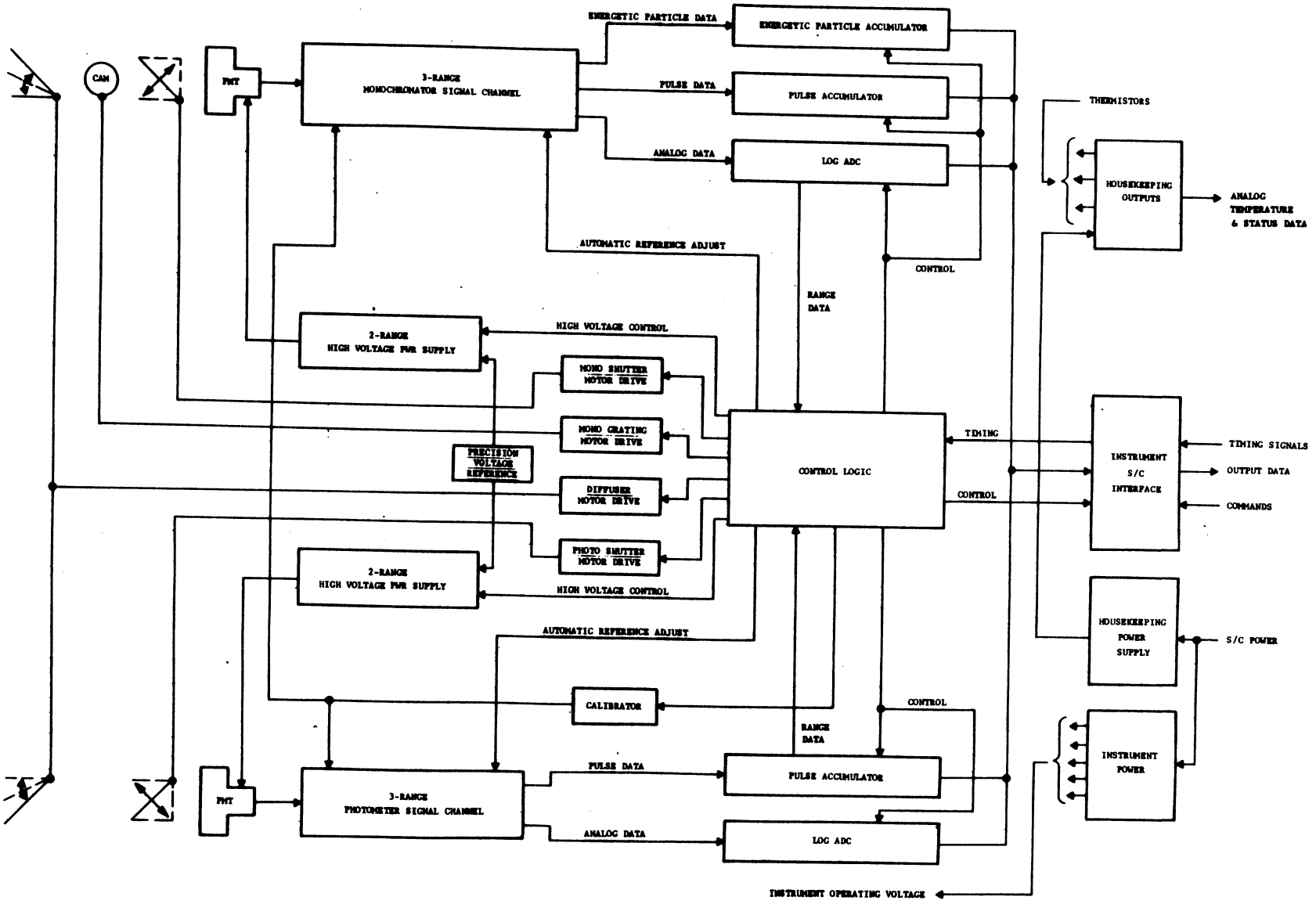

Figure 5-19. BUV Instrument, Simplified Functional Block Diagram

TABLE 5-1. ELECTROMETER RANGES AND SIGNAL LEVELS

Range	Signal Levels
$R_f = 10^7\ \Omega$; $C_f = 10$ pF; $G_{PMT} = 2 \times 10^6$	0 to 10 V
$R_f = 10^7\ \Omega$; $C_f = 10$ pF; $G_{PMT} = \begin{matrix} 80\ (P) \\ 1350\ (M) \end{matrix}$	0.1 V to 10.0 V
$R_f = 2 \times 10^9\ \Omega$; $C_f = 10$ pF; $G_{PMT} = \begin{matrix} 80\ (P) \\ 1350\ (M) \end{matrix}$	0.1 V to 31.6 V
$R_f = 3 \times 10^{10}\ \Omega$; $C_f = 0$ pF; $G_{PMT} = \begin{matrix} 80\ (P) \\ 1350\ (M) \end{matrix}$	0.1 V to 31.6 V

NOTE: PMT Gains Nominal Only -- Refer to paragraph 2.2.3 for actual gains.

When the levels indicated in Table 5-1 are exceeded, the ARS reduces the overall gain of the signal channel. If the system is in the high gain or pulse counting mode, the ARS reduces the PMT high voltage whenever the signal exceeds the specified level. When the photomultiplier gain is reduced, the electrometer gain is switched to the least sensitive level ($R_F = 10^7$ ohms). The system is then allowed to uprange to obtain an on-scale reading from the analog-to-digital converter.

Besides the normal electrometer signal ranges, an over-scale mode is incorporated. In the presence of a signal that causes the PMT anode current to exceed 1 μa, the high voltage power supply is switched off. The high voltage power supply is then periodically re-energized. When the overload condition no longer exists, the ARS resumes the normal ranging sequence.

5.3.5 High Voltage Power Supplies

The BUV programmable high voltage power supplies are shown functionally in Figure 5-20, and schematically in Figure 5-21. There are two separate identical high voltage systems, one for each photomultiplier channel. The only common element is the precision regulator which supplies the reference voltage to both high voltage supplies.

Each supply consists of a double differential comparator amplifier, a tuned Class C sinewave oscillator with current limiting, and a low ripple voltage quadrupler.

The high voltage control switches driven by the ARS logic provide an interface between the 3/0 electronics module and the input resistors located in the

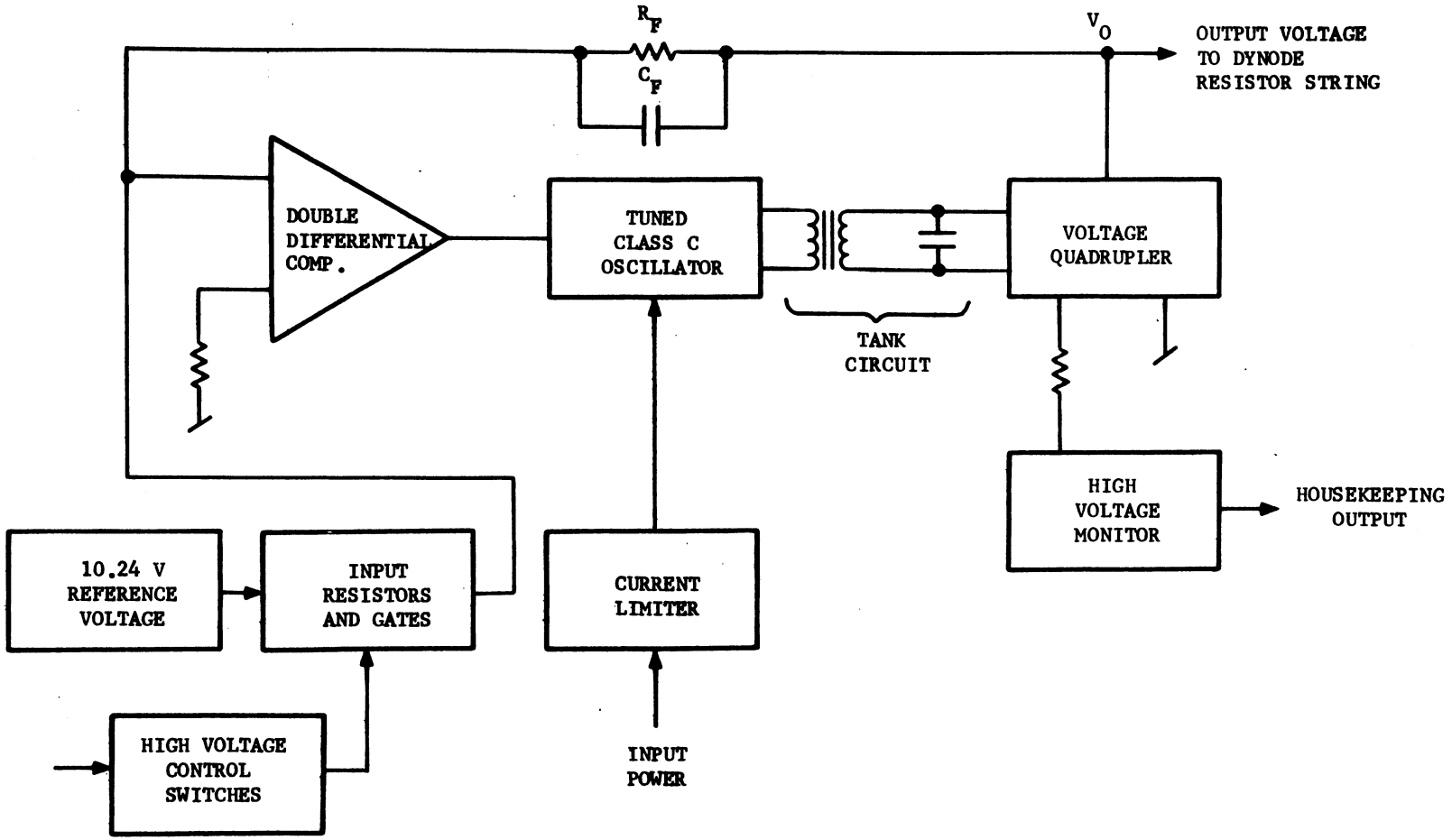

Figure 5-20. Programmable High-Voltage Photomultiplier Supply Block Diagram

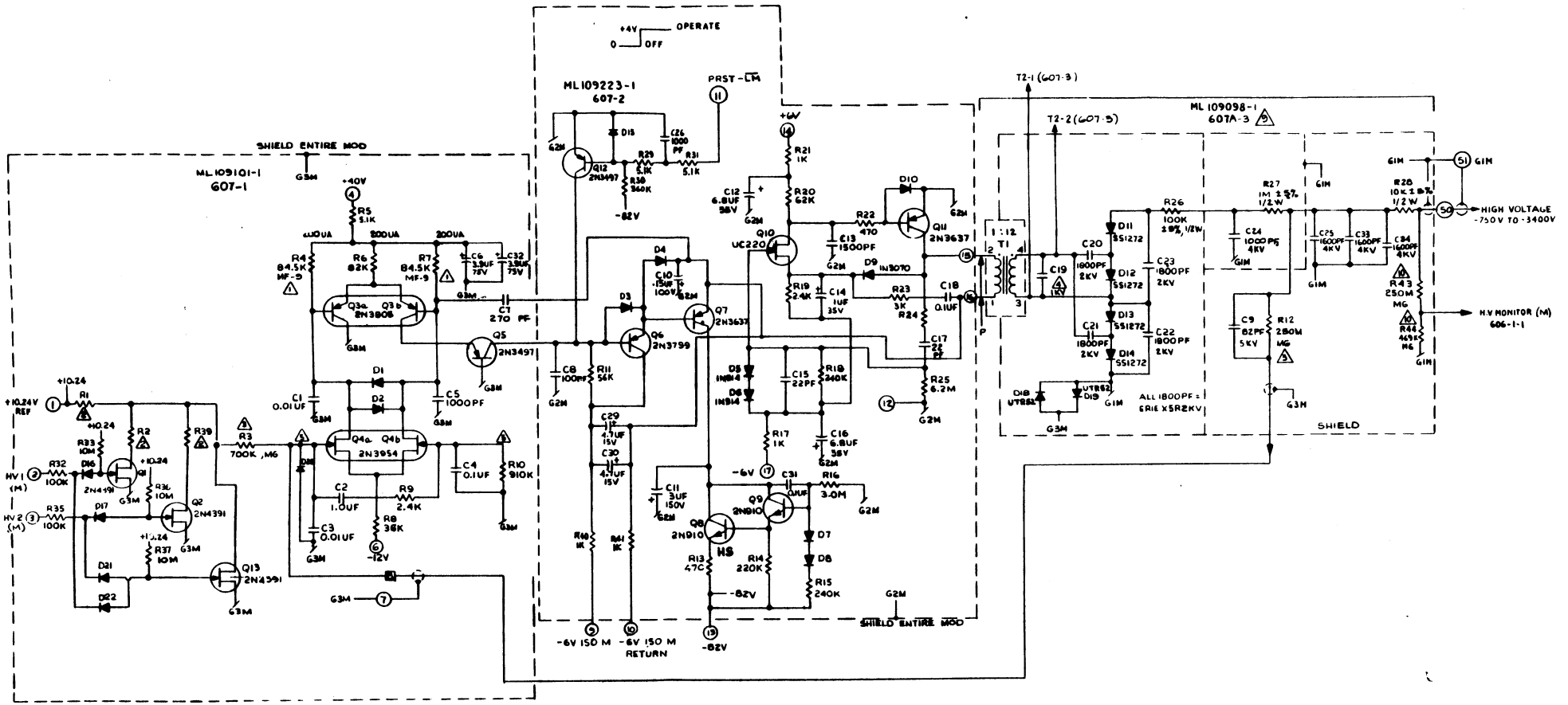

M MATCHED SET ATC A109253

4 SHIELD MOD 607-3 AS SHOWN

8. DELETED

7. COMPONENT DESIGNATIONS USED: R1 THRU R42, D1 THRU D22 Q1 THRU Q13, C1 THRU C32 & T1 NOT USED C27, C28, R34, R38

6. ALL OTHER DIODES FD333 (1N3595)

5 THESE NODES SHALL BE ON TEFLON STANDOFFS

4 TUNING CAPACITOR SELECTED AT ASSEMBLY FOR F_o = 18 KHZ

3 THESE RESISTORS SHALL RATIO WITHIN 0.05% - 10 TO +60°C A109287

2 SELECTED FOR PMT-T9 T.C. R1, R2 AND R39 MUST BE SELECTED AT PMT TEST

1 MATCHED TO 0.1% AT 25°C-T9 T.C. A109288

NOTES: UNLESS OTHERWISE SPECIFIED

12. RESISTORS ARE 1/4W, ±5%

11. RESISTORS VALUES ARE IN OHMS

Figure 5-21. High Voltage Supply - Monochromator, Schematic Diagram

Sensor 3 electronics package. When the correct set of commands is received, a fixed voltage is placed on the input to the double differential stage, setting the level of the high voltage output. The "drop-dead" state occurs when both input signals are true, turning off the high voltage output.

A high voltage monitor is provided which contains the circuitry required to convert the high voltage supply output to the range of 0 to -6.375 volts required for analog inputs to the VIP in the spacecraft.

5.3.6 Data Handling

Digital data handling involves the acquisition of bi-level data from the various sections of the BUV instrument, processing the data and delivering to the NIMBUS "D" spacecraft for relay to the ground. These data range from single status bits to the output pulses from the anti-coincident circuit and the monochromator high-level discriminator. They are presented to VIP by multiplexing seven individual data words with a ten bit length onto a single data line. These words are described in Figure 5-22.

The three pulse outputs which must be handled by the data handling logic are outputs from the monochromator high-level discriminator and outputs from the photometer and monochromator anti-coincident circuits. The maximum pulse rate of these outputs is approximately 1 MHz, necessitating the use of a 21 bit accumulator with an overflow indicator bit. Since the output data word length cannot exceed ten bits, the pulse data are compressed into ten bit words whenever the most significant bit is in or is past the eleventh stage of the 21 bit accumulator. Three indicators contained in word 2 and word 4 indicate compressed status. Two other bits in word 2 indicate when a counter overflow occurs in the monochromator or photometer pulse data accumulators.

WORD ASSIGNMENT

W1	PHOTOMETER DATA (2 BITS RANGE, 8 BITS DATA)
W2	PHOTOMETER STATUS
W3	MONOCHROMATOR DATA (2 BITS RANGE, 8 BITS DATA)
W4	MONOCHROMATOR STATUS
W5	PHOTOMETER PULSE DATA
W6	MONOCHROMATOR PULSE DATA
W7	MONOCHROMATOR ENERGETIC PARTICLE DATA (A DATA SEQUENCE ONLY)

WORD FORMAT

BIT NUMBER	WORD	W1, W3	W2 (PHOTOMETER)	W4 (MONOCHROMATOR)	W5,6,7
MSB 1		RANGE -2	HV 2	HV 2	PULSE COUNTER DATA
2		RANGE -1	HV-1	HV 1	
3		LOG ADC OUTPUT	PULSE DATA COMPRESSED	PULSE DATA COMPRESSED	
4			COUNTER O/F (MONOCHROMATOR)	ENERGETIC PULSE DATA COMPRESSED	
5			COUNTER O/F (PHOTOMETER)	CAM IN MOTION	
6			DIFF NOT DEPLOYED (S2)	CAM POSITION MONITOR	
7			DIFF NOT NORMAL (S1)		
8			DATA A B,C D E		
9			0 0 0 0 1		
LSB 10			0 0 1 1 0		
			0 1 0 1 0 DATA MODE		

RANGE CODING

RF	RANGE 1	RANGE 2
10^7	1	1
2×10^9	1	0
3×10^{11}	0	0

H.V CODING

PMT	HV 1	HV 2
OFF	1	1
10^2	1	0
$2 \cdot 10^6$	0	0

Figure 5-22. Data Word Format

The accumulators are binary ripple counters. The outputs of these counters are parallel transferred to shift registers for compression and readout. The ripple counters are enabled for an accumulation period of 1.8 seconds, and at the end of this period the data are gated into the shift register. The data are then shifted out to the VIP as described earlier.

The monochromator 21 bit shift register handles both the energetic particle (word 7) and the monochromator anti-coincidence pulse data (word 6). In addition, ten bits of status data are acquired by the shift register and transferred to the VIP in word 4.

The photometer 21 bit shift register handles the photometer data (word 5); the 8 bits of log ADC and 2 bits of electrometer range data from the monochromator and photometer channels (words 1 and 3); and ten bits of status data related to the experiment (word 2).

A functional block diagram of the basic BUV instrument-to-VIP data flow is shown in Figure 5-23.

5.3.7 Sequencer

The output from the sequencer (word generator) controls the operation of the BUV instrument. These outputs are derived from the A_{16} and MFP functions from the VIP. The word generator consists of a ripple counter using the A_{16} pulse as the clock and a series of decoding gates to generate the seven output data words. A description of these words and their sequence is given in Figure 5-22.

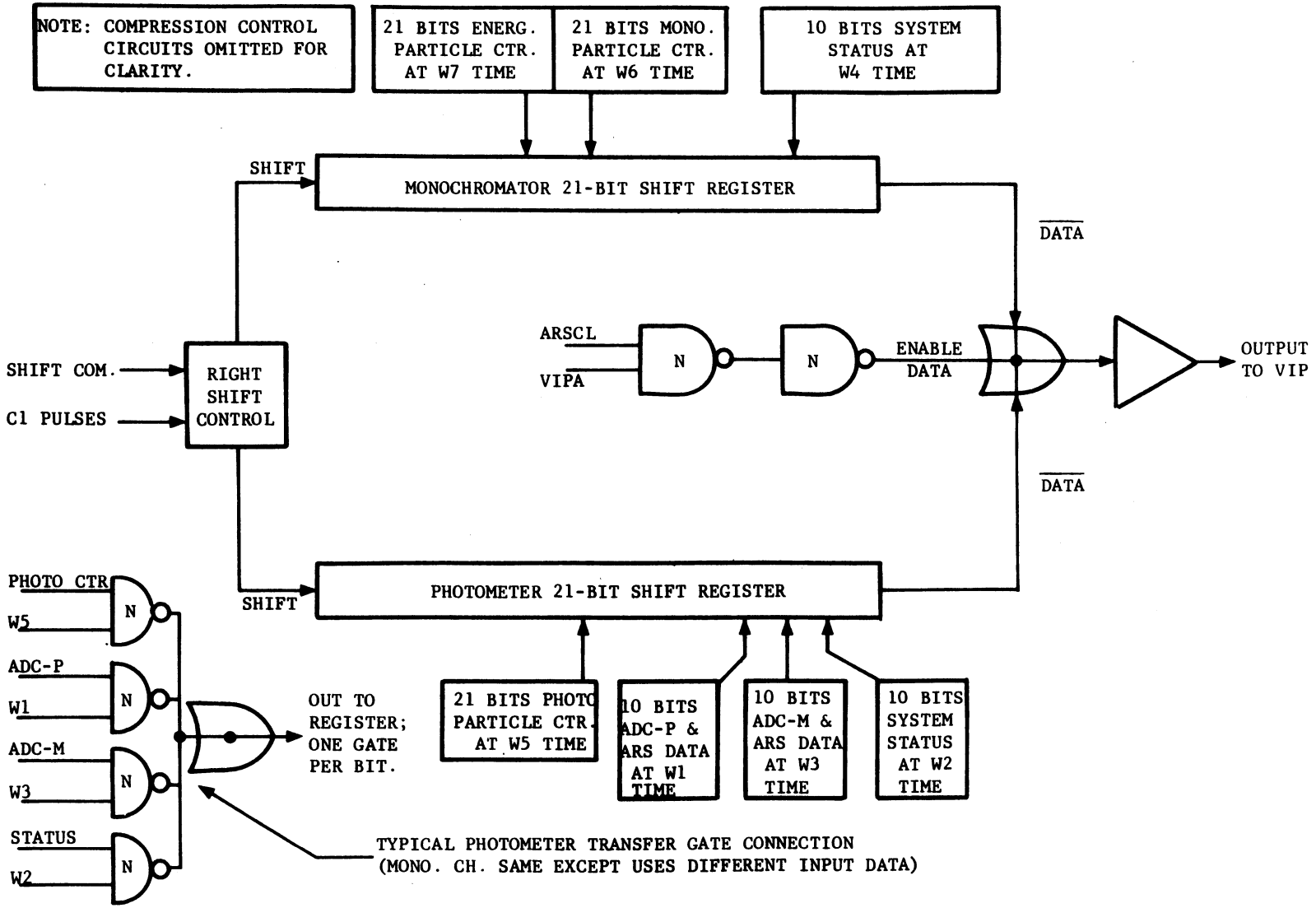

Figure 5-23. Basic Instrument-to-VIP Data Flow Functional Block Diagram

There are 192 BUV minor data frames in each BUV experiment cycle. Each BUV minor data frame is equal to two spacecraft major data frame sequences (16 seconds each) and is synchronized by MFP at every other one.

The 32 second BUV minor data frames consist of data samples in the fixed sequence shown in Figure 5-24, taken at 200 millisecond intervals as controlled by the A_{16} signal. The rotational speed of the cam that moves the wavelength grating into the correct position is slaved to the spacing of these samples and is established to allow the fixed sampling sequence to fit within each step, resulting in the unequal intervals shown in Figure 5-22. The 2.6 second steps are called A intervals and the 2.4 second steps are called B intervals.

The seven data words in the BUV sampling sequence are as follows. Word 1, containing the photometer analog data, has 8 bits of binary coded data plus two bits of electrometer range information. Word 3 is identical to word 1 except that it is reserved for monochromator data and electrometer range information.

Words 2 and 4 contain operational status information on performance parameters within the BUV instrument that are necessary to determine if the instrument is operating properly, and to allow interpretation of the scientific data. Many of the data bits in these two words are redundantly transmitted as discrete bits over the digital B output lines.

Words 5, 6, and 7 contain accumulated pulse data of two types: pulses produced by light incident on the photomultipliers, and by energetic particles striking the photomultipliers. These data are stored in overflow protected 21 bit

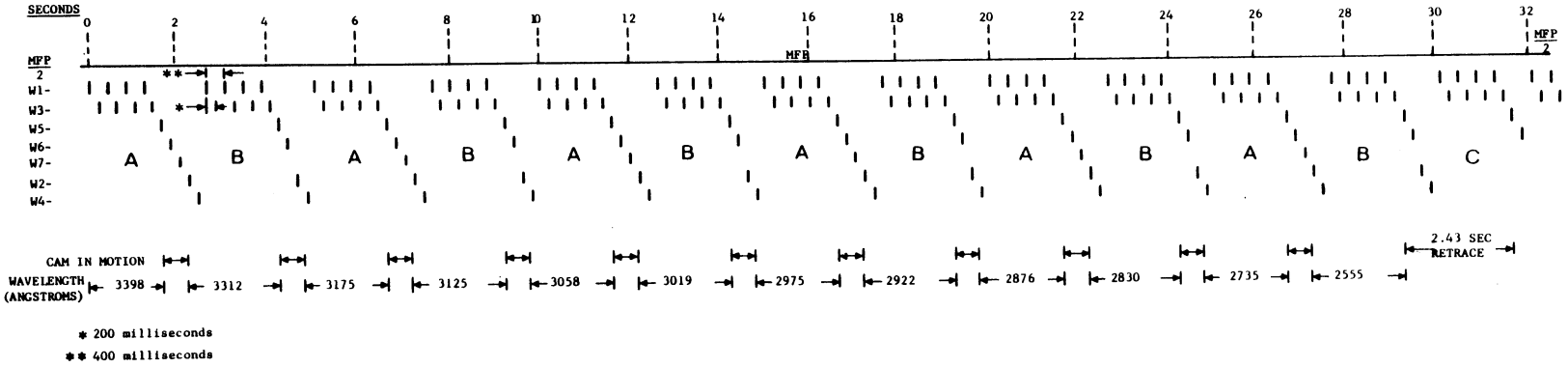

Figure 5-24. Fixed Sequence of 32 Second BUV Minor Data Frames

accumulators and are compressed for transmission to VIP, if the most significant bit in the register exceeds the 2^9 state.

There are 12 wavelength steps in each 32 second scan after which the cam returns to the start position and repeats.

The following is a detailed description of the information content of the seven words:

Word 1 (Photometer Analog Data) - Four Digits - X_1, X_2, X_3, * X_4 D

Word 3 (Monochromator Analog Data) - Four Digits - X_1, X_2, X_3 * X_4 D

X_1 X_2 X_3 - Will range from 0 to 255 maximum - 255 is meaningless, since it indicates the ADC is off-scale.

Use Table to convert counts to PMT anode current, using column corresponding to X_4, decoded range. If more resolution is required, use the formula for I_A given on page 5-43.

X_4 = Electrometer gain

0 = 3×10^{10}

1 = 0 (Normally cannot occur)

2 = 2×10^9

3 = 1×10^7

TABLE 5-2.

TYPICAL READINGS

	Anode Current		
ADC Counts	$R_{FB}=1x10^{7}$	$R_{FB}=2x10^{9}$	$R_{FB}=3x10^{10}$
10	.125	.062	.04
20	.157	.079	.052
30	.2	.1	.065
40	.25	.125	.082
50	.31	.15	.103
60	.39	.2	.13
70	.49	.25	.16
80	.62	.31	.203
90	.78	.39	.255
100	.97	.49	.32
110	1.22	.61	.4
120	1.52	.78	.51
130	1.9	.96	.62
140	2.4	1.2	.8
150	3.0	1.5	1.0
160	3.75	1.9	1.26
170	4.7	2.38	1.8
180	5.9	2.96	1.9
190	7.4	3.7	2.5
200	9.1	4.5	3.0
210	11.5	5.7	3.8
220	14.4	7.2	4.8
230	18.0	9.0	6.0
240	22.5	11.2	7.5
250	28.0	14.0	9.3
Current Multiplier →	$x10^{-7}$	$x10^{-9}$	$x10^{-10}$

1μa ≈204 on 10^{7} Gain

$$I_A = .1 \text{ EXP } \frac{\left(\frac{\text{Data \#}}{44}\right)}{R_{FB}}$$

Word 5 (Photo), Word 6 (Mono), Word 7 (Energ. Part.) - 4 Digits - X_1, X_2, X_3, X_4 *

TABLE 5-3.

PULSE COUNTS

UNCOMPRESSED

1st Digit	2nd Digit	3rd Digit	4th Digit
0 = 0	0 = 0	0 = 0	0 = 0
1 = 256	1 = 64	1 = 8	1 = 1
2 = 512	2 = 128	2 = 16	2 = 2
3 = 768	3 = 192	3 = 24	3 = 3
		4 = 32	4 = 4
		5 = 40	5 = 5
		6 = 48	6 = 6
		7 = 56	7 = 7

HIGH RATE CORRECTION: $R_T = \frac{R_M}{1-(R_M T_D)}$; $T_D = 1 \times 10^{-6}$ (Nominal)

CONVERSION: Divide total reading by 1.8 to get Hz,

i.e., $\frac{X_1 + X_2 + X_3 + X_4}{1.8}$ - Pulse rate in Hz. For equiv. anode current at $G_{PMT} = 2 \times 10^6$, multiply by 3.2×10^{-13}.

COMPRESSED

1st and 2nd Digits	3rd Digit	4th Digit
02 = 16	0 = 64	0 = 0
21 = 32	1 = 72	1 = 1
30 = 64	2 = 80	2 = 2
12 = 128	3 = 88	3 = 3
23 = 256	4 = 96	4 = 4
31 = 512	5 = 104	5 = 5
32 = 1024	6 = 112	6 = 6
13 = 2048	7 = 120	7 = 7
03 = 4096		
01 = 8192		
00 = 16,384		

W5 (P) Compr. Tag - W2, 2nd Digit = 2 or 3
W6 (M) Compr. Tag - W4, 2nd Digit = ODD
W7 (En)Compr. Tag - W4, 3rd Digit = 2 or 3

CONVERSION: Multiply sum of 3rd & 4th digits by multiplier, Then divide by 1.8 to get Hz,

i.e., $\frac{X_1 \ X_2 \text{ (DECODED)} \times (X_3 + X_4)}{1.8}$ = Pulse rate in Hz.

For equivalent anode current at $G_{PMT} = 2 \times 10^6$, multiply by 3.2×10^{-13}.

TABLE 5-4.

Word 2 - Four Digits - X_1, X_2, X_3, X_4 C

		STATUS		
1st Digit Photometer High Voltage	2nd Digit Compressed (P) + OVFL (M)	3rd Digit Diffuser + OVFL (P)		4th Digit Mode
0 = 2×10^6	0 = No OVFL (M) No Compr. (P)	1 = Diff. Depl.		0 = Data
10^2 = 1 = 10^2	1 = OVFL (M) No Compr. (P)	2 = Diff. Retr.	No Photo Ctr. OVFL	1 = MCSA
	2 = No OVFL (M) Compr. Data (P)	3 = Diff. in Motion		2 = MCSB,C
3 = OFF	3 = OVFL (M) Compr. Data (P)	5 = Diff. Depl.	Photo. Ctr. OVFL.	3 = MCSD
		6 = Diff. Retr.		4 = MDSE
		7 = Diff. in Motion		

TABLE 5-5.

Word 4 - Five Digits - X_1, X_2, X_3, X_4, X_5 A

STATUS

1st & 2nd Digits Monochromator High Voltage + Compressed	3rd Digit Energetic Part. and Cam Motion	4th and 5th Digits Cam Position
0 0 = 2×10^6 and not compr.	0 = Not compr. and stopped	00 - 3398 10 - 2735
0 1 = 2×10^6 and compr.	1 = Not compr. and moving	01 - 3312 11 - 2555
0 2 = 10^2 and not compr.	2 = Compr. and stopped	02 - 3175 15 - CAGED
0 3 = 10^2 and compr.	3 = Compr. and moving	03 - 3125 19 - 2522
		04 - 3058 20 - 2527
		05 - 3019 21 - 2532
		06 - 2975 22 - 2537
		07 - 2922 23 - 2542
1 2 = OFF and not compr.		08 - 2876 24 - 2547
1 3 = OFF and compr.		09 - 2830 25 - 2552
		(SEE NOTE BELOW)

NOTE: Any additional numbers up to 31 indicate cam was in motion when read.

CAM IN MOTION TAG:

W4, 3rd DIGIT - ODD

5.3.8 Command Relays

The command relays provide isolation between the VIP command matrix and the instrument. There are five command relays, three magnetically latching relays and two nonlatching relays. The two nonlatching relays are the deploy diffuser and store diffuser relays. The reception of these two commands is stored within the instrument following actuation of the relay.

The latching relays store the launch/normal mode commands, the inhibit/enable calibrate commands, and the instrument power on/off commands.

5.3.9 Low Voltage Power Supplies

There are two electrically isolated low voltage power supplies in the instrument; one supplies housekeeping and motor current limiter voltages and the other supplies the remainder of the instrument low voltage operating power. Each of these supplies consists of a two-core static inverter operating in a driven mode at a frequency of 10 KHz. The inverters normally are synchronized to 10 KHz, but can run free at a lower frequency (dependent upon the input voltage) if synchronization is lost. Each inverter will sync and phase lock exactly at 10 KHz and a known phase relation when the spacecraft supplies the 10 KHz signal.

The housekeeping static inverter supplies power to the cam motor drive limiter, shutter, and diffuser motor drive limiters. The static inverter also furnishes voltage to the housekeeping precision regulator and synchronizing drive signals to the static inverter number 2, the main power converter unit (PCU).

The -24.5 volt input spacecraft power is supplied from a non-switched source through input filters to a current limiter and voltage limiter. The housekeeping inverter runs at a frequency above that of static inverter No. 2 so that in the event of failure of the 10 KHz sync input, inverter No. 2 can still be driven by inverter No. 1. Synchronous operation of these inverters is desired to prevent difference frequency beating which would generate especially undesirable system noise. The free running inverter frequencies are directly dependent upon input voltage and since the noise generated would be a function of input voltage, filtering would be extremely difficult. The current limiter is designed to prevent destruction of the power supply due to long term overload or due to slowly increasing overloads with time constants greater than 200 milliseconds.

5.3.10 Motor Drives

Four identical circuits are used to provide power for the stepper motors. These motors position the wavelength cam, the monochromator and photometer shutters, and the diffuser plate. Working in conjunction with the cam control are five cam encoders for position sensing.

5.3.10.1 Cam Drive

Each phase of the cam motor is individually controlled by separate driver circuits. To provide the required isolation between the logic reference and the motor power lines, a carrier system is used. When any of the drive signals go "true", one of a series of transformer drivers is switched on and saturated. This allows 10 KHz pulses to be placed across the transformer primary. Rectification in the secondary turns on the motor drivers for that

phase until the termination of the 50 Hz input. Each phase is activated in turn, resulting in the motor stepping from one position to the next.

The shaft encoder lamps are energized during cam motion. The shaft encoder contains a hole pattern which allows light to fall on photo sensitive diodes in a fixed sequence. This sequence is directly related to grating position, hence the wavelength of the energy that is passed to the monochromator photomultiplier tube. The photo sensitive diode outputs are amplified and applied to gates in the cam motor drive module, causing the cam to be positioned in accordance with the encoder disc hole pattern. In addition, the position of the shaft encoder is contained in the last five bits of the monochromator status word, word 4, which is multiplexed on to the VIP digital output line.

5.3.10.2 Shutter Drives

The monochromator and photometer shutter drive control logic positions the shutters to one of three positions (photometer) or one of four positions (monochromator) in response to the sequencer state for calibration cycles. Shutter position is sensed by magnetically actuated reed switches, which then control the duration of the drive signal to the individual motors. The isolated motor drive operation is as described for the cam motor drive.

5.3.10.3 Diffuser Drive

The diffuser motor drive circuitry is used to move a diffuser plate into and out of the path of the backscattered energy to provide a diffused solar or lunar energy to both photomultipliers. The diffuser mode can only be activated by ground command and is normally deactivated by a built-in timing mechanism backed up by a ground command. The diffuser position is also sensed by magnetically actuated reed switches.

5.4 PHOTOMULTIPLIER RESULTS

5.4.1 Shields

The final PMT shield configuration is shown in Figure 5-25. The tube itself, with the first nine dynode resistors,is potted within a fiberglass sleeve. The potting material is Sylgard No. 185, with 10 percent eccospheres. At the base of the tube a three-segment copper cup holds various electronic components used to interface with the high voltage supply. Around the copper cup and most of the fiberglass shell is wrapped an electrostatic shield of .004 thick copper, which is then soldered to the cup at several points. This is followed by two layers of mylar insulation.

Next comes a magnetic shield composed of two wraps of 0.004 thickness Co-netic, followed by two more layers of mylar. The entire assembly is then inserted in an aluminum tube, as shown. The tube is slipped into a radiation shield, rigidly mounted to the casting by plastic clamps. The radiation shield is made from a sandwich of aluminum and tungsten alloy, selected to minimize orbital radiation effects on the photocathode.

Previous experiments have established that PMT's operated with a negative high potential on the photocathode are adversely affected by external surfaces at low potential near the photocathode. This is avoided in the 541N-05M-14-M9 tube by incorporating a 0.003 copper shield within the fiberglass sleeve. This shield extends 0.5 inch ahead of the cathode and 0.9 inch behind; it is internally connected to the photocathode. The remainder of the tube, after a 1 inch gap, is then covered by the external copper shield, as mentioned. The external shield is connected to a "quiet" ground within the electronics package.

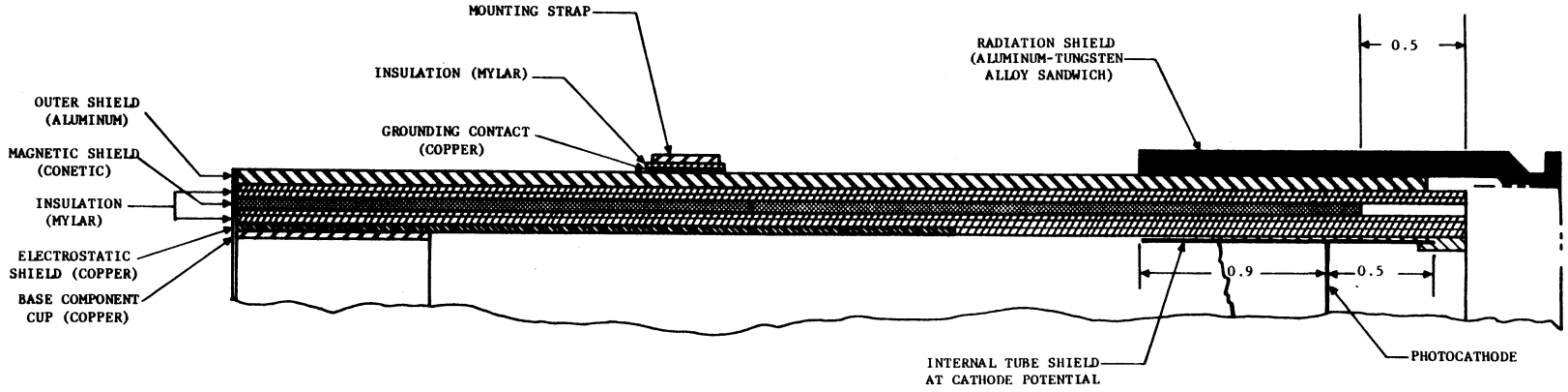

Figure 5-25. Final PMT Shield Configuration

In addition, a copper contact strip under the mounting strap (mylar-isolated from the strap) is connected to the grounded copper shield. This serves to ground the outer aluminum sleeve and the radiation shield, which it contacts via a sliding fit as the photomultiplier assembly is inserted in the casting. Thus, no metallic portion of the assembly is allowed to contact the casting directly; controlled grounding is accomplished to a single selected ground point, as explained.

Figure 5-26 shows the arrangement of components and wiring within the base-mounted cup. After initial tests, this area is potted using a formulation of Solithane 113 with an opaque dye added. The potting is extended back past the top central portion of the cup to serve as a wire retention device for the PMT leads connecting to the electrometer, dynode buffers, and high voltage power supply. Component designations are referred to Figure 5-27.

5.4.2 Testing Methods

Before shipment, the PMT's were tested by the manufacturer (Electro Mechanical Research) as follows:

1. Device connected as a diode; 4100Å light adjusted for diode current of 10^{-11} amperes.
2. Device connected as photomultiplier tube. Light level same as in Step 1. Voltage adjusted for anode current of 10^{-7} amperes. This is the voltage for 10^4 gain.
3. Voltage same as in Step 2. Light reduced until anode current is 10^{-8} amperes. Voltage then adjusted for anode current of 10^{-7} amperes. This is the voltage for 10^5 gain.

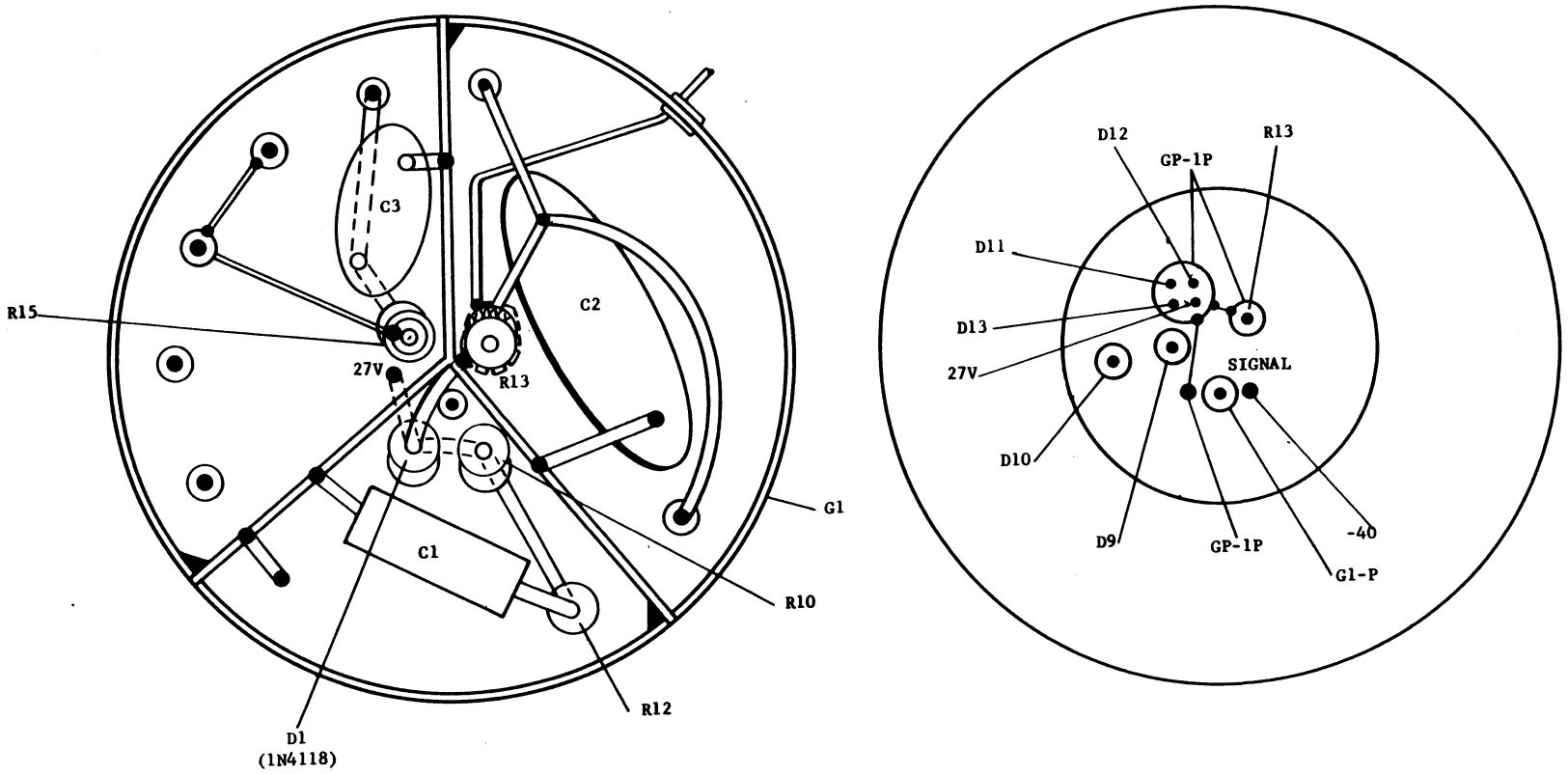

Figure 5-26. Base Mounted Cup Internal Wiring and Component Arrangement

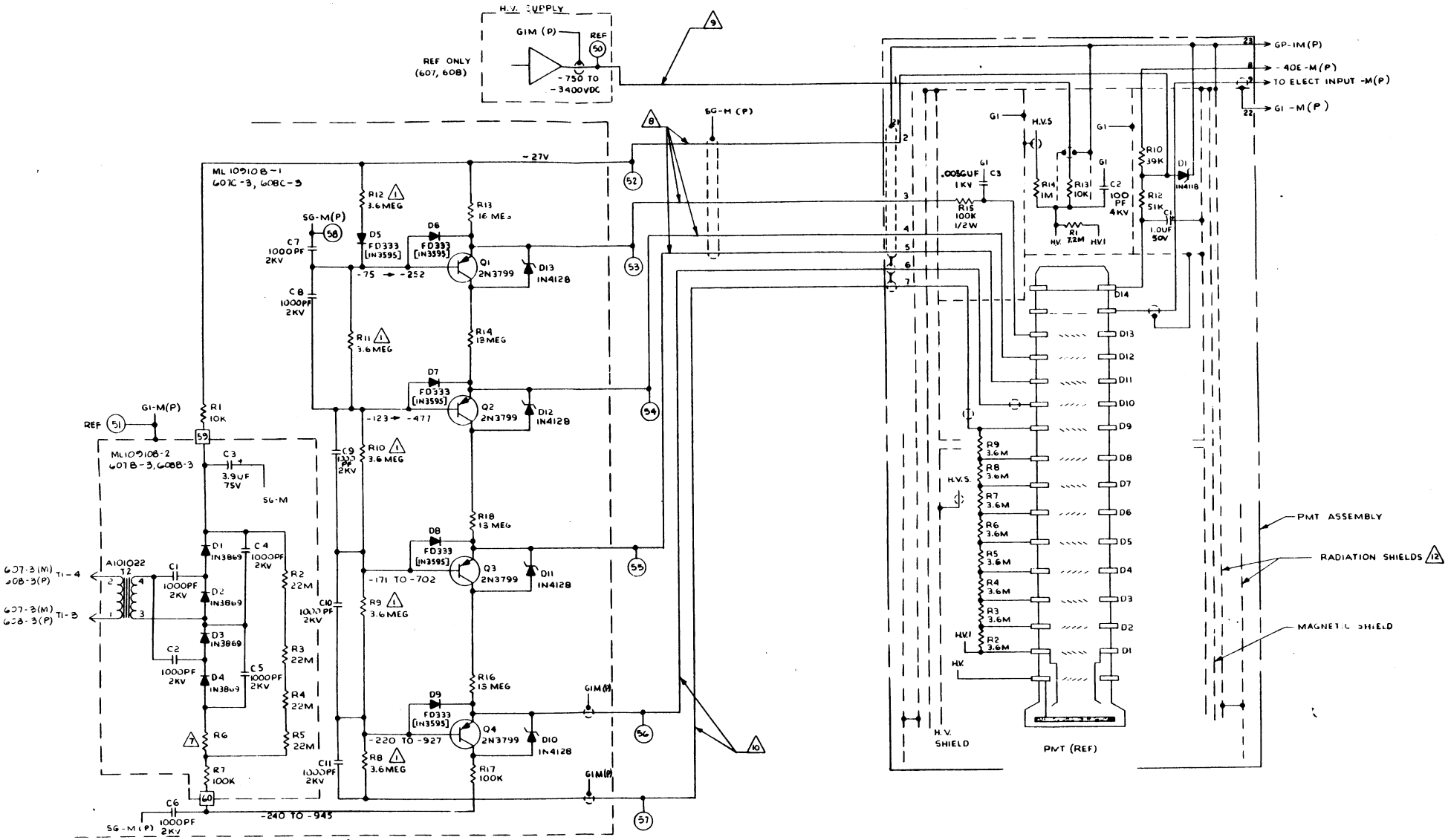

Figure 5-27. PMT Dynode Buffers, Monochromator and Photometer Schematic Diagram

4. This procedure is repeated: light level decreased so that anode current is reduced by a factor of ten, then applied voltage increased to re-establish 10^{-7} amperes anode current, until 3600 volts is reached.

As a cross check, the photomultiplier tubes for the prototype and flight model BUV's were tested in the following sequence:

1. Measure the gain and dark current of the tube as it is received from the manufacturer.
2. Wrap a temporary set of shields on the tube and measure the gain and dark current again to evaluate the effects of the shields.
3. Prepare the base for the tube for the potting operation. This includes the installation of a zener diode voltage regulator on the 14th dynode. Then measure the gain and dark current with no shields.
4. Wrap the final shield configuration on the tube and recheck the gain and dark current.
5. Remove the shields and pot the base of the tube.
6. Recheck the dark current with the base potted and no shields.
7. Wrap the final set of shields on the tube and check the dark current.

The direct gain measurements were made using chopped monochromatic light from a Beckman DU monochromator. The wavelength was 4100Å. The chopped light was diffused and applied to the PMT as an input signal. The output of the PMT was detected using a Princeton Applied Research "Lock-in Amplifier" which was synchronized to the light chopper. A test connection block diagram is shown in Figure 5-28.

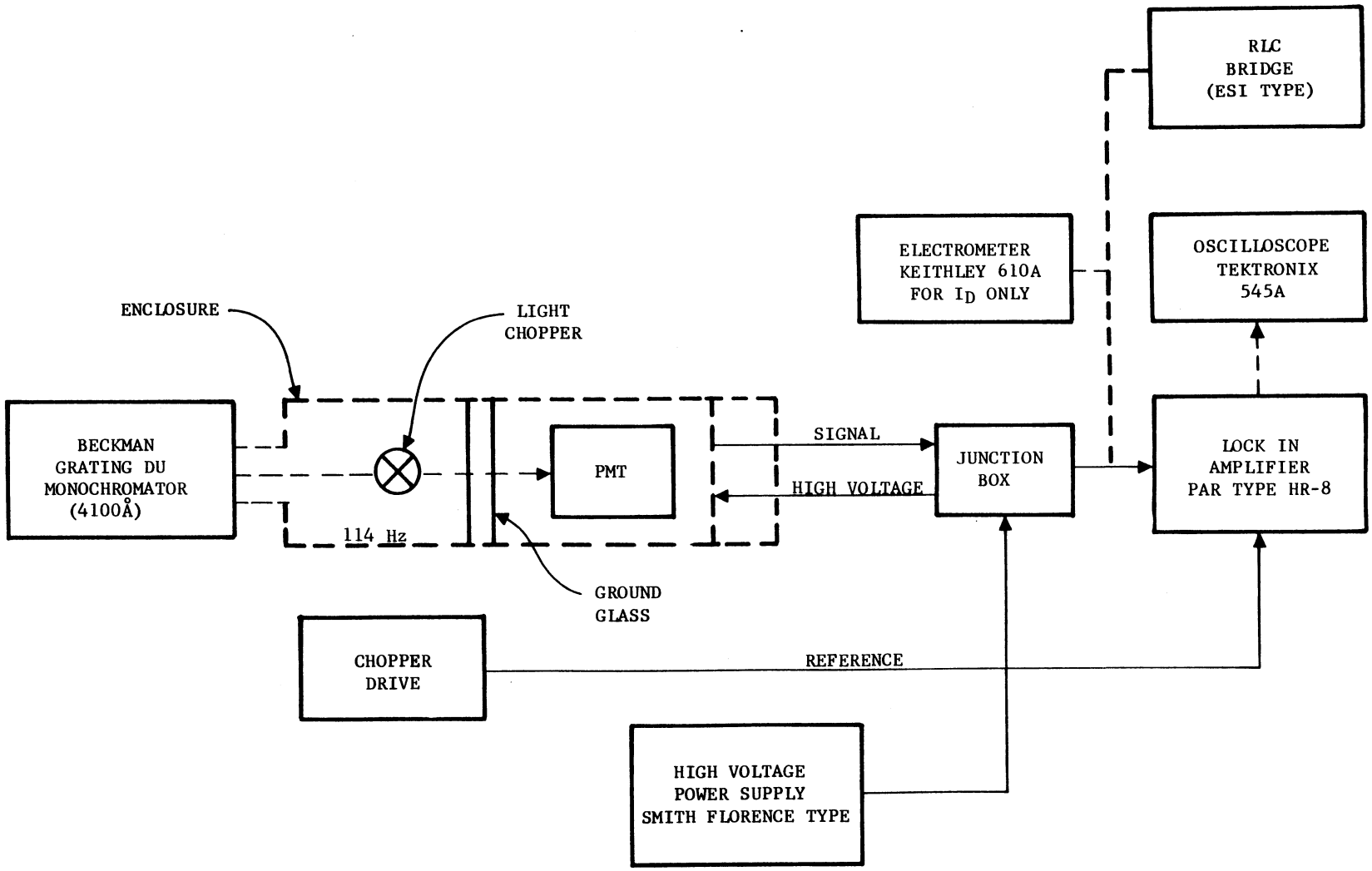

Figure 5-28. BUV Photomultiplier Tube Test Setup

The test procedure is as follows:

1. Connect the tube as a diode. Apply -100 V dc to the cathode.
2. Set the slits of the DU so the diode current is in the order of 1×10^{-11}A.
3. Record the slit width and the PAR amplifier reading with the tube connected as a diode.
4. Turn off the high voltage and connect the RLC bridge to the PAR amplifier signal input. Measure the capacity across the input.
5. Connect the tube as a PMT.
6. Measure the capacity across the PAR amplifier input. Add sufficient capacity so that the total is within 50 pf of the capacity measured as a diode.
7. Use the same slit-width as that used in the diode measurement. Set The PMT dynode voltage to 500 V and read the PAR amplifier output.
8. Increase the dynode voltage in 100 V steps to 1000 V and in 200 V steps above 1000 V. Read the PAR amplifier at each step and record the readings.
9. As the anode current approaches 1 μA, as calculated from the PAR input voltage across the input impedance, reduce the slit width so that the PAR amplifier output drops by a factor of 10 and continue to take readings.
10. Allow the tube to stabilize in the dark for about 12 hours and record the dark current at a nominal gain of 1×10^6 and 2×10^6. Use the Keithley 610A electrometer to measure dark current.

Direct gain measurements made by this method were repeatable to within 10 percent. The gain curves agreed closely with the curves made by the PMT manufacturer for three of the four tubes tested.

5.5 RECOVERY TIME MEASUREMENTS

During system acceptance testing, the photomultiplier tubes' time-response was measured by comparing the dark current before and after exposure to high intensity light, as follows:

1. After a several hour stabilization period with shutters closed, many data samples were taken and averaged.
2. The shutters were opened and light entered the instrument until 1 microampere of anode current was produced on the high gain range.
3. The shutters were closed, and continuous data samples taken for 5 minutes. These were reduced for each 1.8 second sample period to determine when the dark current had decayed to twice its pre-exposure value.

Results for the two instruments are as follows:

Equipment	Pre-Exposure Dark Current		Recovery Time (Seconds)
	Pulse Counts	Anode Current x 10^{-11}	
P103, M	145 ±41	5.14 ±1.45	6
P103, P	140 ±44	4.2 ±1.3	129
F104, M	57.5 ±49.2	1.93 ±1.67	3
F104, P	101.5 ±29.7	3.42 ±1.01	20

SECTION VI

SYSTEM TESTING AND RESULTS

6.1 GENERAL

Tests performed by Beckman on the BUV instruments include the following:

- o Vibration
- o Acceleration
- o Thermal-Vacuum
- o Bench Acceptance Tests, Optical and Electrical
- o Interface Acceptance Test, Primarily Electrical

The tests and results of Bench and Interface acceptance tests have been documented previously, and will not be repeated here; a summary of the results appears in Section VII. The tests of Vibration, Acceleration, and Thermal Vacuum (TV) are given in the GSFC Environmental Test Specification S-320-NI-3-A, as revised by GSFC communications, and implemented by previously submitted detailed test plans.

6.2 ENVIRONMENTAL TESTS

6.2.1 Vibration

The breadboard sensor module (without electronics) was tested in October 1967, and several minor changes were incorporated as a result. For a detailed analysis, see PR-2475-8, Beckman Monthly Report No. 8 for the period ending November 30, 1967.

Model P103 vibration testing results are given in Table 6-1, and F104 results in Table 6-2.

Figures 6-1 and 6-2 define the instrument axes.

6.2.2 Acceleration

The P103 unit was subjected to 30 g acceleration for 5 minutes along the thrust (Z) axis as specified in S-320-NI-3-A. The test was performed on 4-10-69; before and after performance comparisons showed that the instrument was unaffected by the applied acceleration.

6.2.3 Thermal Vacuum

Both the P103 and F104 Instruments were subjected to thermal-vacuum (TV) testing as specified in S-320-NI-3-A, modified by GSFC instructions. Figure 6-3 shows the P103 test regime, and Figure 6-4 specifies the test regime for the F104 Instrument.

During the tests, internal calibrations were performed periodically. Calibration results are discussed in Section VII of this report.

In addition to the tests shown in Figures 6-3 and 6-4, both instruments were later exposed to several abbreviated thermal or thermal-vacuum cycles following repair or rework. The P103 unit was also subjected to an extensive thermal-vacuum test program at General Electric, Valley Forge. (Calibration Run Results at General Electric are found in Section VII.)

ITEM	DATE	TEST DESCRIPTION	AXIS	REMARKS
Sensor	1-30,31-69	1 & 4 g Sine	Z,Y,X	Exploratory Survey
Sensor	1-31,2-1-69	10 g/rms Random	X,Z,Y	Exploratory Survey (Note 1)
3/0	2-1-69	1 and 7.5 g Sine	Y,Z,X	Survey and Specification
3/0	2-1-69	20 g/rms Random	Y,Z,X	Specification Levels (Note 2)
Sensor	2-8-69	7.5 g Sine	Y	Spec Levels (Note 3)
3/0	2-11-69	11.7 g/rms Random	X	Workmanship for repair of 2-1-69 Failure
Sensor	2-17-69	7.5 g Sine	X	Spec Levels (Note 4)
Sensor	3-29-69	7.5 g Sine	X	Repeat of 2-17 Test (Sine) (Note 5)
Sensor	3-30-69	7.5 g to 40 g at 800 Hz	Z	Accelerometer Mount Failure
Sensor	3-31-69	7.5 g Sine, 15 g/rms Random	Y	Repeat of 2-8 Test Sine and Spec Random
Sensor	4-1-69	7.5 g Sine, 800 to 2000 Hz	Z	Completion of 3-30 Test
Sensor	4-1-69	15 g/rms Random	X	Repeat of 2-17 Test (Random)
Sensor	4-1-69	20 g/rms Random	Z	Diffuser Plates Incorrectly Mounted
3/0	5-16-69	11.7 g/rms Random	X	Workmanship for repair of failure in TV Test
3/0	9-13-69	11.7 g/rms Random	X	Workmanship after rework
Sensor	9-19-69	11.7 g/rms Random	X	Workmanship after rework
3/0	9-22-69	11.7 g/rms Random	X	Workmanship for repair of failure in A.T.

NOTES

1. Two wires in the electronics package were broken. See failure report A-01604.
2. A pinched wire caused destruction of a logic element. See failure report A-01603.
3. A photometer shutter pin loosened during the test and was epoxied in place. See failure report A-01606.
   Several wires were broken in the electronics package. See failure reports A-01605 and A-01607.
4. Many wires were broken in the electronics package, see failure reports A-01608, A-01609, A-01611. Following this test, all the sensor electronics packages were reworked to withstand more rugged operations.
5. A loose diffuser plate clamp was loctited after this test.
6. All sine vibration tests were limited to D.A. displacement of 1 2-inch maximum, at a sweep speed of 2 octaves per minute from 5 to 2000 Hz.
7. All random vibration tests were 2 minutes per axis per test, 20 to 2000 Hz spectrum.

Table 6-1. Results of Vibration Testing, P103

ITEM	DATE	TEST DESCRIPTION	AXIS	REMARKS
3/0	5-19,20-69	5 g Sine	X,Y,Z	Specification Level
3/0	5-21-69	11.7 g/rms Random	Y,Z,X	Specification Level
Sensor	6-25-69	11.7 g/rms Random	Z	Specification Level (Note 1)
Sensor	6-27-69	5 g Sine, 11.7 g/rms Random	X,Y,Z	Specification Level
Sensor	7-22-69	11.7 g/rms Random	X	Workmanship for repair of TV Failure
Sensor	9-10-69	11.7 g/rms Random	X,Z	Workmanship after rework
Sensor	10-1-69	11.7 g/rms Random	X,Z	Workmanship for repair of A.T. Failure
3/0	10-1-69	11.7 g/rms Random	X	Workmanship for repair of A.T. Failure
Sensor	3-17-70	11.7 g/rms Random	X	Workmanship for repair of A.T. Failure

NOTES:
1. The monochromator shutter magnet plate was reworked following this test. See failure report A-01615.
2. All sine vibration tests were limited to a D.A. displacement of 1/2-inch maximum at a sweep speed of 2 octaves per minute from 5 to 2000 Hz.
3. All random vibration tests were 2 minutes per axis per test, 20 to 2000 Hz spectrum.

Table 6-2. Results of Vibration Testing, F104

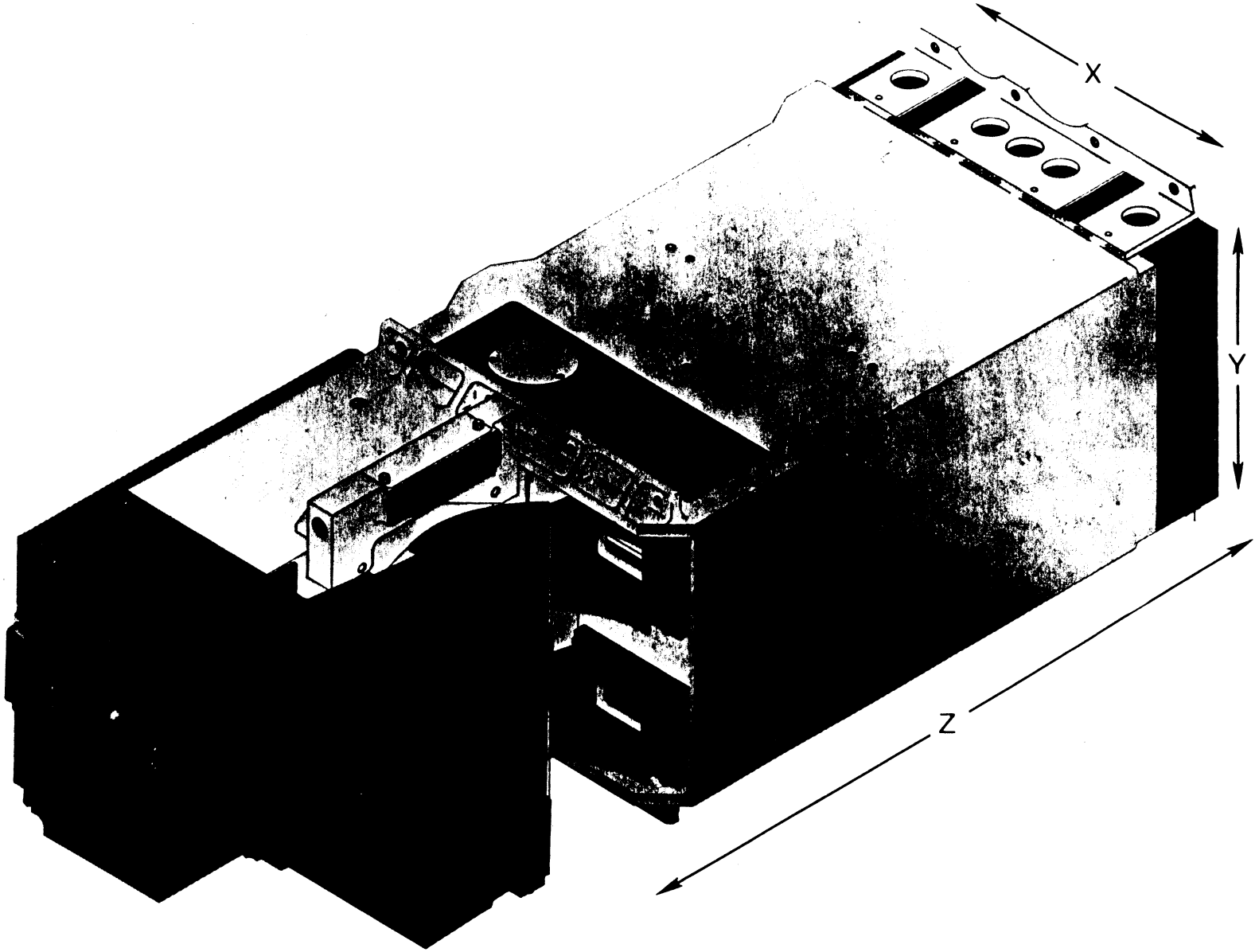

Figure 6-1. Sensor Module Axis Definition

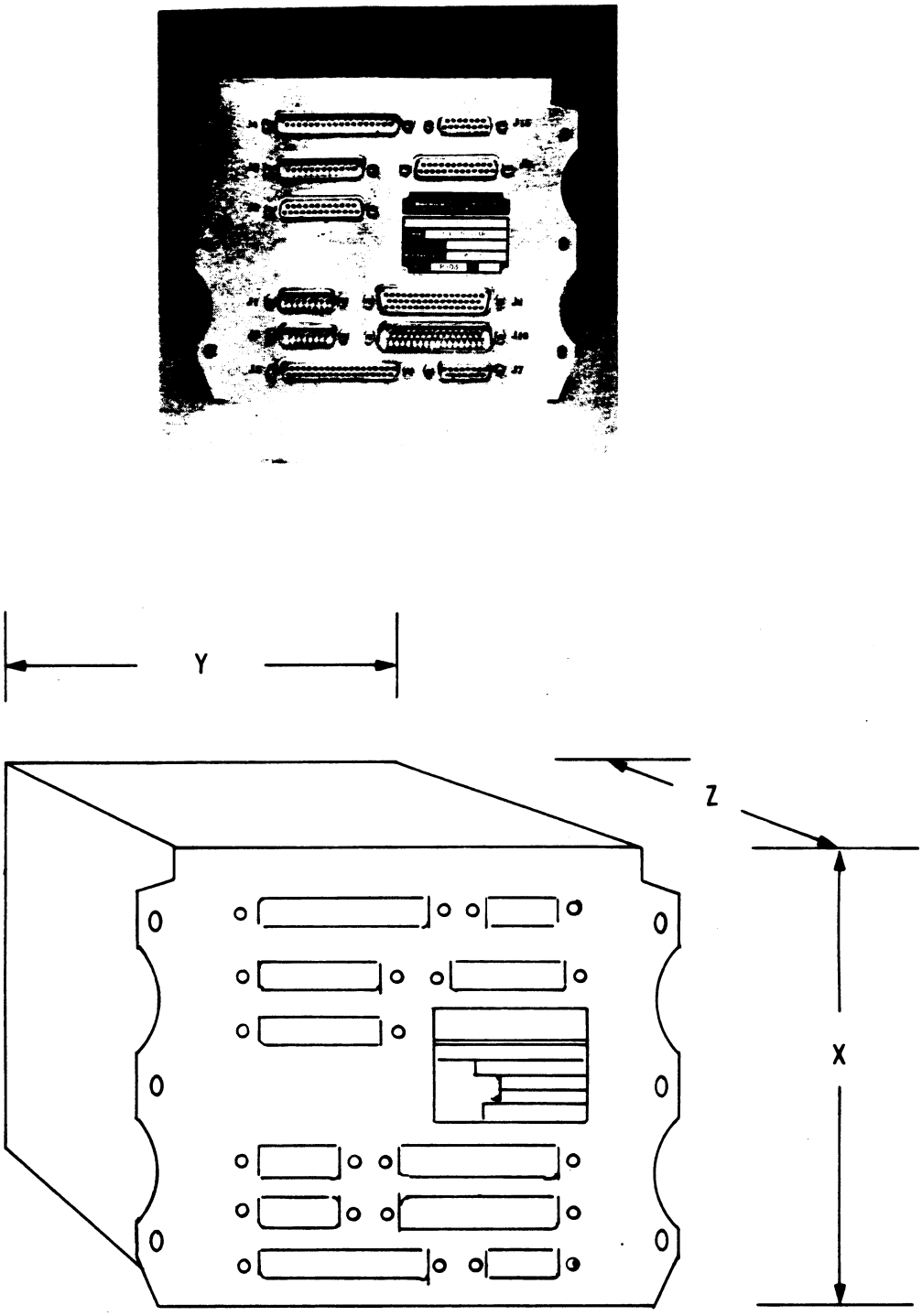

Figure 6-2. 3/0 Electronics Module Axis Definition

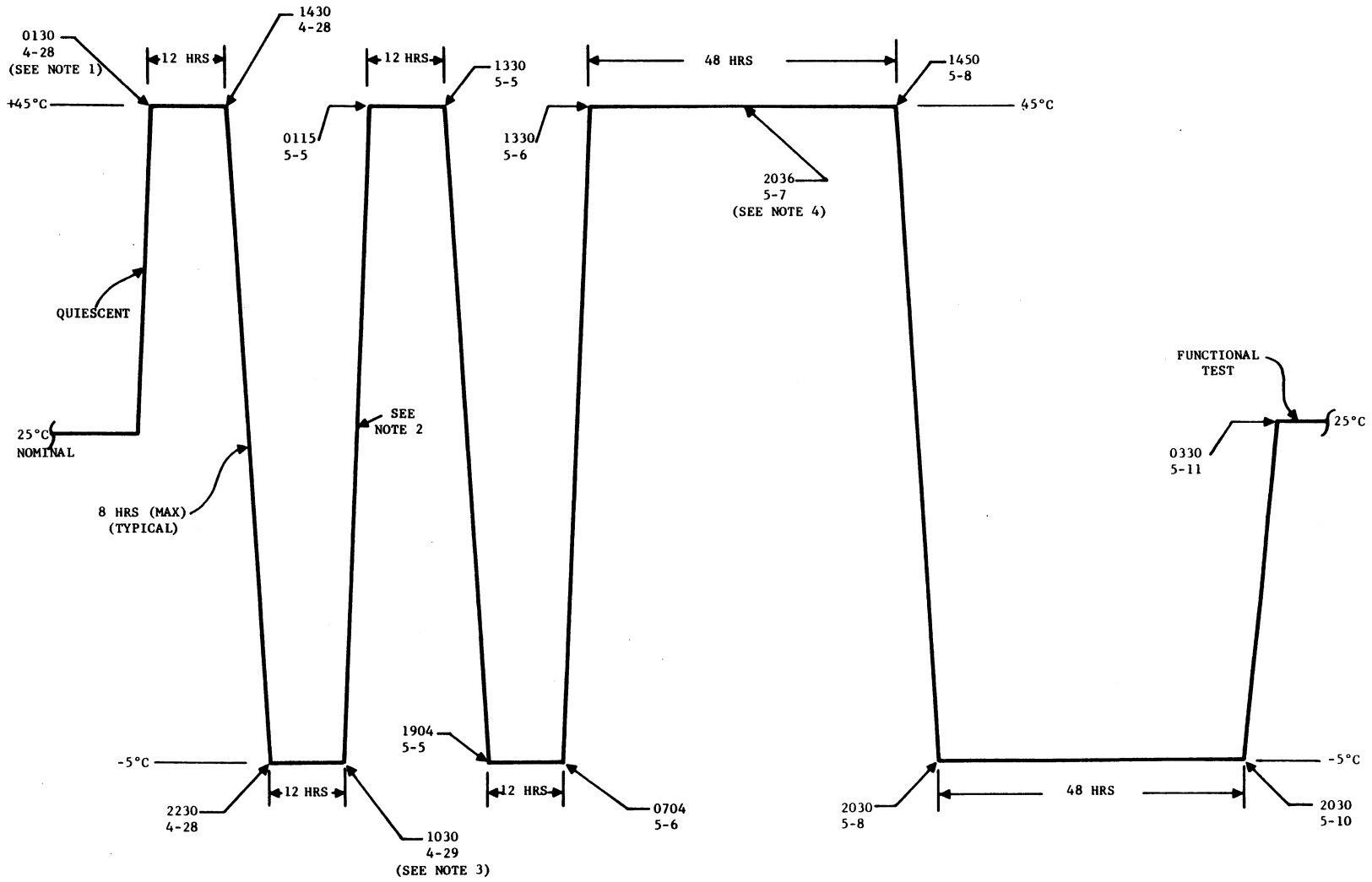

NOTES:
1. OPERATE CONTINUOUSLY IN NORMAL MODE WITH CALIBRATION ENABLED FOR FIRST FOUR HOURS AND MAKE HOURLY FUNCTIONAL TESTS. REMAINING EIGHT HOURS - QUIESCENT EXCEPT FOR FUNCTIONAL TEST EVERY FOUR HOURS.
2. BROKE VACUUM SEVERAL TIMES DURING THIS RAMP BECAUSE OF PUMP MALFUNCTION AND LOW PUMPING RATE.
3. INTERRUPTED TEST HERE - RESUMED AT 2200 on 5-1 (SEE FAILURE REPORT-A-01613).
4. PUMP MALFUNCTIONED LOST VACUUM FOR 70 MINUTES.
5. VACUUM: 10^{-5} mm Hg OR LESS.

Figure 6-3. Thermal Vacuum Tests, P103

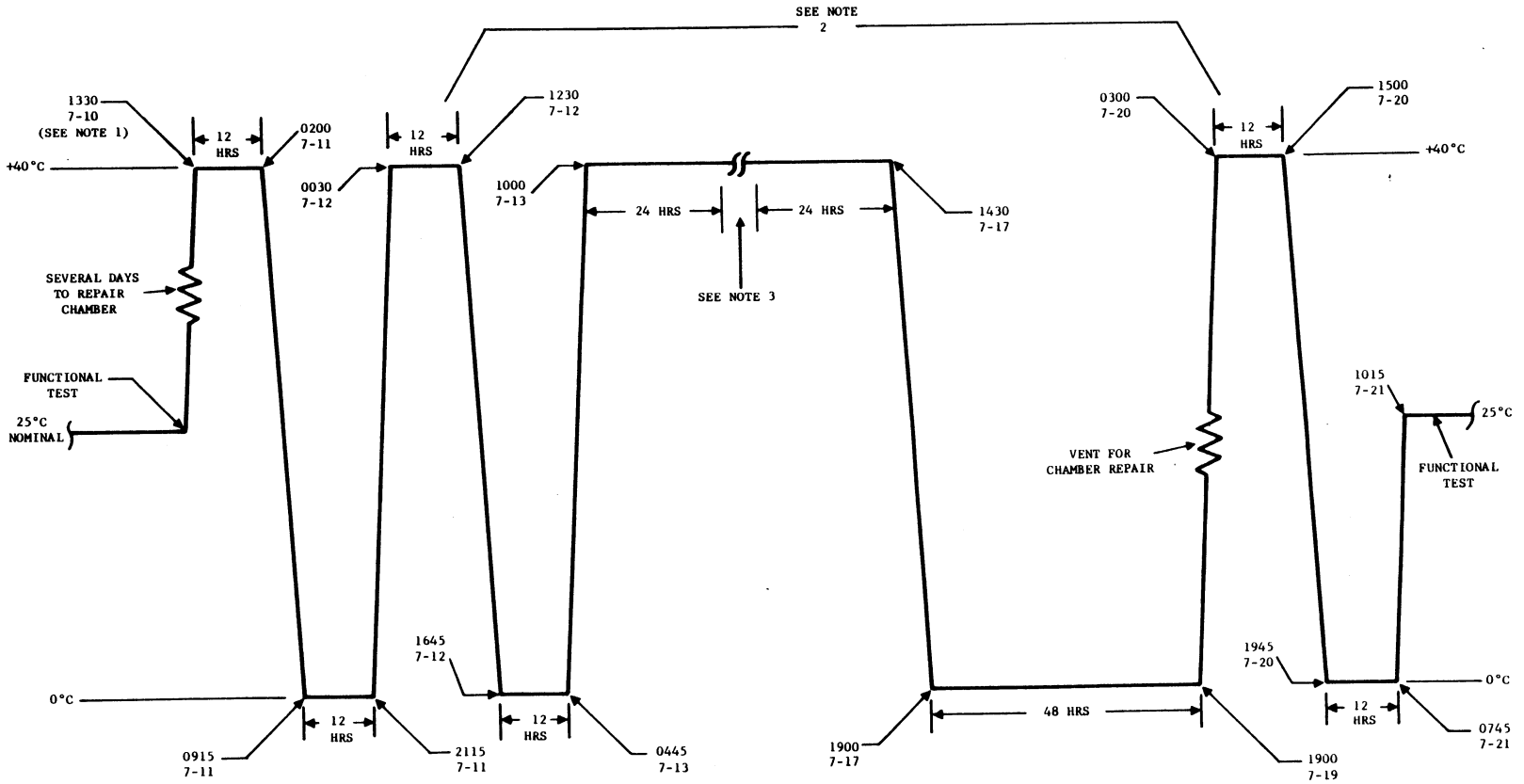

NOTES:

1. FIRST FOUR HOURS OF CONTINUOUS OPERATION.
2. INSTRUMENT QUIESCENT DURING REMAINING DWELL TIMES, WITH FUNCTIONAL TEST AT FOUR HOUR INTERVALS.
3. INTERRUPTED FOR REPAIR (SEE FAILURE REPORT A-01616).
4. VACUUM: 10^{-5} mm Hg OR LESS.

Figure 6-4. Thermal Vacuum Test, F104

6.3 IRRADIATION TESTING

6.3.1 General

The optical components used in the BUV Instrument are discussed with respect to their function in paragraph 2.3.3 of the Technical Manual. The following is a discussion of the results of transmission and reflectance tests performed on these optical components.

All transmitting optical components such as monochromator transfer prisms, monochromator exit lens, monochromator wavelength calibration prism, monochromator attenuation filter, and photometer exit lens are constructed of fused silica SUPRASIL I. Everyone of these components was checked for transmission. A representative sample of SUPRASIL I was irradiated to test for degradation with exposure to radiation. The scan before and after radiation (Figures 6-5 and 6-6) show that no transmission loss was experienced.

Figures 6-5 and 6-6 also show the graphs for the sapphire used as a shield for the two depolarizer calcite plates. The actual pieces of sapphire which were used in the P103 Instrument have not been irradiated. A similar sample was irradiated with 2×10^{14} e/cm^2 at 1.0 MeV. Figure 6-6 shows that there is a slight amount of transmission loss towards the lower wavelengths of the BUV range.

The graphs for the calcite used in the construction of the depolarizer before irradiation are shown in Figures 6-7 and 6-8. Figures 6-9 and 6-10 show the calcite after irradiation. The 100-percent line was established with two 10-millimeter pieces of SUPRASIL as shown on the graph. The "Sample" SUPRASIL cube was then replaced with the calcite cube for the test run. Again, the calcite experiences some degradation of transmission after irradiation with the same exposure to radiation.

The monochromator collimating mirrors are coated with vacuum-deposited aluminum. At one time it was under consideration to coat these mirrors with vacuum-deposited magnesium fluoride. Tests were conducted to establish the

transmission characteristics of the hard- and soft-coated magnesium fluoride before and after irradiation. Figures 6-11, 6-12, and 6-13 show the graph before irradiation, and Figures 6-14 and 6-15 show graphs after irradiation. Only a small degradation in transmission can be observed due to irradiation damage. Subsequently, it was decided not to use any magnesium fluoride coating on the mirrors. The substrates used in these transmission measurements were fused silica, SUPRASIL I, which has a known resistance to irradiation damage. The hard and soft magnesium fluoride coatings were also tested when deposited on aluminum mirrors (with fused silica substrates). The reflectivity of these coatings before irradiation is shown in Figures 6-16, 6-17, and 6-18, and the reflectivity of these coatings after irradiation is shown in Figures 6-19 and 6-20. Again, there is very little degradation due to irradiation damage. As stated before, the magnesium fluoride overcoat was not used on the final mirrors. The mirror used in the first monochromator had a special antireflection coating deposited by NASA at Goddard Space Flight Center, and the resistance to degradation due to irradiation damage was checked by NASA.

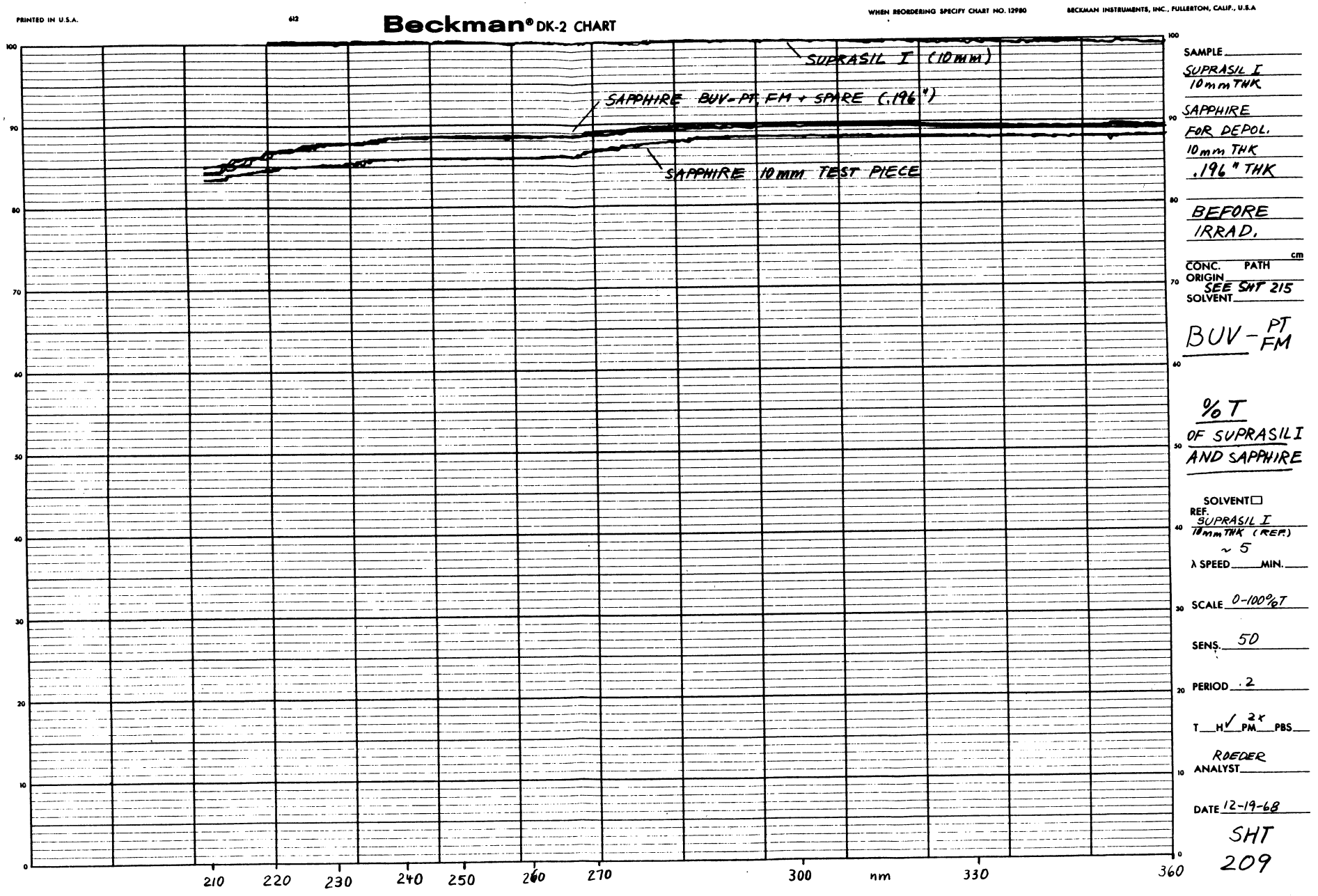

Figure 6-5. SUPRASIL I and Sapphire Percent Transmission Graph (before irradiation)

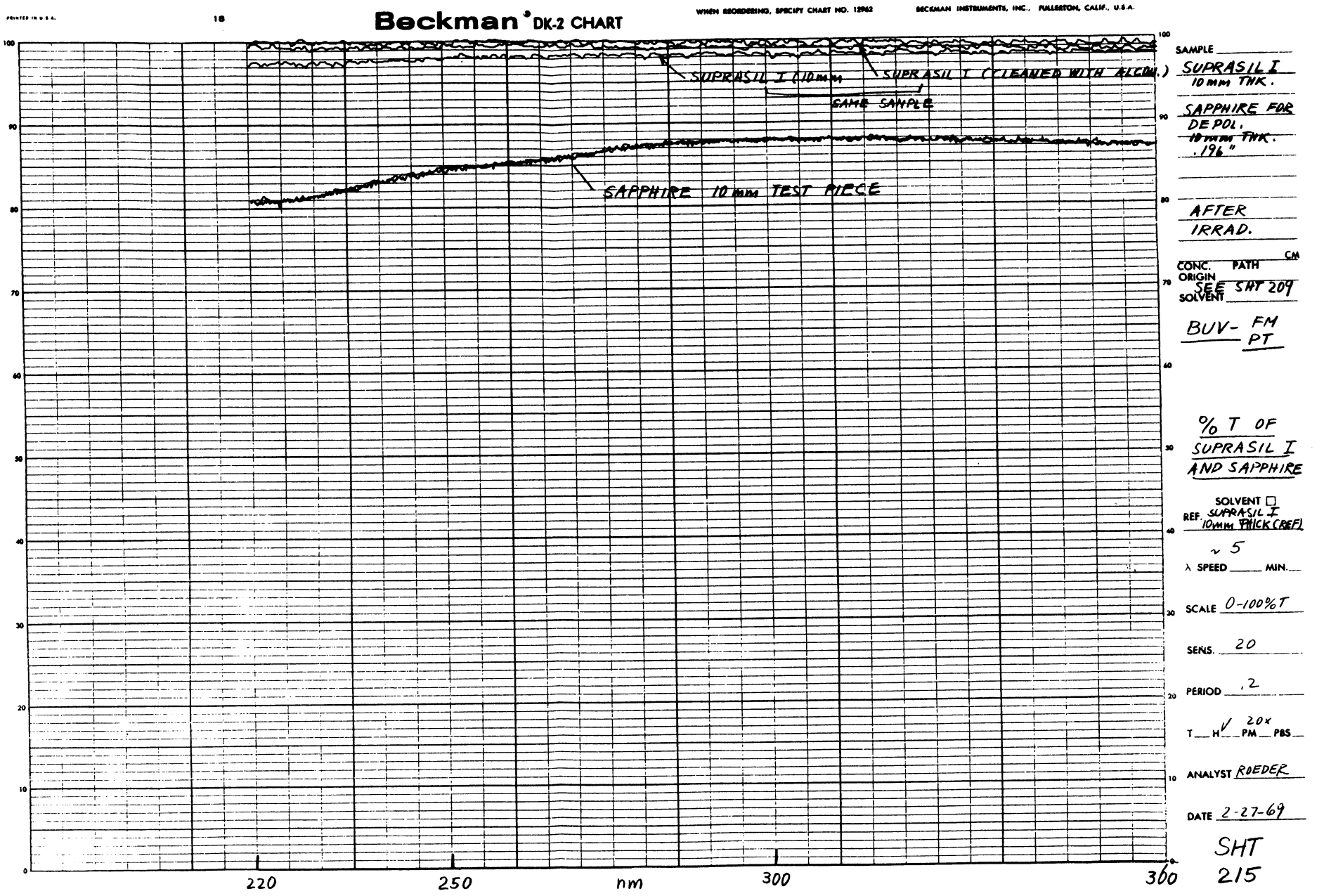

Figure 6-6. SUPRASIL I and Sapphire Percent Transmission Graph (After Irradiation)

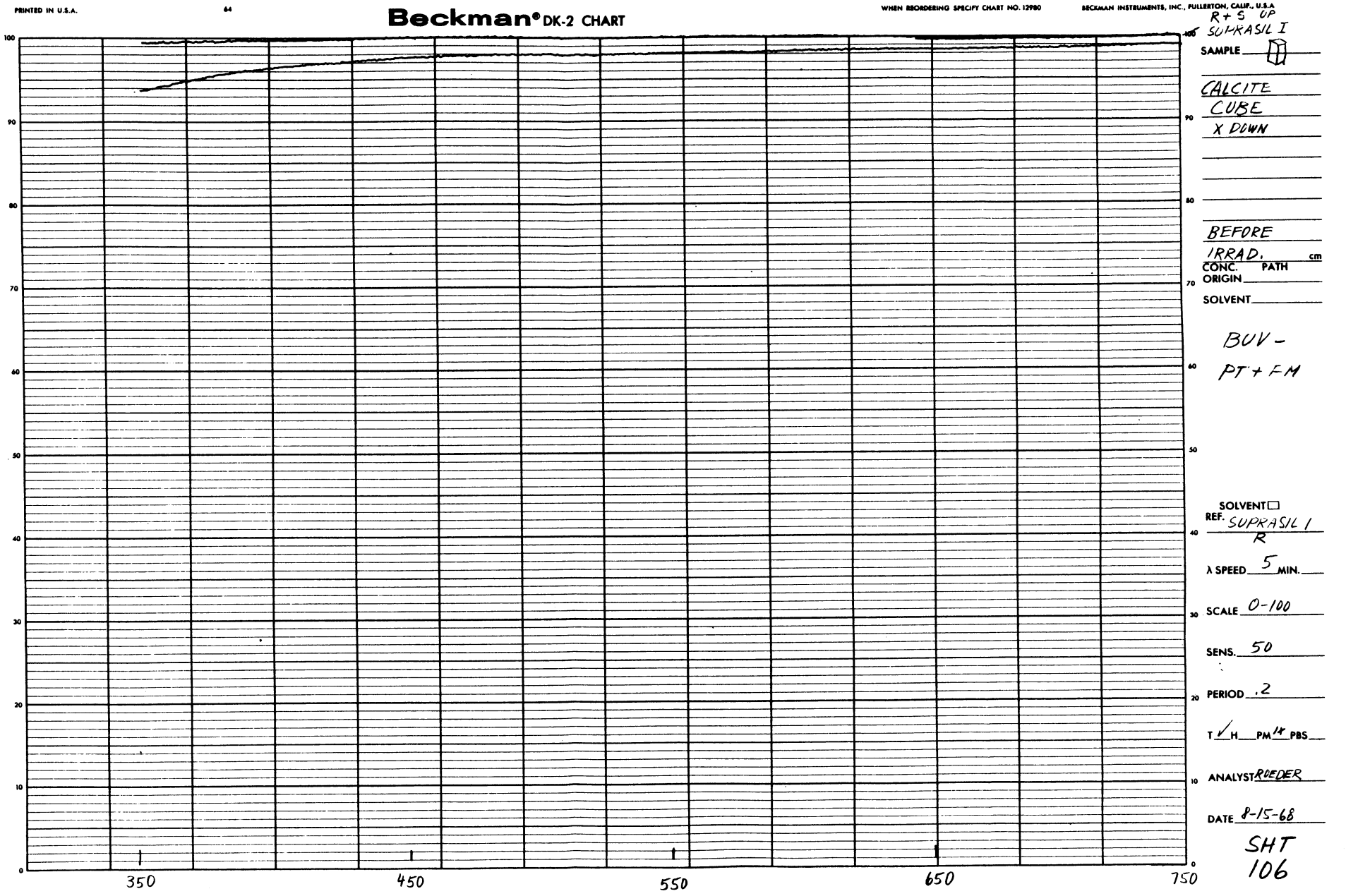

Figure 6-7. Calcite Percent Transmission Graph No. 1 (Before Irradiation)

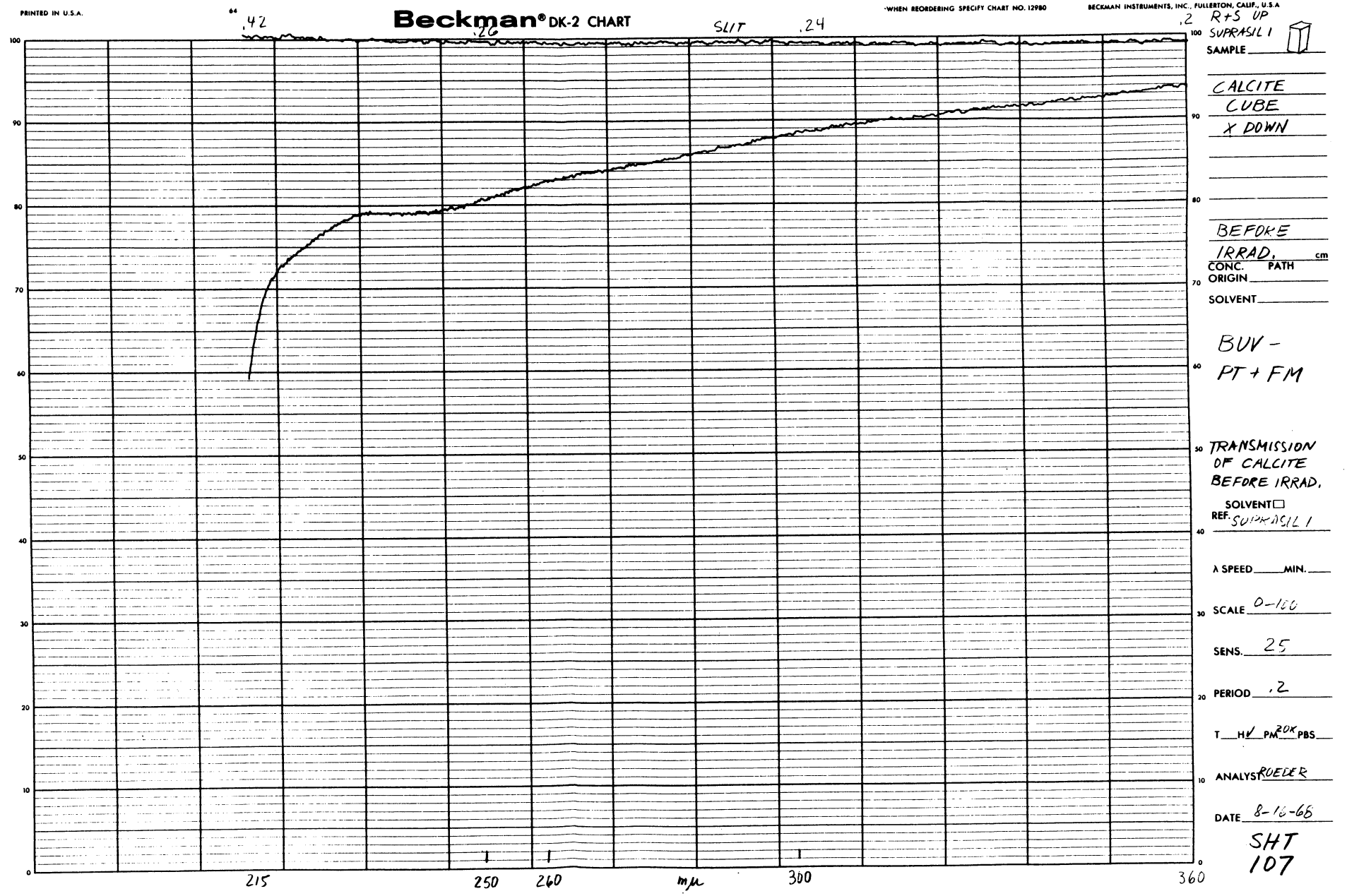

Figure 6-8. Calcite Percent Transmission Graph No. 2 (Before Irradiation)

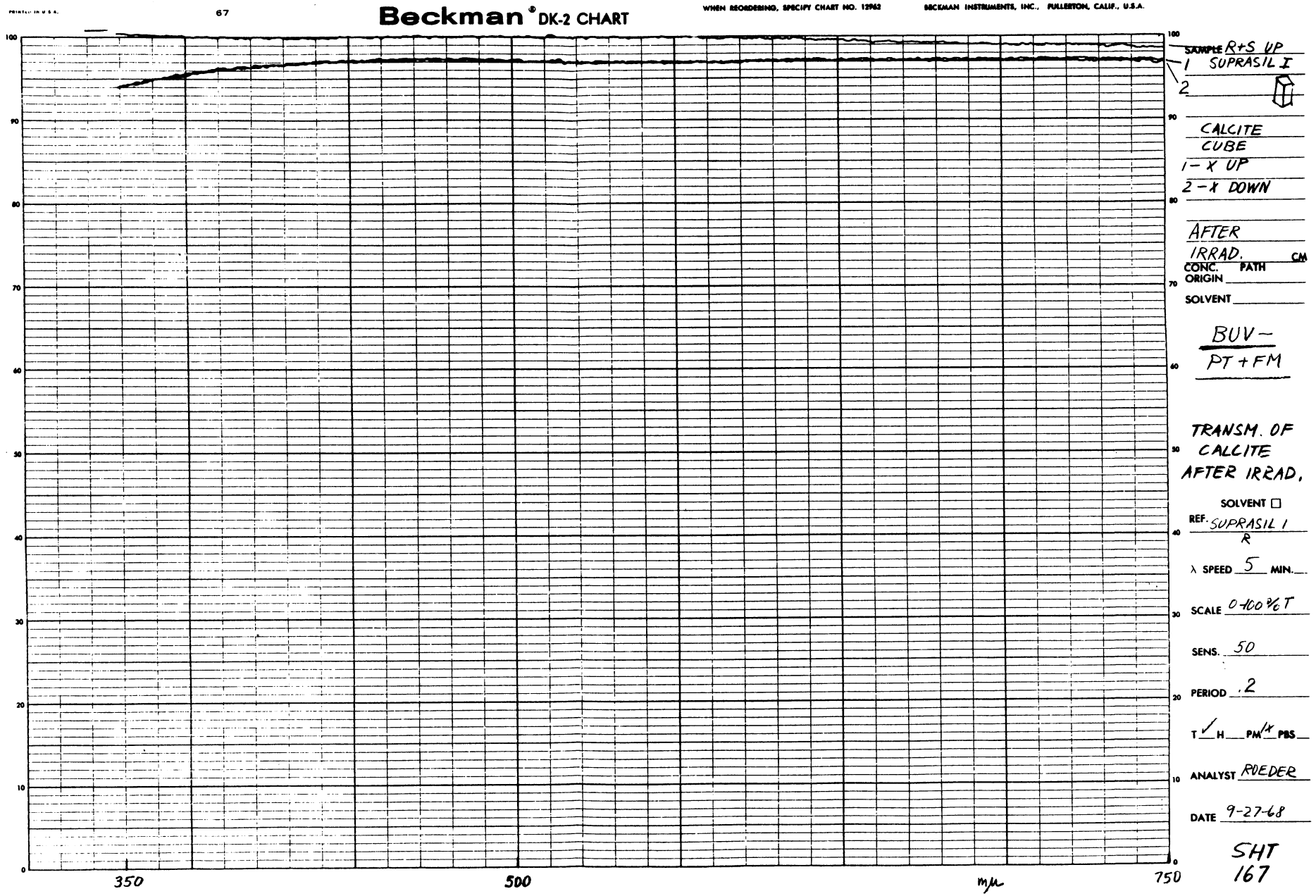

Figure 6-9. Calcite Percent Transmission Graph No. 1 (After Irradiation)

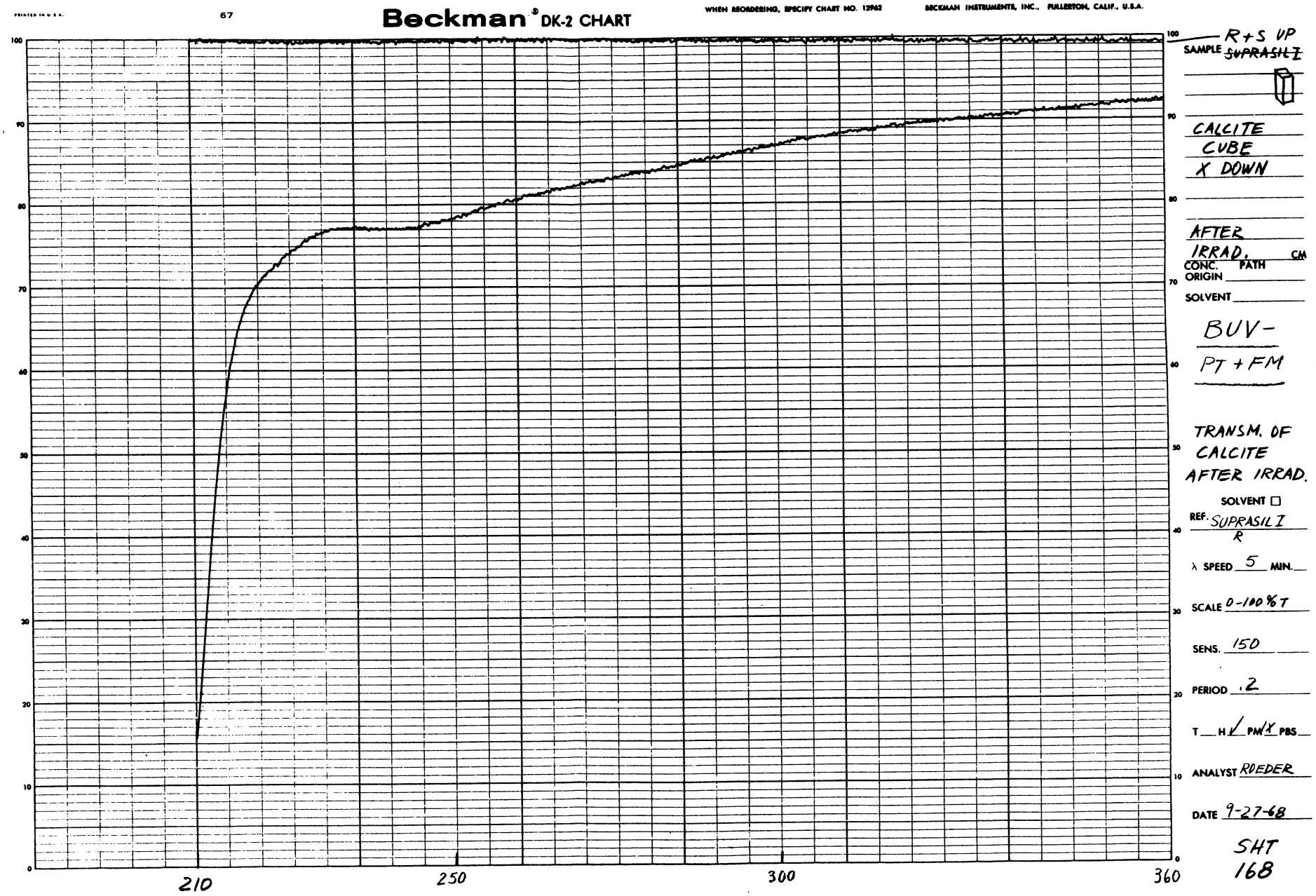

Figure 6-10. Calcite Percent Transmission
Graph No. 2 (After Irradiation)

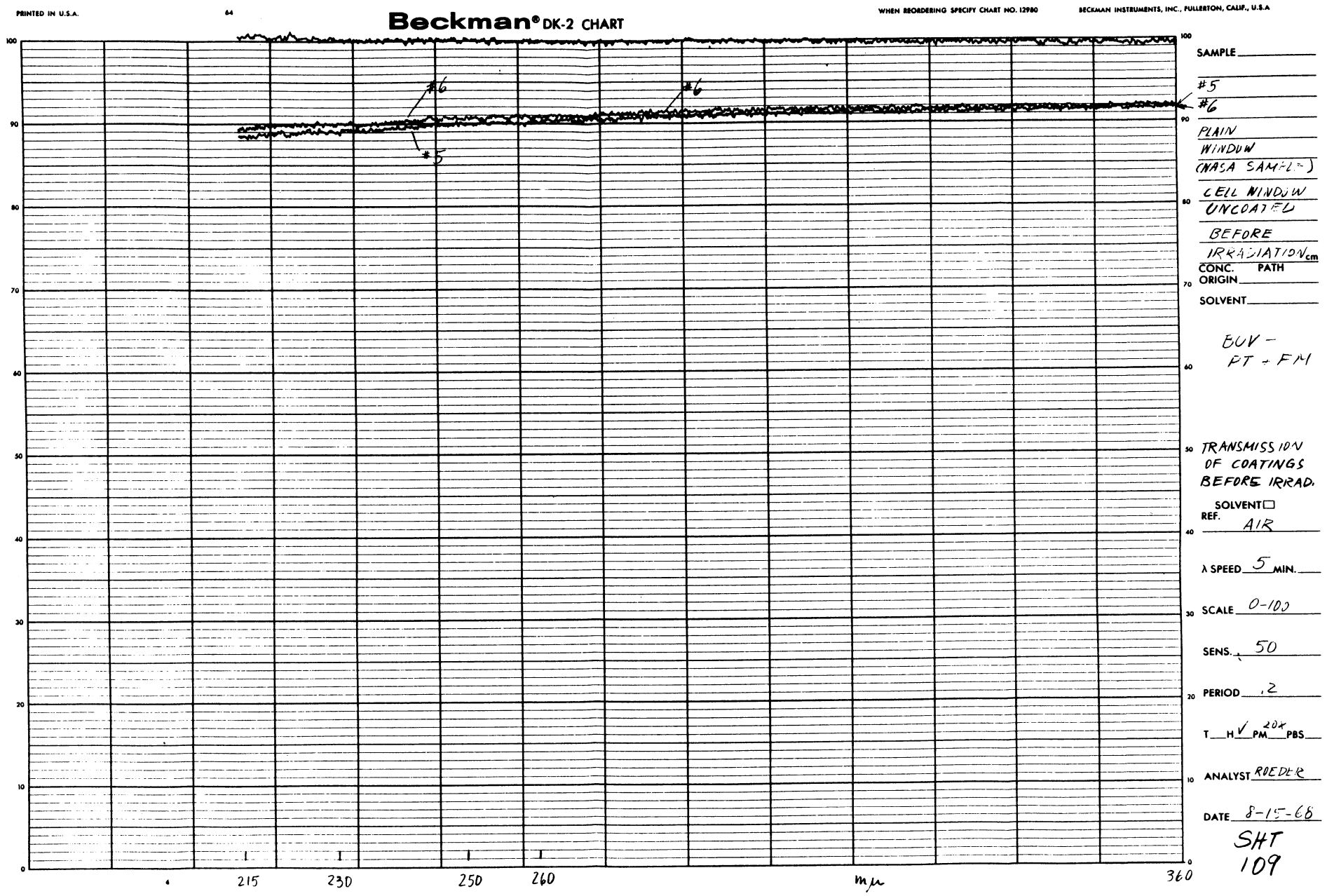

Figure 6-11. Percent Transmission of Coatings No. 1 (Before Irradiation)

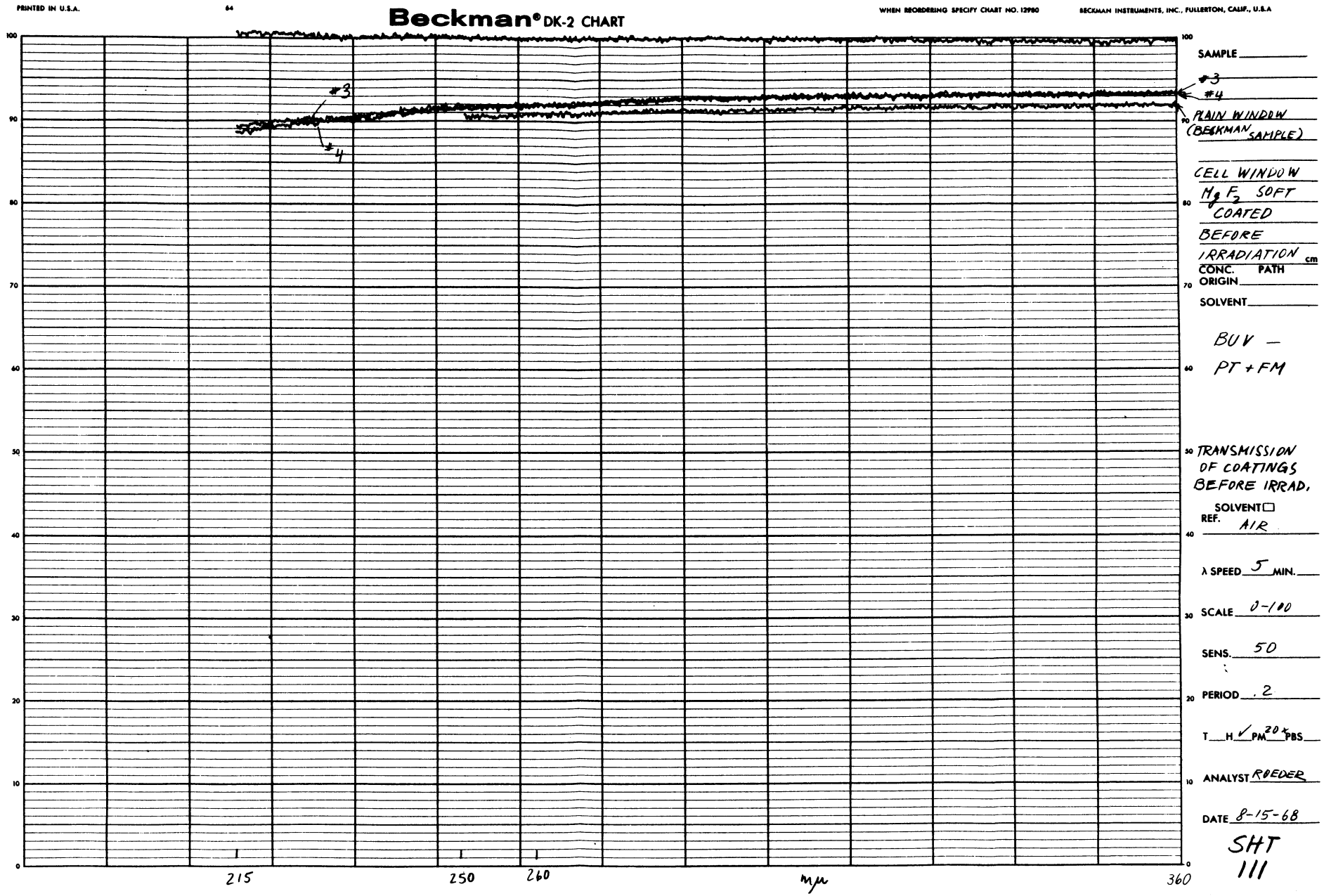

Figure 6-12. Percent Transmission of Coatings No. 2 (Before Irradiation)

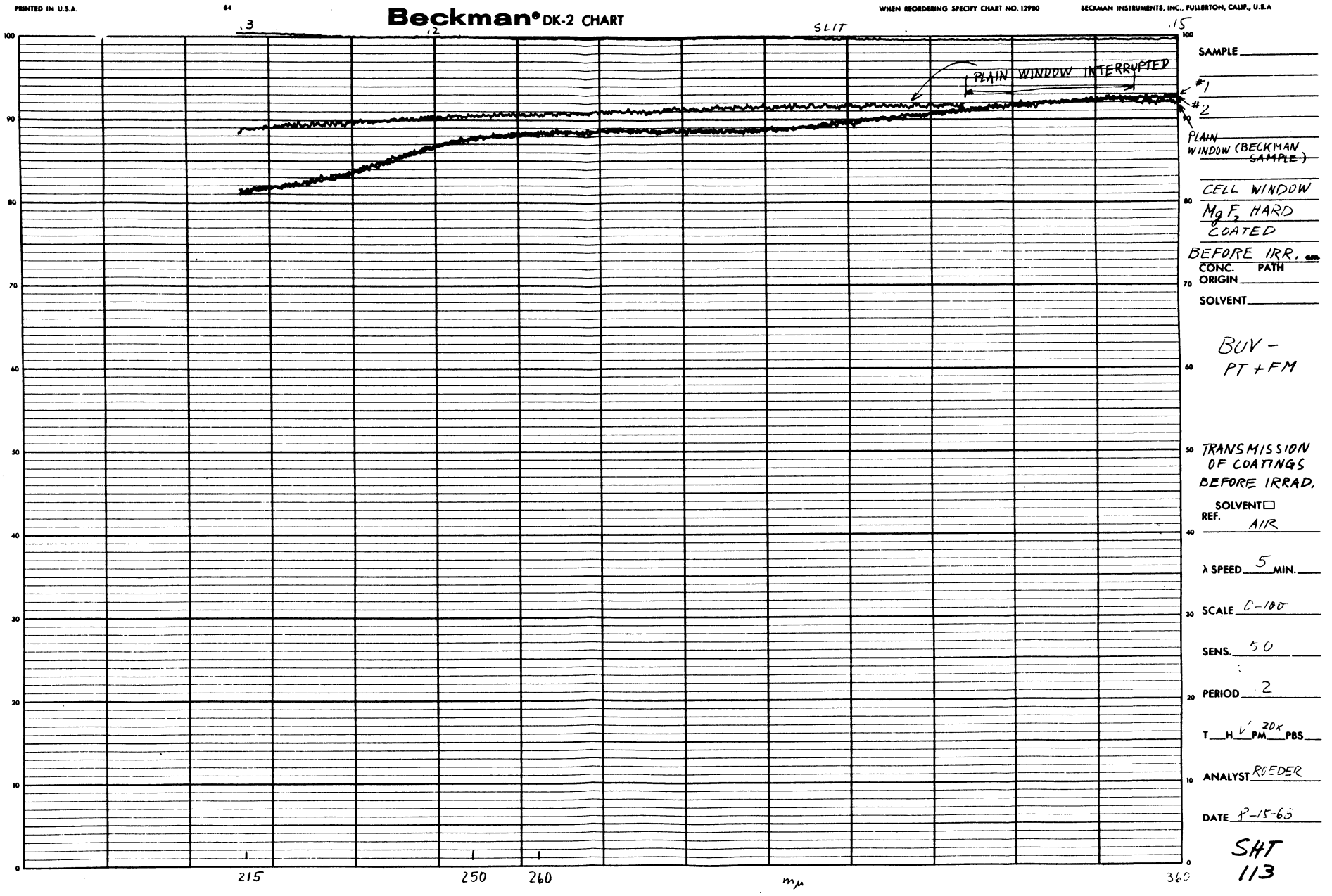

Figure 6-13. Percent Transmission of Coatings No. 3 (Before Irradiation)

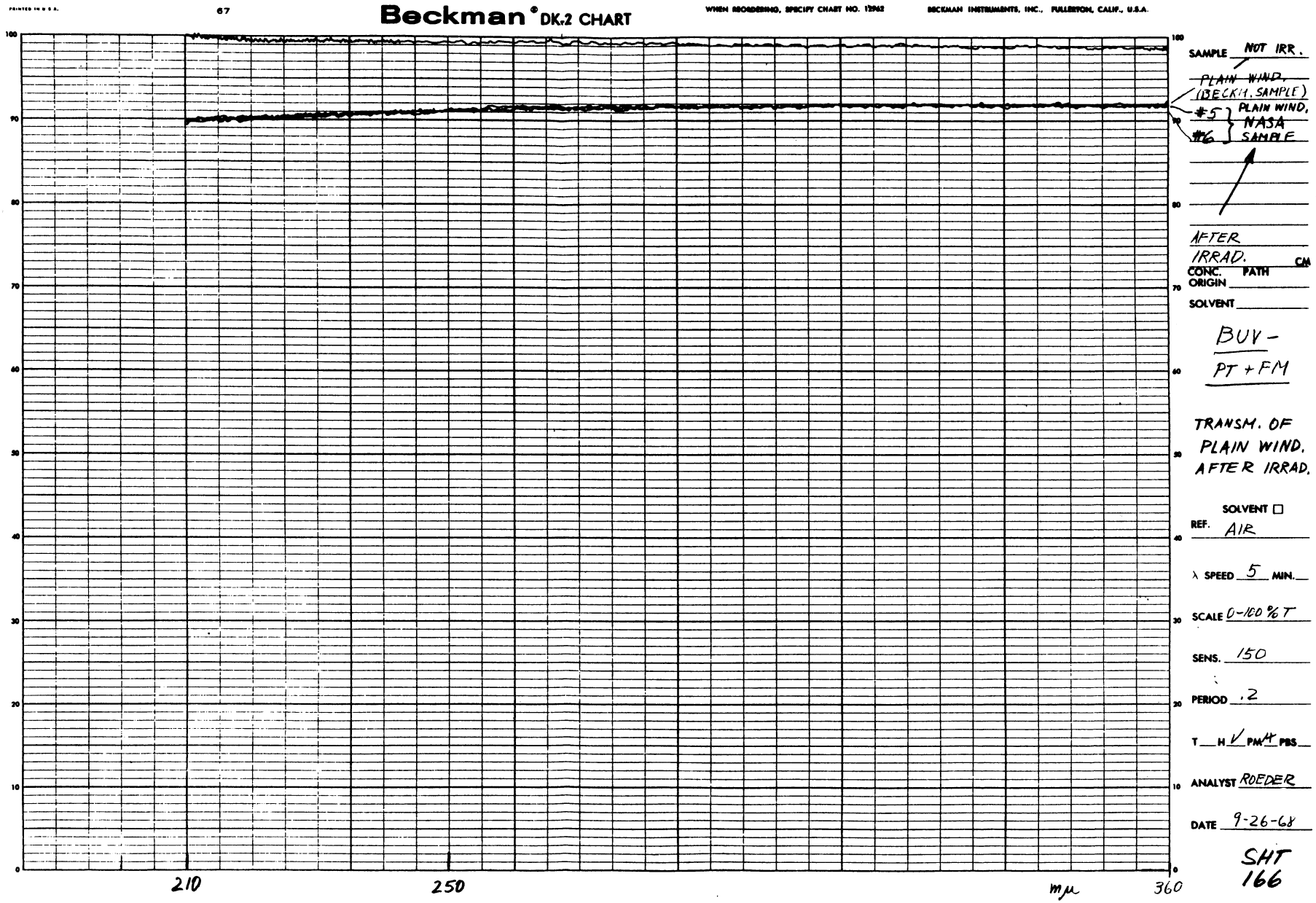

Figure 6-14. Percent Transmission of Coatings No. 1 (After Irradiation)

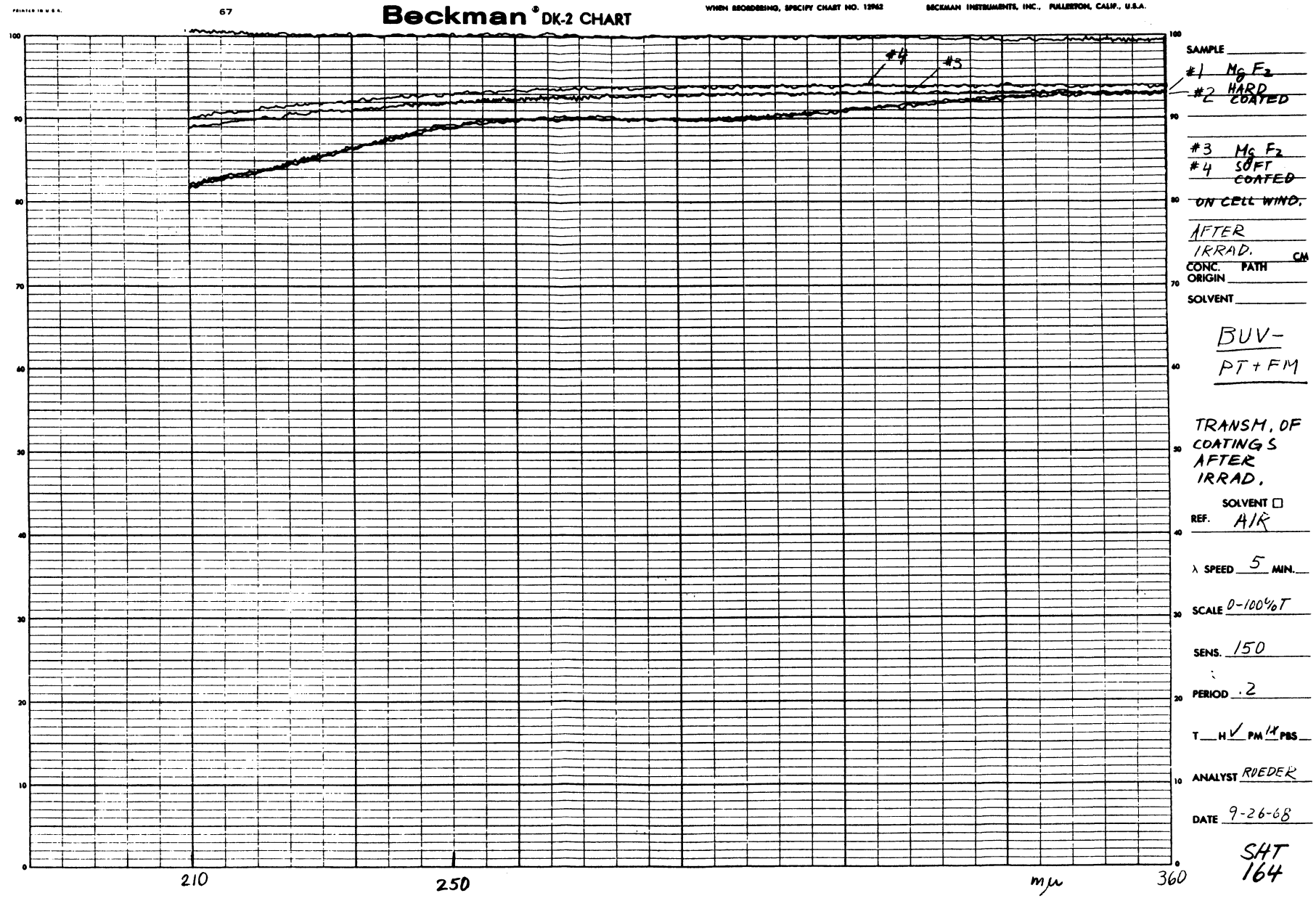

Figure 6-15. Percent Transmission of Coatings No. 2 (After Irradiation)

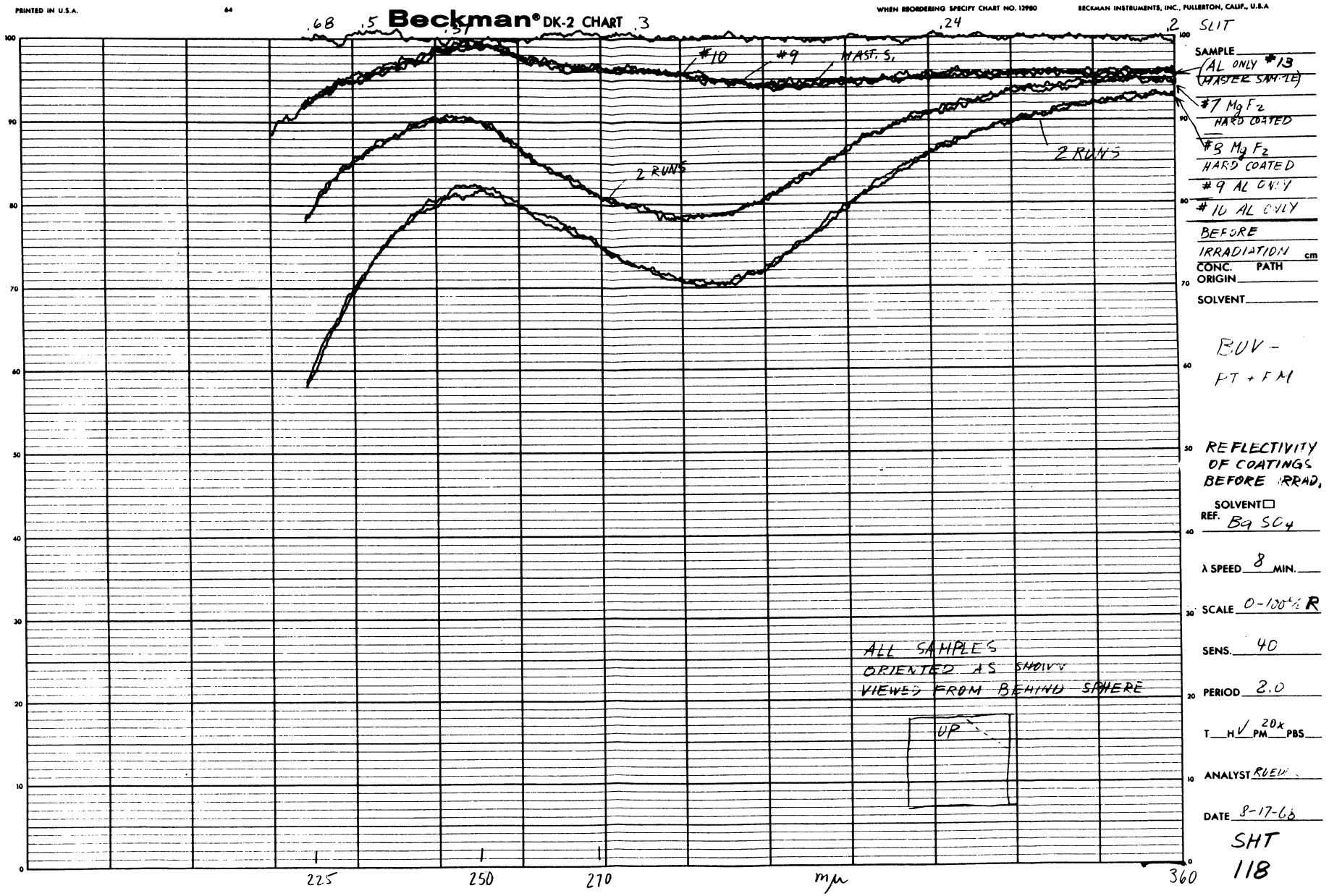

Figure 6-16. Percent Reflectivity of Coatings No. 1 (Before Irradiation)

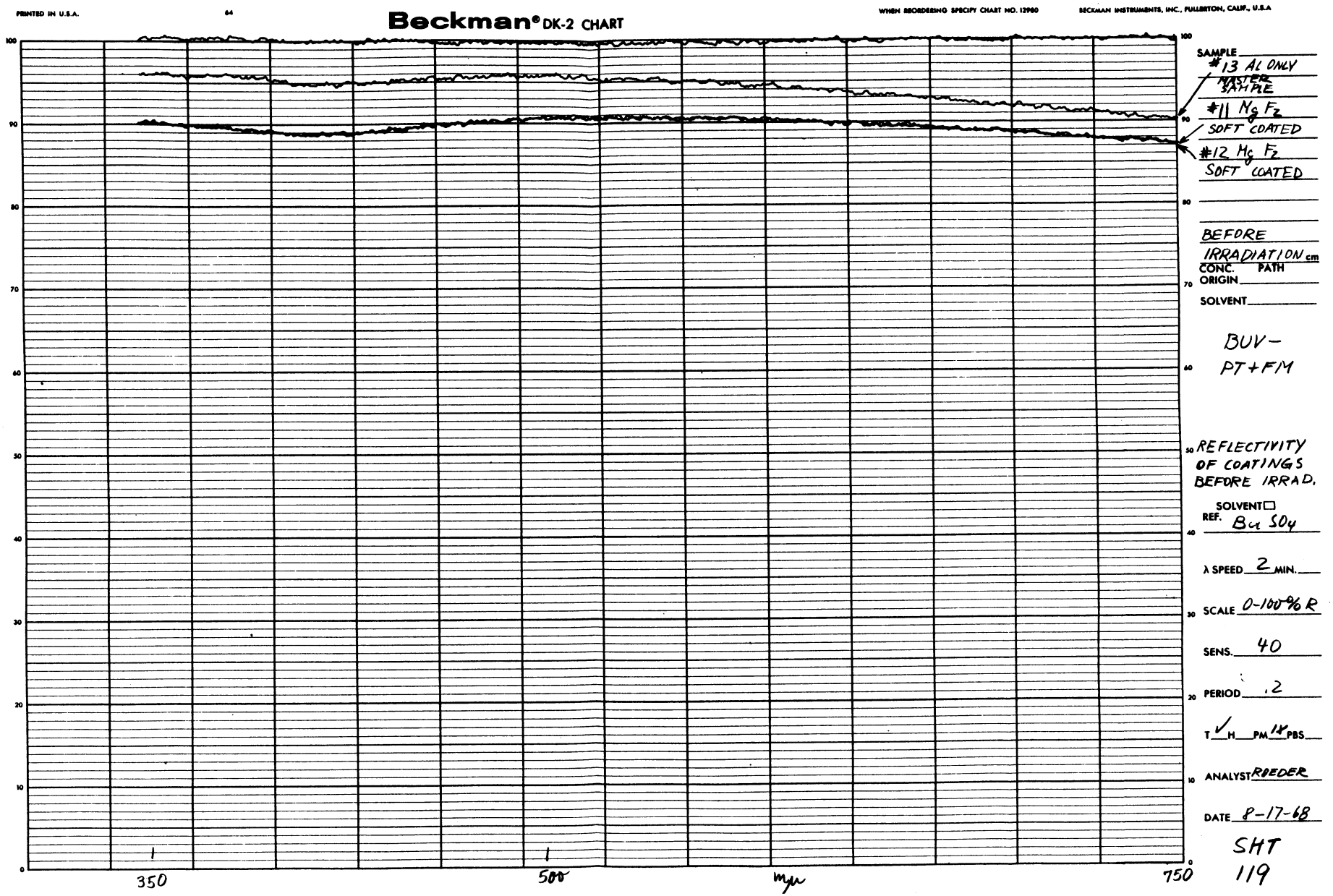

Figure 6-17. Percent Reflectivity of Coatings No. 2 (Before Irradiation)

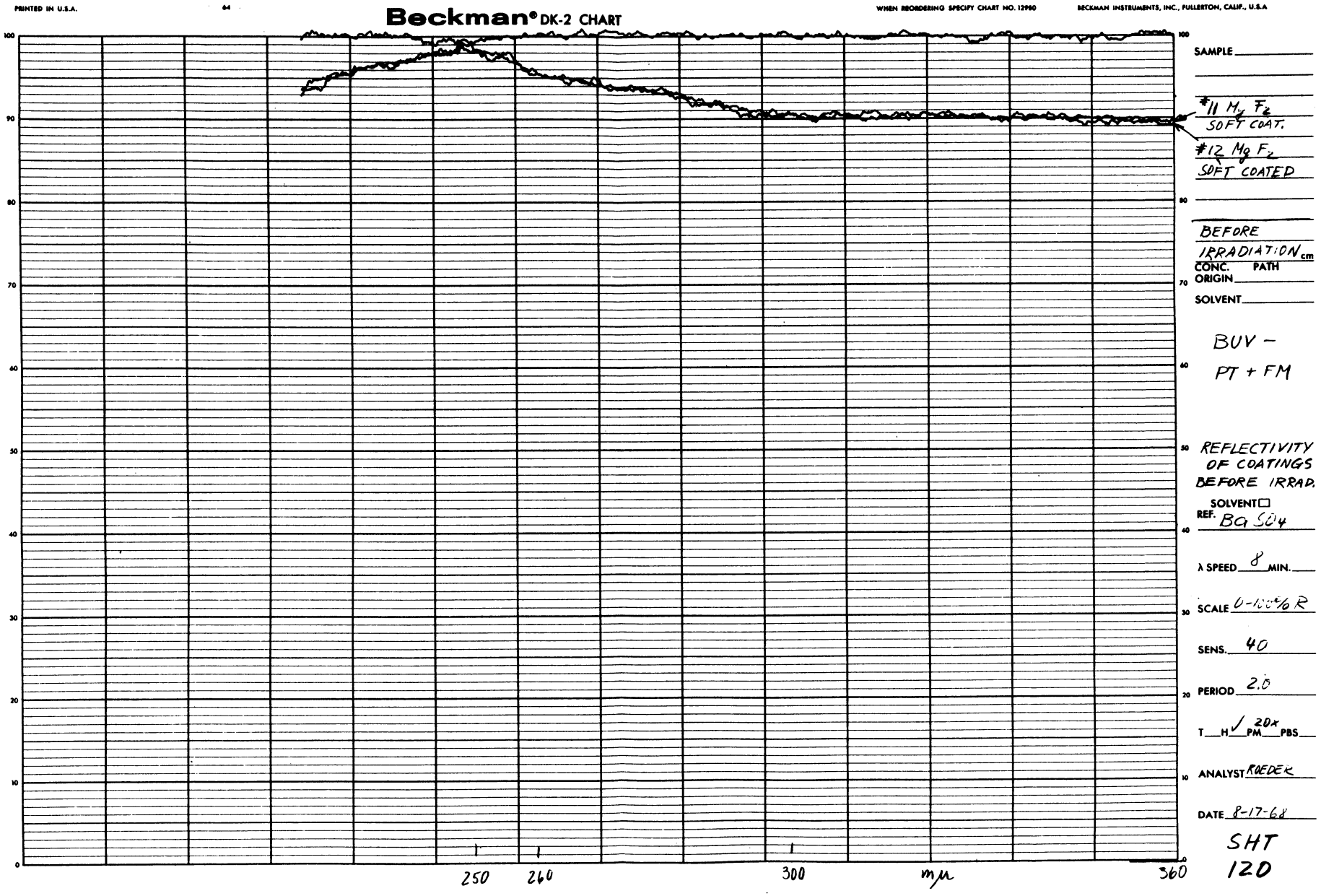

Figure 6-18. Percent Reflectivity of Coatings No. 3 (Before Irradiation)

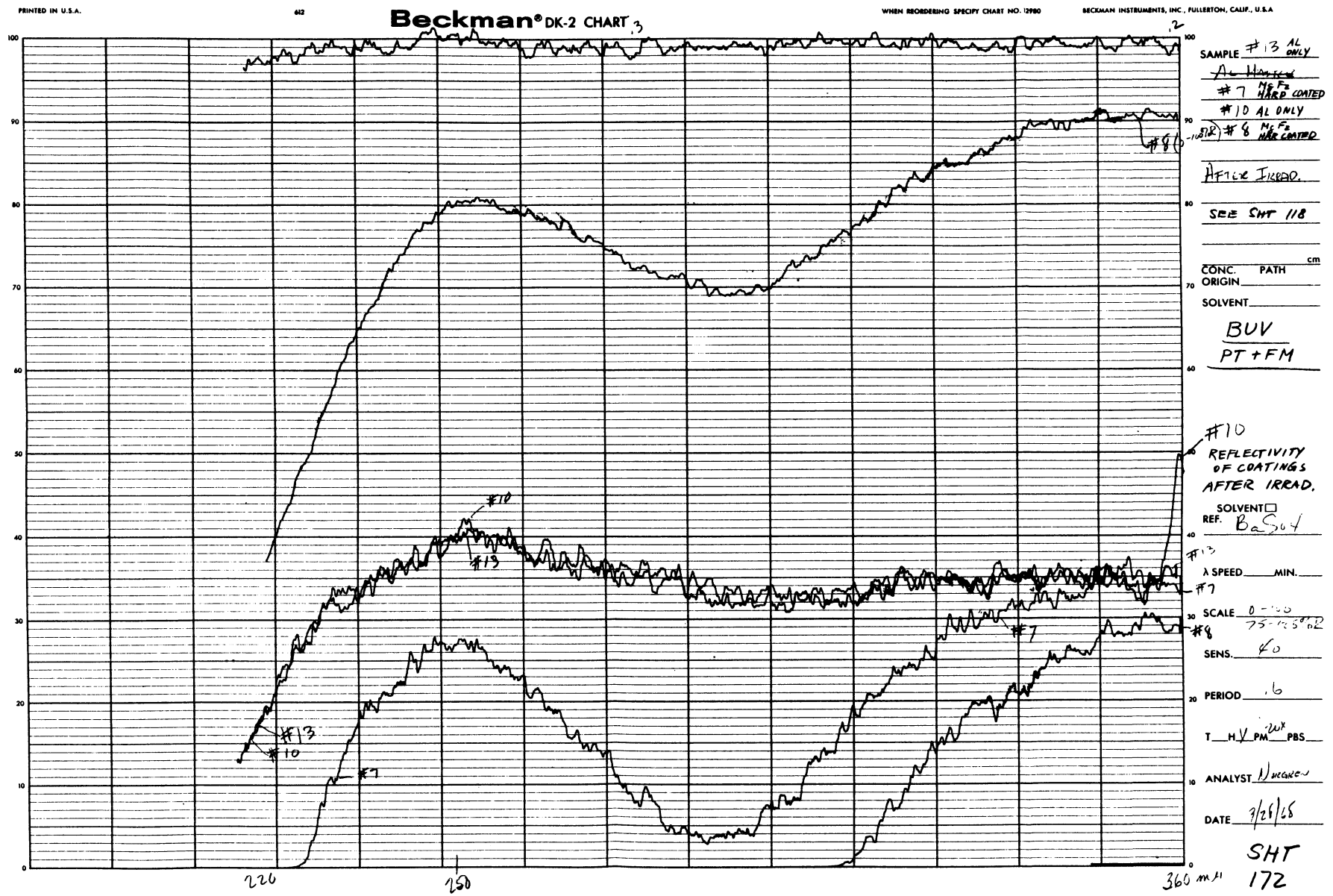

Figure 6-19. Percent Reflectivity of Coatings No. 1 (After Irradiation)

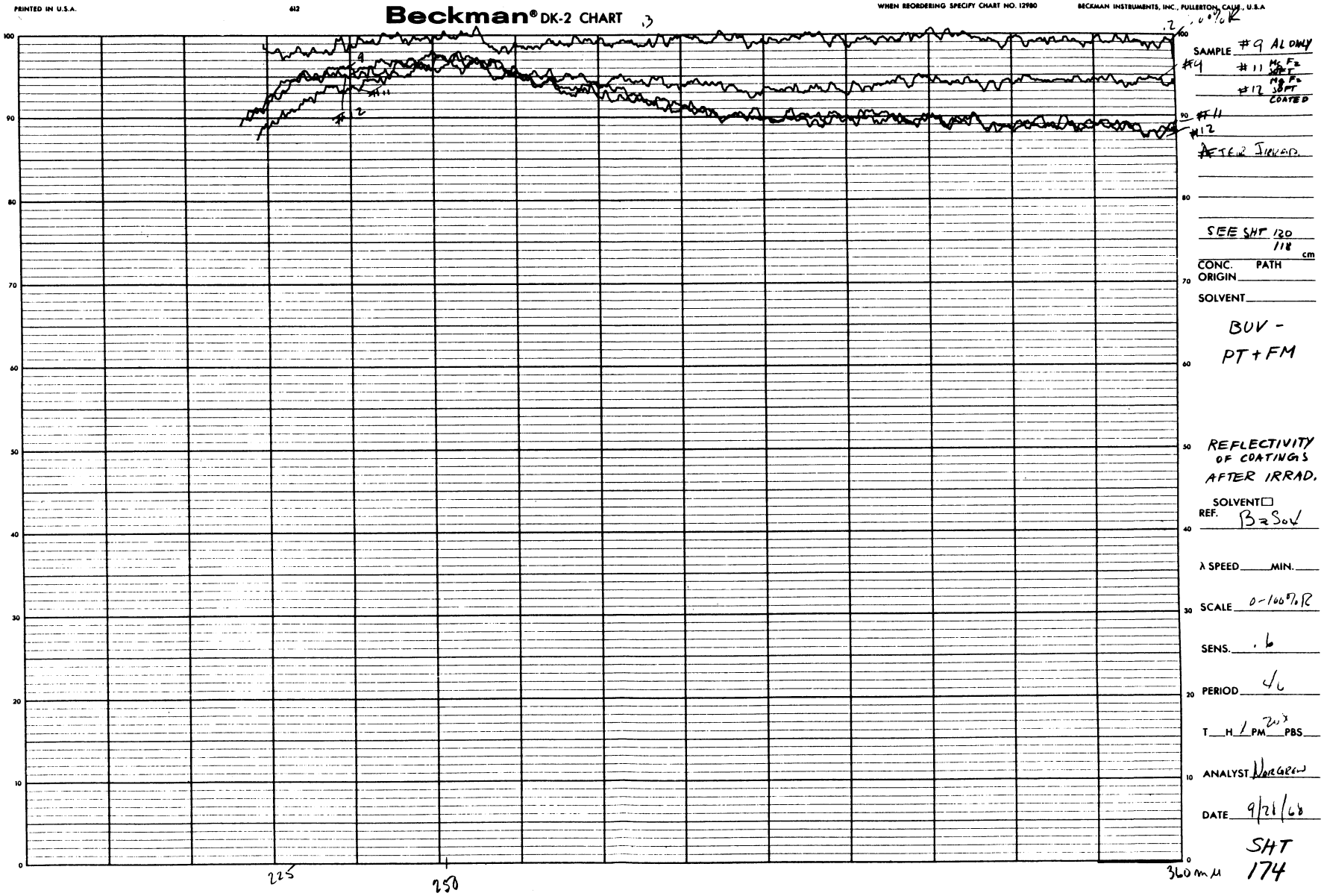

Figure 6-20. Percent Reflectivity of Coatings No. 2 (After Irradiation)

SECTION VII

CALIBRATION

7.1 GENERAL

This section is concerned with the verification of the concepts and theories of the BUV Instrument design through tests performed on the actual hardware.

Most of the calibration data herein was obtained before the hardware components were subjected to environmental tests. Where it was thought that the environmental testing might change the calibration, post-environmental tests were performed.

7.2 CALIBRATION DESCRIPTION

7.2.1 Photometric Sources

Applicable documentation are Beckman drawings:

147418 Photometric Source--Monochromator, and
147419 Photometric Source--Photometer

Two photometric sources are employed in the BUV Instrument to supply an independent, stable reference for calibration. The sources are UV-emitting tritium phosphors rated at 2 curies, and are mounted in a two-part silicon resin (Sylgard 185, Dow-Corning). The monochromator source peaks at 3100 Å, the photometer source at 3800 Å (Figures 7-1 and 7-2). The curves depict linear intensity data. Linearization is accomplished by correcting the response of a Beckman Linear Spectroradiometer to a standard lamp quartz-iodine spectrum.

In the monochromator, the photometric source is located at right-angles to the optical axis next to the entrance slit. In the photometric calibrate position a mirror mounted on the rotating shutter assembly directs the energy into the first monochromator while blocking all external energy.

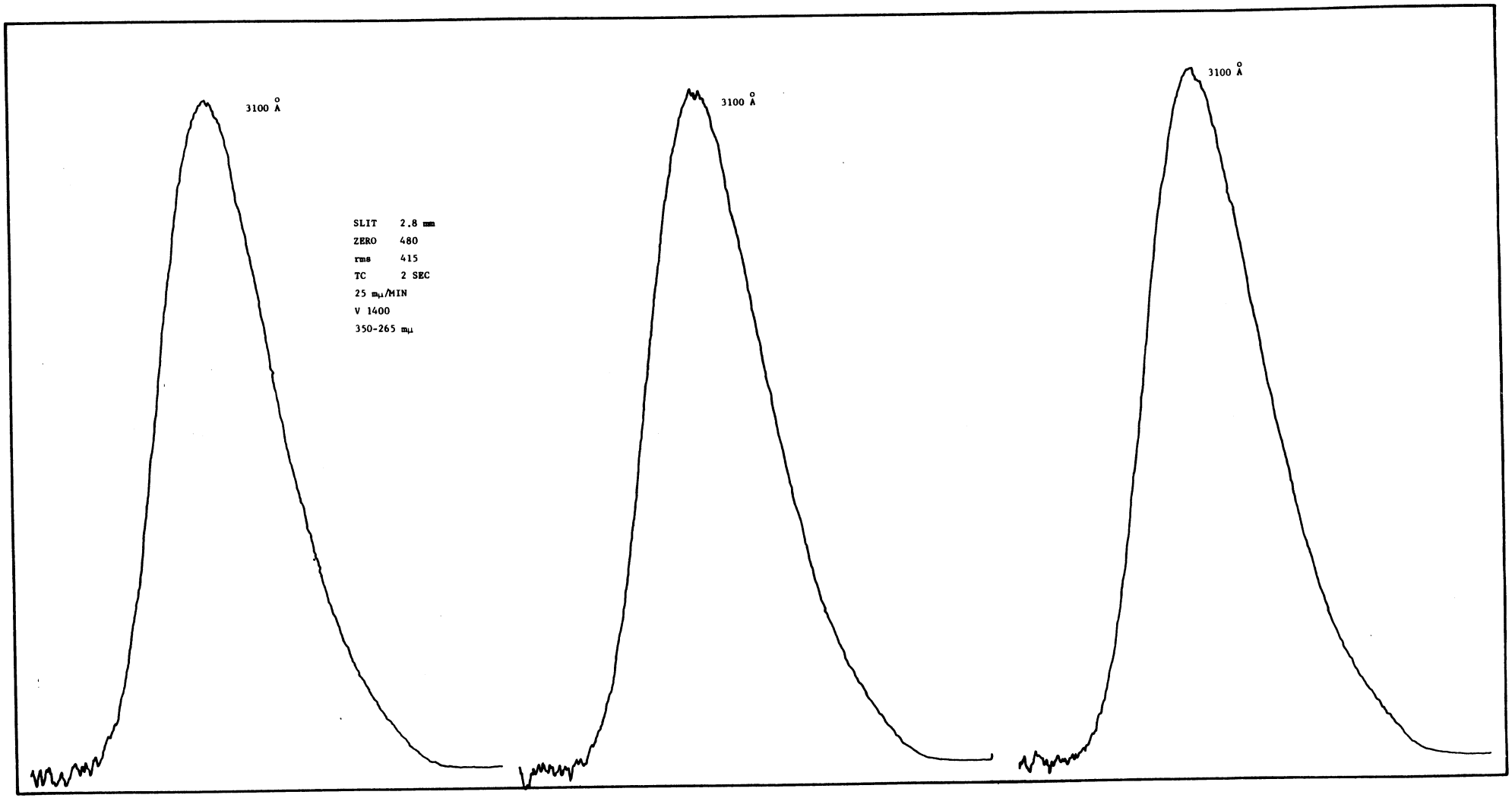

Figure 7-1. Monochromator Source Curve

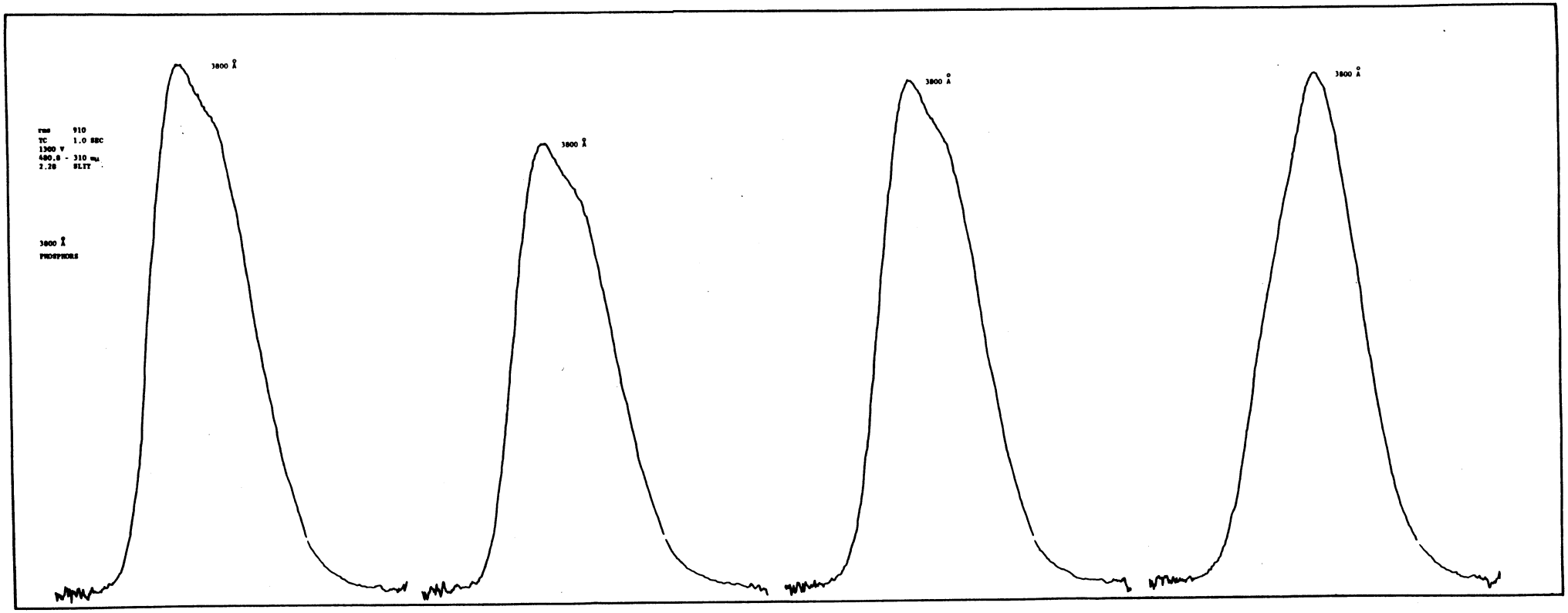

Figure 7-2. Photometer Source Curve

In the photometer, the source in the calibrate position directs its energy onto the interference filter and photomultiplier while external energy is blocked by a rotating shutter. The radioactive gas and the phosphor are housed in a SUPRASIL I envelope which is mounted in an aluminum disc. Manufacturer of the sources is American Atomics.

The photometric sources allow measurement of system degradation with respect to time. Degradation could result from irradiation damage and the loss of sensitivity due to gain changes in the electronic or optical systems. The sources are somewhat affected by temperature changes. While data on source change with temperature was unavailable from American Atomics, a measurement of the influence of temperature can be derived from the environmental test results obtained at Beckman and General Electric.

A compilation of the instrument sensitivity to the source output is shown in Tables 7-1 and 7-2. From these tables, a scan is constructed from the very first and the very last sensitivity data, indicating a relative change of this sensitivity with respect to time and changes in instrument parameters. In addition to using this photometric calibration source during the environmental testing (vibration and thermal), the sensitivity was measured every time the instrument was returned to the optics laboratory. Plots of Table 7-1, columns 1 and 4, are shown in Figures 7-3 and 7-4, and plots of Table 7-2, columns 3 and 9, are shown in Figures 7-5 and 7-6.

Tritium gas in the sources has a half-life of 12 years, with corresponding decrease in output of the sources. The scans showing the sensitivity of the photometric sources in the BUV Instrument are not corrected for dark current, which is too small to make a significant error. The output of the photometer channel photometric source was also recorded during the environmental testing of the Instrument.

American Atomics was also questioned about the effect of 10^6 rad of irradiation exposure on the sources. Information was not available, but the effects would depend largely upon how the exposure was received. The sources are, however, exposed to 1.7×10^6 rad per hour normally, due to the internal tritium gas activity.

			1	2	3	4	5
			Before vibration, after reassembly of collimating mirror and grating mount PMT 12735 1940 V	After 7-1/2 g sine 20 g random Z axis 15 g random X and Y axis Hi volt = 2×10^6 gain (nom) Electrom. gain = 10^7	After all environmental tests Acceptance Tests	Before environmental tests; after feedback resistors were changed	After vibration and thermal cycle; before shipment to GSFC 9-24-69
			3-27-69	4-8-69	4-8-69	9-17-69	9-22-69
Step	Wavelength Å	Micrometer Setting	Keithley Amperes ($\times 10^{-8}$)	Keithley Volts	Keithley Volts	Keithley Volts	Keithley Volts
00	3398	0.719	0.003	0.002	0.23(1)	0.21(1)	-
01	3312	0.651	0.009	0.0045	0.65(1)	0.60(1)	-
02	3175	0.545	0.06	0.024	3.8	3.8	-
03	3125	0.506	0.105	0.042	6.6	6.5	1.34
04	3058	0.455	0.19	0.078	11.6	11.5	2.24
05	3019	0.426	0.235	0.10	14.4	14.2	2.72
06	2975	0.392	0.255	0.112	15.5	15.5	3.00
07	2922	0.352	0.21	0.09	12.5	12.6	2.45
08	2876	0.318	0.12	0.054	7.1	7.2	1.54
09	2830	0.283	0.042	0.016	2.3(1)	2.3	-
10	2735	0.212	0.0015	0.002	0.12(1)	0.1	-
11	2555	0.079	0.0010	0.002	0.1(1)	0.07	-

(1) Noise

Table 7-1. Internal Photometric Calibration Source, Monochromator 3050 Å, P103 Instrument

		Before environmental tests PMT 10137; 2800 V	1	2	3	4	4a	5	6	7	8	9
			Before environmental tests and electronic integration; PMT 12313 2400 V	Before environmental tests; after electr. integration; PMT 12735 $2x10^6$ Hi V; 10^7 electr.	After 11.7 g random Z axis; after entrance shutter magnet replaced $2x10^6$ Hi V; 10^7 electr.	$2x10^6$ Hi V; $2x10^9$ electr. BUV zeroed before every reading	After complete vibration F104 Instrument 11.7 g rand. X Y Z axes $2x10^6$ Hi V; $2x10^9$ electr. BUV zeroed before every reading	After TV, after workmanship shake $2x10^6$ Hi V; $2x10^9$ electr. BUV zeroed before every reading	After install. of addit. stray light shield and removal of both PMT's (cleaning of compartment) $2x10^6$ Hi V; $2x10^9$ electr.	After vibration in X and Z axes $2x10^6$ Hi V; $2x10^9$ electr.	After workmanship vibra. & thermal cycling; after extensive rework by ATC & changes in gain settings $2x10^6$ Hi V; $2x10^9$ electr.	
			1-30-69	4-16-69	5-14-69	6-27-69	6-27-69	6-29-69	7-23-69	9-9-69	9-11-69	10-3-69
Step	Wavelength Å	Micrometer Setting	Keithley Amperes ($x10^{-10}$)	Keithley Amperes ($x10^{-10}$)	Keithley Volts	Keithley Volts	Keithley[3] Volts	Keithley[4] Volts	Keithley[4] Volts	Keithley Volts	Keithley Volts	Keithley Volts
00	3398	0.709	-	0.4	0.003(1)	0.0002	0.04	0.04(1)	0.04(1)	0.03(1)	0.032(1)	0.1(1)
01	3312	0.642	2.5	0.62	0.004(1)	0.0005	0.13	0.135(1)	0.13(1)	0.13(1)	0.012(1)	0.38(1)
02	3175	0.536	5.9	3.0	0.008	0.005	1.1	1.05	1.00(1)	1.00(1)	0.92(1)	2.9(1)
03	3125	0.498	9.5	5.2	0.012	0.010	1.85	1.85	1.72	1.70	1.68	5.2(1)
04	3058	0.446	18.0	9.5	0.024	0.018	3.30	3.40	3.22	3.20	3.05	9.3(1)
05	3019	0.417	21.0	1.2	0.029	0.025(2)	4.30	4.20	4.05	3.90	3.80	11.5
06	2975	0.384	22.5	1.32	0.031	0.028(2)	4.70	4.70	4.40	4.22	4.15	12.8
07	2922	0.344	17.4	1.13	0.027	0.0235(2)	3.95	3.80	3.60	3.50	3.40	10.5
08	2876	0.309	9.10	6.4	0.016	0.0145(2)	2.20	2.30	1.95	1.90	1.90	6.0
09	2830	0.275	5.60	2.5	0.007	0.006	0.75	0.75	0.75	0.66	0.64	1.9(1)
10	2735	0.204	2.35	0.45	0.003(1)	0.0022	0.03	0.06(1)	0.07(1)	0.015(1)	0.015(1)	0.03(1)
11	2555	0.071	-	0.32	0.003(1)	0.0020	0.015(1)	0.015(1)	0.003(1)	0.006(1)	0.007(1)	0.01(1)

NOTES:

(1) Noisy
(2) Instrument zeroed before this reading
(3) Instrument zeroed before every reading after (1.1)
(4) Instrument zeroed before every reading

Table 7-2. Internal Photometric Calibration Source, Monochromator 3050 Å, F104 Instrument

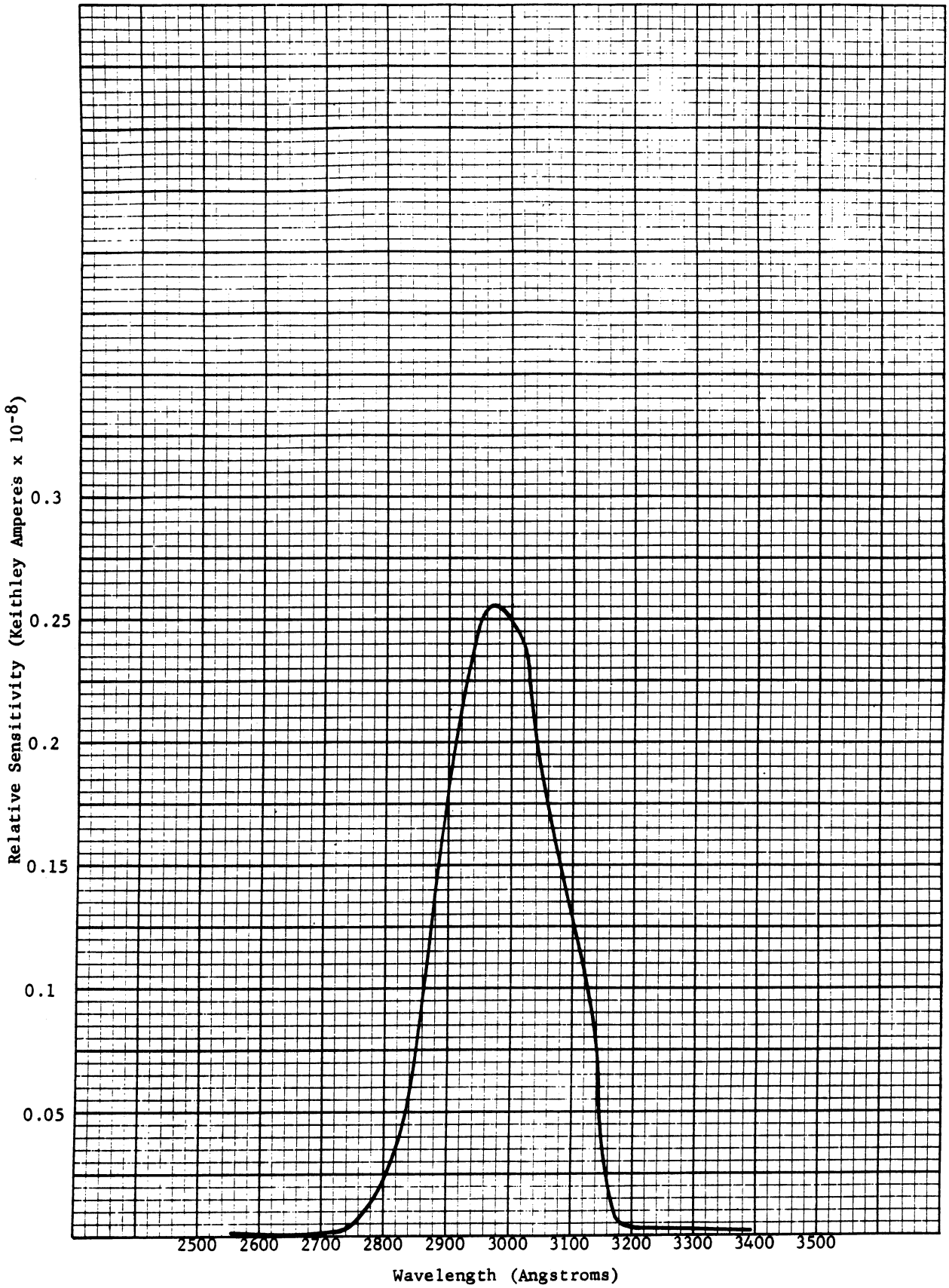

Figure 7-4. Internal Photometric Calibration After Vibration Tests (P103 Instrument)

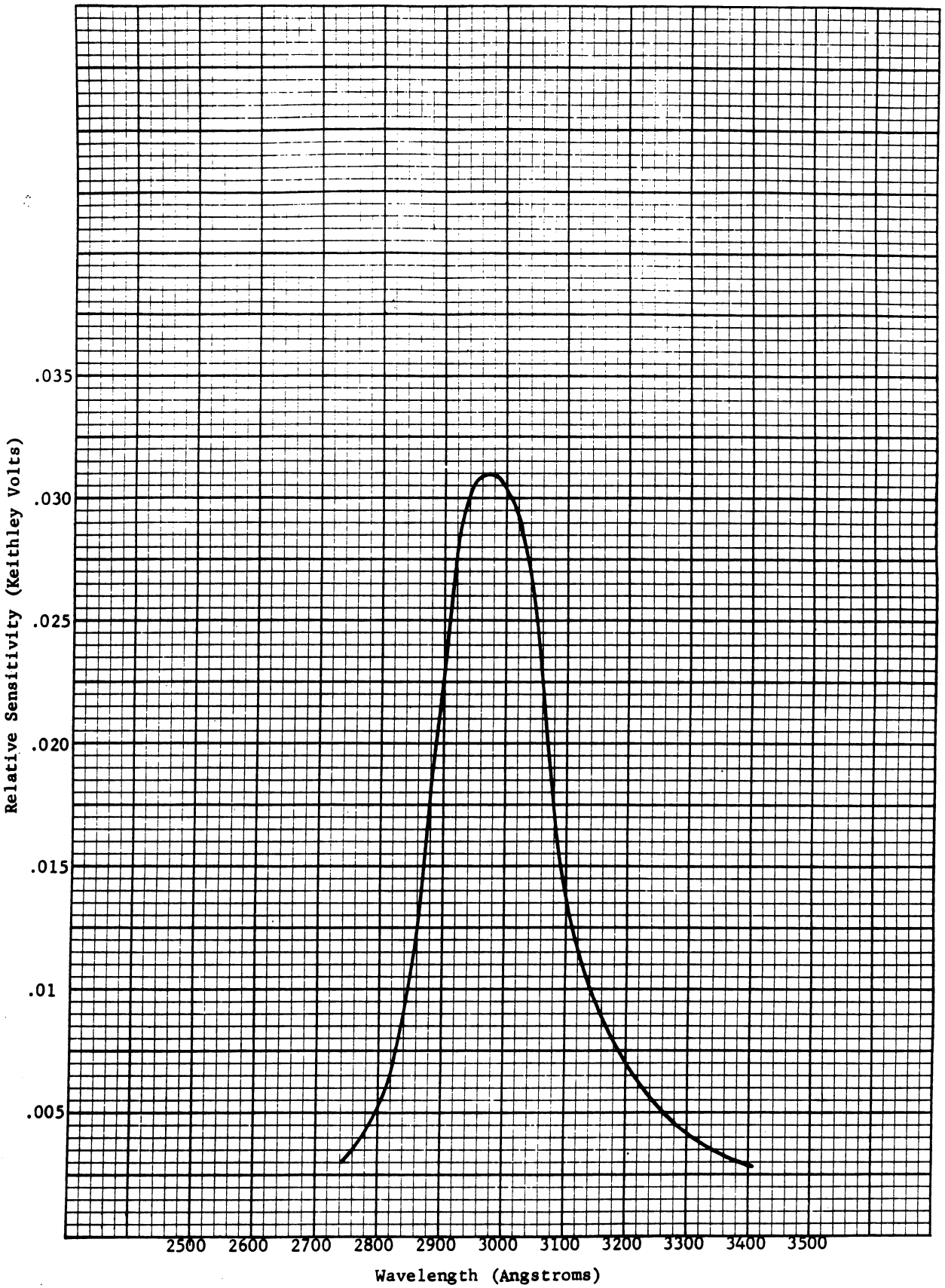

Figure 7-5. Internal Photometric Calibration Before Environmental Tests (F104 Instrument)

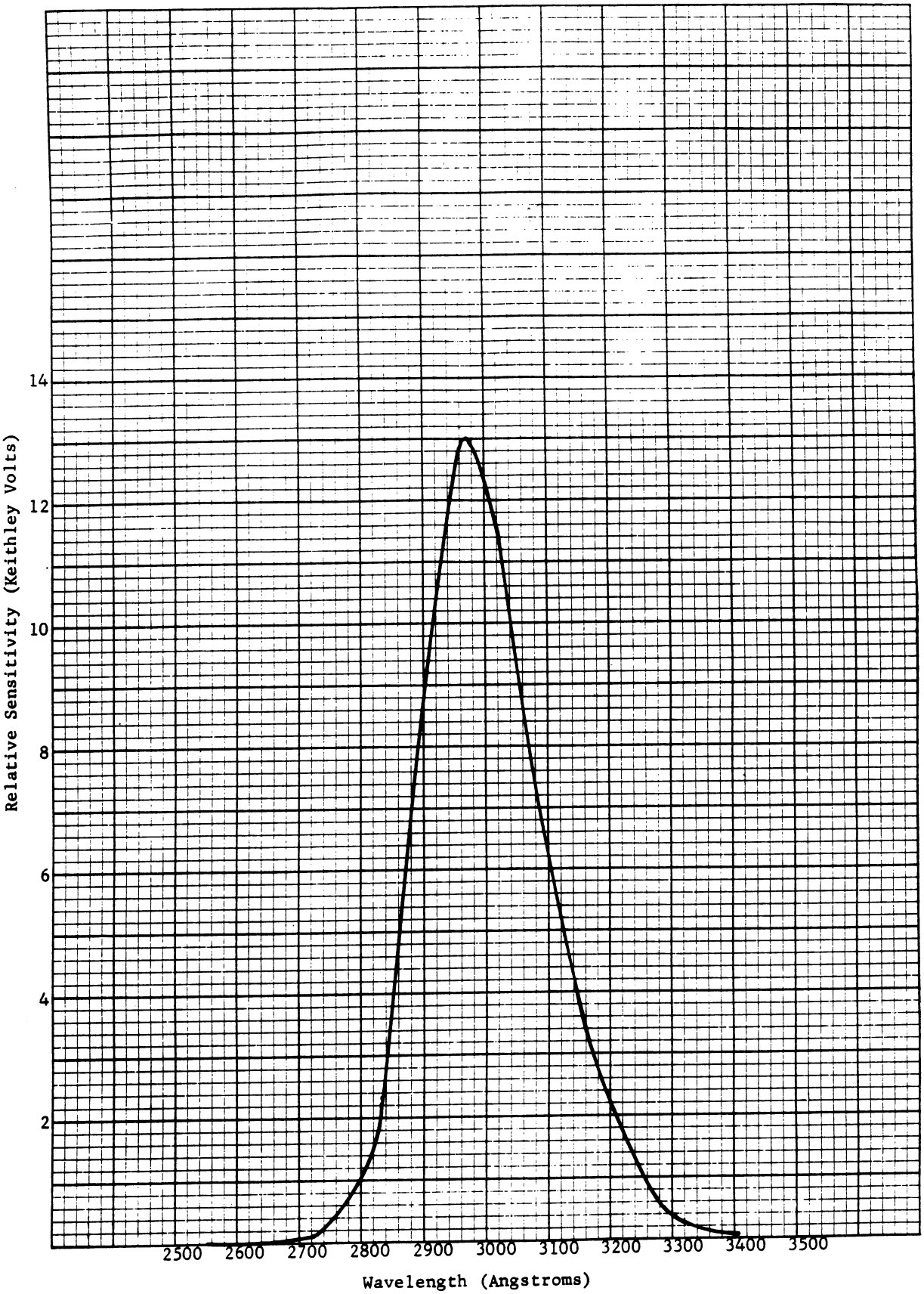

Figure 7-6. Internal Photometric Calibration After Environmental Tests (F104 Instrument)

7.2.2 Wavelength Calibration

The wavelength scan of the BUV Instrument contains twelve sampling steps in the wavelength range 2500 to 3400 Å, and seven wavelength calibration steps grouped around the 2537 Å mercury line. The half-bandwidths of all steps are nominally 10 Å wide.

A wavelength scan starts at 3400 Å and continues sequentially through the sampling steps and seven calibration steps before returning to the 3400 Å starting point.

The scan dwells for two seconds at each sampling step and moves to the next step in 0.5 second. During the 2-second measuring interval, any given wavelength is displayed at the exit slit to an accuracy of +0.2 Å. A complete scan is accomplished in 32 seconds with 2 seconds for each sampling step, and 0.5-second movement to the next step.

The positions of the wavelength scan steps are cut into a continuous cam. One cam revolution contains all sampling and calibration steps. The sampling steps are 10° wide and the calibration steps are 8° wide. Table 7-3 shows the sampling and calibration wavelengths, and separation between steps.

Step Number	Wavelength Å	Separation Å	Step Number	Wavelength	Separation Å	
00	3398	86	10	2735	180	
01	3312	137	11	2555		
02	3175	50	19	2522	5	Calibration Steps
03	3125	67	20	2527	5	
04	3058	39	21	2532	5	
05	3019	44	22	2537	5	
06	2975	53	23	2542	5	
07	2922	46	24	2547	5	
08	2876	46	25	2552	5	
09	2830	95				

Table 7-3. Sampling and Calibration Wavelengths

Note that in the region where ozone backscattering occurs, the sampling points are more closely spaced, and that the wavelength calibration steps have a fixed 5 Å separation.

The wavelength accuracy of the BUV is checked with the internal mercury calibration lamp, and with a PEN RAY Mercury Light Pencil. To accomplish this, a micrometer is installed in the instrument, as shown in Figure 7-7.

The micrometer settings (which place the cam follower in contact with the cam steps) are recorded for each step of the wavelength cam. Also recorded is the micrometer setting corresponding to the peak PMT output current at 2537 Å when the instrument is illuminated by its own mercury calibration lamp through the auxiliary slit. The micrometer setting gives peak PMT output current at each mercury line when the BUV is illuminated externally by a PEN RAY Mercury Light Pencil diffused from a MgO plate.

From the data taken by diffused external illumination, the micrometer reading versus wavelength was plotted for each mercury line except 2537 Å. The mean slope of that plot was used to determine the spectral displacement of each cam step from the nearest mercury line to determine the wavelength associated with each cam step. The deviation of the actual wavelength from the design wavelength at each step versus wavelength was plotted. Using the value of the mean slope, the deviation of the 2537 Å cam step position from the 2537 Å calibration lamp output was determined and plotted on the deviation curve.

The following mercury emission lines of the PEN RAY Mercury Light Pencil were used for calibration:

3341.47, 3131.83, 3125.67, 3124, 2967.28,
2892.6. 2752.78, 2652.8, 2537.26

None of these lines exactly matches a cam step and thus cannot be used for a direct measurement.

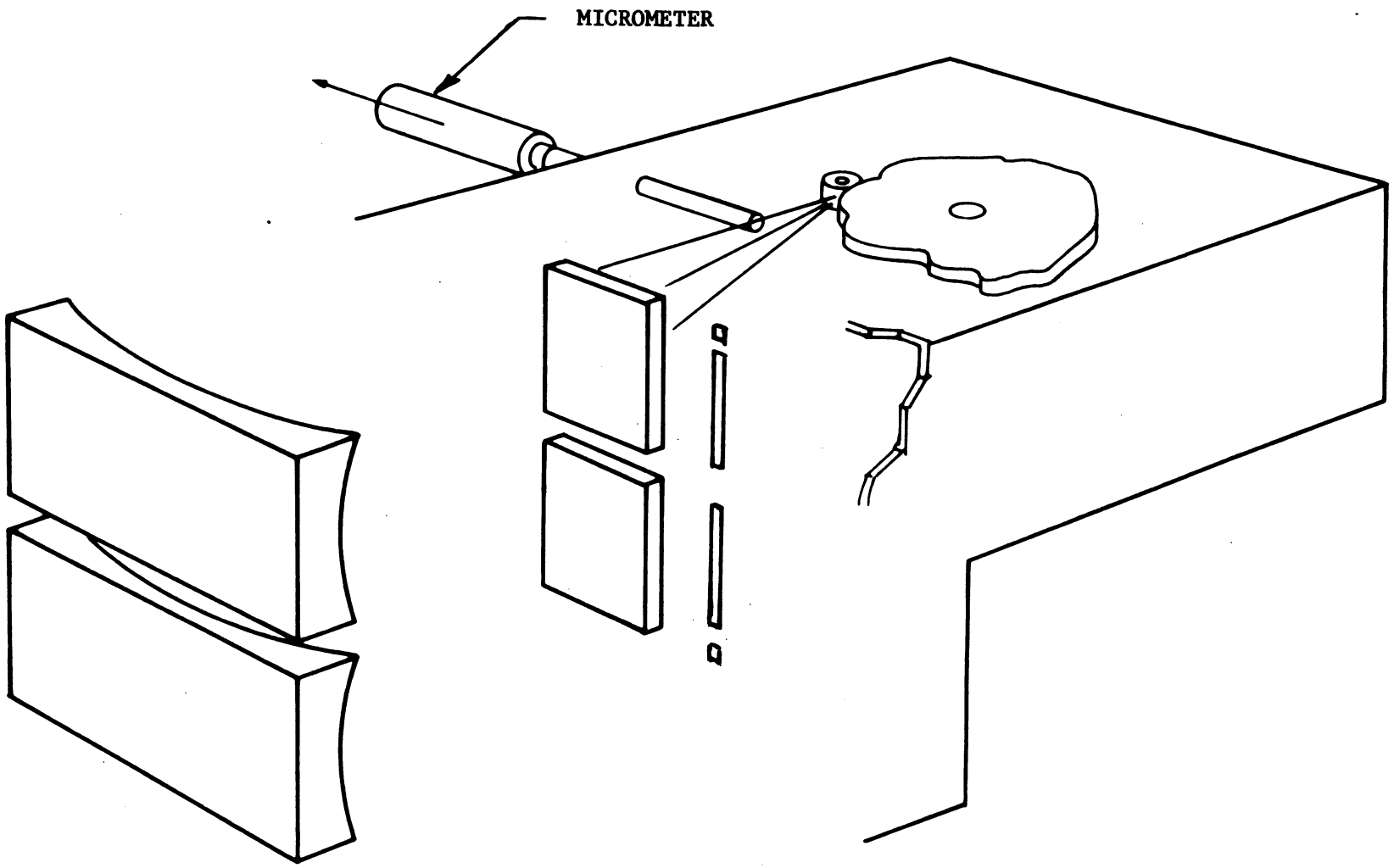

Figure 7-7. BUV External Micrometer Installation

A verification of the correct alignment of the optics is obtained with a scan of the internal mercury calibration lamp. Figure 7-8 shows a typical scan for the F104 instrument. The P103 instrument is similar.

The seven calibration steps are grouped in such a way that the fourth step corresponds to the 2537 Å mercury emission line. The 5 Å separation between the steps permits viewing of the 10 Å half-bandwidth lines with steps 3 and 5. If the shoulders of steps 3 and 5 are of equal heights, then the 2537 Å line is correctly placed on step 4. The spike response just prior to step 1 is the 2537 Å mercury line, which must be passed to get on the first calibration step at 2522 Å.

The internal mercury calibration lamp scan, Figure 7-8, and the external PEN RAY scan determine the correct location of the cam steps in the spectrum. Table 7-4 lists the final values for the cam steps of the BUV P103 and F104 Instruments.

Step Number	Wavelength Step Desired (Å)	Actual Wavelength Step (Å) BUV P103	BUV F104
00	3398	3400.77	3398.61
01	3312	3314.62	3312.09
02	3175	3176.8	3374.76
03	3125	3126.42	3124.48
04	3058	3059.86	3058.71
05	3019	3021.01	0318.73
06	2975	2976.9	2975.14
07	2922	2924.06	2921.84
08	2876	2878.18	2876.21
09	2830	2832.42	2830.42
10	2735	2737.65	2735.3
11	2555	2557.34	2555.11
12	2537	2539.62	2537.34

Table 7-4. Final Values for Cam Steps

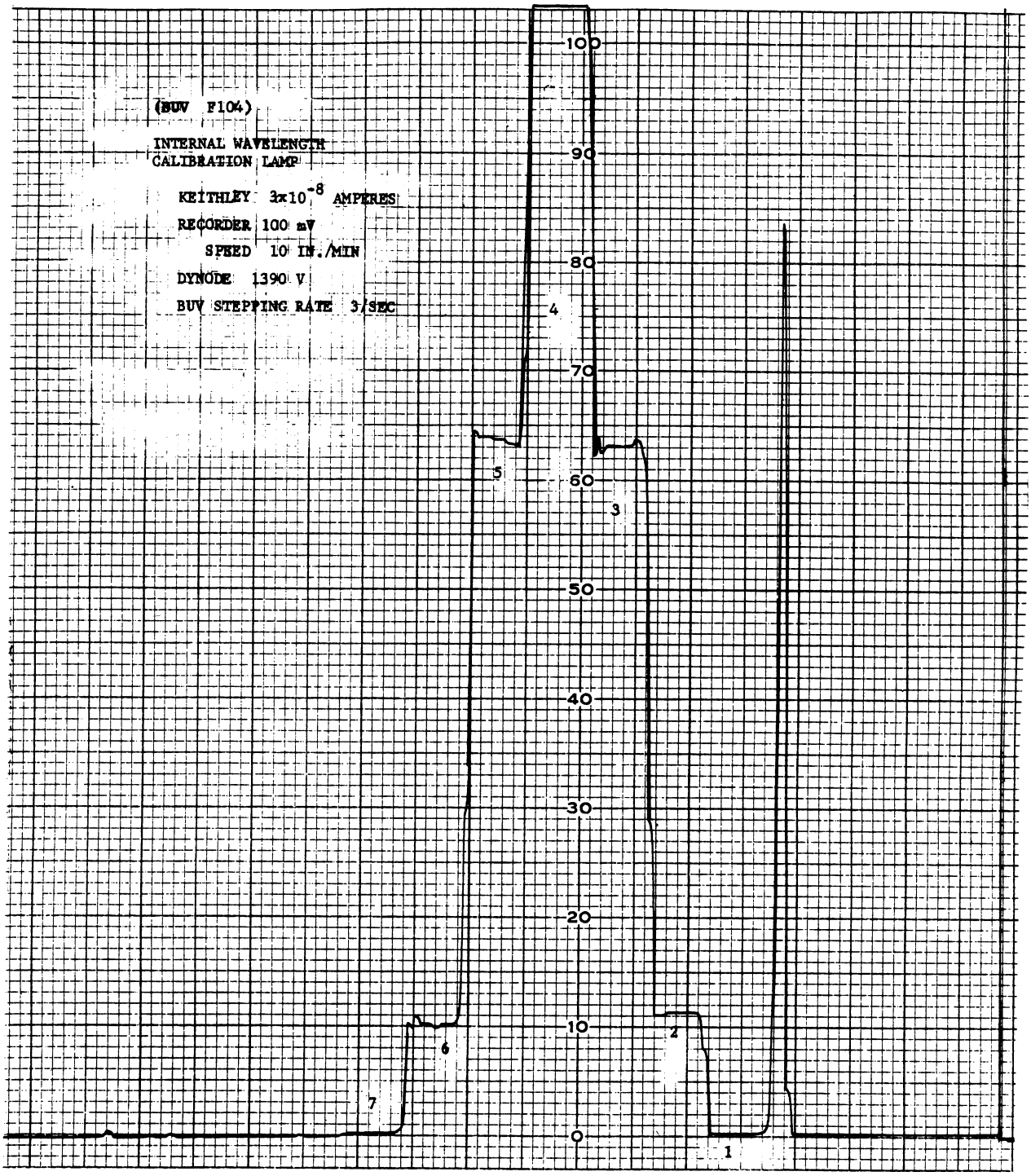

Figure 7-8. Wavelength Calibration Lamp Scan

The wavelength accuracy of P103 and F104 were monitored through all environmental tests. The manual PEN RAY external and the mercury lamp internal calibration methods were used employing the micrometer screw after the vibration, acceleration, and thermal vacuum tests. The internal mercury lamp method was employed during all environmental tests with the resultant data plotted in Figures 7-22 through 7-25 (see Section 7.3.1.3).

The final wavelength steps were calculated using five mercury calibration lines in the BUV wavelength range instead of the seven formerly used. The peaks of the two wavelengths eliminated (3131-3125 Å group, and the 2652.8 Å line) could not be exactly located on the BUV for final calibration. The wavelength data of the five mercury lines was obtained from Beckman Instruction Manual 1220-A, "Model DK-A Recording Spectrophotometers". The calibration points reflect an "in air" environment.

The final data for the best possible values was determined with the least squares method using a computer program. Reproductions of the computer data are shown on the following pages.

7.2.3 Radiant Sensitivity, Q.I. Lamp

The radiant sensitivity measurements were conducted to establish the response of the BUV Instrument to a calibrated light source with a known flux output.

Quantum efficiency and gain of the photomultiplier may be deduced using the measured transmission and reflectance values of the optical components. A calibrated 1000 W quartz-iodine lamp is used for the calibration. Instructions for using this standard of spectral irradiance are listed in paragraph 7.2.6 of the Instruction Manual. Copies of the flux output for several calibrated lamps are also contained in that paragraph.

FINAL WAVELENGTH STEPS FOR P103 INSTRUMENT

POLFIT 18:12 LA 024 06/10/70

VERSION 7/1/69

LEAST-SQUARES POLYNOMIALS

NUMBER OF POINTS = 5
MEAN VALUE OF X = .33492
MEAN VALUE OF Y = 2898.09
STD ERROR OF Y = 297.236

NOTE: CODE FOR 'WHAT NEXT?' IS:

Q = STOP PROGRAM
1 = COEFFICIENTS ONLY
2 = ENTIRE SUMMARY
3 = FIT NEXT HIGHER DEGREE

POLYFIT OF DEGREE 2 INDEX OF DETERM = .999996 WHAT NEXT? 2

TERM	COEFFICIENT
0	2.4495382E+03
1	1.3678590E+03
2	-6.2655730E+01

X-ACTUAL	Y-ACTUAL	Y-CALC	DIFF	PCT-DIFF
.6728	3341.48	3341.47	8.01849E-03	2.39969E-04
.3851	2967.28	2967.01	.27129	9.14355E-03
.3293	2892.6	2893.18	-.579857	-2.00422E-02
.2237	2752.78	2752.39	.387161	1.40664E-02
.0637	2536.33	2536.42	-8.65593F-02	-3.41266E-03

STD ERROR OF ESTIMATE FOR Y = .53258

WHAT NEXT? 0

WVCAL3 19:00 LA 024 06/10/70

WAVELENGTHS CALCULATED WITH SECOND ORDER POLYNOMIAL

ALL WAVELENGTHS IN ANGSTROMS, MICROMETER READINGS IN INCHES

WVLNGTH, SPEC	WVLNGTH, CALC	(SPEC)-(CALC)	MICROM
3398	3400.77	-2.76602	.7191
3312	3314.62	-2.61844	.6519
3175	3176.8	-1.80089	.5453
3125	3126.42	-1.41537	.5066
3058	3059.86	-1.86029	.4557
3019	3021.01	-2.00706	.4261
3975	2976.9	-1.90221	.3926
2922	2924.06	-2.05549	.3526
2876	2878.18	-2.18136	.318
2830	2832.42	-2.42367	.2836
2735	2737.65	-2.64717	.2127
2555	2557.34	-2.34381	.0791

CALCULATED VALUES BELOW WERE CORRECTED FOR 4A OFFSET
OF INTERNAL CALIBRATION AUXILIARY SLIT.

2522	2524.53	-2.52718	.0579
2527	2529.83	-2.83258	.0618
2532	2534.86	-2.86415	.0655
2537	2539.62	-2.62216	.069
2542	2544.38	-2.37864	.0725
2547	2549.54	-2.54107	.0763
2552	2554.43	-2.43013	.0799

THE AVERAGE DEVIATION IS:-2.32725
THE STANDARD DEVIATION IS: 2.35896

THE VALUES OF A,B,AND C USED WERE***
A= 2449.54 B= 1367.86 C=-62.6557

FINAL WAVELENGTH STEPS FOR F104 INSTRUMENT

```
POLFIT          15:15          06/11/70

                    *** VERSION OF 08/01/69 ***

L E A S T - S Q U A R E S   P O L Y N O M I A L S

        NUMBER OF POINTS = 5
         MEAN VALUE OF X = 0.32758
         MEAN VALUE OF Y = 2898.09
          STD ERROR OF Y = 297.236

   NOTE:  CODE FOR 'WHAT NEXT?' IS:

            0 = STOP PROGRAM
            1 = COEFFICIENTS ONLY
            2 = ENTIRE SUMMARY
            3 = FIT NEXT HIGHER DEGREE


POLYFIT OF DEGREE 2
INDEX OF DETERMINATION = 0.999999
   WHAT NEXT? 2


TERM            COEFFICIENT

 0               2457.99
 1               1372.48
 2              -64.3426

X-ACTUAL        Y-ACTUAL        Y-CALC          DIFF            PCT-DIFF

 0.6644          3341.48         3341.47         1.37024E-2      4.10071E-4
 0.3776          2967.28         2967.07         0.213257        7.18746E-3
 0.3219          2892.6          2893.13        -0.526398       -1.81948E-2
 0.2167          2752.78         2752.39         0.393127        1.42831E-2
 0.0573          2536.33         2536.42        -9.33533E-2     -3.68051E-3

STD ERROR OF ESTIMATE FOR Y = 0.492963

   WHAT NEXT? 0
```

WVCAL8 7:45 LA 024 06/12/70

WAVELENGTHS CALCULATED WITH SECOND ORDER POLYNOMIAL

ALL WAVELENGTHS IN ANGSTROMS, MICROMETER READINGS IN INCHES

WVLNGTH, SPEC	WVLNGTH, CALC	(SPEC)-(CALC)	MICROM
3398	3398.61	-.606384	.7089
3312	3312.09	-8.64944E-02	.6416
3175	3174.76	.237156	.5357
3125	3124.48	.518948	.4972
3058	3057.71	.288177	.4463
3019	3018.73	.269966	.4167
2975	2975.14	-.137688	.3837
2922	2921.84	.155056	.3435
2876	2876.21	-.209358	.3092
2830	2830.42	-.422375	.2749
2735	2735.3	-.298229	.204
2555	2555.11	-.111725	.071

CALCULATED VALUES BELOW WERE CORRECTED FOR 4A OFFSET
OF INTERNAL CALIBRATION AUXILLIARY SLIT.

2522	2522.18	-.179923	.0498
2527	2527.23	-.233509	.0535
2532	2532.42	-.421841	.0573
2537	2537.34	-.335392	.0609
2542	2542.25	-.247272	.0645
2547	2547.29	-.293858	.0682
2552	2551.93	7.02934E-02	.0716

THE AVERAGE DEVIATION IS:-.107603
THE STANDARD DEVIATION IS: .303756

THE VALUES OF A,B,AND C USED WERE***
A= 2457.99 B= 1372.48 C=-64.3426

The radiant sensitivity measurement setup is shown in Figure 7-9. The Sensor Module is protected from the heat of the lamp by a metal plate. A flat, black coating on the plate minimizes back-reflection against the envelope of the lamp. A hole in the plate permits illumination of only the diffuser plates.

The calibrated lamp is positioned perpendicular to the optical axis of the instrument and the outboard mounting surface, as shown in Figure 7-9, with the center line going through a point on the diffuser plate where the optical axis intercepts the plate.

To change from the photometer to the spectrometer position, the lamp is moved vertically only. For the calibration measurements of the spectrometer, the lamp is positioned 50 cm away from the diffuser plates and is operated at 8.3 amperes (measured on a 0.25 percent ac meter). The anode current should not exceed one microampere at maximum response. The wavelength positions are then scanned either with the micrometer screw or the cam drive, and the response recorded.

Figure 7-10 shows the output of a standard quartz-iodine lamp. Figures 7-11 and 7-12 show the response curves of P103 and F104 Instruments to a calibrated lamp. In the 2900 to 3400 Å region, the curve shape is largely influenced by the special coating of the first collimating mirror.

7.2.4 MCS B,C

As mentioned in paragraph 7.2.1, two photometric sources are employed to supply stable reference for calibration. In the monochromator, the photometric source is located at right-angles to the optical axis next to the entrance slit. In the photometric calibrate position, a mirror mounted on the rotating shutter assembly directs the energy into the first monochromator while blocking all external energy.

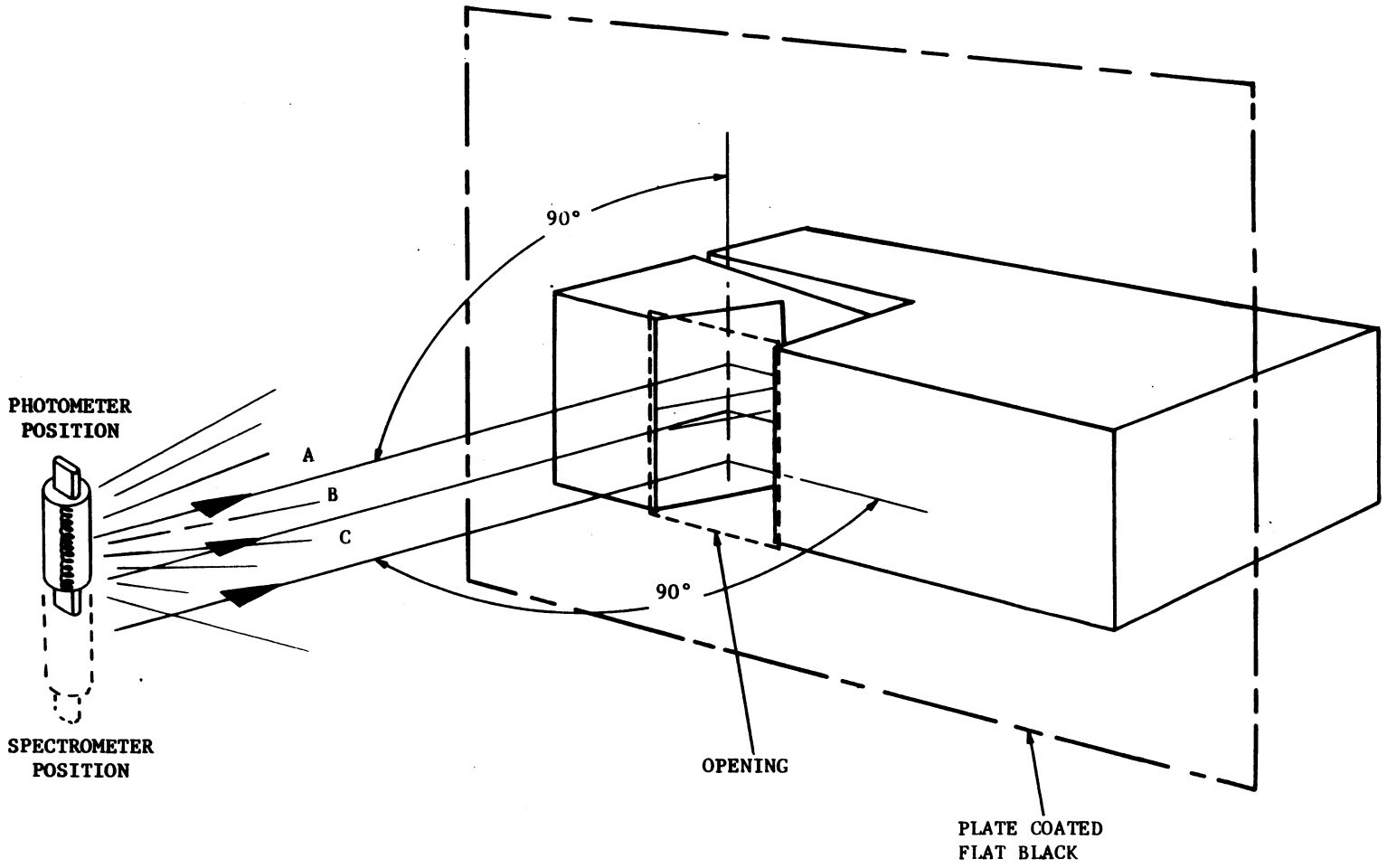

Figure 7-9. Radiant Sensitivity Measurement Set-up

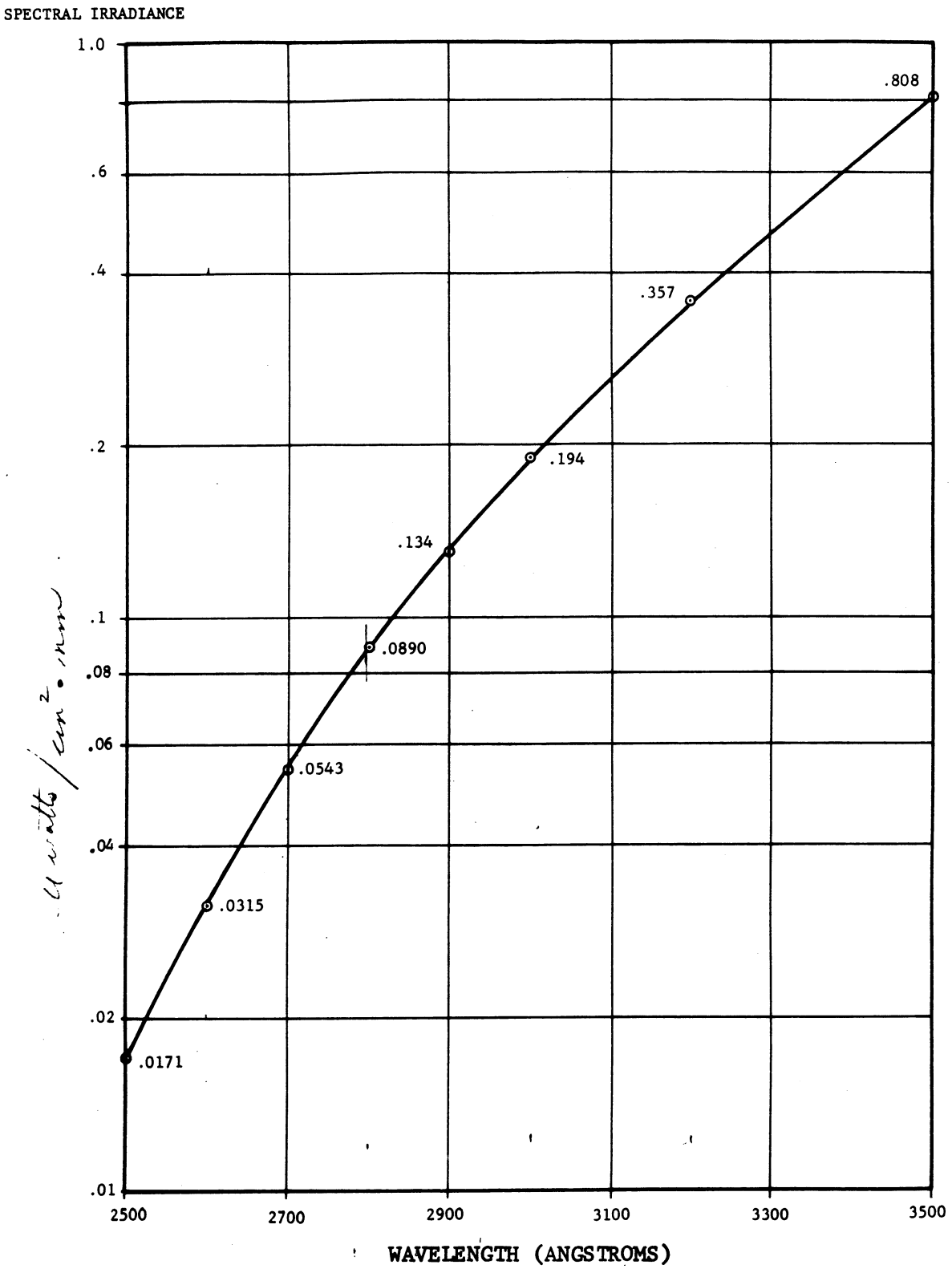

Figure 7-10. Spectral Irradiance in Microwatts Per (cm^2-nanometer) at a Distance of 50 cm of Lamp No. EPI-1258 Operated at 8.3 Amperes

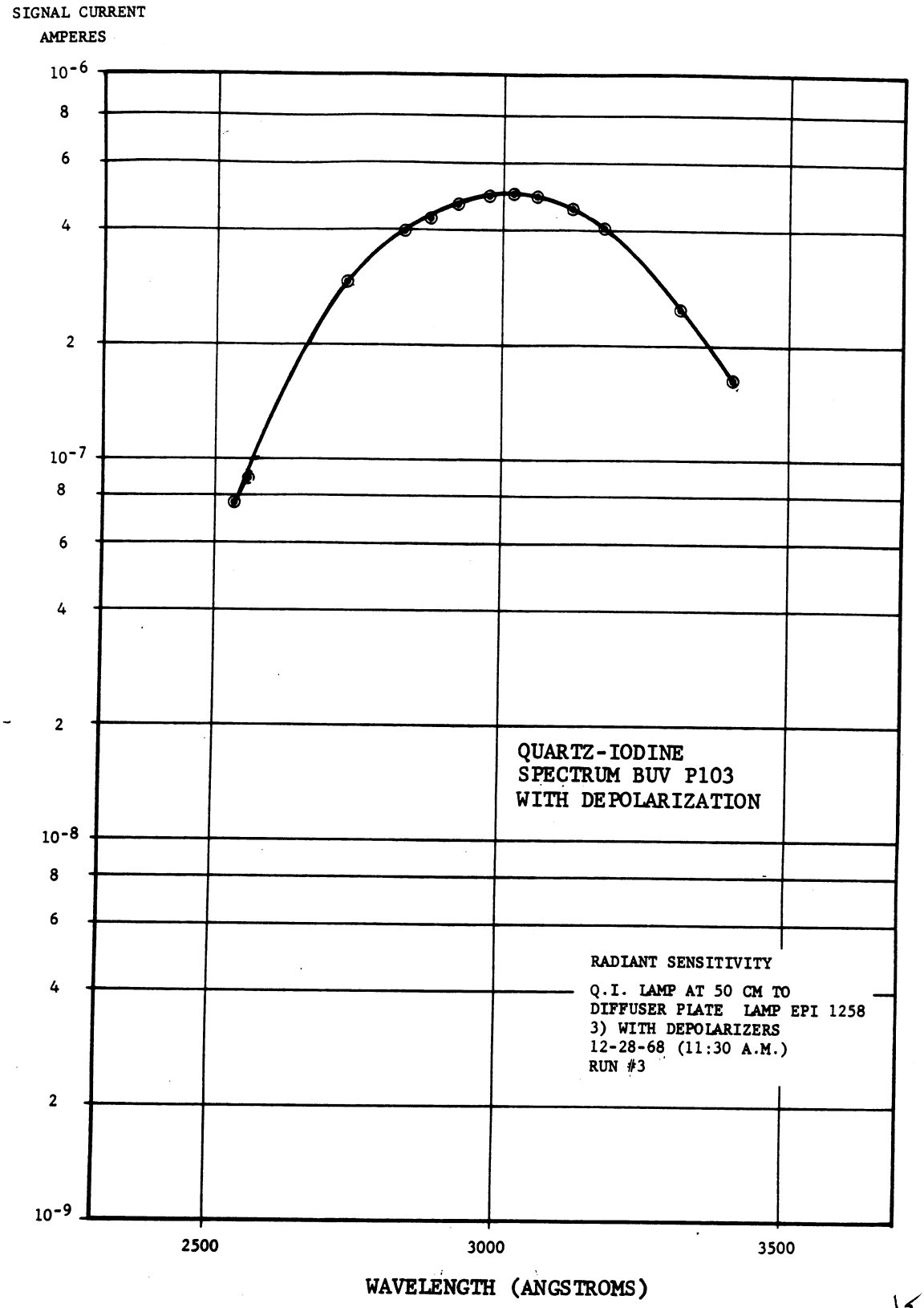

LOG P55
P/F OPTICAL LOG

Figure 7-11. P103 Instrument Response Curve

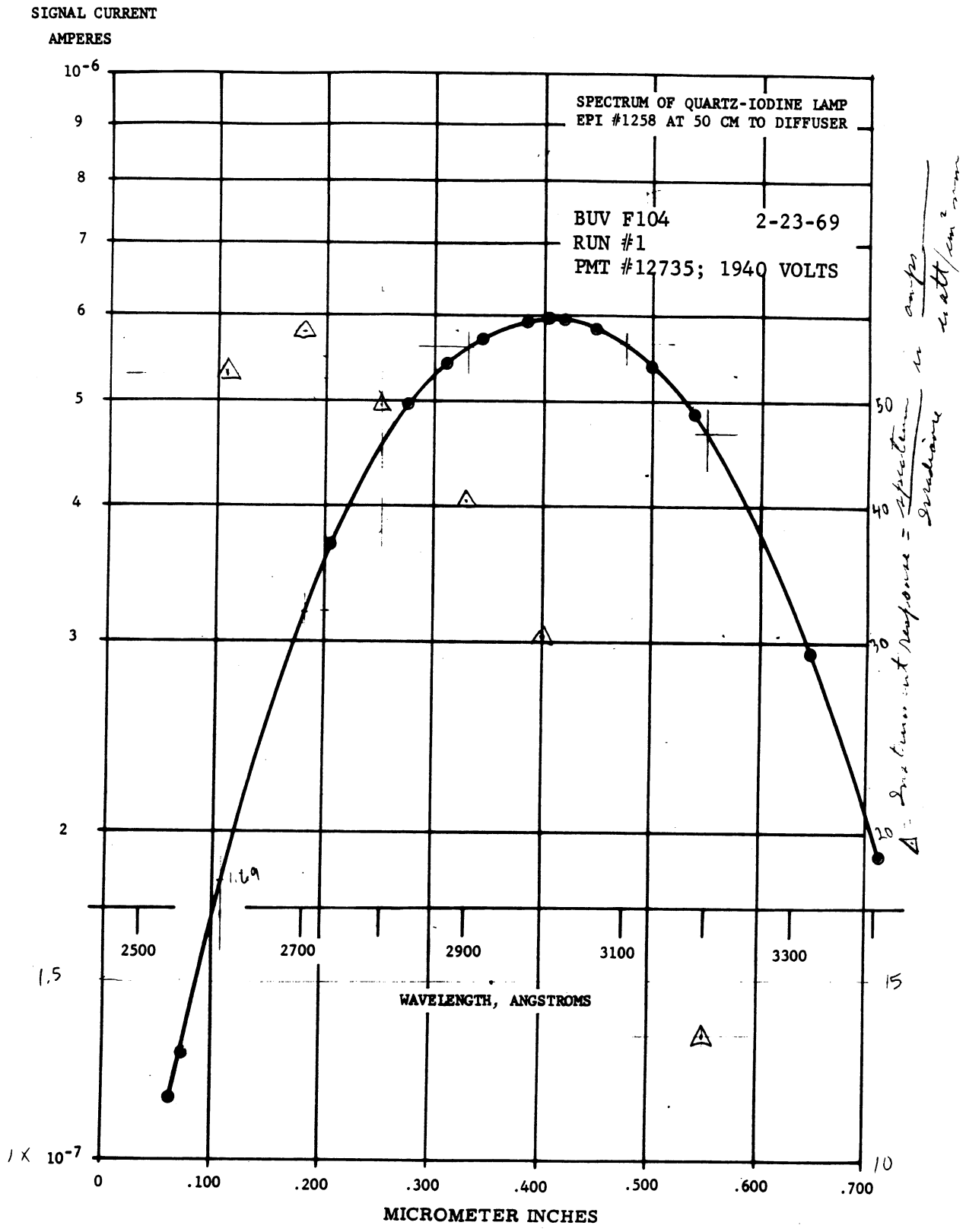

Figure 7-12. F104 Instrument Response Curve

In the photometer, the source in the calibrate position directs its energy onto the interference filter and photomultiplier while external energy is blocked by a rotating shutter.

Figure 7-13 shows that the tritium decay rate will result in an approximate 6-percent decrease in the output of the sources during the first year of operation.

During MCS B, the monochromator PMT voltage is forced to the high-gain state and the electrometer is allowed to free-range. During MCS C, which occurs simultaneously with MCS B, the photometer PMT voltage is forced to the low-gain state and the electrometer allowed to free-range.

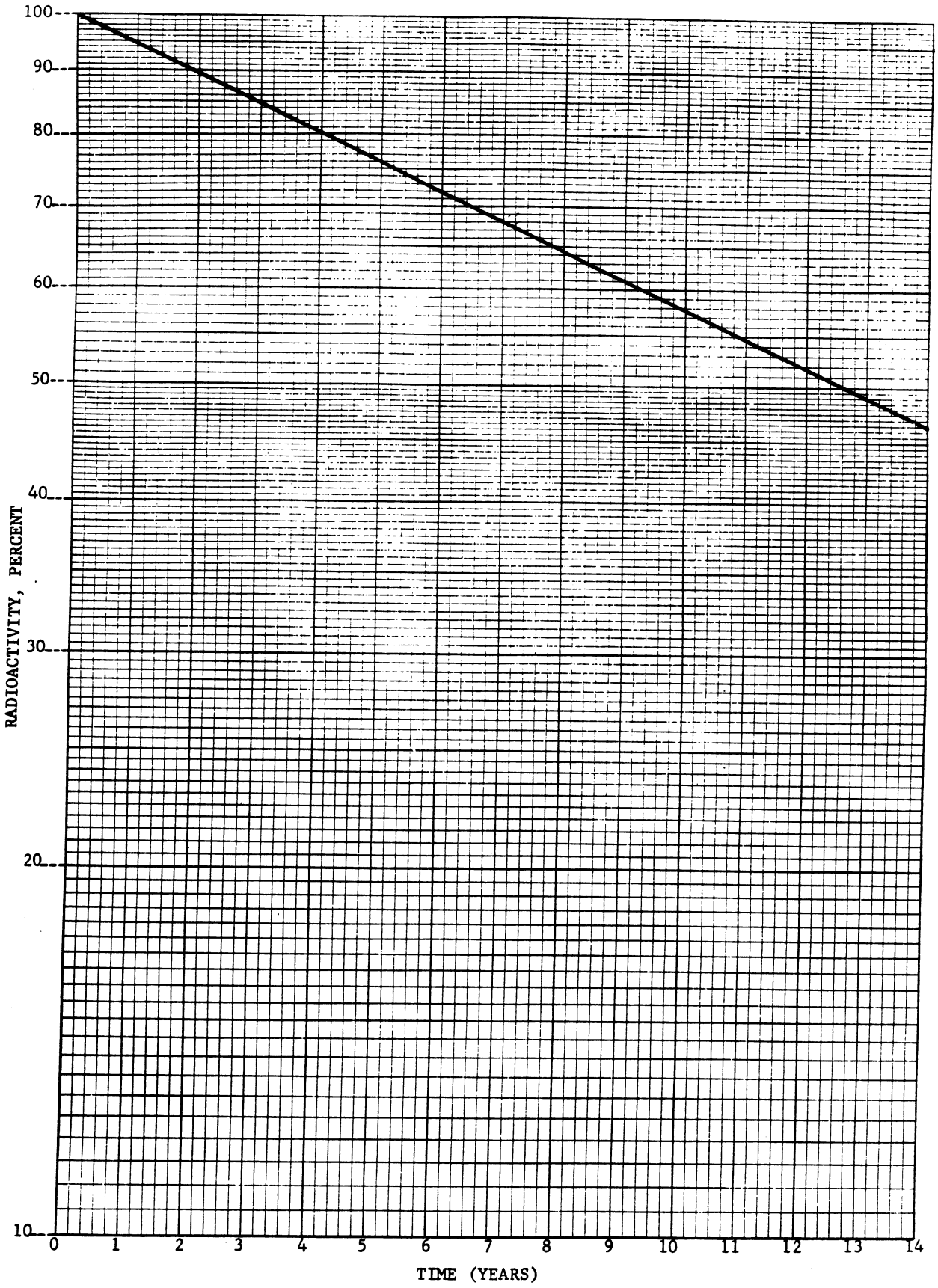

Figure 7-13. Radioactive Decay of Tritium (Half-Life = 12.6 years)

7.2.5 MCS D, E

During the last minor data frame of the 24th Master Data Frame, a wavelength calibration of the monochromator channel is performed. The first 7.5 seconds are used to step the wavelength cam to the wavelength calibrate position and to rotate the shutters to view the wavelength calibration source (a Mercury Argon lamp). During the next 14 seconds, the cam is stepped from the 2522 Å position to the 2552 Å position in 5 Å steps, dwelling 2 seconds at each step. The remainder of the 32-second frame is used to position the cam to the start position.

The next data frame is used for a secondary wavelength calibration. During this frame, the grating is stepped through the normal positions while the monochromator views the wavelength source. The final 2.5 seconds of the frame are used to reposition the shutters to the data position.

While in the WAVELENGTH CALIBRATION position, the entrance shutter is closed, but in a position 180° from the DARK CURRENT position. The Wavelength Calibration Lamp is turned on, and the light beam passes through a filter and a Transfer Prism. The light beam continues through an auxiliary slit and into the monochromator system.

The attenuation filter is mounted directly in front of the wavelength calibration lamp. The filter is a circular disc of fused silica with an aluminum coating. The coating passes one percent of the incident energy at 2537 Å, the wavelength calibration line of the mercury arc lamp.

The transfer prism, constructed of SUPRASIL I fused silica, is mounted in front of the Wavelength Calibration Lamp and directs the energy of this lamp into the monochromator. The two transmitting surfaces of the prism are covered with aluminum coatings which transmit 9 percent and 0.9 percent of the incident energy at 2537 Å, the wavelength calibration mercury line, for a total attenuation of approximately 10^3.

The small rectangular auxiliary slit is located directly beneath the main entrance slit. Slit Dimensions are 2 mm high and 1.2 mm wide, and it is cut into the same plate as the main entrance slit.

The Wavelength Calibration Lamp is mounted directly beneath the depolarizer on the common mounting plate which also houses the entrance and exit slit and the exit lens. The lamp is a small (1-3/4 in. long by 9 mm in diameter) arc lamp filled with mercury argon gas; the envelope is fused quartz.

During MCS DE, the monochromator PMT voltage is forced to the high-gain state, and the electrometer is allowed to free range. Results of the MCS D calibration are given in paragraph 7.3.1.

Figure 7-14 is a plot of the results of a typical MCS D calibration made on the P103 instrument. The point at which the 2537 Å mercury line peaks was determined by the intersection of two straight lines through pairs of points on either side of the peak. The "two point" forms of the two lines were rearranged and solved for the "X" value of their intersection. A less accurate method is to plot the data on linear graph paper and determine the intersection by use of a straight edge.

For the P103 unit, two sets of lines were used:

a. Lines joining cam steps 19, 20 and 23, 24 (called the intermediate skirt), and

b. Lines joining cam steps 20, 21 and 22, 23 (called upper skirt).

Note that the intermediate skirt center wavelength values follow those derived from the upper skirt data, but magnify any shift which occurs. It thus appears that an additional effect contributes to the actual wavelength shift when using the lower value data. For this reason, the F104 instrument was evaluated using only the data from the 20, 21 and 23, 24 point pairs. Note that point 22 was not used since it lay very close to the calculated intersection and thus would distort the results of the method as used.

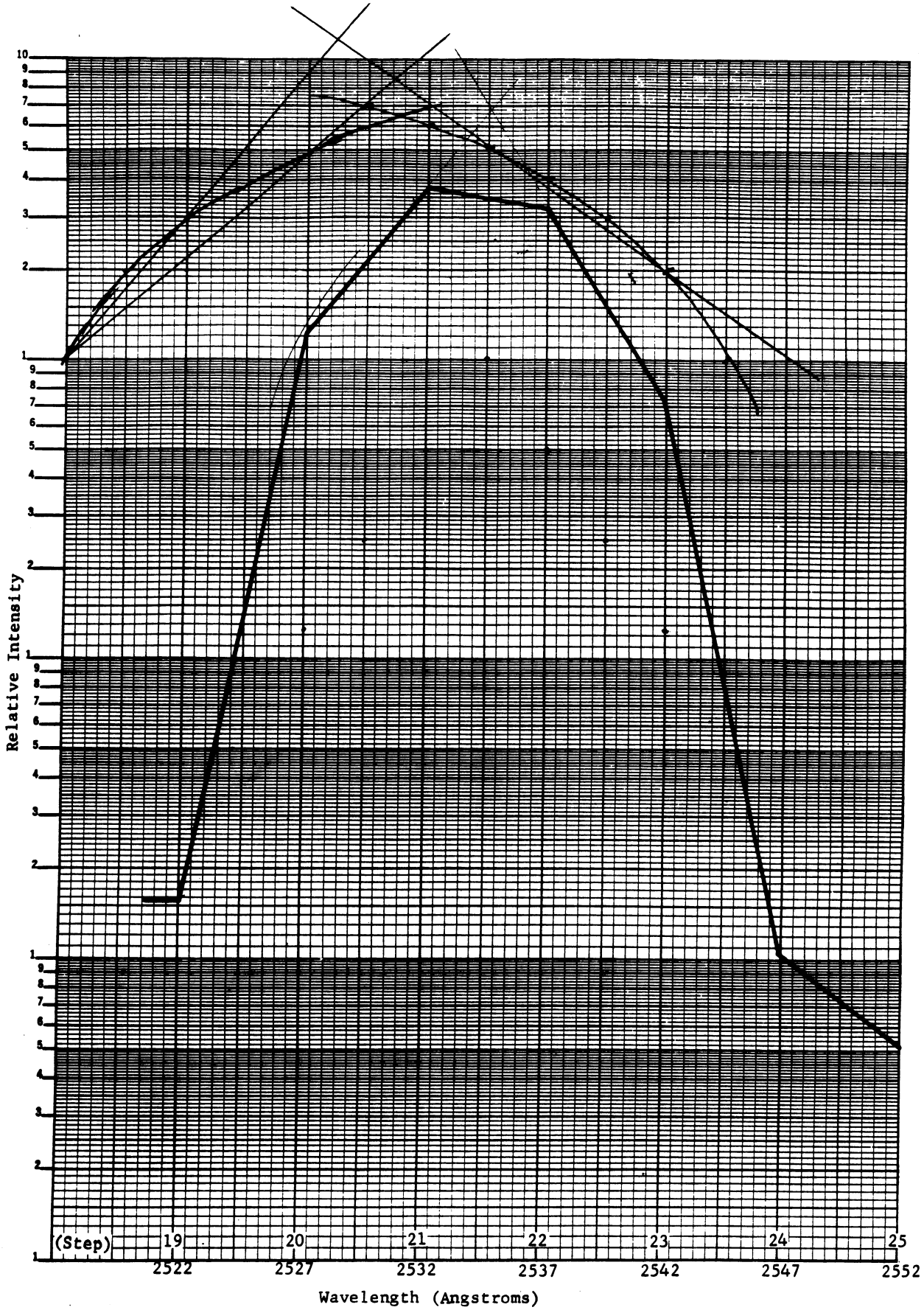

Figure 7-14. Typical MCS, D Calibration Curve for the P103 Instrument

7.3 CALIBRATION RESULTS AND DERIVATIONS

The results presented were obtained during performance of various environmental tests or, for quartz-iodine data, during bench acceptance tests. Data for the P103 Instrument comes primarily from tests performed at General Electric, Valley Forge, while most F104 Instrument data was derived from tests at Beckman's facilities.

7.3.1 MCS B C, D E, and Q I Tests

7.3.1.1 Dark Current

Figure 7-15 shows the temperature dependence of dark current observed during thermal-vacuum tests at General Electric on the P103 Instrument. Figures 7-16 and 7-17 show the corresponding data for the F104 Instrument taken at Beckman during TV (thermal vacuum) testing in February, 1970.

7.3.1.2 MCS B,C

Figure 7-18 shows the temperature dependency of the photometer photometric calibration during TV testing at General Electric, while Figures 7-19 and 7-20 show comparable data on the monochromator in both pulse counts and analog values for selected wavelengths.

Figure 7-21 shows equivalent data for the F104 Instrument, taken at Beckman during TV testing in February, 1970.

7.3.1.3 MCS D,E

Figures 7-22, 7-23, and 7-24 show the apparent wavelength shift as a function of test activity during pre-thermal vacuum testing of the P103 Instrument. Similar data for the F104 Instrument is shown in Figure 7-25. Refer to paragraph 7.2.4 for an explanation of the derived data.

Figure 7-26 shows the large temperature dependency of the internal calibration lamp perceived intensity, and Figure 7-27 shows the resulting variations in

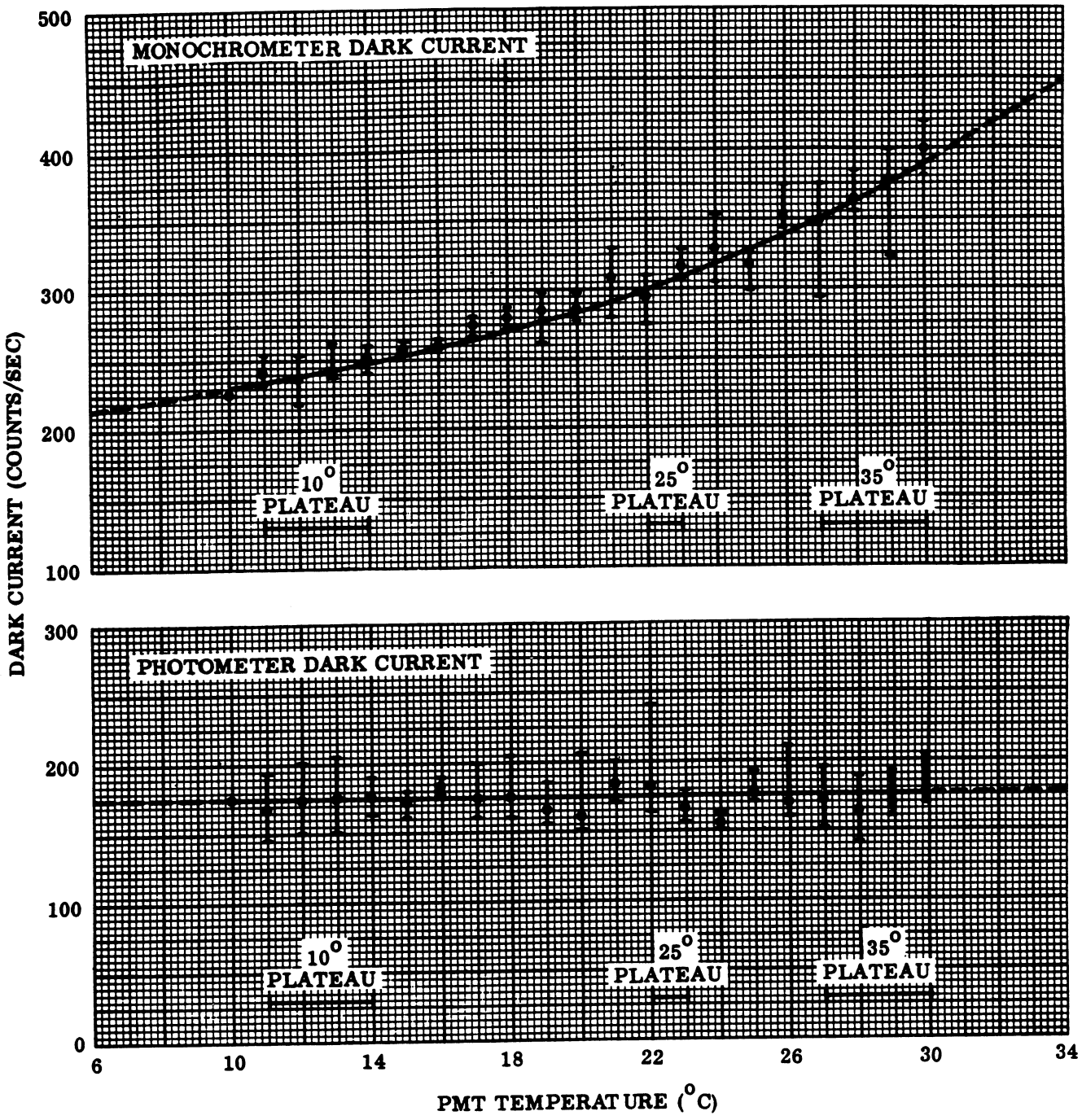

Figure 7-15. Photomultiplier Tube (PMT) Dark Currents Versus PMT Temperature, P103 Instrument

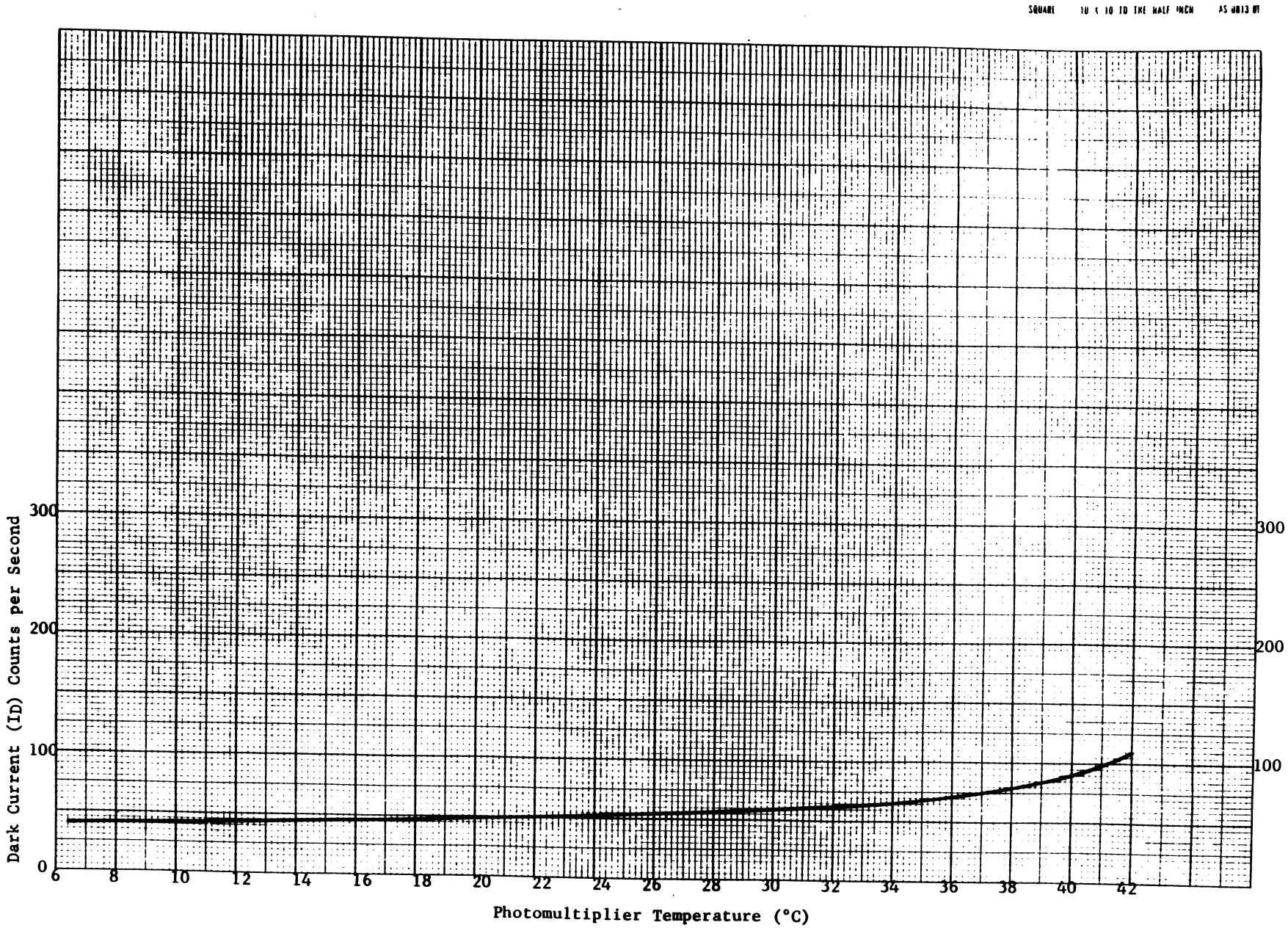

Figure 7-16. Monochromator Thermal Vacuum Test Results, F104 Instrument

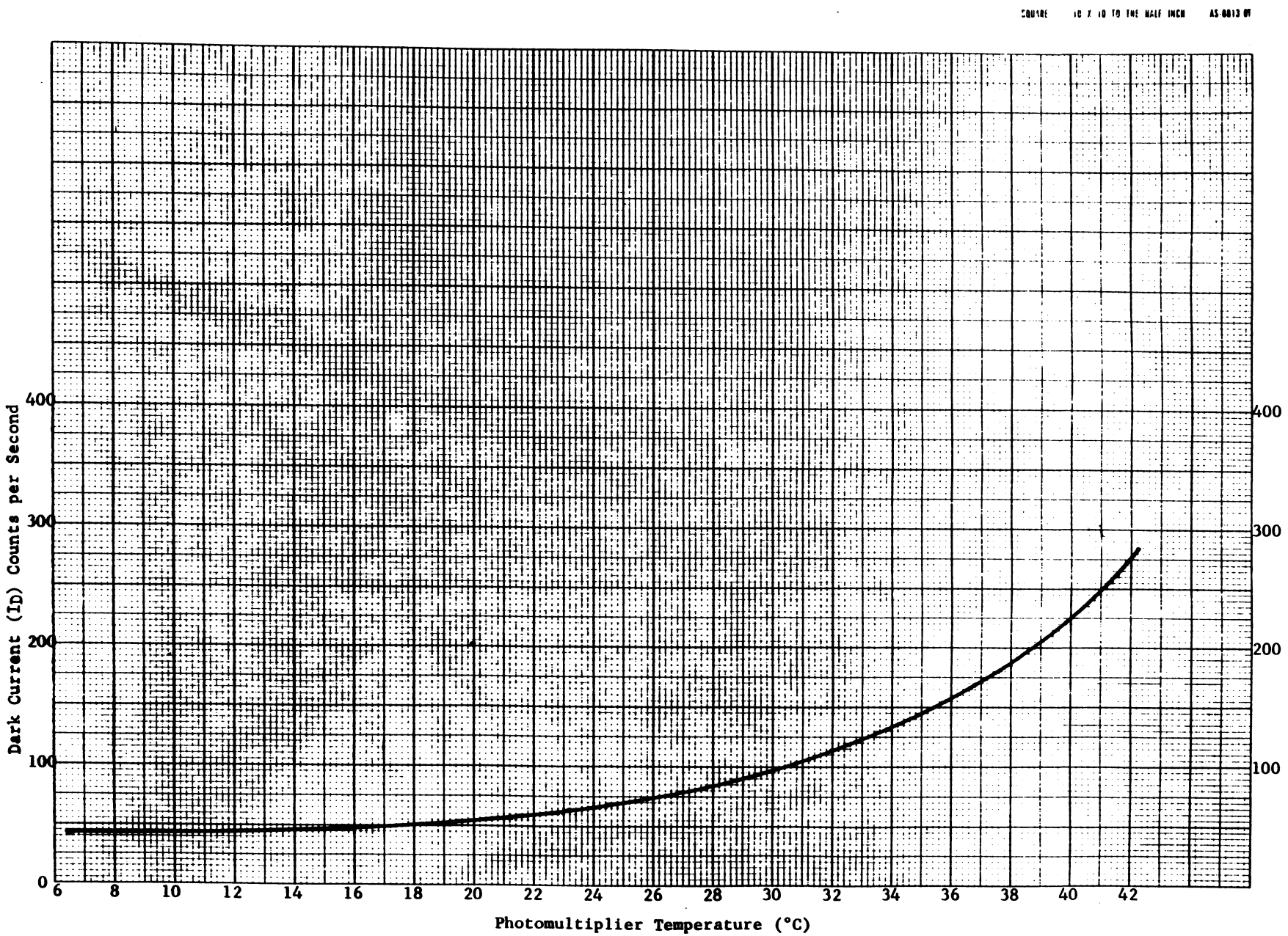

Figure 7-17. Photometer Thermal Vacuum Test Results, F104 Instrument

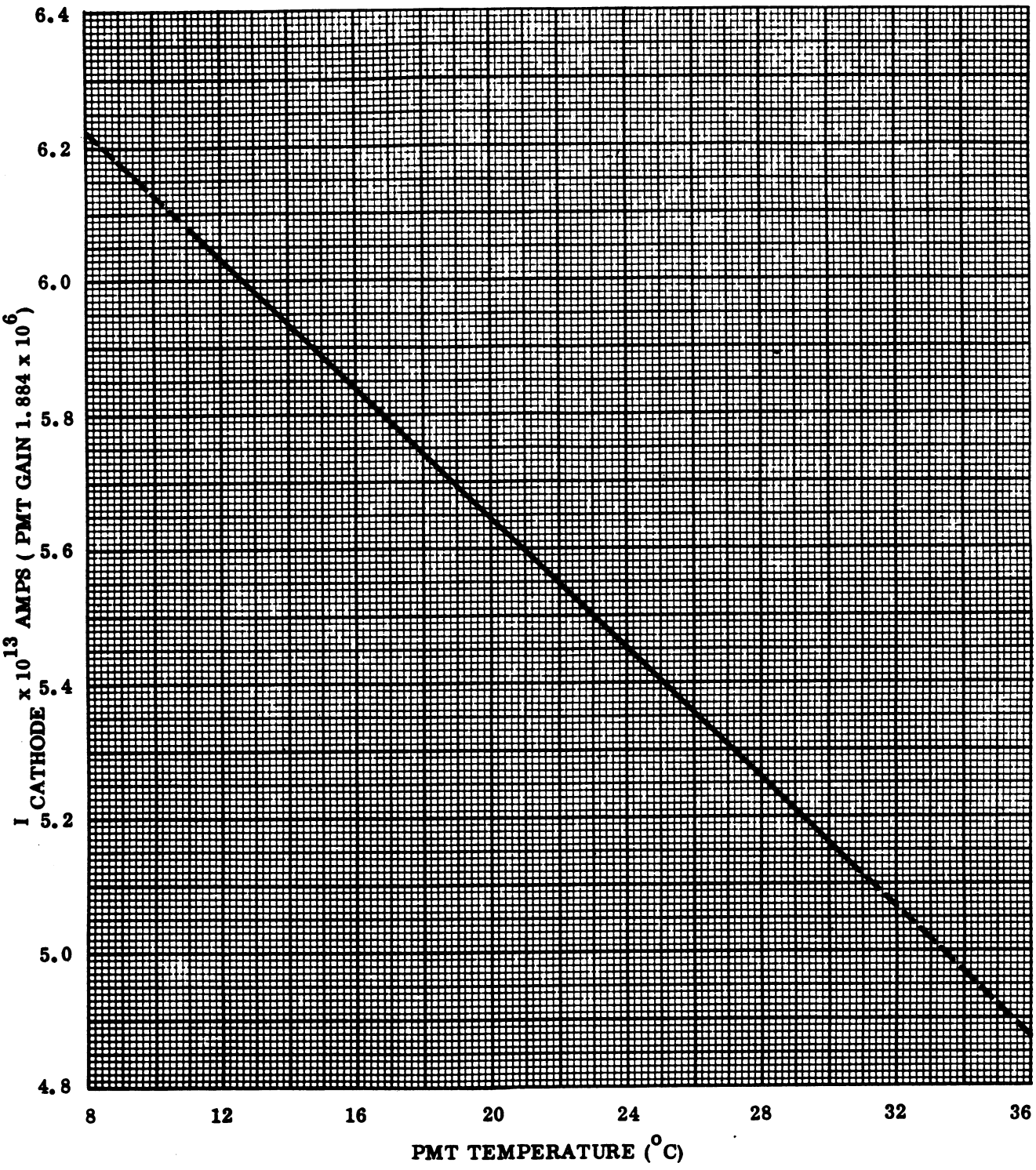

Figure 7-18. MCSC Level Versus PMT Temperature

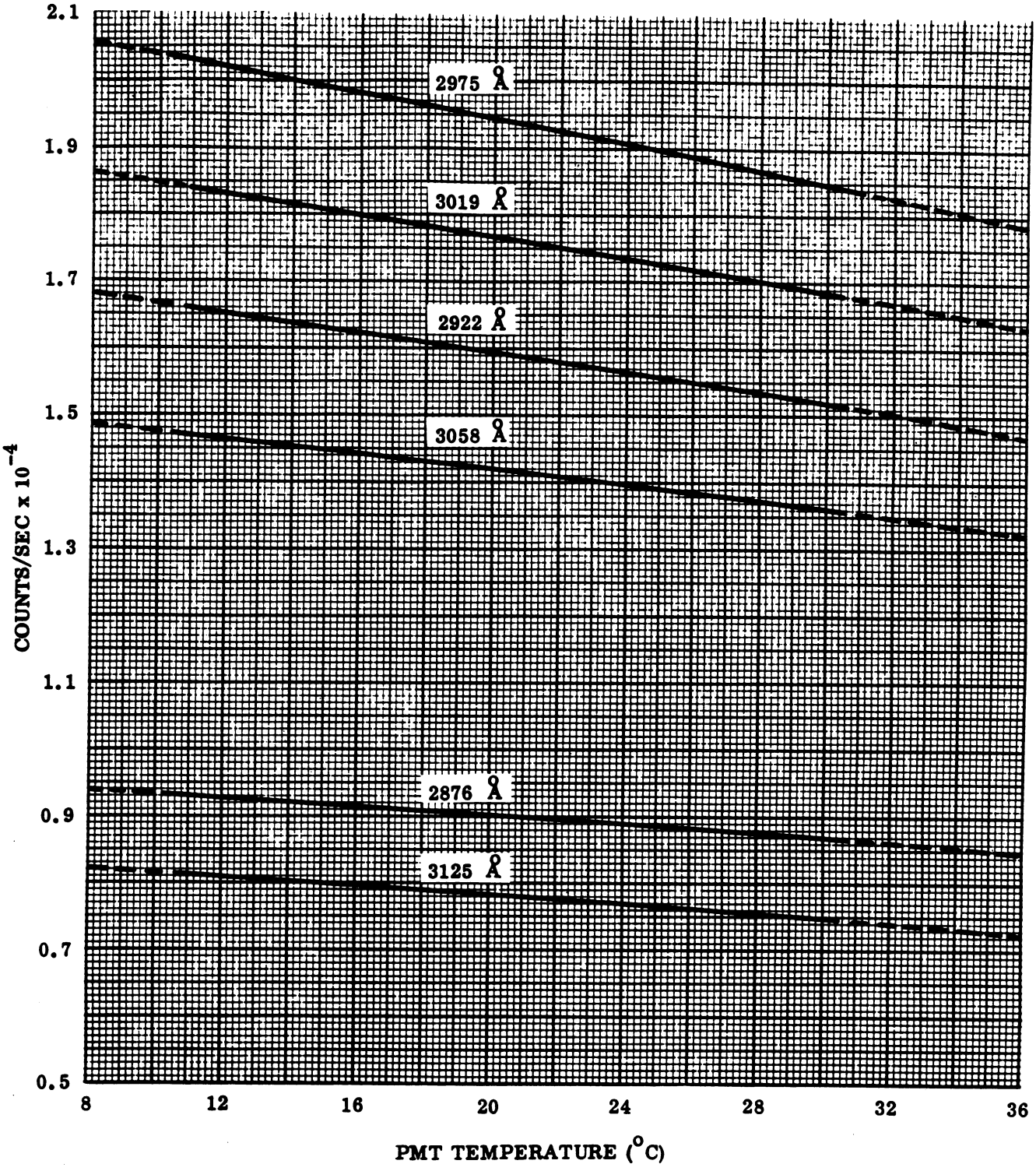

Figure 7-19. MCS B Pulse Count Values Versus PMT Temperature

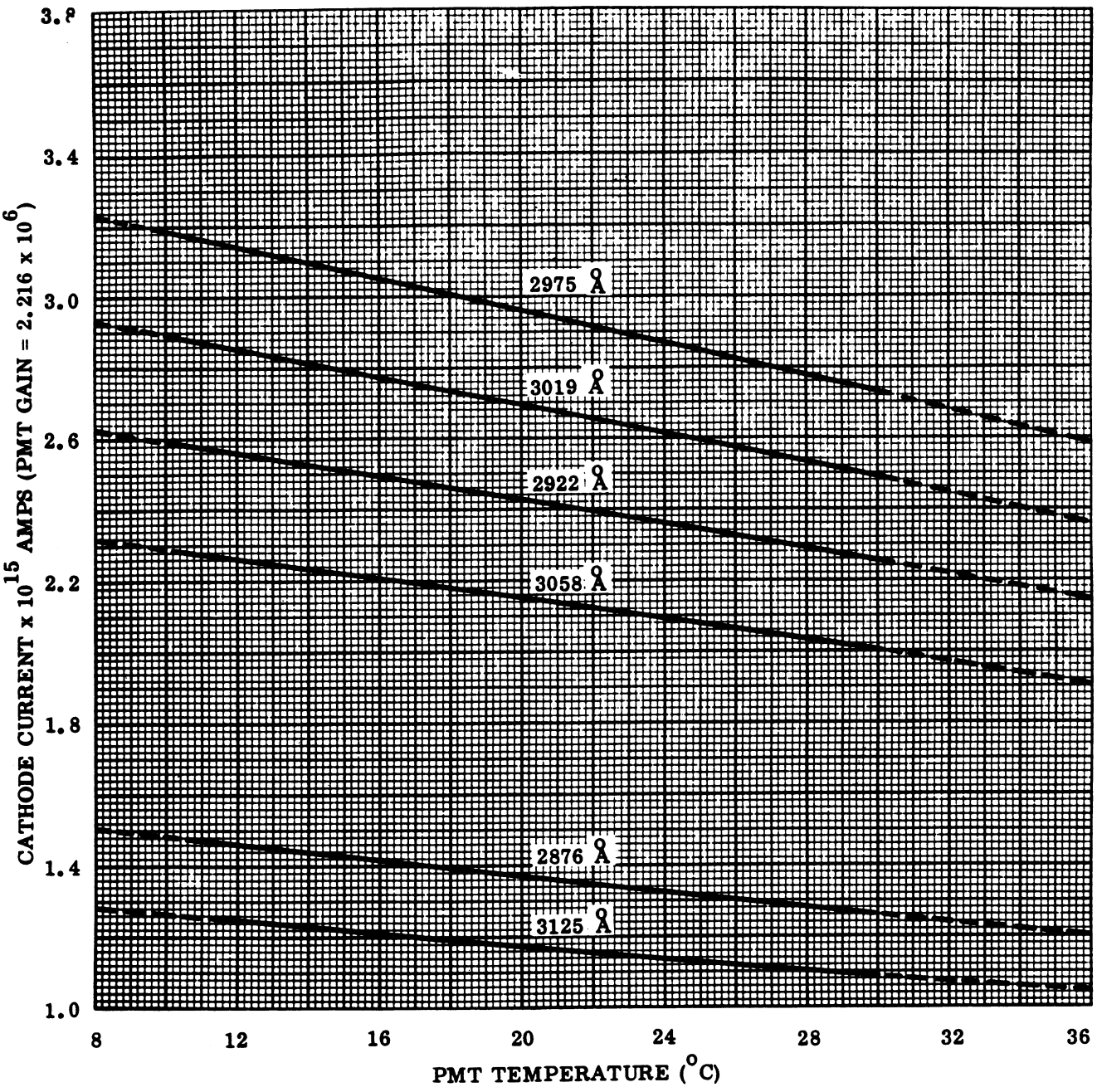

Figure 7-20. MCS B Analog Values Versus PMT Temperature

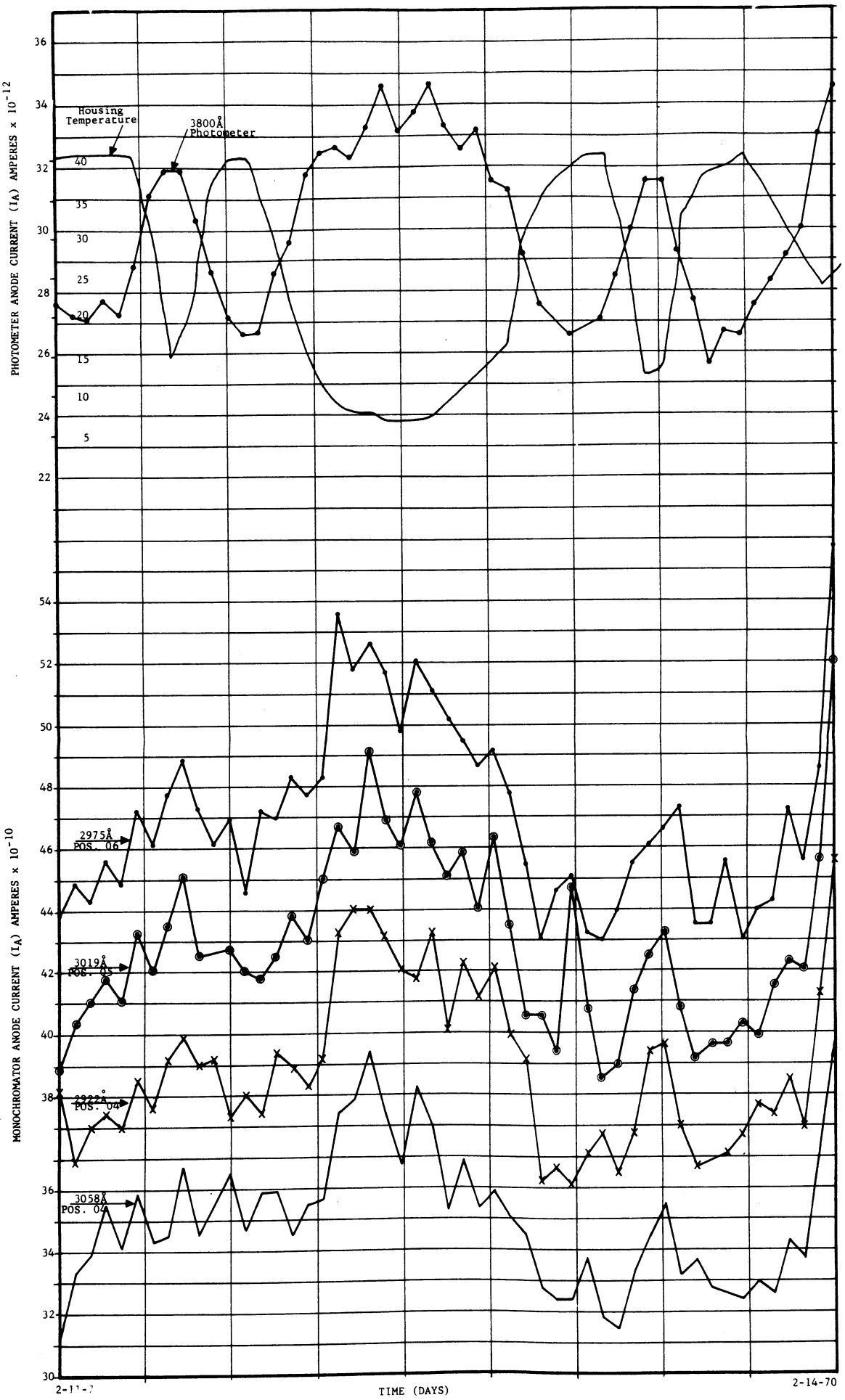

Figure 7-21. Internal Photometer Calibration vs. Temperature, F104 Instrument

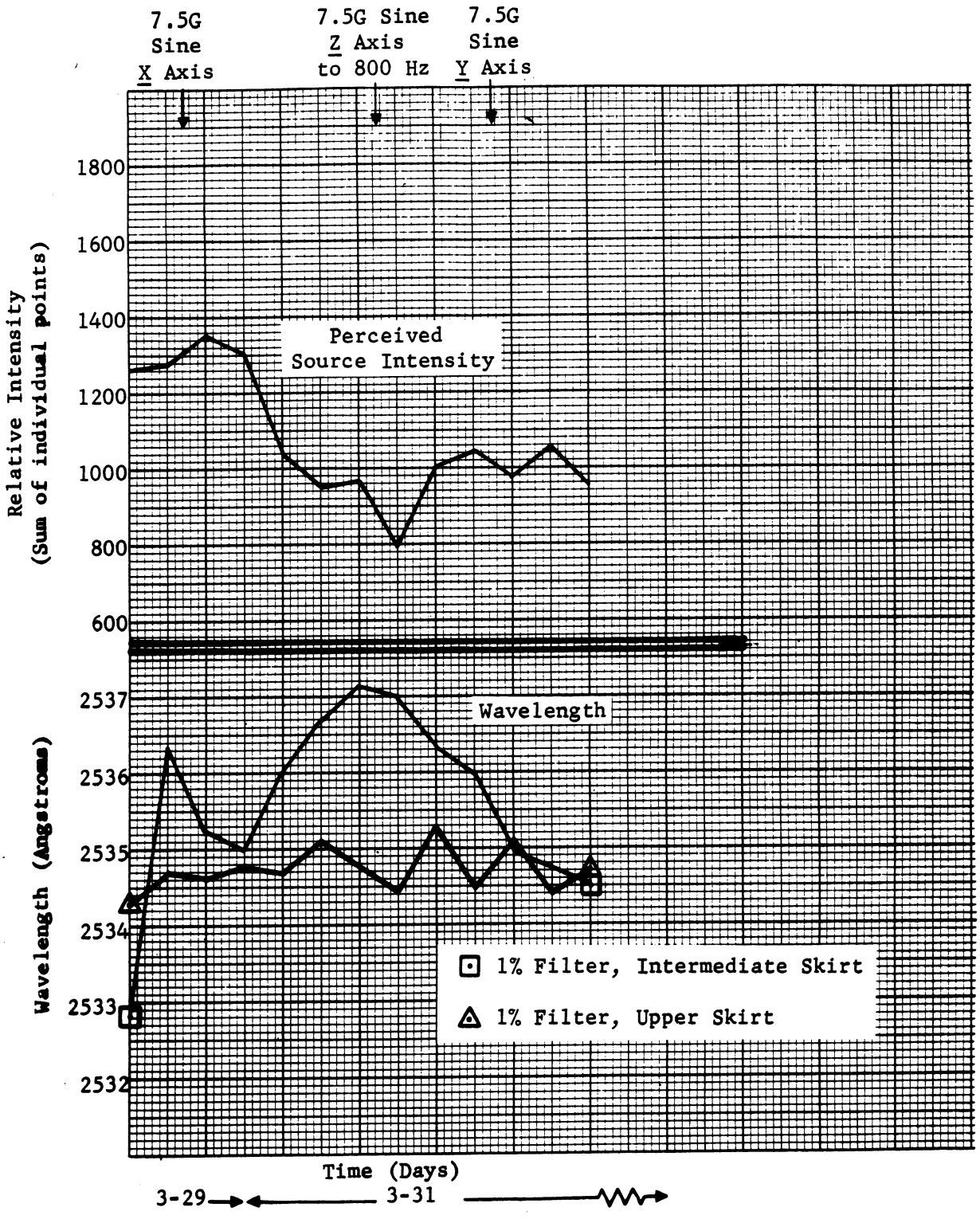

Figure 7-22. Wavelength Shift Due to Pre-Thermal Vacuum Testing from 3-29 to 3-31, P103 Instrument

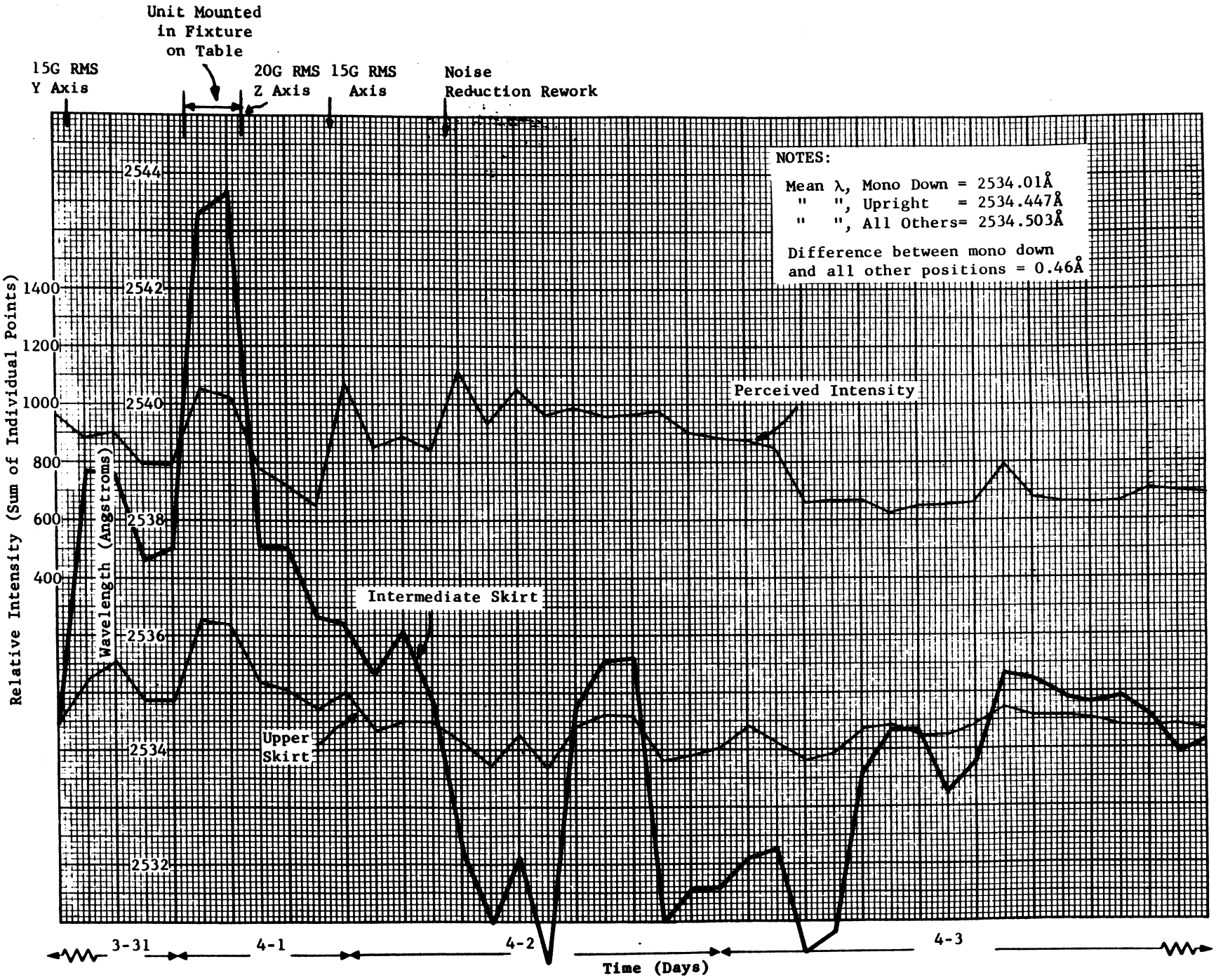

Figure 7-23. Wavelength Shift Due to Pre-Thermal Vacuum Testing, from 3-31 to 4-3, P103 Instrument

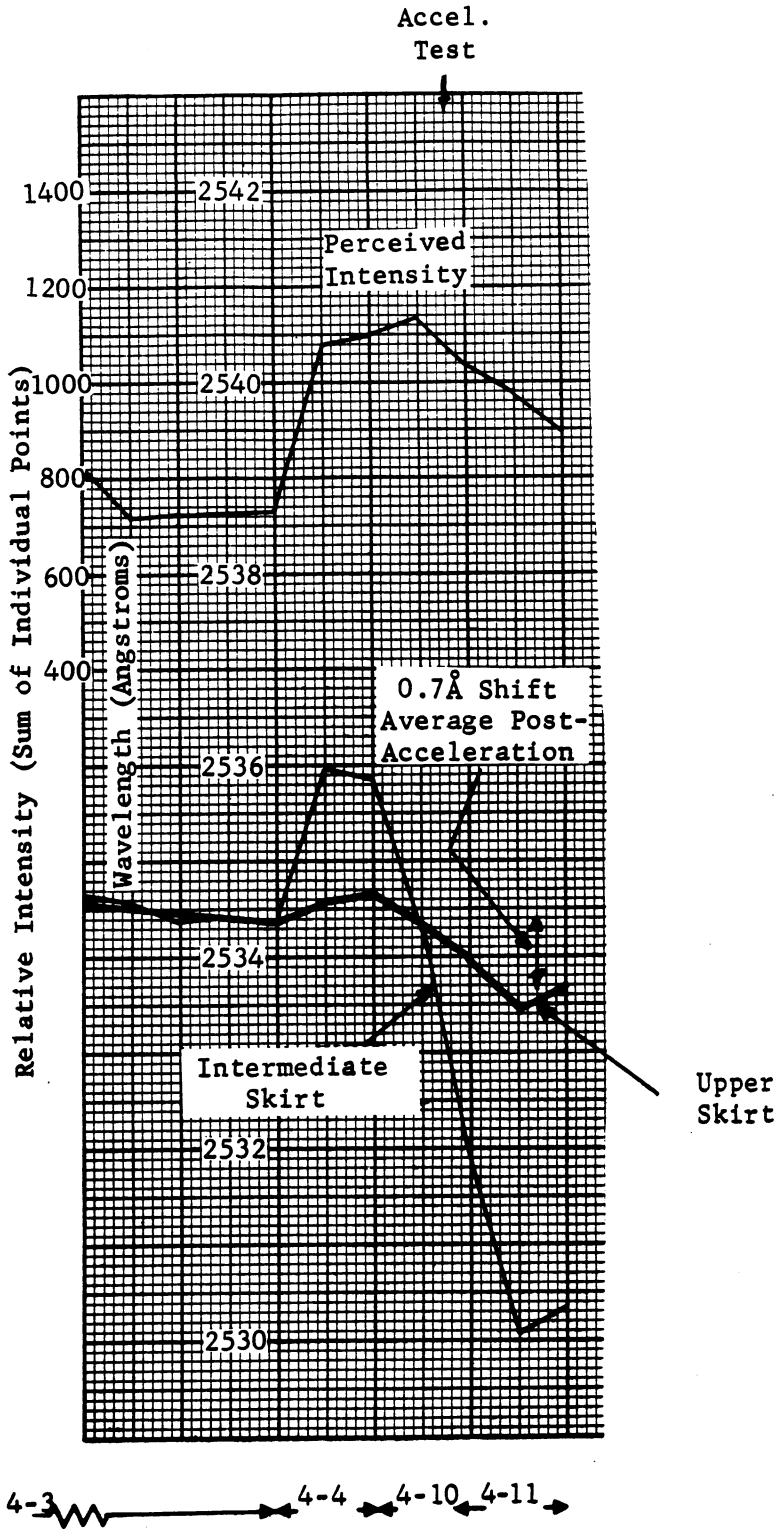

Figure 7-24. Wavelength Shift Due to Pre-Thermal Vacuum Testing, from 4-3 to 4-11, P103 Instrument

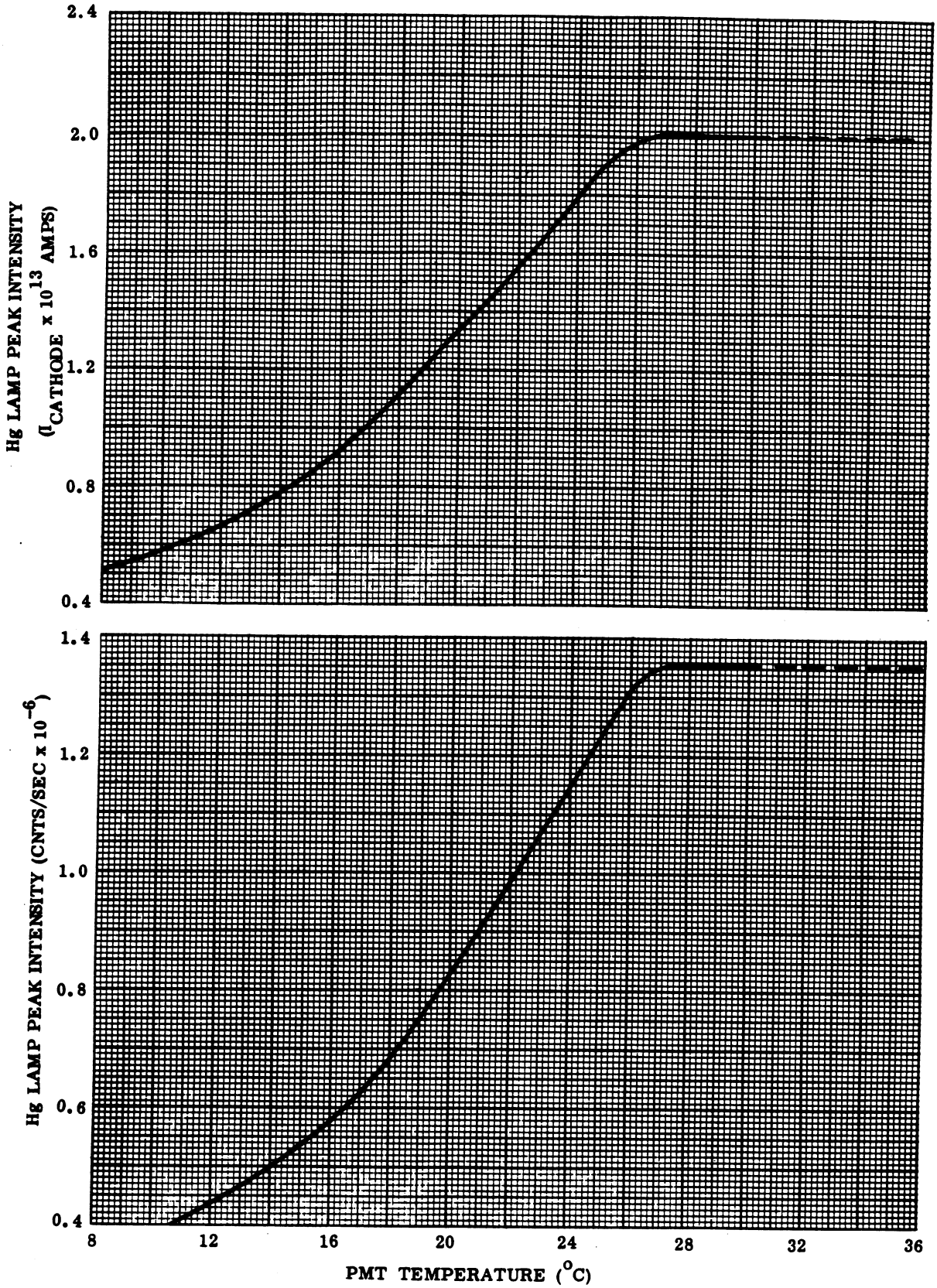

Figure 7-26. Hg Lamp Intensity Versus PMT Temperature

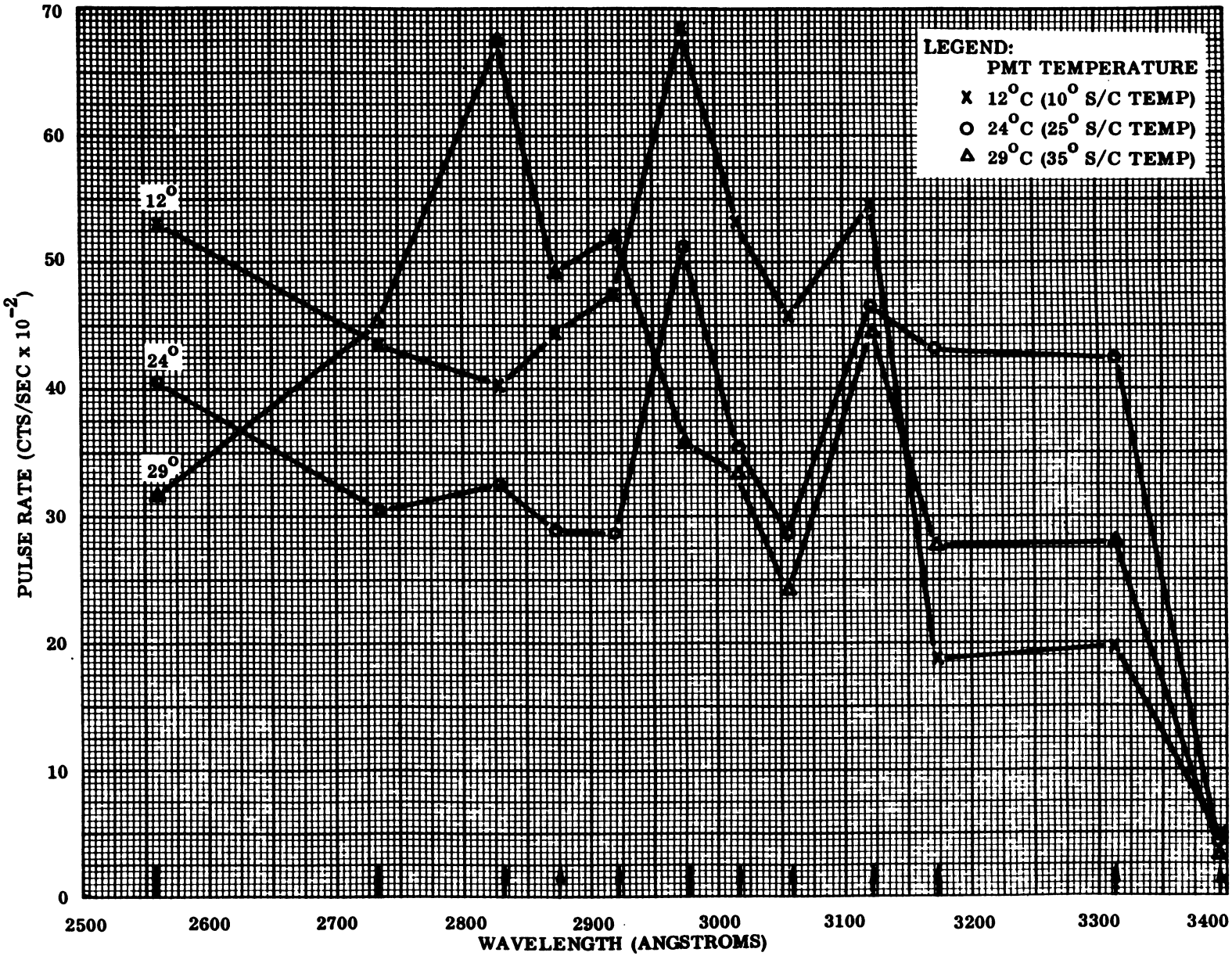

Figure 7-27. MCSE Calibration--PMT Temperature Correlation

Figures 7-28 and 7-29 are plotted from data taken on the F104 Instrument at Beckman during TV testing in February and March, 1970. On Figure 7-29, temperature is plotted only during the first transition to show the slope of the slight wavelength shift; thereafter, data was taken at the temperature plateaux only, and is indicated on the graph by a single entry.

7.3.1.4 Quartz-Iodine (Absolute) Tests

Tables 7-5 and 7-6 show comparative data for the P103 and F104 Instruments taken at Beckman and General Electric. Table 7-7 shows comparative data for the F104 Instrument taken at Beckman on 10-5-69 and 3-1-70, using the same Q-I lamp. Percentages given are with respect to the earlier reading in all cases.

7.3.2 PMT Gains and T_d Values

Determining PMT gains and discriminator "dead times" is basically a two-step procedure, with a third step giving a check of the results of the first two. The steps are as follows:

1. Determine PMT gain independently of dead time.
2. Determine dead time using the gain value of Step 1.
3. Measure system response using six screens having known percentages of transmittance, and readjust gains and dead times as required.

Step 1:

The PMT is operated in the high-gain mode, and stimulated by a Q-I lamp. The light level is set, by varying the lamp current, to give an analog output just over the ADC threshold. Several runs are made and the pulse-count values for corresponding ADC readouts are recorded. The pulse count measured (R_m) should be kept in the 30K to 70K pps region to minimize dead time correction effects. Since the pulse count readout will be compressed, the maximum resolution uncertainty is 1.5 percent, which is magnified by the relation:

$$\text{Error } (\%) = \frac{1.5}{1 - R_m T_d}$$

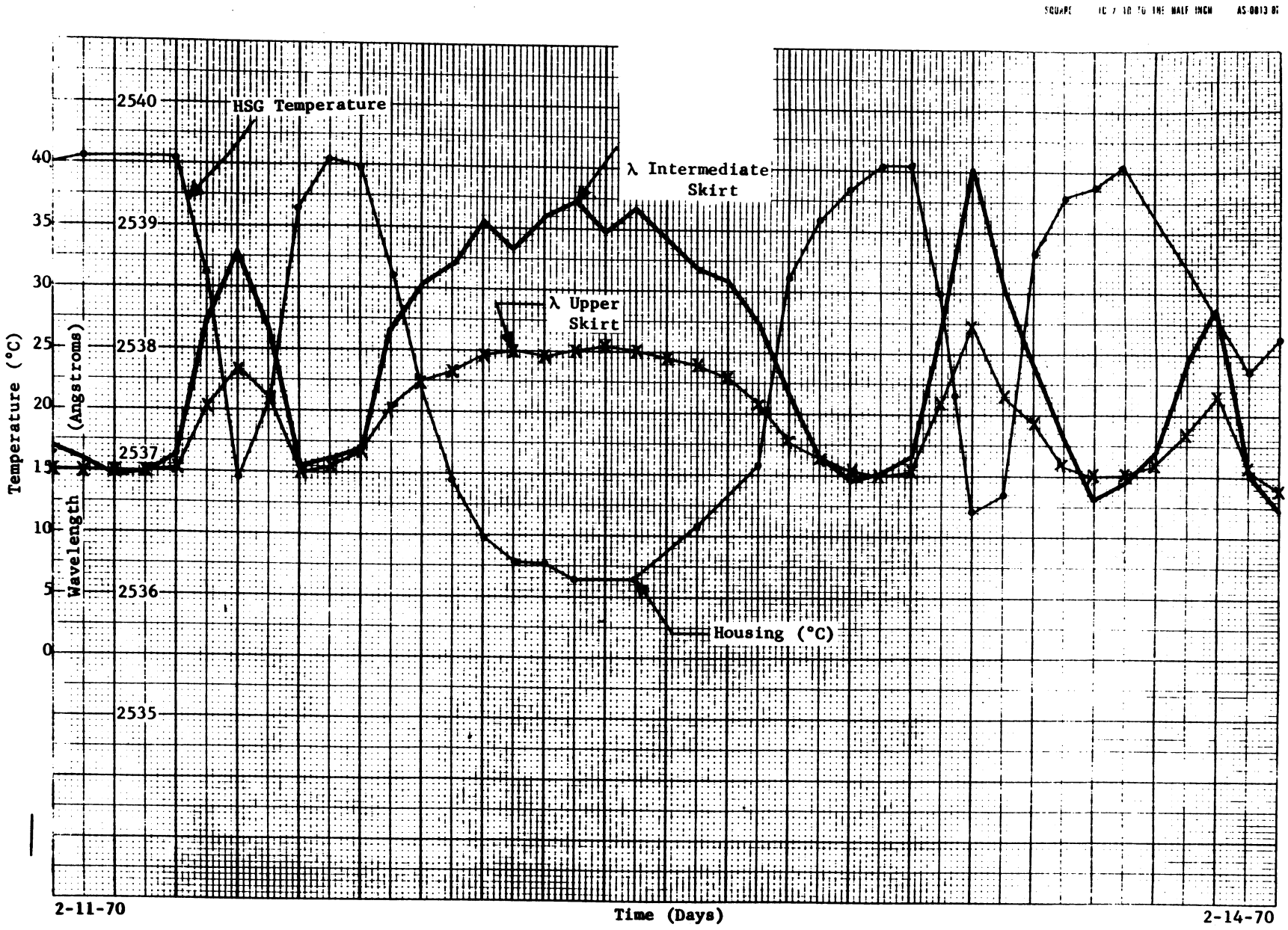

Figure 7-28. Wavelength vs. Housing Temperature, F104 Instrument (Pressure < 0.1 mm Hg)

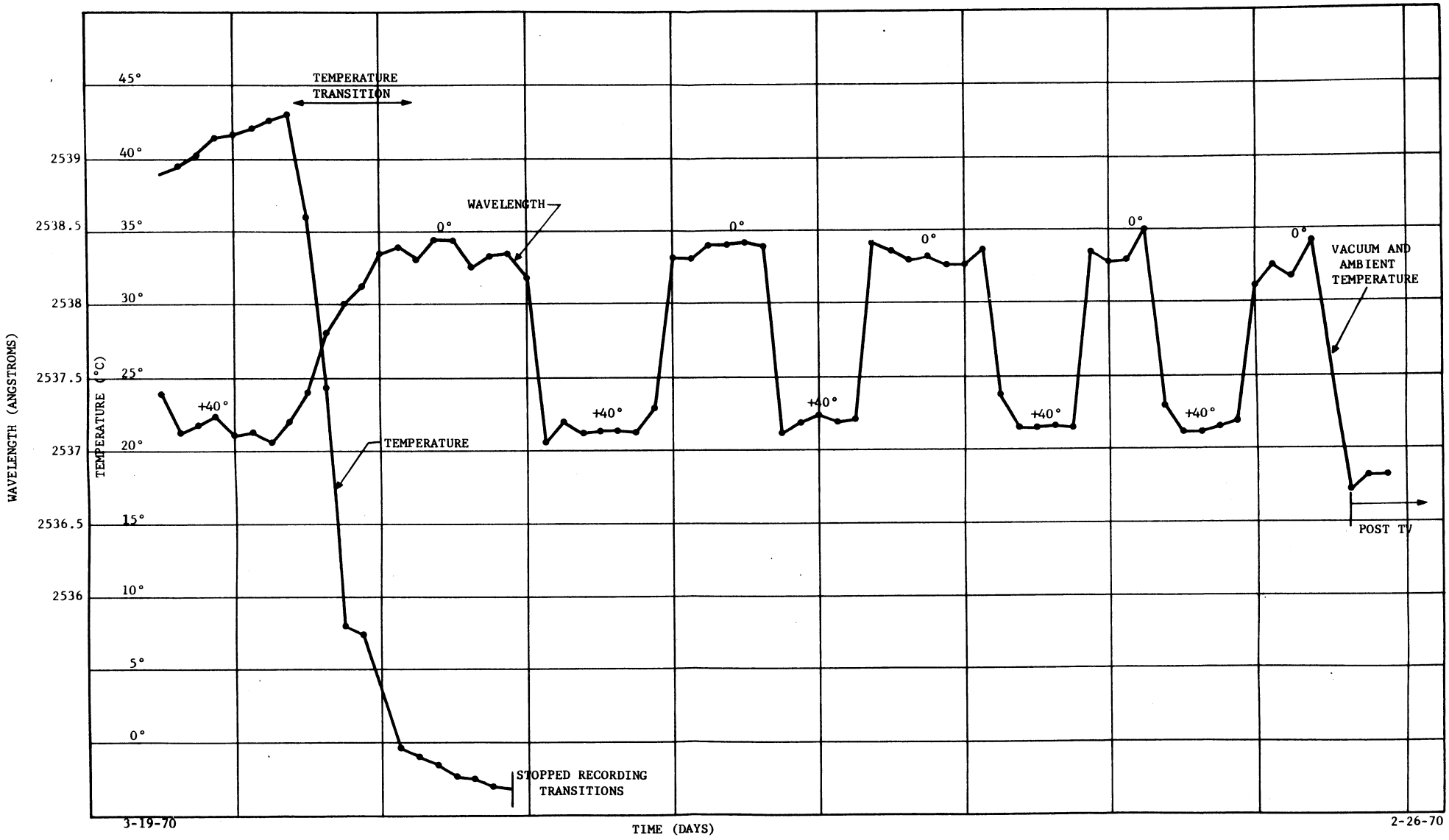

Figure 7-29. Wavelength vs. Housing Temperature, F104 Instrument) (Pressure < 10^3 Torr)

Wavelength (Angstroms)	Expected* Ipc x 10^{13} (Amperes)	Measured** Ipc x 10^{13} (Amperes)	Difference (%)
3398	2.70	2.70	0
3312	3.84	3.80	-1.05
3175	5.13	5.04	-1.78
3125	5.47	5.39	-1.48
3050	5.66	5.56	-1.79
3019	5.62	5.52	-1.81
2975	5.47	5.35	-2.24
2922	5.08	5.00	-1.6
2876	4.61	4.57	-0.87
2830	4.12	4.04	-1.98
2735	2.82	2.76	-2.17
2555	0.792	0.792	0
3800	323.	297.	-8.75

Source: 1000 watt Q-I lamp S/N EPI 1260, filament 8.3 amperes, source-to-instrument distance = 50 cm.

* Photocathode currents measured at Beckman Instruments during BAT of 9-23-69.

** Values measured at General Electric during BAT of 9-29-69.

Table 7-5. Absolute Calibration Data, P103 Instrument

Wavelength (Angstroms)	Expected* Ipc x 10^{13} (Amperes)	Measured** Ipc x 10^{13} (Amperes)	Difference (%)
3398	2.3549	2.1623	- 8.9
3312	3.3676	3.0753	- 9.5
3175	5.1284	4.956	- 3.47
3125	5.4592	5.1876	- 5.23
3058	5.7454	5.1876	-10.75
3019	5.7781	5.1876	-11.38
2975	5.5529	5.0706	- 9.51
2922	5.3059	4.8455	- 9.5
2876	4.9559	4.4242	-12.01
2830	4.4744	4.0399	-10.75
2735	3.3487	2.9598	-13.13
2555	1.1124	1.0096	-10.18
3800	109.39	191.1	+ 0.37

Source: 1000 watt QI lamp S/N EPI 1262, filament current - 8.3 amperes, and source-to-diffuser distance at 50 cm.

* Photocathode currents as measured at Beckman Instruments during bench acceptance test of 10-5-69.

** Photocathode currents measured at General Electric during bench acceptance test of 10-11-69.

Table 7-6. Absolute Calibration Data, F104 Instrument

Wavelength (Angstroms)	10-5-69 Expected Ipc x 10^{13} (Amperes)	3-1-70 Measured Ipc x 10^{13} (Amperes)		Difference (%)	
		$2x10^9$ R_{FR}	$3x10^{10}$ R_{FR}	$2x10^9$	$3x10^{10}$
3398	2.3549	2.433	2.596	+3.31	+10.23
3312	3.3676	3.465	3.608	+2.89	+ 7.13
3175	5.1284	5.054	5.347	-1.47	+ 4.26
3125	5.4592	5.364	5.686	-1.77	+ 4.15
3050	5.7454	5.617	5.848	-2.28	+ 1.78
3019	5.7781	5.588	5.848	-3.4	+ 1.2
2975	5.5529	5.429	5.686	-2.28	+ 2.39
2922	5.3059	5.22	5.474	-1.64	+ 3.16
2876	4.9559	5.003	5.023	+ .95	+ 1.35
2830	4.4744	4.35	4.557	-2.85	+ 1.84
2735	3.3487	3.198	3.393	-4.71	- 4.71
2555	1.1124	1.072	1.149	-3.76	+ 3.29

Table 7-7. Comparative Absolute Calibration Data, F104 Instrument

Thus, R_m should be kept low for this measurement. R_t is calculated using the relationship $R_t = \frac{R_m}{1 - R_m T_d}$, assuming a T_d of 1 μsec.

The PMT gain is then calculated at several light levels using the relationship:

$$G_{PMT} = \frac{I_A(ADC)}{1.602 \times 10^{-19} \times R_t}$$

(The denominator represents equivalent photocathode current.)

Step 2:

The light level is increased to give pulse counts in the 100K to 800K pps range, and several runs made recording pulse counts vs. ADC readout. T_d is then calculated from:

$$T_d = \frac{R_t - R_m}{R_t R_m}$$

where

$$R_t = \frac{I_{A(ADC)}}{G_{PMT} \times 1.602 \times 10^{-19}}$$

Steps 1 and 2 can be iterated several times to get a high confidence level for the gain and dead time values.

As a further check, an EPUT meter can be used at the output of the low-level discriminator and its readings compared with those produced, in compressed form, in words 5 and 6.

For calculating T_d, the energetic particle count should be added to the R_m value given in words 5 and 6 (but <u>not</u> to the EPUT readings). The monochromator energetic particle count appears in W7, and typically runs 1 to 2 percent of the W6 values.

NOTE

The energetic particle count is assumed equal to the monochromator in percentage when calculating photometer parameters

Step 3:

Several runs are made, using constant Q-I lamp current for each run, with the calibrated filters interposed between the light and the instrument. Using the 100 percent I_A (ADC) value as a base, the percentages are calculated for the I_A (ADC) readings and compared with the independently measured transmission percentages to establish confidence in the test configuration.

Then, using the previously derived T_d, the pulse count reading percentages are obtained. (As a double check, both the 100 percent value and the minimum percentage value may be used as bases for calculation.)

Since the I_A (ADC) percentage values are independent of absolute gain values, agreement between pulse count (R_t) percentages and I_A (ADC) percentages gives a good indication of the accuracy of the derived T_d.

To minimize compression truncation errors, it is useful to interpolate between discrete R_m values by noting W5 and W6 LSB variations. E.g., if, out of five readings, three are nominal, one is LSB + 1 and one is LSB - 1, then the R_m value should be taken as the midpoint between the nominal value and the nominal value plus LSB; if three are nominal and two are LSB + 1, then the R_m value should be taken as midpoint + 2/5 of the difference, etc.

During all the above tests, the wavelength cam is stopped at a selected position (usually 04 or 07) by opening a switch inserted in the cam motor drive line, and the Q-I lamp is driven by a regulated supply to prevent intensity fluctuations due to changes in the line voltage.

7.4 LINEARITY CALIBRATION PERFORMANCE

Using the calibrated screens described in paragraph 7.3.2, runs were made on several gain ranges at various light intensities. Figures 7-30 through 7-36 show the results obtained on both signal channels for the P103 Instrument. To normalize the graphs, the ordinate is given in percentage of full scale rather than in absolute units. The 100 percent value is given in all cases.

7.5 RANGE OVERLAP

To determine the various electrometer and PMT gains, two points were taken as reference points. The first was the PMT high gain value as determined using the methods of paragraph 7.3.2. It was felt that the methods used were valid, and the final results gave good percentage-point agreement for the linearity runs.

The second point of reference was the electrometer feedback resistance of 10^7 ohms. Confidence in this value arises from knowledge of the resistor construction, its screening tests, and the fact that it is orders-of-magnitude lower in value than the other feedback resistors, and thus less likely to change value with time or environment.

With these two points as references, gain crossover runs then establish the remaining values. In all cases, light intensity remains constant after being set to fall in the overlap region. Manual interposition of an opaque screen causes the instrument to auto-range, and allows comparison of the two sets of output readings, as follows:

Monochromator

1. The 2×10^9-ohm resistor value is determined by comparing 1×10^7 vs. 2×10^9 runs, both at low PMT voltage (PMT gain does not affect this ratio).

2. The low PMT gain is determined by comparing 2×10^9 and low voltage (LoV) vs. 1×10^7 and high voltage (HiV), using the corrected 2×10^9-ohm value found in Step 1.

3. The 3×10^{10}-ohm resistor value is determined by comparing 2×10^9 vs. 3×10^{10}, both at low voltage, using the corrected value of the 2×10^9-ohm resistor.

Photometer

1. Determine the 2×10^9-ohm resistor by inference to the percentage change seen in the monochromator channel, since the same history applies to both components from the same manufacturing lot. This assumption resulted in derived gain results consistent with other tests.

2. Determine the 3×10^{10}-ohm resistor value by comparing 2×10^9 vs. 3×10^{10}, both at low voltage.

3. Determine the low voltage gain by comparing 1×10^7 and high voltage vs. 3×10^{10} and low voltage, using the corrected 3×10^{10}-ohm value found in Step 2.

The photometer is difficult to cross-check between 1×10^7 and 2×10^9 at low voltage due to the low gain at low PMT voltage.

Values determined for both instruments using the foregoing methods are given in Section II, paragraph 2.2.

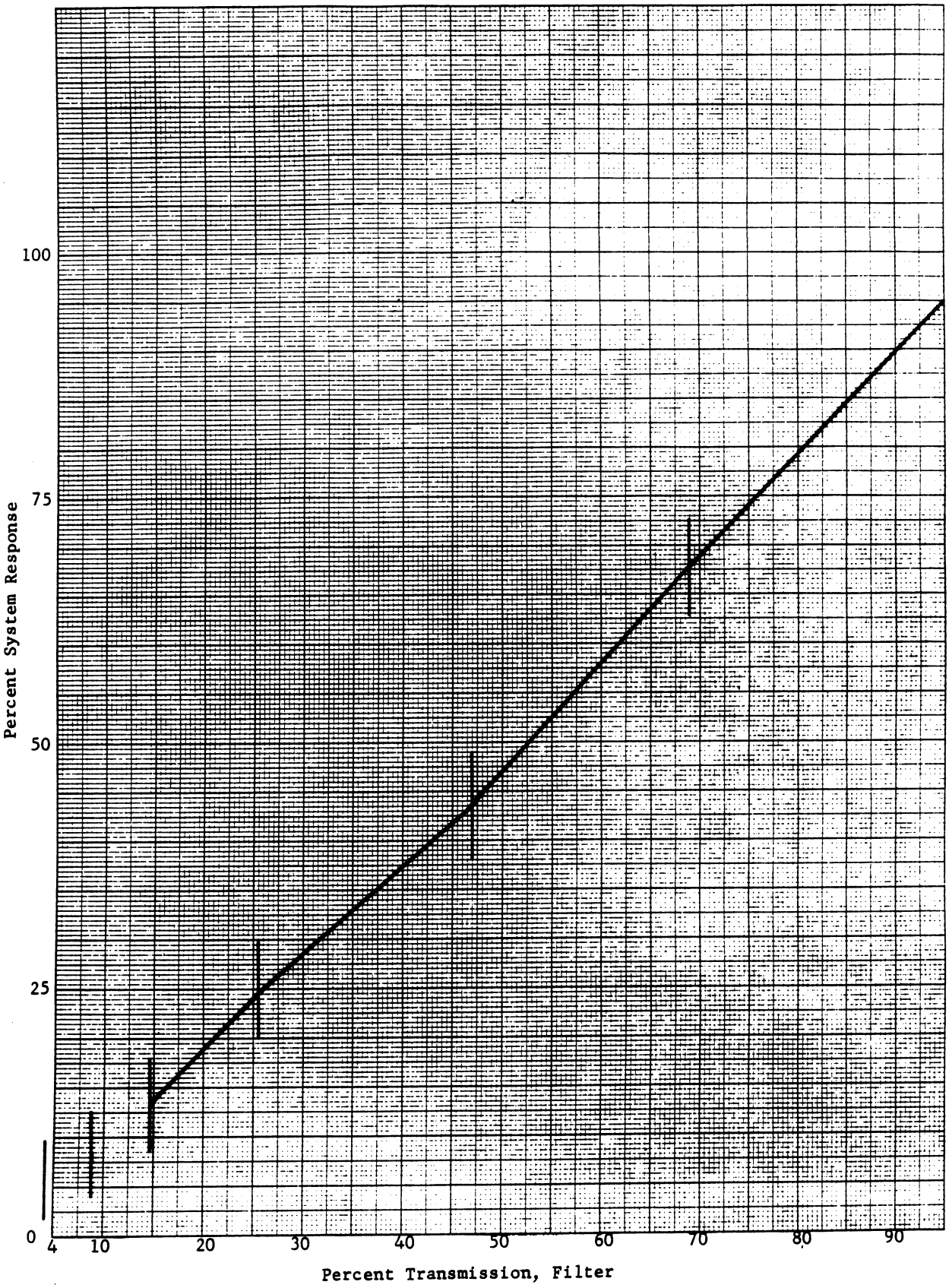

Figure 7-30. Linearity Calibration Performance, Monochromator (Buffer Filter, LoV = 2×10^9; 100% = 1.015 V.)

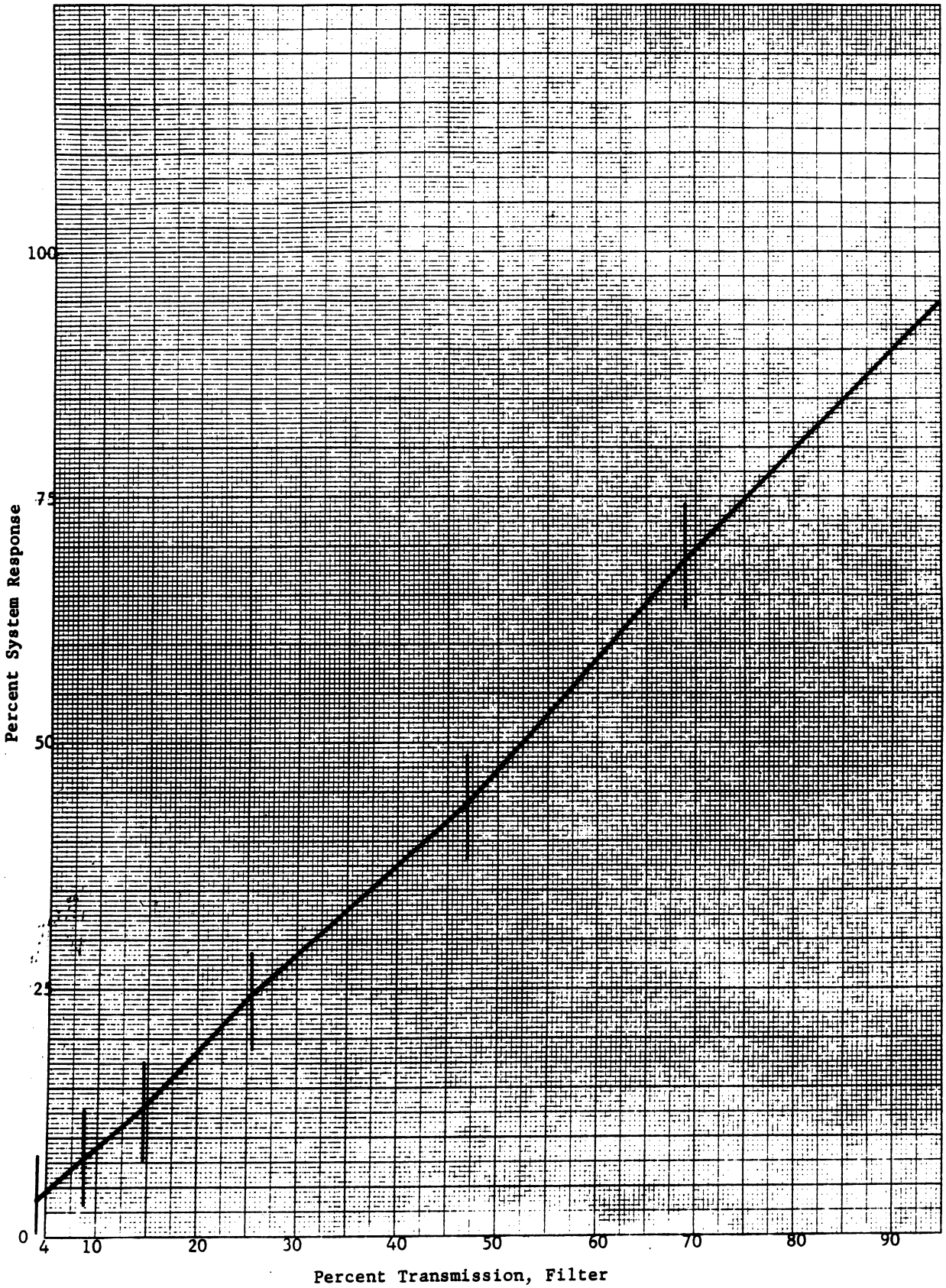

Figure 7-31. Linearity Calibration Performance, Monochromator (Pulse Counts T_D = 1.1×10^{-6}; 100% = 2.89 MHz)

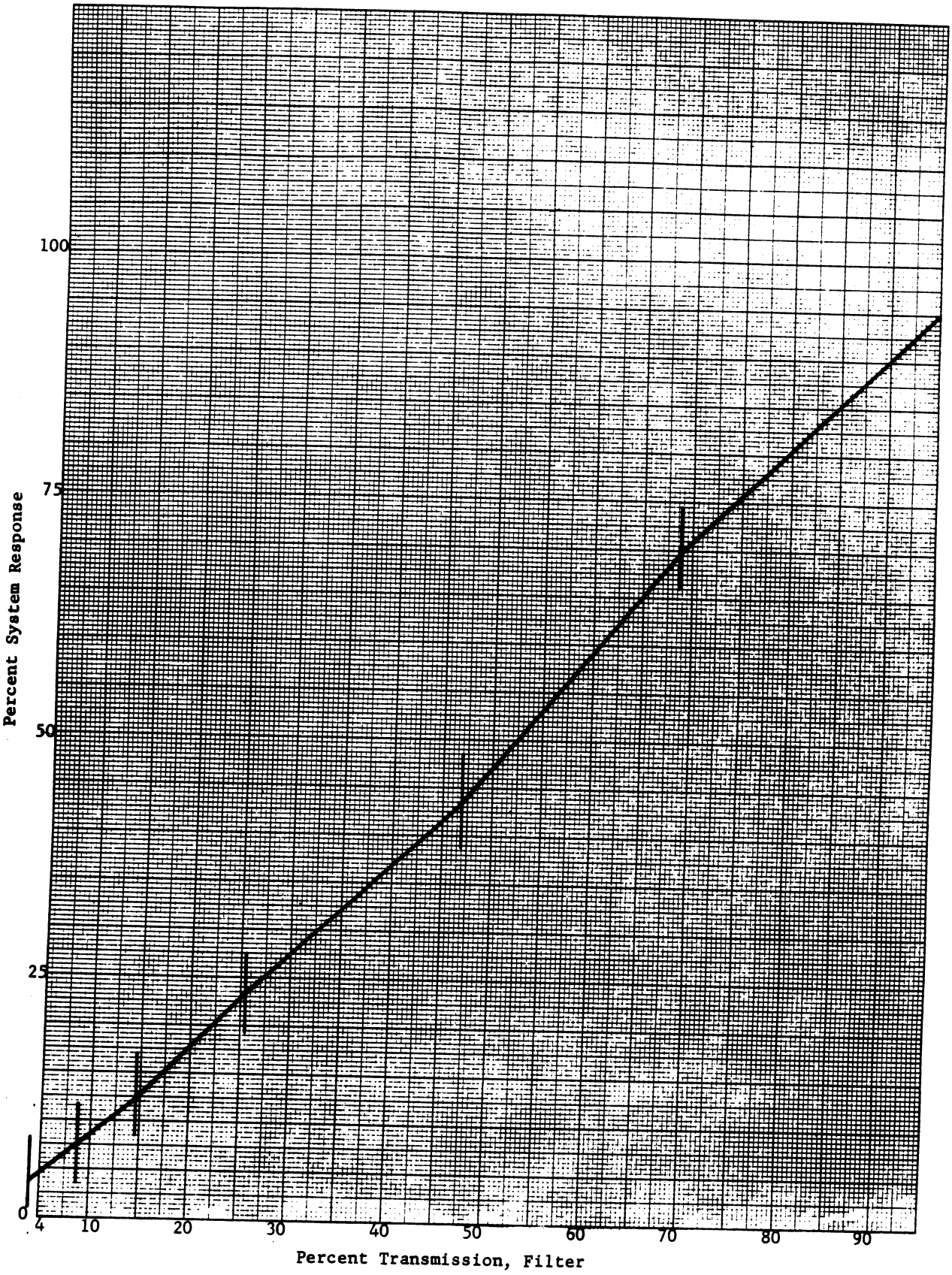

Figure 7-32. Linearity Calibration Performance, Monochromator (Buffer Filter Output, Hi V = 10^7; 100% = 9.9 V)

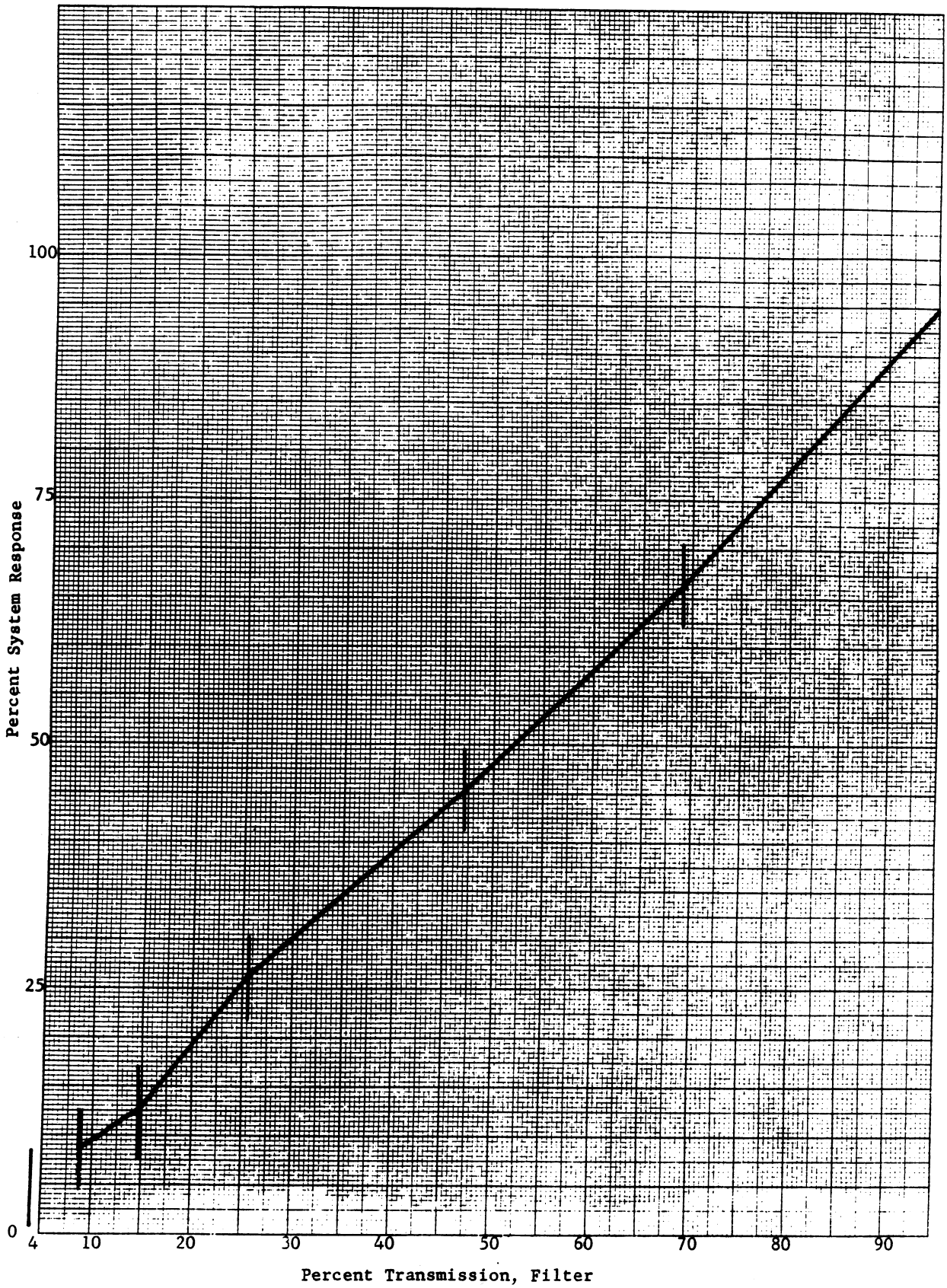

Figure 7-33. Linearity Calibration Performance, Photometer (ADC Data, Lo V = 2×10^{9}; 100% = 1.173×10^{-10} Amperes)

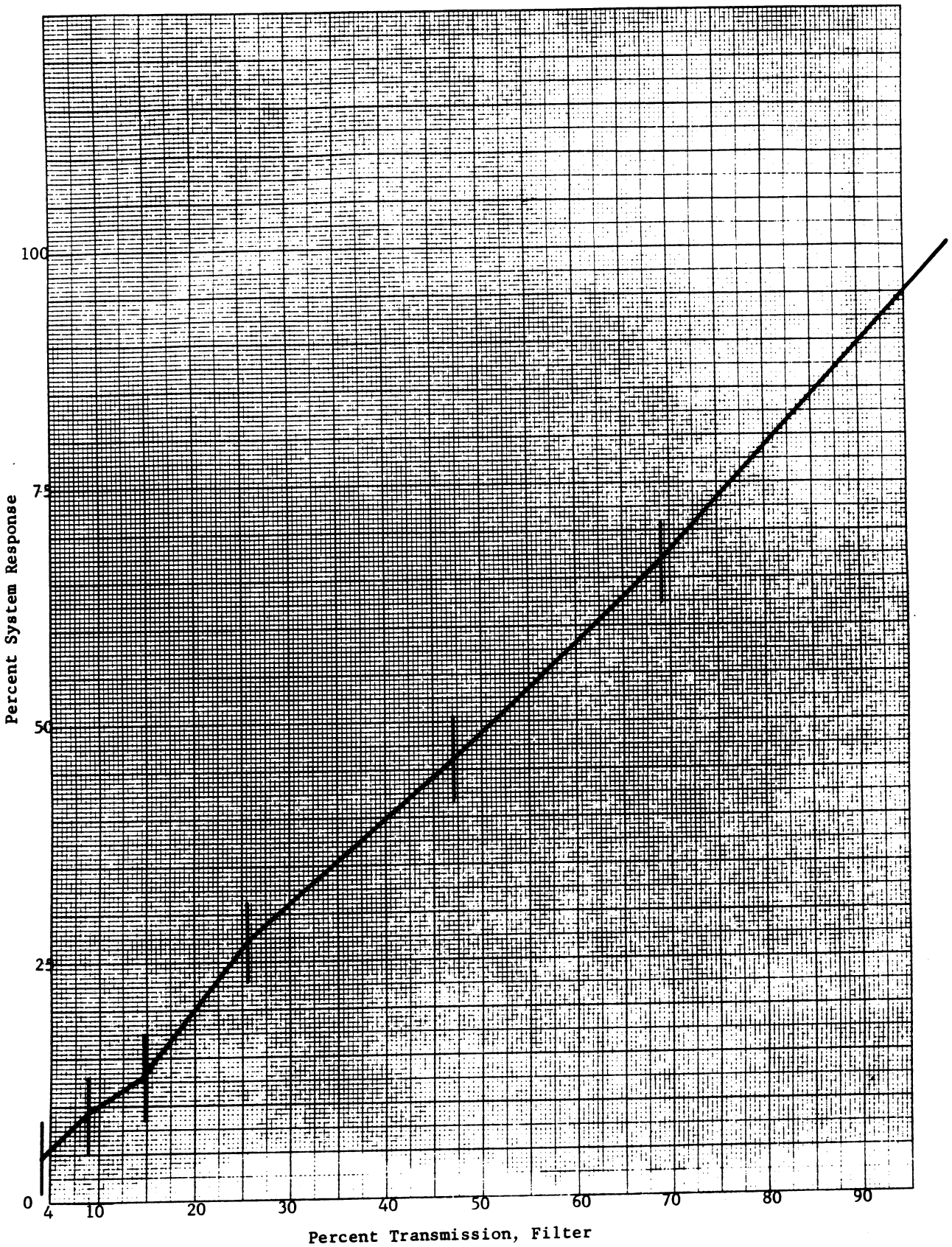

Figure 7-34. Linearity Calibration Performance, Photometer (ADC Data, Lo V = 3×10^{10}; 100% = 3.72×10^{-10} Amperes)

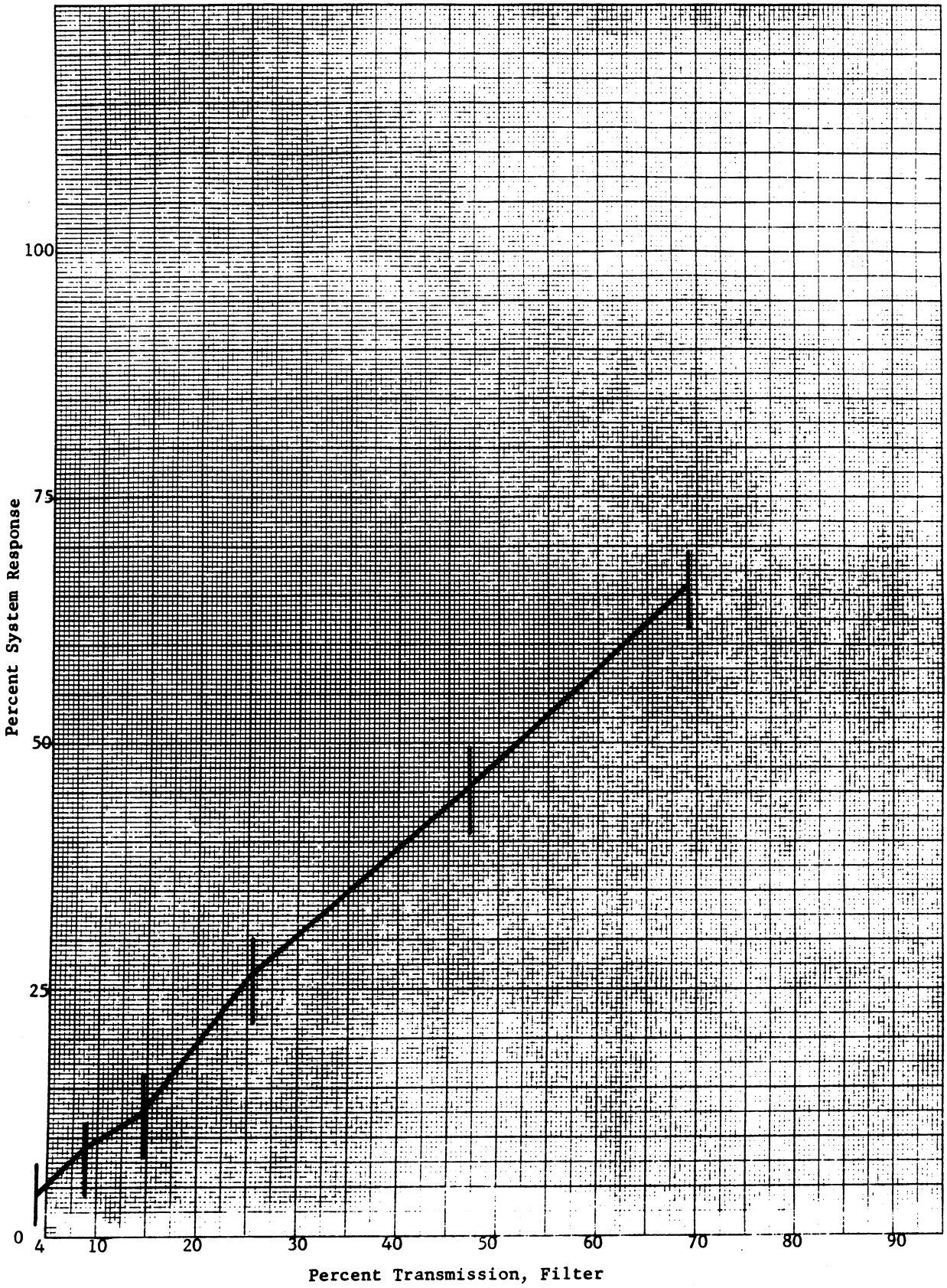

Figure 7-35. Linearity Calibration Performance, Photometer (Pulse Counts, T_D=1.33x10^{-6}; 100%=3.2 MHz, Based on 1% Value)

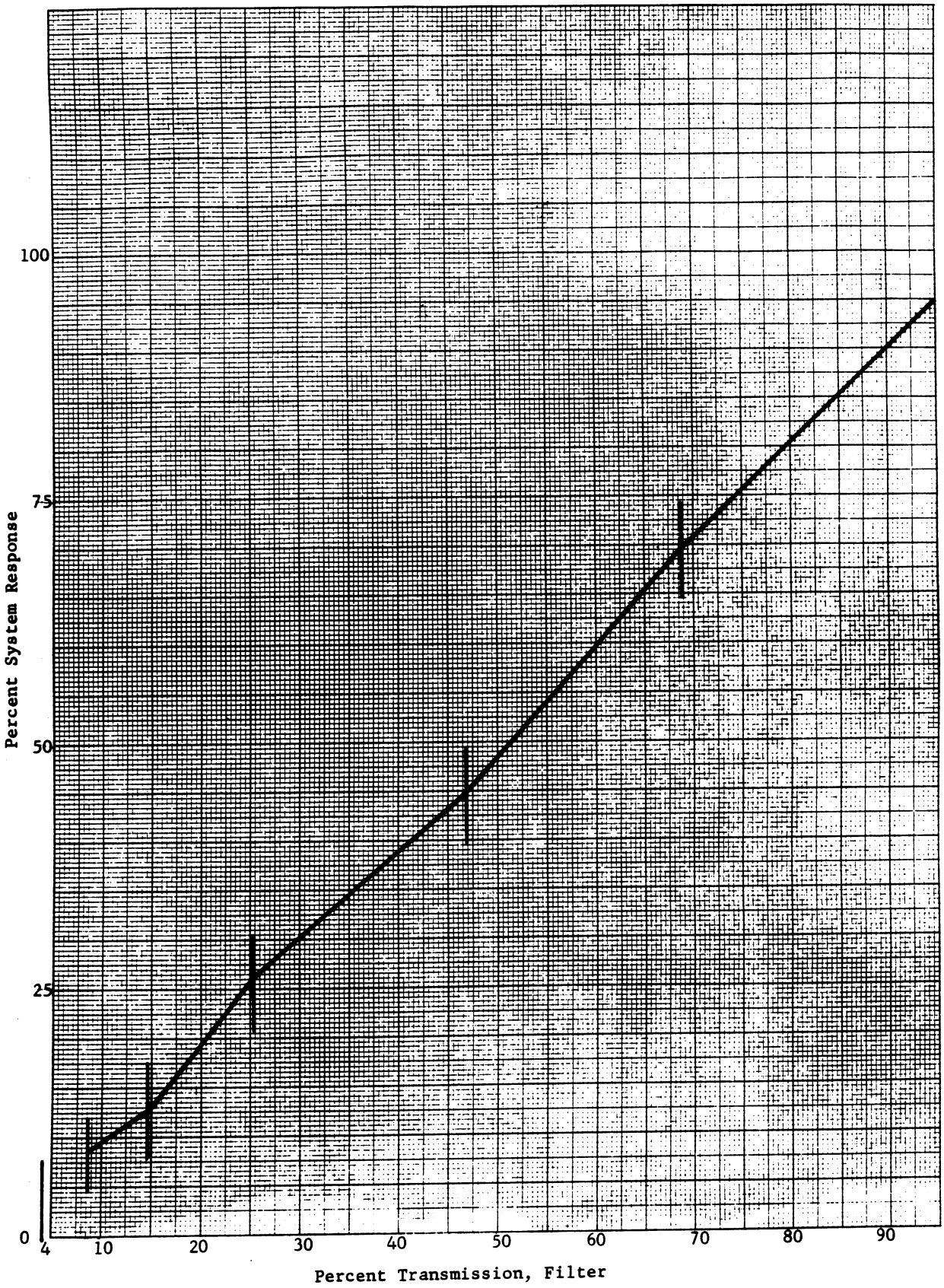

Figure 7-36. Linearity Calibration Performance, Photometer (ADC Data, LoV = 2×10^9; 100% = 11.77×10^{-10} Amperes)

SECTION VIII

QUALITY ASSURANCE AND RELIABILITY

8.1 GENERAL

The Quality Assurance Department of Beckman maintained surveillance with reference to the approved Quality Control Program Plan during the fabrication of the Engineering, P103, and F104 Instruments for the BUV, both in-house and at subcontractor and supplier locations. Quality Assurance assisted in setting up manufacturing processes for all units including handling, fabrication, and environment and acceptance testing. The Quality Assurance department initiated the Equipment Log Book which was maintained with the Engineering, P103, and F104 Instruments.

8.2 METHODS USED FOR SELECTION OF HIGH-GRADE COMPONENTS

Component parts used for the BUV P103 and F104 Instruments were selected by Beckman and ATC from the GSFC Preferred Parts List and from other Preferred Parts Lists which referenced high reliability or military part specifications. Parts and materials lists were submitted to the Technical Officer for review by the NRO and were accompanied by Beckman and ATC generated parts and material specifications.

Parts were screened by following the provisions of GSFC Specifications S-450-P-3, Screening of Semiconductors for the Nimbus Meteorological Satellite Program, and S-450-P-4, Screening of High Usage Electronic Parts for the Nimbus Satellite Program. Beckman Quality Assurance and Reliability monitored this activity and also submitted non-standard part approval requests initiated from both in-house and from the subcontractor.

8.3 FAILURE MODE AND EFFECT ANALYSIS REPORT

Beckman Reliability performed a Failure Mode and Effect Analysis (FMEA) on the BUV Instrument interface. A copy of the FMEA is included in this Final Report.

8.4 FAILURE REPORT SUMMARY

Malfunction reporting was conducted in accordance with procedures given in Section 3.18 of GSFC Specification S-450-P-1A, Quality and Reliability Provisions for Nimbus D Procurements.

Malfunctions were reported on GSFC Malfunction Report Form 4-2. The Malfunction Report numbers for the P103 and F104 Instruments are as follows:

P103: No. A-01602 through No. A-01613,
No. A-01624.

F104: No. A-01615 through No. A-01623,
No. A-01625 through No. A-01631.

FAILURE MODE AND EFFECT ANALYSIS

BACKSCATTER ULTRAVIOLET (BUV) INSTRUMENT INTERFACE

CONTRACT NO. NAS 5-10381

AUGUST 14, 1969

Prepared for:

NATIONAL AERONAUTICS AND SPACE ADMINISTRATION
Goddard Space Flight Center
Greenbelt, Maryland 20771

Prepared by:

BECKMAN INSTRUMENTS, INC.
Advanced Technology Operations
Fullerton, California 92634

Beckman® INSTRUMENTS, INC.
ADVANCED TECHNOLOGY OPERATIONS
2500 HARBOR BOULEVARD, FULLERTON, CALIFORNIA • 92634
(714) 871-4848; TWX: 714-871-1790 • TELEX: 06-78813

Document No. _____
Rev____ Rev Date_____

Title: FAILURE MODE AND EFFECT ANALYSIS

BACKSCATTER ULTRAVIOLET (BUV) INSTRUMENT INTERFACE

Prepared for:

National Aeronautics and Space Administration
Goddard Space Flight Center
Greenbelt, Maryland 20771

Prepared by: R L Cramer	8/26/69	Approved by: W Summers	9/9/69
Originator	Date	R&D Manager	Date
Approved by: P L Stern	9/9/69	Approved by: B T Anderson	9/8/69
Project Engineer	Date	QA/R Manager	Date
Approved by: M A Robinson	9/9/69	Approved by: C Reese	9/9/69
Program Manager	Date	ATO Manager	Date
Approved by: N/A		Approved by: Earl Jones	9/9/69
Documen.Control	Date	Contract Admin.	Date

Beckman INSTRUMENTS, INC.
FULLERTON, CALIFORNIA
ADVANCED TECHNOLOGY OPERATIONS
AREA CODE 714 - 871-4848

FAILURE MODE AND EFFECT ANALYSIS

BACKSCATTER ULTRAVIOLET (BUV) INSTRUMENT INTERFACE

The failure mode and effect analysis (FMEA) for the Backscatter Ultraviolet (BUV) instrument interface is presented on the attached Failure Effect Analysis forms.

The FMEA performed indicates that no problems of excessive high voltage would be encountered at the interface for any assumed failure of the BUV instrument.

The columns on the forms, with additional explanatory statements given, are as follows:

(1) In the column, "Item No. and Name", the interface connector, reference "J", number is presented at the top of the column, followed by the pin numbers in sequence. The interface connectors include J1 through J6.

(2) The column, "Assumed Failure", contains the types of possible failure modes that could be encountered at the BUV instrument interface.

(3) In the column, "Probable Cause", electrical disconnect frequently appears. This could be a disconnect at the connector or at any other tie-point in the BUV instrument.

(4) The columns, "Stress Margin", "$\lambda \times 10^6$", and "Failure Rate Source", were intentionally left blank as they are not required.

(5) The column, "Probable Effect", contains the probable effects at the interface equipment.

(6) The column, "Failure Effect Class", refers to the severity of the assumed failure. The classifications are presented for BUV instrument inputs and for BUV instrument outputs as follows:

BUV instrument inputs:

Class A_1 - Failure which severely degrades the supply voltage or signal from the interface equipment.

Class B_1 - Failure which slightly degrades the supply voltage or signal from the interface equipment.

Class C_1 - Failure which has no direct effect at the interface equipment.

BUV instrument outputs:

Class A_2 - Failure which causes a complete loss of signal to the interface equipment.

Class B_2 - Failure which degrades the performance at the interface such that the indication is in error.

Class C_2 - Failure which has no direct effect at the interface equipment.

(7) The column, "Remarks", is used for additional comments wherever deemed necessary.

FAILURE EFFECT ANALYSIS

EQUIPMENT	Prepared by: DATE	REVISION DATE	APPROVED BY DATE	REFERENCES	EQUIPMENT STATUS
BUV Instrument, Interface Connectors	R. Cramer 8/14/69	N/C			Normal Operation

ITEM NO. & NAME	ASSUMED FAILURE	Probable Cause	Stress MARGIN	λ x 10^6	Failure Rate Source	PROBABLE EFFECT	FAILURE EFFECT CLASS	Remarks
J1								
Pin								
1	Loss of Logic Reference	Electrical disconnect				No effect at VIP	C_1	
2 (Spare)								
3	Loss of Primary Power Return #1	Electrical disconnect				No effect at Power Subsystem	C_1	
4	Loss of Housekeeping Power Return #1	Electrical disconnect				No effect at Power Subsystem	C_1	
5 (Spare)								
6	Loss of Housekeeping Power #1	(1) Electrical disconnect.				(1) No effect at Power Subsystem.	C_1	
		(2) Defective circuit in Static Inverter No. 1.				(2) No effect at Power Subsystem.	C_1	
		(3) Capacitor shorted in Static Inverter No. 1.				(3) -24.5V line from Power Subsystem is reduced to 0 volt.	A_1	
	Voltage level of Housekeeping Power #1 decreases.	Capacitor leakage in Static Inverter No. 1				-24.5V line from Power Subsystem is reduced.	B_1	

FAILURE EFFECT ANALYSIS

EQUIPMENT	Prepared by: DATE	REVISION DATE	APPROVED BY DATE	REFERENCES	EQUIPMENT STATUS
BUV Instrument, Interface Connectors	R.Cramer 8/14/69	N/C			Normal Operation

ITEM NO. & NAME	ASSUMED FAILURE	Probable Cause	Stress MARGIN	λ x 10⁶	Failure Rate Source	PROBABLE EFFECT	FAILURE EFFECT CLASS	Remarks
J1								
Pin								
7	Loss of Housekeeping Power return from GSE	(1) Electrical disconnect.				No effect at GSE.	C_1	
		(2) Diode open in Static Inverter No.1.						
8	Loss of Primary Power #1	(1) Electrical disconnect.				(1) No effect at Power Subsystem.	C_1	
		(2) Defective circuit in Static Inverter No. 2.				(2) No effect at Power Subsystem.	C_1	
		(3) Capacitor shorted in Static Inverter No. 2.				(3) -24.5V line from Power Subsystem is reduced to 0 volt.	A_1	
	Voltage level of Primary Power #1 decreases.	Capacitor leakage in Static Inverter No. 2				-24.5V line from Power Subsystem is reduced.	B_1	
9	Loss of Primary Power #2.	(1) Electrical disconnect.				(1) No effect at Power Subsystem.	C_1	
		(2) Defective circuit in Static Inverter No. 2.				(2) No effect at Power Subsystem.	C_1	
		(3) Capacitor shorted in Static Inverter No. 2.				(3) -24.5V line from Power Subsystem is reduced to 0 volt.	A_1	

FAILURE EFFECT ANALYSIS

EQUIPMENT	Prepared by: DATE	REVISION DATE	APPROVED BY DATE	REFERENCES	EQUIPMENT STATUS
BUV Instrument, Interface Connectors	R.Cramer 8/14/69	N/C			Normal Operation

ITEM NO. & NAME	ASSUMED FAILURE	Probable Cause	Stress MARGIN	λ x 10⁶	Failure Rate Source	PROBABLE EFFECT	FAILURE EFFECT CLASS	Remarks
J1								
Pin								
9 (continued)	Voltage level of Primary Power #2 decreases.	Capacitor leakage in Static Inverter No. 2.				-24.5V line from Power Subsystem is reduced.	B_1	
10	Loss of Primary Power return from GSE	(1) Electrical disconnect. (2) Diode open in Static Inverter No. 2.				No effect at GSE.	C_1	
11	Loss of Primary Power return #2.	Electrical disconnect.				No effect at Power Sub-System.	C_1	
12	Loss of Housekeeping Power return #2.	Electrical disconnect.				No effect at Power Subsystem.	C_1	
13 (Spare)								
14	Loss of Housekeeping Power #2.	(1) Electrical disconnect. (2) Defective circuit in Static Inverter No. 1. (3) Capacitor shorted in Static Inverter No. 1.				(1) No effect at Power Subsystem. (2) No effect at Power Subsystem. (3) -24.5V line from Power Subsystem is reduced to 0 volt.	C_1 C_1 B_1	

FAILURE EFFECT ANALYSIS

EQUIPMENT	Prepared by: DATE	REVISION DATE	APPROVED BY DATE	REFERENCES	EQUIPMENT STATUS
BUV Instrument, Interface Connectors	R.Cramer 8/14/69	N/C			Normal Operation

ITEM NO. & NAME	ASSUMED FAILURE	Probable Cause	Stress MARGIN	λ x 10⁶	Failure Rate Source	PROBABLE EFFECT	FAILURE EFFECT CLASS	Remarks
J1								
Pin								
9 (continued)	Voltage level of Primary Power #2 decreases.	Capacitor leakage in Static Inverter No. 2.				-24.5V line from Power Subsystem is reduced.	B_1	
10	Loss of Primary Power return from GSE	(1) Electrical disconnect. (2) Diode open in Static Inverter No. 2.				No effect at GSE.	C_1	
11	Loss of Primary Power return #2.	Electrical disconnect.				No effect at Power Sub-System.	C_1	
12	Loss of House-keeping Power return #2.	Electrical disconnect.				No effect at Power Sub-system.	C_1	
13 (Spare)								
14	Loss of House-keeping Power #2.	(1) Electrical disconnect.				(1) No effect at Power Subsystem.	C_1	
		(2) Defective circuit in Static Inverter No. 1.				(2) No effect at Power Subsystem.	C_1	
		(3) Capacitor shorted in Static Inverter No. 1.				(3) -24.5V line from Power Subsystem is reduced to 0 volt.	B_1	

FAILURE EFFECT ANALYSIS

EQUIPMENT	Prepared by: DATE	REVISION DATE	APPROVED BY DATE	REFERENCES	EQUIPMENT STATUS
BUV Instrument, Interface Connectors	R.Cramer 8/14/69	N/C			Normal Operation

ITEM NO. & NAME	ASSUMED FAILURE	Probable Cause	Stress MARGIN	λ x 10^6	Failure Rate Source	PROBABLE EFFECT	FAILURE EFFECT CLASS	Remarks
J1								
Pin								
14 (Continued)	Voltage level of Housekeeping Power #2 decreases.	Capacitor leakage in Static Inverter No. 1.				-24.5V line from Power Subsystem is reduced.	B_1	
15	Loss of chassis ground.	Electrical Disconnect.				No effect at VIP.	C_1	May increase noise on J1 voltage levels from interface equipment to BUV.

FAILURE EFFECT ANALYSIS

EQUIPMENT	Prepared by: DATE	REVISION DATE	APPROVED BY DATE	REFERENCES	EQUIPMENT STATUS
BUV Instrument, Interface Connectors	R.Cramer 8/14/69	N/C			Normal Operation

ITEM NO. & NAME	ASSUMED FAILURE	Probable Cause	Stress MARGIN	λ x 10⁶	Failure Rate Source	PROBABLE EFFECT	FAILURE EFFECT CLASS	Remarks
J2								
Pin								
1	Loss of Logic Reference.	Electrical disconnect.				No effect at VIP.	C_2	
2	Loss of Signal Voltage.	(1) Electrical disconnect.				Loss of "Motor current limiter temp." to VIP.	A_2	
		(2) Defective Housekeeping circuit or temp. sensor ckt.						
	Signal Voltage decrease.	Component degradation in Housekeeping circuit or temp. sensor ckt.				Inaccurate "Motor current limiter temp." to VIP.	B_2	
	Signal Voltage increase.	(1) Shorted diode in Housekeeping regulator.				(1) Inaccurate "Motor current limiter temp." to VIP.	B_2	(1) The resulting loss of -6.375V regulation would also be detected via J2-18.
		(2) Component degradation in Housekeeping circuit or temp. sensor ckt.				(2) Inaccurate "Motor current limiter temp." to VIP.		
3	Loss of signal voltage.	(1) Electrical disconnect.				Loss of "Housing temp. gradient" to VIP.	A_2	
		(2) Defective Housekeeping circuit or temp sensor ckt.						

FAILURE EFFECT ANALYSIS

EQUIPMENT	Prepared by: DATE	REVISION DATE	APPROVED BY DATE	REFERENCES	EQUIPMENT STATUS
BUV Instrument, Interface Connectors	R.Cramer 8/14/69	N/C			Normal Operation

ITEM NO. & NAME	ASSUMED FAILURE	Probable Cause	Stress MARGIN	$\lambda \times 10^6$	Failure Rate Source	PROBABLE EFFECT	FAILURE EFFECT CLASS	Remarks
J2								
Pin								
3 (Continued)	Signal voltage decrease.	Component degradation in Housekeeping circuit or temp. sensor ckt.				Inaccurate "Housing temp. gradient" to VIP.	B_2	
	Signal voltage increase.	(1) Shorted diode in Housekeeping regulator.				(1) Inaccurate "Housing Temp. gradient" to VIP.	B_2	(1) The resulting loss of -6.375V regulation would also be detected via J2-18.
		(2) Component degradation in Housekeeping circuit or temp. sensor ckt.				(2) Inaccurate "Housing Temp. gradient" to VIP.	B_2	
4	Loss of signal voltage.	(1) Electrical disconnect.				Loss of "Arm temp. gradient" to VIP.	A_2	
		(2) Defective Housekeeping circuit or temp. sensor ckt.						
	Signal voltage decrease.	Component degradation in Housekeeping circuit or temp. sensor ckt.				Inaccurate "Arm temp. gradient" to VIP.	B_2	
	Signal voltage increase.	(1) Shorted diode in Housekeeping Regulator.				(1) Inaccurate "Arm temp. gradient" to VIP.	B_2	(1) The resulting loss of -6.375V regulation would also be detected via J2-18.

FAILURE EFFECT ANALYSIS

EQUIPMENT	Prepared by: DATE	REVISION DATE	APPROVED BY DATE	REFERENCES	EQUIPMENT STATUS
BUV Instrument, Interface Connectors	R.Cramer 8/14/69	N/C			Normal Operation

ITEM NO. & NAME	ASSUMED FAILURE	Probable Cause	Stress MARGIN	λ x 10⁶	Failure Rate Source	PROBABLE EFFECT	FAILURE EFFECT CLASS	Remarks
J2								
Pin								
4 (Continued)		(2) Component degradation in Housekeeping circuit or temp. sensor ckt.				(2) Inaccurate "Arm temp. gradient" to VIP.	B_2	
5	Loss of signal voltage.	(1) Electrical disconnect.				Loss of "Static Inverter #1" temp. indication to VIP.	A_2	
		(2) Defective Housekeeping circuit or temp. sensor ckt.						
	Signal voltage decrease.	Component degradation in Housekeeping circuit or temp. sensor ckt.				Inaccurate "Static Inverter #1" temp. indication to VIP.	B_2	
	Signal voltage increase.	(1) Shorted diode in Housekeeping regulator.				(1) Inaccurate "Static Inverter #1" temp. indication to VIP.	B_2	(1) The resulting loss of -6.375V regulation would also be detected via J2-18.
		(2) Component degradation in Housekeeping circuit or temp. sensor Ckt.				(2) Inaccurate "Static Inverter #1" temp. indication to VIP.		
6 (Spare)								
7	Loss of signal voltage.	(1) Electrical disconnect.				Loss of "Electronics Module Temp." indication to VIP.	A_2	
		(2) Defective Housekeeping circuit or temp. sensor ckt.						

FAILURE EFFECT ANALYSIS

EQUIPMENT	Prepared by:	DATE	REVISION	DATE	APPROVED BY	DATE	REFERENCES	EQUIPMENT STATUS
BUV Instrument, Interface Connectors	R. Cramer	8/14/69	N/C					Normal Operation

ITEM NO. & NAME	ASSUMED FAILURE	Probable Cause	Stress MARGIN	λ x 10^6	Failure Rate Source	PROBABLE EFFECT	FAILURE EFFECT CLASS	Remarks
J2								
Pin								
7 (Continued)	Signal voltage decrease.	Component degradation in Housekeeping circuit or temp. sensor ckt.				Inaccurate "Electronics Module Temp." indication to VIP.	B_2	
	Signal voltage increase.	(1) Shorted diode in Housekeeping regulator.				(1) Inaccurate "Electronics Module Temp." indication to VIP.	B_2	(1) The resulting loss of -6.375V regulation would also be detected via J2-18.
		(2) Component degradation in Housekeeping circuit or temp. sensor ckt.				(2) Inaccurate "Electronics Module Temp." indication to VIP.	B_2	
8	Loss of signal voltage.	(1) Electrical disconnect.				Loss of "PMT Temp." indication to VIP.	A_2	
		(2) Defective Housekeeping circuit or temp. sensor ckt.						
	Signal voltage decrease.	Component degradation in Housekeeping circuit or temp. sensor ckt.				Inaccurate "PMT Temp." indication to VIP.	B_2	
	Signal voltage increase.	(1) Shorted diode in Housekeeping regulator.				(1) Inaccurate "PMT Temp." indication to VIP.		(1) The resulting loss of -6.375V regulation would also be detected via J2-18.
		(2) Component degradation in Housekeeping circuit or temp. sensor ckt.				(2) Inaccurate "PMT Temp." indication to VIP.	B_2	

FAILURE EFFECT ANALYSIS

EQUIPMENT	Prepared by: DATE	REVISION DATE	APPROVED BY DATE	REFERENCES	EQUIPMENT STATUS
BUV Instrument, Interface Connectors	R.Cramer 8/14/69	N/C			Normal Operation

ITEM NO. & NAME	ASSUMED FAILURE	Probable Cause	Stress MARGIN	λ x 10⁶	Failure Rate Source	PROBABLE EFFECT	FAILURE EFFECT CLASS	Remarks
J2								
Pin								
9	Loss of signal voltage.	(1) Electrical disconnect. (2) Defective Housekeeping circuit or temp. sensor ckt.				Loss of "Housing absolute inboard casting wall temp." indication to VIP.	A_2	
	Signal voltage decrease.	Component degradation in Housekeeping circuit or temp. sensor ckt.				Inaccurate "Housing absolute inboard casting wall temp." indication to VIP.	B_2	
	Signal voltage increase.	(1) Shorted diode in Housekeeping regulator. (2) Component degradation in Housekeeping circuit or temp. sensor ckt.				(1) Inaccurate "Housing absolute inboard casting wall temp." indicationto VIP. (2) Inaccurate "Housing absolute inboard casting wall temp." indication to VIP.	B_2 B_2	(1) The resulting loss of -6.375V regulation would also be detected via J2-18.
10 (Spare)								
11, 12	Loss of Housekeeping reference.	Electrical disconnect				Loss of Housekeeping signals to VIP.	A_2	
13 (Spare)								
14	Loss of signal voltage.	(1) Electrical disconnect. (2) Defective circuit in sensor module.				Loss of "Monochromator high voltage" indication to VIP.	A_2	

FAILURE EFFECT ANALYSIS

EQUIPMENT	Prepared by: DATE	REVISION DATE	APPROVED BY DATE	REFERENCES	EQUIPMENT STATUS
BUV Instrument, Interface Connectors	R.Cramer 8/14/69	N/C			Normal Operation

ITEM NO. & NAME	ASSUMED FAILURE	Probable Cause	Stress MARGIN	λ x 10^6	Failure Rate Source	PROBABLE EFFECT	FAILURE EFFECT CLASS	Remarks
J2								
Pin								
14 (Continued)	Signal voltage decrease or increase.	Component degradation in sensor module.				Inaccurate "Monochromator high voltage" indication to VIP.	B_2	
15	Loss of signal voltage.	(1) Electrical disconnect.				Loss of "Photometer high voltage" indication to VIP.	A_2	
		(2) Defective circuit in sensor module.						
	Signal voltage decrease or increase.	Component degradation in sensor module.				Inaccurate "Photometer high voltage" indication to VIP.	B_2	
16	Loss of wire shield.	Electrical disconnect.				May cause increased noise on high voltage indications to VIP.	C_2	
17 (Spare)								
18	Loss of signal voltage.	(1) Electrical disconnect.				Loss of "Thermistor bias (-6.375V) monitor" to VIP.	A_2	
		(2) Defective Housekeeping circuit.						
	Signal voltage decrease.	Component degradation in Housekeeping circuit.				Inaccurate "Thermistor bias (-6.375V) monitor" to VIP.	B_2	
	Signal voltage increase.	(1) Shorted diode in Housekeeping regulator.				(1) Inaccurate "Thermistor bias (-6.375V) monitor" to VIP.	B_2	(1) Would have loss of -6.375V regulation.

FAILURE EFFECT ANALYSIS

EQUIPMENT	Prepared by: DATE	REVISION DATE	APPROVED BY DATE	REFERENCES	EQUIPMENT STATUS
BUV Instrument, Interface Connectors	R.Cramer 8/14/69	N/C			Normal Operation

ITEM NO. & NAME	ASSUMED FAILURE	Probable Cause	Stress MARGIN	$\lambda \times 10^6$	Failure Rate Source	PROBABLE EFFECT	FAILURE EFFECT CLASS	Remarks
J2								
Pin								
18 (Continued)		(2) Component degradation in Housekeeping circuit.				(2) Inaccurate "Thermistor bias (-6.375V) monitor" to VIP.	B_2	
19	Loss of signal voltage.	(1) Electrical disconnect.				Loss of "Sensor module electronic temp." indication to VIP.	A_2	
		(2) Defective Housekeeping circuit or temp. sensor ckt.						
	Signal voltage decrease.	Component degradation in Housekeeping circuit or temp. sensor ckt.				Inaccurate "Sensor module electronics temp." indication to VIP.	B_2	
	Signal voltage increase.	(1) Shorted diode in Housekeeping regulator.				(1) Inaccurate "Sensor module electronics temp." indication to VIP.	B_2	(1) The resulting loss of -6.375V regulation would also be detected via J2-18.
		(2) Component degradation in Housekeeping circuit or temp. sensor ckt.				(2) Inaccurate "Sensor module electronics temp." indication to VIP.	B_2	
20, 21 (Spares)								
22	Loss of signal voltage.	(1) Electrical disconnect.				Loss of "+4V monitor" to VIP.	A_2	
		(2) Defective Housekeeping circuit.						

FAILURE EFFECT ANALYSIS

EQUIPMENT	Prepared by: DATE	REVISION DATE	APPROVED BY DATE	REFERENCES	EQUIPMENT STATUS
BUV Instrument, Interface Connectors	R.Cramer 8/14/69	N/C			Normal Operation

ITEM NO. & NAME	ASSUMED FAILURE	Probable Cause	Stress MARGIN	$\lambda \times 10^6$	Failure Rate Source	PROBABLE EFFECT	FAILURE EFFECT CLASS	Remarks
J2								
Pin								
22 (Continued)	Signal voltage decrease.	Component degradation in Housekeeping circuit				Inaccurate "+4V monitor" to VIP.	B_2	
	Signal voltage increase.	(1) Shorted diode in Housekeeping regulator.				Inaccurate "+4V monitor" to VIP.	B_2	The resulting loss of -6.375V regulation would also be detected via J2-18.
		(2) Component degradation in Housekeeping circuit.						
23, 24 (Spares)								
25	Loss of chassis ground.	Electrical disconnect.				No effect at VIP.	C_2	May increase noise on the signals from J2 to the interface equipment.

16. Shigley, "Mechanical Engineering Design," p. 246.

17. Military Standard MS 16995.

18. Greenwood, Douglas C., "Geneva Wheel Design," Product Engineering, May 26, 1958.

19. Jensen, Preven W., "Geneva Mechanisms," Design Data, Design News, September 29, 1965.

20. Fenton, R.G., "Geneva Mechanisms," Machine Design, January 21, 1965.

21. Lichtwitz, Otto, "Mechanisms for Intermittent Motion," Machine Design, December 1951.

22. Johnson, Ray C., "Geneva Mechanisms," Machine Design, March 22, 1956.

23. Polymer Corporation, "Nimbus B approved material and Processes List," p. 42.

24. Timoshenk, S., and Young, D.H., "Elements of Strength of Materials," pp 212, 247, (Princeton, New Jersey, Van Nostrand Co., Inc. 1962).

25. Roark, Raymond J., "Formulas for Stress and Strain," New York, McGraw-Hill Book Co., Inc., 1965, p. 194, 320.

26. Dow Chemical Corporation, "Physical Properties of Magnesium Casting Alloys," Table II, Bulletin 141-176.

27. MIL Handbook, "5A Metallic Materials & Elements for Aerospace Vehicle Structures," p. 4.2.8.

28. Wirsching, P.H., "Random Vibrations," Product Engineering, Vol. 22, p. 108, 1964.

SECTION X

BIBLIOGRAPHY

1. Lyot, Ann. Observatoire Astron. Phys. de Paris (Meudon)--Tomi i Fasc. 1-2 8, 102 (1928).

2. Billings, Bruce H., "A Monochromatic Depolarizer," Journal of the Optical Society of America, Volume 41, No. 12, December 1951.

3. Peters, C.J., "Light Depolarizer," Applied Optics, Vol. 3, No. 12, pp 1502, December 1951.

4. Shurcliff, Wm. A., "Polarized Light," Harvard University Press.

5. Description of the Backscatter Ultraviolet Experiment by Dr. J. V. Dave and Dr. D. F. Heath.

6. Billings, Bruce H., and Land, E.H., "A Comparative Survey of Some Possible Systems of Polarized Headlights," Journal of Optical Society of America, Vol. 38, N. 10, pp 819, October 1948.

7. Dave, J.V., and Furukawa, P.M., "Scattered Radiation in the Ozone Absorption Bands at Selected Levels of a Terrestrial," Rayleigh Atmosphere, Vol. 7, No. 29, Published by American Meteorological Society, Boston, Mass., Jan. 1966.

8. Freberg and Kemler, "Elements of Mechanical Vibration," pp 28, 127, and 142.

9. IEEE Transactions on Nuclear Science, Volume NS-13, No. 6, December 1966.

10. Battelle Memorial Institute, "Space Radiation Damage to Electronic Components and Materials," Report No. 39, January 31, 1966.

11. GSFC Specification, "An Environmental Specification for Nimbus B Subsystems," p. 5.

12. Product Engineering, June 22, 1964, p. 108.

13. Metals Handbook, p. 1038.

14. General Electric Fused Quartz Catalog, p. 5.

15. Nimbus Handbook for Experimenters, Figure 13, III-5.

9.3.5 Test Point Buffers

Additional buffering by active elements is needed for isolation of sensitive test points. The buffers could be incorporated in a small amplifier box powered by the BTU and mounted on the instrument proper during bench test.

9.3.6 Real Time Analog Readout

Additional meters should be provided in the BTU, driven by the buffers discussed in Paragraph 9.3.5. Several important test parameters such as buffer-filter output, high voltage monitor, etc., could then be continuously monitored on a simultaneous basis.

9.3.7 "Disable" Switches

The test harness should be built to allow insertion of BTU-mounted switches into various control lines. These lines would include the various motor drive lines, high voltage and feedback control lines, etc. Much more flexible operation would be afforded by providing for independent control of these functions during test. Also, the Mini-Computer discussed in Paragraph 9.3.1 could perform automatic modification of the instrument operating condition, if desired, by using remotely controlled switches.

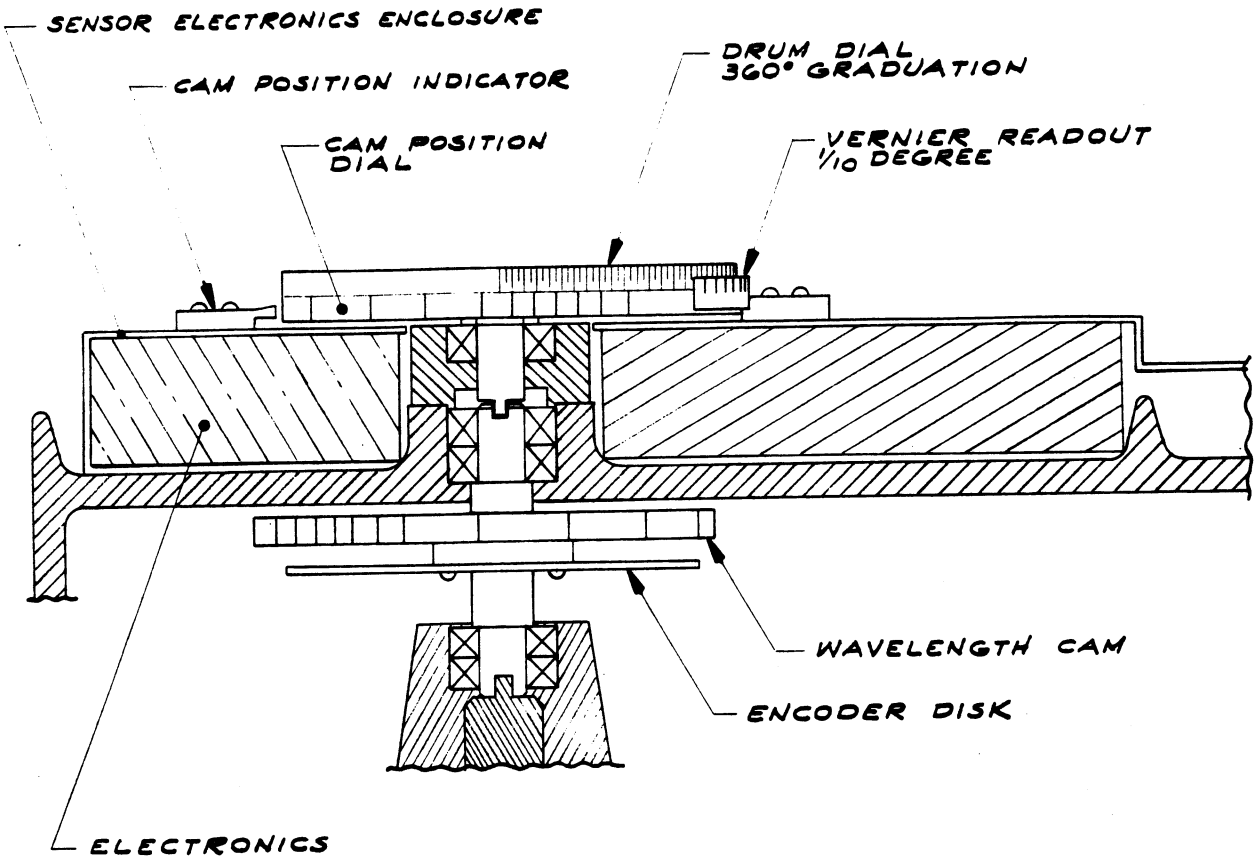

Figure 9-1. External Cam Position Indicator

9.3.4 External Cam Position Indicator (Mechanical)

Various testing, adjusting, and calibration requirements revealed the need for continuous direct identification of the actual wavelength-cam position.

An external dial readout should be provided for future instruments. This drum type dial would consist of a removable accessory with the vernier readout attached to a base or bracket that in turn could be mounted onto the main BUV housing (Figure 9-1).

The wavelength cam shaft presently hidden under the cover of the sensor electronics package could be made accessible and the shaft end within the ball-bearing provided with a slot, that in turn would accommodate a mating part as continuous extension of the wavelength dial.

The dial would represent the actual cam steps of the 12 monitor and the 7 calibrating positions. Below the cam-step locations would be a secondary dial with a 360° scale in increments of 1/2°; position and direction of scale to be consistent with the cam layout.

Tied in with the cam configuration and position is the encoder. The encoder provides both cam position control and housekeeping information. It would be extremely helpful to have access to the encoder disc and/or readout to provide the ability for corrective adjustment between the cam and encoder. The encoder itself should be of a type that would provide better resolution than the one presently used.

various reasons. This would allow extremely rapid evaluation of the effect of configuration changes and afford a means for rapid optimization of various test setups.

e. Control of a small line printer for producing hard copy records of various decoded parameters.

f. Rapid correlation, during environmental testing, between instrument outputs and changes in test conditions.

g. Complete automatic control of the instrument operating sequence. This would function in conjunction with the Preset Frame Counter discussed in Paragraph 9.3.3.

9.3.2 Different PMT

The use of sapphire as a window material in the PMT's may be undesirable, due either to its proximity to the photocathode or its response to energetic particles. A side view tube would allow greater separation between the window and the photocathode. A different material could be used for the present configuration, or a combination could be tried. This would require investigation before selection of future tubes for orbital flight.

9.3.3 Preset Frame Counter

A method should be provided to allow setting of the internal sequence controller (calibration sequencer) to any desired state. This would require only a small increase in the instrument digital logic elements and the addition of not more than ten external connections. The sequencer could then be set to any desired frame by manual switches or controlled automatically with the Mini-Computer discussed in Paragraph 9.3.1. The ten additional lines could also be used to detect the state of the internal sequencer at any time.

SECTION IX

RECOMMENDATIONS

9.1 GENERAL

During the course of the BUV program, several possible improvements were evident. These were incorporated when not ruled out by schedule and funding considerations. For similar programs of the future, the following suggestions may be fruitful.

9.2 SUMMARY

Almost all items deal with bench test of the instrument, since that is the area requiring the greatest concentration of effort. The exception is a possible PMT improvement discussed in Paragraph 9.3.2.

9.3 DETAILED RECOMMENDATIONS

9.3.1 Mini-Computer in BTU

A small computer could be added to the Bench Test Unit for monitoring the digital output lines. Among the expanded capabilities are:

a. Real time conversion of the instrument digital output (VIP A) to equivalent PMT anode or cathode current.

b. Continuous comparison of the stripped-out status bits with the Digital B signals.

c. Evaluation of internal calibration results as compared to stored norms.

d. Performance of the calibration methods of Section VII on a continuous real-time basis to detect gain or dead-time variations caused by

FAILURE EFFECT ANALYSIS

EQUIPMENT	Prepared by: DATE	REVISION DATE	APPROVED BY DATE	REFERENCES	EQUIPMENT STATUS
BUV Instrument, Interface Connectors	R.Cramer 8/14/69	N/C			Normal Operation

ITEM NO. & NAME	ASSUMED FAILURE	Probable Cause	Stress MARGIN	λ x 10^6	Failure Rate Source	PROBABLE EFFECT	FAILURE EFFECT CLASS.	Remarks
J6								
Pin								
24	Loss of Major Frame Pulse Shield.	Electrical disconnect.				No effect at VIP.	C_1	
25	Loss of Chassis Ground.	Electrical disconnect.				No effect at VIP.	C_1	May cause noise on J6 digital signals.

FAILURE EFFECT ANALYSIS

EQUIPMENT	Prepared by: DATE	REVISION DATE	APPROVED BY DATE	REFERENCES	EQUIPMENT STATUS
BUV Instrument, Interface Connectors	R.Cramer 8/14/69	N/C			Normal Operation

ITEM NO. & NAME	ASSUMED FAILURE	Probable Cause	Stress MARGIN	λ x 10^6	Failure Rate Source	PROBABLE EFFECT	FAILURE EFFECT CLASS	Remarks
J6								
Pin								
11 (Spare)								
12	Loss of Major Frame Pulse.	(1) Electrical disconnect. (2) Defective Major Frame pulse circuit.				No effect at VIP.	C_1	
13 (Spare)								
14	Loss of Logic Reference 2.	Electrical disconnect.				No effect at VIP.	C_1	
15	Loss of Sample Data A1 line Shield.	Electrical disconnect.				No effect at VIP.	C_1	
16, 17 (Spares)								
18	Loss of Shield Return for B1 Line.	Electrical disconnect.				No effect at VIP.	C_1	
19 (Spare)								
20	Loss of Shield Return for C1 Line.	Electrical disconnect.				No effect at VIP.	C_1	
21, 22 (Spares)								
23	Loss of Digital D1 data Out Shield.	Electrical disconnect.				No effect at VIP.	C_1	May cause noise on Digital D1 data out line to VIP.

FAILURE EFFECT ANALYSIS

EQUIPMENT	Prepared by: DATE	REVISION DATE	APPROVED BY DATE	REFERENCES	EQUIPMENT STATUS
BUV Instrument, Interface Connectors	R.Cramer 8/14/69	N/C			Normal Operation

ITEM NO. & NAME	ASSUMED FAILURE	Probable Cause	Stress MARGIN	λ x 10⁶	Failure Rate Source	PROBABLE EFFECT	FAILURE EFFECT CLASS	Remarks
J6								
Pin								
1	Loss of Logic Reference 1.	Electrical disconnect.				No effect at VIP.	C_1	
2	Loss of Sample Data A1 Line Pulses.	(1) Electrical disconnect. (2) Defective A1 line circuit.				No effect at VIP.	C_1	
3, 4 (Spares)								
5	Loss of Timing B1 Line Pulses.	(1) Electrical disconnect. (2) Defective B1 line circuit.				No effect at VIP.	C_1	
6 (Spare)								
7	Loss of C1 line shift pulses.	(1) Electrical disconnect. (2) Defective C1 line circuit.				No effect at VIP.	C_1	
8, 9 (Spares)								
10	Loss of Digital D1 data Out Pulses.	(1) Electrical Disconnect. (2) Defective D1 line circuit.				Loss of Digital D1 data out pulses to VIP.	A_2	

FAILURE EFFECT ANALYSIS

EQUIPMENT	Prepared by: DATE	REVISION DATE	APPROVED BY DATE	REFERENCES	EQUIPMENT STATUS
BUV Instrument, Interface Connectors	R.Cramer 8/14/69	N/C			Normal Operation

ITEM NO. & NAME	ASSUMED FAILURE	Probable Cause	Stress MARGIN	λ x 10^6	Failure Rate Source	PROBABLE EFFECT	FAILURE EFFECT CLASS	Remarks
J5								
Pin								
1	Loss of Logic Reference.	Electrical disconnect.				No effect at VIP.	C_1	
2 (Spare)								
3	Loss of 10KH$_z$ Clock Signal.	(1) Electrical disconnect.				No effect at clock subsystem.	C_1	Loss of 10KH$_z$ clock can be detected at VIP via J3-7.
		(2) Defective 10KH$_z$ Clock Circuit.						
	10KH$_z$ Clock Signal Unstable.	Defective 10KH$_z$ clock circuit.				No effect at clock subsystem.	C_1	Unstable 10KH$_z$ clock can be detected at VIP via J3-7.
4-9 (Spares)								
10	Loss of 10KH$_z$ clock shield.	Electrical disconnect.				No effect at clock subsystem.	C_1	May cause noise on the 10KH$_z$ clock signal.
11	Loss of 10KH$_z$ clock signal return.	Electrical disconnect.				No effect at clock subsystem.	C_1	
12, 13, 14 (Spares)								
15	Loss of Chassis Ground.	Electrical disconnect.				No effect at VIP.	C_1	May increase noise on J5 clock signals from interface equipment to BUV.

FAILURE EFFECT ANALYSIS

EQUIPMENT	Prepared by: DATE	REVISION DATE	APPROVED BY DATE	REFERENCES	EQUIPMENT STATUS
BUV Instrument, Interface Connectors	R.Cramer 8/14/69	N/C			Normal Operation

ITEM NO. & NAME	ASSUMED FAILURE	Probable Cause	Stress MARGIN	$\lambda \times 10^6$	Failure Rate Source	PROBABLE EFFECT	FAILURE EFFECT CLASS	Remarks
J4								
Pin								
33	Loss of "Set Calib. Inhibit Return".	Electrical disconnect.				No effect at Command Subsystem.	C_1	
34 (Spare)								
35	Loss of "Remove Calib. Inhibit Return".	Electrical disconnect.				No effect at Command Subsystem.	C_1	
36 (Spare)								
37	Loss of Chassis Ground.	Electrical disconnect.				No effect at VIP.	C_1	May increase noise on the command signals on J4 from the interface equipment to the BUV.

FAILURE EFFECT ANALYSIS

EQUIPMENT	Prepared by: DATE	REVISION DATE	APPROVED BY DATE	REFERENCES	EQUIPMENT STATUS
BUV Instrument, Interface Connectors	R.Cramer 8/14/69	N/C			Normal Operation

ITEM NO. & NAME	ASSUMED FAILURE	Probable Cause	Stress MARGIN	λ x 10⁶	Failure Rate Source	PROBABLE EFFECT	FAILURE EFFECT CLASS	Remarks
J4								
Pin								
18, 19 (Spares)								
20	Loss of "Deplo Diffuser retur	lectrical disconnect.				No effect at Command Subsystem.	C_1	
21	Loss of "Return Diffuser to Normal" return.	Electrical disconnect.				No effect at Command Subsystem.	C_1	
22	Loss of "Set Launch Mode Return".	Electrical disconnect.				No effect at Command Subsystem.	C_1	
23	Loss of "Reset Launch Mode Return".	Electrical disconnect.				No effect at Command Subsystem.	C_1	
24 (Spare)								
25	Loss of "Switch-On Power Relay Return".	Electrical disconnect.				No effect at Command Subsystem.	C_1	Will cause lack of primary power to Static Inverter #2 in BUV.
26 (Spare)								
27	Loss of "Switch-Off Power Relay Return".	Electrical disconnect.				No effect at Command Subsystem.	C_1	Will prevent switch-off of primary power to Static Inverter #2 in BUv.
28-32 (Spares)								

FAILURE EFFECT ANALYSIS

EQUIPMENT	Prepared by:	DATE	REVISION	DATE	APPROVED BY	DATE	REFERENCES	EQUIPMENT STATUS
BUV Instrument, Interface Connectors	R.Cramer	8/14/69	N/C					Normal Operation

ITEM NO. & NAME	ASSUMED FAILURE	Probable Cause	Stress MARGIN	$\lambda \times 10^6$	Failure Rate Source	PROBABLE EFFECT	FAILURE EFFECT CLASS	Remarks
J4								
Pin								
5	Loss of "Reset Launch Mode" command.	(1) Electrical disconnect. (2) Defective relay K3 in module 202.				No effect at Command Subsystem.	C_1	
6 (Spare)								
7	Loss of "Switch-On Power Relay".	(1) Electrical disconnect. (2) Defective relay K6 in module 202.				No effect at Command Subsystem.	C_1	Will cause lack of primary power to Static Inverter #2 in BUV.
8 (Spare)								
9	Loss of "Switch-Off Power Relay".	(1) Electrical disconnect. (2) Defective relay K6 in module 202.				No effect at Command Subsystem.	C_1	Will prevent switch-off of primary power to Static Inverter #2 in BUV.
10-14 (Spares)								
15	Loss of "Set Calib. Inhibit" Command.	(1) Electrical disconnect. (2) Defective relay K4 in module 202.				No effect at Command Subsystem.	C_1	
16 (Spare)								
17	Loss of "Remove Calib. Inhibit" Command.	(1) Electrical disconnect. (2) Defective relay K4 in module 202.				No effect at Command Subsystem.	C_1	

FAILURE EFFECT ANALYSIS

EQUIPMENT	Prepared by: DATE	REVISION DATE	APPROVED BY DATE	REFERENCES	EQUIPMENT STATUS
BUV Instrument, Interface Connectors	R. Cramer 8/14/69	N/C			Normal Operation

ITEM NO. & NAME	ASSUMED FAILURE	Probable Cause	Stress MARGIN	λ x 10⁶	Failure Rate Source	PROBABLE EFFECT	FAILURE EFFECT CLASS	Remarks
J4								
Pin								
1	Loss of Logic Reference.	Electrical disconnect.				No effect at VIP.	C_1	
2	Loss of "Deploy Diffuser" command.	(1) Electrical disconnect. (2) Defective relay K1 in module 202. (3) Defective logic circuit.				No effect at Command Subsystem.	C_1	
3	Loss of "Return Diffuser to Normal" Command.	(1) Electrical disconnect. (2) Defective relay K2 in module 202. (3) Defective logic circuit.				No effect at Command Sub-System.	C_1	
4	Loss of "Set Launch Mode" command.	(1) Electrical disconnect. (2) Defective relay K3 in module 202. (3) Defective LM circuit.				No effect at Command Subsystem.	C_1	

FAILURE EFFECT ANALYSIS

EQUIPMENT	Prepared by:	DATE	REVISION	DATE	APPROVED BY	DATE	REFERENCES	EQUIPMENT STATUS
BUV Instrument, Interface Connectors	R.Cramer	8/14/69	N/C					Normal Operation

ITEM NO. & NAME	ASSUMED FAILURE	Probable Cause	Stress MARGIN	λ x 10⁶	Failure Rate Source	PROBABLE EFFECT	FAILURE EFFECT CLASS	Remarks
J3								
Pin								
27	Loss of Digital "B" Signal.	(1) Electrical disconnect. (2) Defective digital "B" circuitry.				Loss of "Monochromator Dark Current/Wavelength monitor" to VIP.	A_2	
28, 29 (Spares)								
30	Loss of Digital "B" Signal.	(1) Electrical disconnect. (2) Defective digital "B" circuitry.				Loss of "Monochromator Photometric Calibrate monitor" to VIP.	A_2	
31, 32 (Spares)								
33	Loss of Signal.	(1) Electrical disconnect. (2) Defective relay K6 in module 202. (3) Defective -6.375V supply circuitry.				Loss of "Power relay Status" to VIP.	A_2	
34, 35, 36 (Spares)								
37	Loss of chassis ground.	Electrical disconnect.				No effect at VIP.	C_2	May increase noise on the signals from J3 to the interface equipment.

FAILURE EFFECT ANALYSIS

EQUIPMENT	Prepared by: DATE	REVISION DATE	APPROVED BY DATE	REFERENCES	EQUIPMENT STATUS
BUV Instrument, Interface Connectors	R. Cramer 8/14/69	N/C			Normal Operation

ITEM NO. & NAME	ASSUMED FAILURE	Probable Cause	Stress MARGIN	λ x 10⁶	Failure Rate Source	PROBABLE EFFECT	FAILURE EFFECT CLASS	Remarks
J3								
Pin								
20	Loss of Digital "B" Signal.	(1) Electrical disconnect. (2) Defective digital "B" circuitry.				Loss of "Electronics calib. monitor (MSC-A)" to VIP.	A_2	
21	Loss of Digital "B" Signal.	(1) Electrical disconnect. (2) Defective digital "B" circuitry.				Loss of "Cam Position - λ2" to VIP.	A_2	
22	Loss of Digital "B" Signal.	(1) Electrical disconnect. (2) Defective digital "B" circuitry.				Loss of Monochromator shutters open monitor" to VIP.	A_2	
23	Loss of Digital "B" Signal.	(1) Electrical disconnect. (2) Defective digital "B" circuitry.				Loss of "Photometer calibrate monitor" to VIP.	A_2	
24, 25 (Spare)								
26	Loss of Digital "B" Signal.	(1) Electrical disconnect. (2) Defective digital "B" circuitry.				Loss of "Calibrate inhibit Relay monitor" to VIP.	A_2	

FAILURE EFFECT ANALYSIS

EQUIPMENT	Prepared by: DATE	REVISION DATE	APPROVED BY DATE	REFERENCES	EQUIPMENT STATUS
BUV Instrument, Interface Connectors	R.Cramer 8/14/69	N/C			Normal Operation

ITEM NO. & NAME	ASSUMED FAILURE	Probable Cause	Stress MARGIN	$\lambda \times 10^6$	Failure Rate Source	PROBABLE EFFECT	FAILURE EFFECT CLASS	Remarks
J3								
Pin								
14	Loss of Digital "B" Signal.	(1) Electrical disconnect. (2) Defective digital "B" circuitry.				Loss of "Pre-λ calibrate Indicator" to VIP.	A_2	
15	Loss of Digital "B" Signal.	(1) Electrical disconnect. (2) Defective digital "B" circuitry.				Loss of "Launch Mode Relay Monitor" to VIP.	A_2	
16	Loss of Digital "B" Signal.	(1) Electrical disconnect. (2) Defective digital "B" circuitry.				Loss of "Diffuser Deployed Monitor" to VIP.	A_2	
17	Loss of Digital "B" Signal.	(1) Electrical disconnect. (2) Defective digital "B" circuitry.				Loss of "Diffuser Retracted Monitor" to VIP.	A_2	
18	Loss of Digital "B" Signal.	(1) Electrical disconnect. (2) Defective digital "B" circuitry.				Loss of "Cam Position - λ 1" to VIP.	A_2	
19	Loss of Digital "B" Signal.	(1) Electrical disconnect. (2) Defective digital "B" circuitry.				Loss of "Photometer Dark Current Monitor" to VIP.	A_2	

FAILURE EFFECT ANALYSIS

EQUIPMENT	Prepared by: DATE	REVISION DATE	APPROVED BY DATE	REFERENCES	EQUIPMENT STATUS
BUV Instrument, Interface Connectors	R. Cramer 8/14/69	N/C			Normal Operation

ITEM NO. & NAME	ASSUMED FAILURE	Probable Cause	Stress MARGIN	$\lambda \times 10^6$	Failure Rate Source	PROBABLE EFFECT	FAILURE EFFECT CLASS	Remarks
J3								
Pin								
7	Loss of Signal.	(1) Electrical disconnect.				Loss of "10KH$_z$ monitor" to VIP.	A_2	
		(2) Defective 10KH$_z$ monitor circuit.						
8	Loss of Digital "B" Signal.	(1) Electrical disconnect.				Loss of "Calibration lamp on/off Indicator" to VIP.	A_2	
		(2) Defective digital "B" circuitry.						
9	Loss of Digital "B" Signal.	(1) Electrical disconnect.				Loss of "Photometer Shutters Open Monitor" to VIP.	A_2	
		(2) Defective digital "B" Circuitry.						
10, 11 (Spares)								
12	Loss of Digital "B" Signal.	(1) Electrical disconnect.				Loss of "Photometric calib. Indicator" to VIP.	A_2	
		(2) Defective digital "B" circuitry.						
13	Loss of Digital "B" signal.	(1) Electrical disconnect.				Loss of "Major Frame Pulse Data Frame Indicator" to VIP.	A_2	
		(2) Defective digital "B" circuitry.						

FAILURE EFFECT ANALYSIS

EQUIPMENT	Prepared by: DATE	REVISION DATE	APPROVED BY DATE	REFERENCES	EQUIPMENT STATUS
BUV Instrument, Interface Connectors	R.Cramer 8/14/69	N/C			Normal Operation

ITEM NO. & NAME	ASSUMED FAILURE	Probable Cause	Stress MARGIN	$\lambda \times 10^6$	Failure Rate Source	PROBABLE EFFECT	FAILURE EFFECT CLASS	Remarks
J3								
Pin								
1	Loss of Logic Reference.	Electrical disconnect.				No effect at VIP.	C_2	
2	Loss of Digital "B" Signal.	(1) Electrical disconnect. (2) Defective digital "B" circuitry.				Loss of "Cam position -λ4" to VIP.	A_2	
3	Loss of Digital "B" Signal.	(1) Electrical disconnect. (2) Defective digital "B" circuitry.				Loss of "Cam Position -λ8" to VIP.	A_2	
4	Loss of Digital "B" Signal.	(1) Electrical disconnect. (2) Defective digital "B" circuitry.				Loss of "Cam Position -λ16" to VIP.	A_2	
5	Loss of Digital "B" Signal.	(1) Electrical disconnect. (2) Defective digital "B" circuitry.				Loss of "Retract Diffuser Command Monitor" to VIP.	A_2	
6	Loss of Digital "B" Signal.	(1) Electrical disconnect. (2) Defective digital "B" circuitry.				Loss of "Deploy Diffuser Command Monitor" to VIP.	A_2	